Springer Protocols

Methods in Molecular Biology 627

Surface Plasmon Resonance

Methods and Protocols

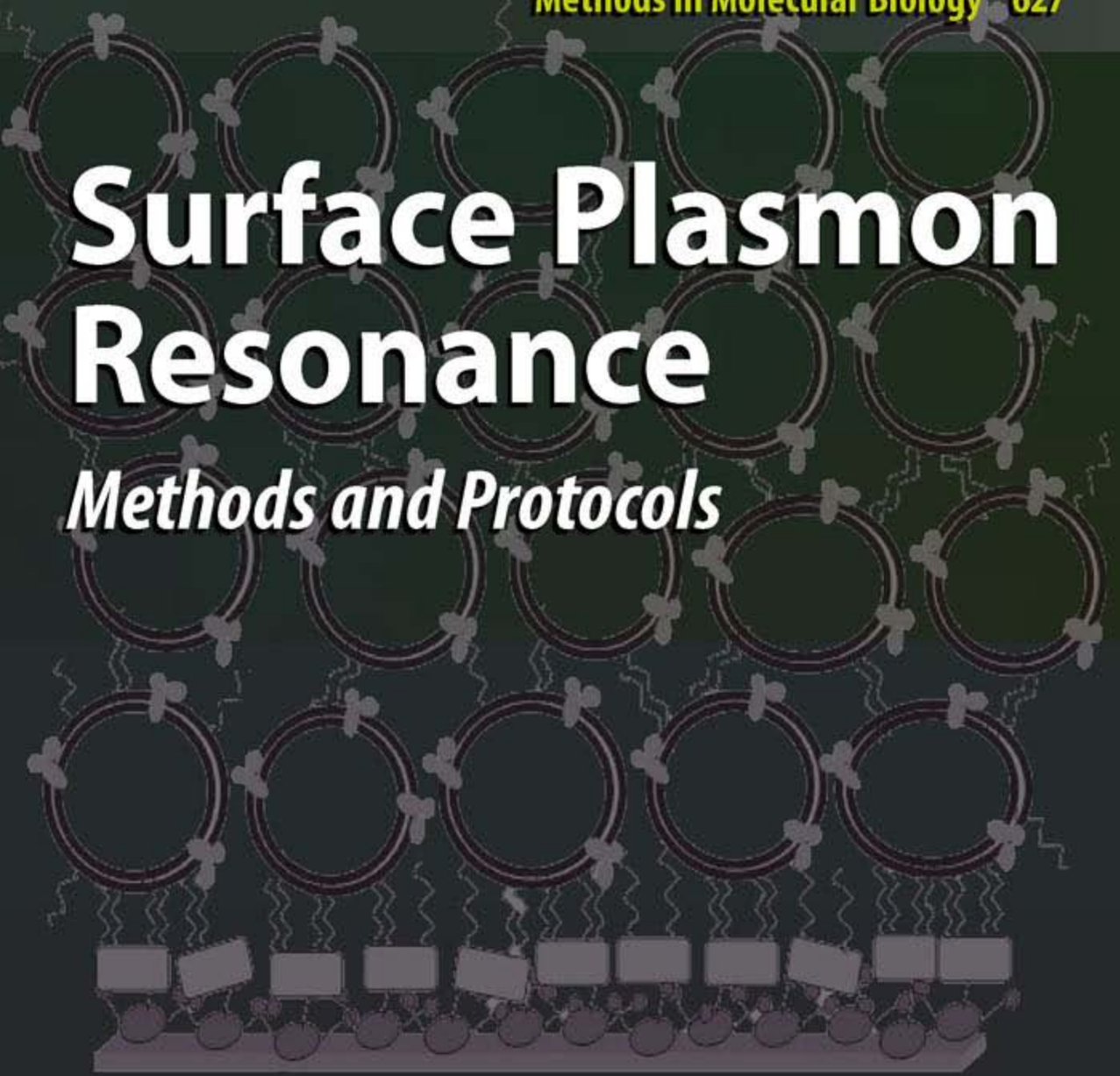

Edited by

Nico J. de Mol

Marcel J. E. Fischer

Humana Press

METHODS IN MOLECULAR BIOLOGY™

Series Editor
John M. Walker
School of Life Sciences
University of Hertfordshire
Hatfield, Hertfordshire, AL10 9AB, UK

For other titles published in this series, go to
www.springer.com/series/7651

Surface Plasmon Resonance

Methods and Protocols

Edited by

Nico J. de Mol, Marcel J. E. Fischer

Utrecht University, Utrecht, The Netherlands

Humana Press

Editors
Nico J. de Mol
Department of Pharmaceutical Sciences
Utrecht University
Sorbonnelaan 16
3585 CA Utrecht
Netherlands
n.j.demol@uu.nl

Marcel J. E. Fischer
Department of Pharmaceutical Sciences
Utrecht University
Sorbonnelaan 16
3585 CA Utrecht
Netherlands
m.j.e.fischer@uu.nl

ISSN 1064-3745 e-ISSN 1940-6029
ISBN 978-1-60761-669-6 e-ISBN 978-1-60761-670-2
DOI 10.1007/978-1-60761-670-2
Springer New York Dordrecht Heidelberg London

Library of Congress Control Number: 2010920287

Cover illustration: The buildup of a proper surface is central in SPR technology. Here a sophisticated example from Chapter 16 is shown for incorporating transmembrane proteins in a supported 3D-matrix of liposomes, which are connected by complementary DNA sequences to the previous layer. From Chapter 16 by Annettte Graneli.

Printed on acid-free paper

Humana Press is part of Springer Science+Business Media (www.springer.com)

Preface

Surface plasmon resonance (SPR) has evolved into an exciting technique in biomolecular interaction analysis. The development of commercial SPR instruments has made the technique available to a wide scientific audience, and the number of publications in which the use of SPR is described is rapidly increasing. SPR is in use for many purposes from food quality control to the study of nanoparticles. Much research is now focused on developing new SPR-related applications, e.g., SPR imaging, SPR arrays, SPR fluorescence, and combinations of SPR with mass spectrometry and with electrochemistry.

Biomolecular interaction analysis is at the core of many research projects. In principle, the setup of an SPR experiment is simple: There is a sensor surface to which one of the interacting partners (the ligand) is immobilized; the other partner (the analyte) is added in a flow or cell-like compartment. The binding phenomenon is monitored in real time as a change in SPR angle.

An important issue is the choice of surface and the immobilization strategy. With SPR, it is possible to mimic the biological environment which is relevant for an interaction. For interactions in a water environment, sensor surfaces with hydrogels are available. Many biomolecular interactions take place in a membrane environment. For this, commercial sensor surfaces are available, or surfaces can be tailor-made. This volume contains several examples of building up of lipophilic surfaces. Nature abundantly makes use of multivalent interactions; multivalency can be mimicked on a sensor surface with immobilized ligands.

In composing this volume, we had users in mind who have access to commercially available SPR instruments. As mentioned above, new technology-driven SPR applications are emerging. These are fascinating and promising but mostly not widely commercially available yet, and therefore not prominent in this volume.

A broad variety of applications is presented. The volume aims to address a wide range of researchers (biochemists, molecular biologists, medicinal chemists, molecular pharmacologists, biophysicists) who would not like to use their SPR instrument as a "black box" but wish to be aware of the processes on and near the sensor that affect the outcome of SPR experiments. Therefore, this volume does not only contain protocol-based chapters but also chapters highlighting backgrounds of vital issues in using SPR, such as processes occurring within the hydrogel environment of sensors and one chapter focusing on lipid membrane surfaces. The information from SPR experiments is very information rich. It cannot only be used for affinity assays but also to gather kinetic information. Proper kinetic analysis may help to understand the binding mode, e.g., conformational changes, dimerization, or heterogeneity.

We expect that this volume fills a need for well-described hands-on SPR experimental protocols. It promises, however, more than details for implementing a described protocol: You may be inspired to develop adaptations to your own need and molecules. This is also how our authors started!

In their 2005 review of the literature, Rich and Myszka conclude that the quality and presentation of SPR work is often pretty poor (1). It is our conviction that this is caused by a lack of knowledge of the processes that influence the SPR signal. Hopefully, this volume

helps to create insight into the great possibilities and also limitations of SPR. Such insight promotes well-designed SPR experiments and adequate presentation in literature. More knowledge also inspires researchers to do more with the SPR signal than is now common practice.

We are thankful to our authors for their enthusiastic reaction to our invitation and for their cooperation and patience. Now overlooking the end result, we are impressed by the high quality of their contributions. It was a pleasure to collaborate with them.

Reference

1. Rich, R. L., and Myszka, D. G. (2006) Survey of the year 2005 commercial optical biosensor literature. *J. Mol. Recognit.* **19**, 478–534.

Nico J. de Mol
Marcel J.E. Fischer

Contents

Contributors

GREGOR ANDERLUH • *Department of Biology, Biotechnical Faculty, University of Ljubljana, Ljubljana, Slovenia*

MARIE-ISABEL AGUILAR • *Department of Biochemistry and Molecular Biology, Monash University, Clayton, Victoria, Australia*

MOJCA PODLESNIK BESENIČAR • *Department of Biology, Biotechnical Faculty, University of Ljubljana; Institute "Jožef Stefan", Ljubljana, Slovenia*

JONAS BORCH • *Institute for Biochemistry and Molecular Biology, University of Southern Denmark, Odense M, Denmark*

BEINING CHEN • *Department of Chemistry, University of Sheffield, Sheffield, UK*

NICO J. DE MOL • *Department of Medicinal Chemistry and Chemical Biology, Utrecht Institute for Pharmaceutical Sciences, Utrecht, The Netherlands*

ERIC DUVERGER • *Glycobiologie, Centre de Biophysique Moléculaire, CNRS et Université d'Orléans, Orléans, France*

MARCEL J.E. FISCHER • *Department of Medicinal Chemistry and Chemical Biology, Utrecht Institute for Pharmaceutical Sciences, Utrecht, The Netherlands*

NATACHA FRISON • *Glycobiologie, Centre de Biophysique Moléculaire, CNRS et Université d'Orléans, Orléans, France*

NAOKI GOSHIMA • *Protein Expression Team, Biological Information Research Center, National Institute of Advanced Industrial Science and Technology, Tokyo, Japan*

ANNETTE GRANÉLI • *Department of Physics, University of Gothenburg, Gothenburg, Sweden*

KRISTOPHER HALL • *Department of Biochemistry and Molecular Biology, Monash University, Clayton, Victoria, Australia*

VESNA HODNIK • *Department of Biology, Biotechnical Faculty, University of Ljubljana, Ljubljana, Slovenia*

XU HOU • *Department of Biochemistry and Molecular Biology, Monash University, Clayton, Victoria, Australia*

STEPHANIE Q. HUTSELL • *Department of Biochemistry and Biophysics, The University of North Carolina, Chapel Hill, NC, USA*

ADAM J. KIMPLE • *Department of Pharmacology, The University of North Carolina, Chapel Hill, NC, USA*

RANDALL J. KIMPLE • *Department of Radiation Oncology, The University of North Carolina, Chapel Hill, NC, USA*

KARL-WILHELM KOCH • *Biochemistry Group, IBU, University of Oldenburg, Oldenburg, Germany*

KONSTANTIN E. KOMOLOV • *Biochemistry Group, IBU, University of Oldenburg, Oldenburg, Germany*

NATHALIE LAMERANT-FAYEL • *Glycobiologie, Centre de Biophysique Moléculaire, CNRS et Université d'Orléans, Orléans, France*

JOHN S. MITCHELL • *The Horticulture and Food Research Institute of New Zealand Ltd., Hamilton, New Zealand*

MICHEL MONSIGNY • *Glycobiologie, Centre de Biophysique Moléculaire, CNRS et Université d'Orléans, Orléans, France*

ROBIN E. MULLER • *Department of Pharmacology, The University of North Carolina, Chapel Hill, NC, USA*

DOBRIN NEDELKOV • *Intrinsic Bioprobes Inc., Tempe, AZ, USA*

NOBUO NOMURA • *Protein Expression Team, Biological Information Research Center, National Institute of Advanced Industrial Science and Technology, Tokyo, Japan*

SARA PEETERS • *Nano Engineered Component Science Research, IMEC vzw, Leuven, Belgium; Department of Medical Diagnostic Sciences, KUleuven, Leuven, Belgium*

PETER ROEPSTORFF • *Institute for Biochemistry and Molecular Biology, University of Southern Denmark, Odense M, Denmark*

PETER SCHUCK • *Dynamics of Macromolecular Assembly, Laboratory of Bioengineering and Physical Science, National Institute of Biomedical Imaging and Bioengineering (NIBIB), National Institutes of Health, Bethesda, MD, USA*

DAVID P. SIDEROVSKI • *Department of Pharmacology, UNC Neuroscience Center and Lineberger Comprehensive Cancer Center, The University of North Carolina, Chapel Hill, NC, USA*

DAVID H. SMALL • *Menzies Research Institute, University of Tasmania, Hobart, Tasmania, Australia*

TIM STAKENBORG • *Nano Engineered Component Science Research, IMEC vzw, Leuven, Belgium*

HIROYUKI TAKEDA • *Protein Expression Team, Japan Biological Information Research Center, Japan Biological Informatics Consortium, Tokyo, Japan*

FRANCIS S. WILLARD • *Department of Pharmacology, The University of North Carolina, Chapel Hill, NC, USA*

YINQIU WU • *The Horticulture and Food Research Institute of New Zealand Ltd., Hamilton, New Zealand*

HUAYING ZHAO • *Dynamics of Macromolecular Assembly, Laboratory of Bioengineering and Physical Science, National Institute of Biomedical Imaging and Bioengineering (NIBIB), National Institutes of Health, Bethesda, MD, USA*

Chapter 1

Surface Plasmon Resonance: A General Introduction

Nico J. de Mol and Marcel J. E. Fischer

Abstract

Surface plasmon resonance (SPR) analysis is rather unique in that it allows assay of binding constants (affinity) and kinetic analysis of binding phenomena. This introductory chapter deals with some specific features that are relevant to many diverse applications. The role and impact of kinetics in biomolecular interactions is highlighted. A concise description of the physical principles of the SPR phenomenon is given from a practical point of view, such that some possibilities and limitations of the method can be rationalized, e.g., depth of the evanescent field. A specific condition that may come forward in kinetic analysis is mass transport limitation (MTL). A practical model is presented, which allows estimation of the extent of MTL. Based on this model it can be rationalized whether MTL can be avoided by experimental design. In this framework also rules are presented to convert SPR signals (RU or millidegree) to mass/surface unit. The chapter concludes with an overview of commercially available SPR equipment.

Key words: Surface plasmon resonance (SPR), kinetics, SPR equipment, SPR physical principles, mass transport, SPR bulk effects, evanescent field.

1. Introduction

Biomolecular interactions are at the core of virtually every biological phenomenon: ligand–receptor interactions, signal transduction, regulation of gene expression, etc., are all controlled by specific recognition of interacting partners. So it is not surprising that there is a keen interest in and need for methods and technologies to characterize biomolecular interactions. Such methods and technologies have been developed and improved, especially in recent years. In the broad spectrum of technologies for interaction analysis, label-free biomolecular interaction analysis has a special place. The introduction of labels, e.g., fluorescent labels,

N.J. de Mol, M.J.E. Fischer (eds.), *Surface Plasmon Resonance*, Methods in Molecular Biology 627,
DOI 10.1007/978-1-60761-670-2_1, © Springer Science+Business Media, LLC 2010

to study molecular interactions has brought great progress, but also has drawbacks like the risk to intervene in the binding event. The last decade we have seen tremendous progress in equipment for label-free biosensor techniques, like microcalorimeters, quartz crystal microbalances, reflectometric interference spectrometers, and, not least, surface plasmon resonance (SPR) equipment.

SPR has become very important with a yearly impressive increase in number of publications (1). Because it is a label-free technique, only one of the interacting partners has to be immobilized on a sensor surface. SPR has been applied in a wide range of settings, even mimicking biological environments like membranes and surfaces with multiple-binding partners. In the next section, the principles of the SPR phenomenon are described briefly. In essence a mass change near a thin gold (or other metal) surface is detected in real time. This implies that the change in SPR signal over time (as depicted in a sensorgram, *see* **Fig. 1.1**) also contains kinetic information. Ideally, the sensorgram contains kinetic information, but also information upon reaching equilibrium (steady state). The signals at equilibrium can be readily used for assay of equilibrium-binding constants (K_A or K_D, e.g., *see* **Chapter 6**). The kinetic phase (association and dissociation) can be used for kinetic analysis, and may yield under proper conditions also equilibrium-binding constants. Kinetic analysis can be easily performed if a simple one-to-one interaction model describes the data, yielding the association rate (k_{on}) and the dissociation rate (k_{off}), e.g., *see* **Chapter 2**. In practice, often more complex binding models may apply, e.g., due to mass transport (*see* **Section 2** and **Chapter 2**), heterogeneity of the surface (*see* **Chapter 2**), conformational change, multivalent binding, dimer formation. In such cases so-called global kinetic analysis may be performed using specific software like CLAMP or Scrubber (2).

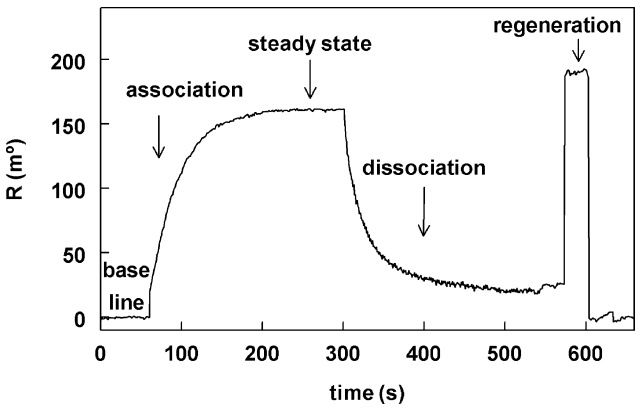

Fig. 1.1. Typical sensorgram of a molecular interaction. The various phases of a SPR experiment are shown. The SPR signal (R) is here expressed as change in SPR angle in millidegree (m°) (*see* text).

In this respect, SPR analysis is rather unique in that it is one of the few techniques that generates equilibrium data and kinetic data.

1.1. Kinetics: Slow or Fast, Which Is the Best?

Most of us are familiar with equilibrium-binding constants as an expression for the strength of the binding. Usually, in screening of drug candidates, those compounds that have high affinity for the target are selected for further development. Interpretation and exploitation of *kinetic* information is not so straightforward. Intuitively we assume that it plays an important role in biological processes, e.g., in homeostasis of transient cellular processes, when short residence times are needed, or on contrary, in situations where it is efficient during receptor occupation to activate multiple cycles of a process. In general, it is not known what the impact is of the residence time of an agonist on the receptor, which is primarily dictated by k_{off}. There are only few examples of receptors for which residence time has been assigned a clear and important role in biological activity. Such examples are given by Tummino and Copeland: For example, the residence time of peptide–MHC complexes at the T-cell receptor in general correlates with the degree of T-cell activation, and the life time of proteinase–natural protein inhibitor complexes is crucial for control of proteinase activity (3). From our own research we observed that interactions of phosphotyrosine-containing peptides with SH2 domains are characterized by extreme high on-rates of approximately 5×10^6 $M^{-1}s^{-1}$, and extreme high off-rates of approximately 1 s^{-1} (4). Such high rates and short residence times are consistent with a role of these interactions in transient signal transduction processes. Multivalent interactions, e.g., involving tandem SH2 domains, allow to combine high dissociation rates with high affinity and specificity, resulting from a multitude of weak interactions (5, 6). These insights might have important implications for drug design, questioning the current paradigm to hunt for highest affinity (7). Transient drugs can be based on high off-rates, multivalent approaches, and multiple targets. SPR is a valuable tool to study such drug candidates, as it allows kinetic characterization of biomolecular interactions.

1.2. How SPR Developed into a Biomolecular Interaction Analysis Tool

Before describing the physical principles of the SPR phenomenon here, a concise overview is given of how it developed into a technique, which is widely used in binding studies.

The first observations of the SPR phenomenon were obtained at the beginning of the twentieth century, when Wood detected an anomalous diffraction pattern of light and dark bands when visible polarized light reflects on a metal grating (8). It took until the late 1960s, before the phenomenon of SPR could be exploited by Otto and Kretschmann as an optical excitation of surface plasmons. In this setting light falls through a glass prism under conditions of total reflection and onto a metal film evaporated on the

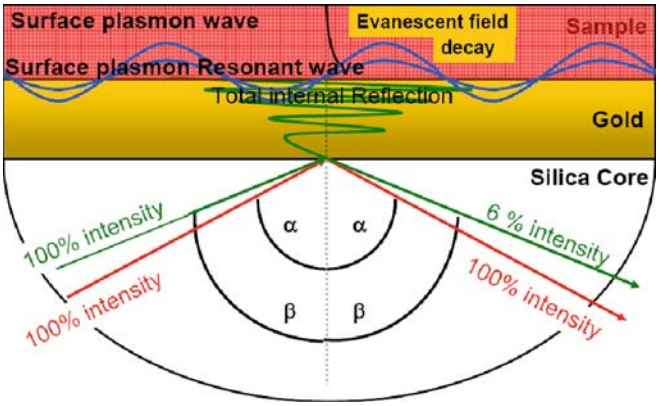

Fig. 1.2. SPR effect at attenuated total reflection (ATR). An SPR sensor is shown in the Kretschmann configuration. Below a hemi-cylindrical prism is shown, covered with a sensor chip with a gold layer on which a ligand can be immobilized (sample compartment). The surface is irradiated with polarized visible light with a range of incident angles (e.g., α and β). Under conditions of attenuated total reflection (ATR) (angle α) a dip in the intensity of reflected light is observed and the electrons in the gold layer absorb the energy of the light, resulting in a surface plasmon resonant wave. Figure by courtesy of Jan Castrop, Metrohm Autolab, Utrecht, The Netherlands.

glass (*see* **Fig. 1.2**) (9, 10). This provided the basic configuration for an SPR sensor. In the 1980s Liedberg et al. first realized that SPR-based sensors can be used to study binding, as the SPR signal is sensitive to a change in refractive index. The refractive index is influenced by the accumulation of mass (molecules) near the metal surface (11). The configurations for SPR sensors developed by Kretschmann and Otto opened the way for development of commercial SPR instrumentation, initially by Pharmacia Biosensor in Sweden, a predecessor of what now is GE-Biacore. Next to Biacore instruments, various other types of SPR instrumentation are available (*see* **Section 3**)

1.3. The Physical Principles of Surface Plasmon Resonance

This section gives a simplified qualitative description of the principles of SPR. For a physicist it probably is an oversimplification, but the emphasis in this volume is on practical aspects of the SPR technique, and it is our aim here to give such a description that some limitations and possibilities of application of the technique can be rationalized and understood from its principles. For a more thorough treatment of the physics of SPR the reader is referred to specialized literature (12, 13).

SPR is an optical phenomenon involving excitation of free oscillating metal electrons. The energy carried by photons of light is transferred to packages of electrons on a metal surface. The optical excitation of plasmons occurs only under proper resonance conditions, that is, under conditions of attenuated total reflection (ATR) when the energy of the photons of light exactly equals the quantum energy level of the plasmons.

A configuration according to Kretschmann, existing of a prism coated with a thin metal film to generate surface plasmons, is shown in **Fig. 1.2**. At a particular incident angle (β) light impinging on the prism penetrates into the metal film and the ATR conditions are met. These are the conditions for plasmon generation, and energy is transferred from the photons to the metal electrons. The electromagnetic field associated with the incident light is coupled to the oscillations of the free electrons. The plasmon state is a highly delocalized state of the metal electrons, resulting in a plasmon resonant wave at the interface of the metal and a dielectric medium. An evanescent electromagnetic field is connected with this plasmon resonant wave. This evanescent field has a limited penetration depth into the dielectric medium (*see* **Section 1.5**)

The ATR conditions can be explored by varying the incident angle of the light and the detection of the intensity of reflected light. This yields characteristic SPR curves with a sharp minimum in reflection (approximately to 6%), upon variation of the angle of light incidence (*see* **Fig. 1.3**). The shape of the SPR curve is characterized by three elements: the angular position, the angular width, and the depth in the reflectance. This shape is strongly dependent on the nature of the metal, the wavelength of the

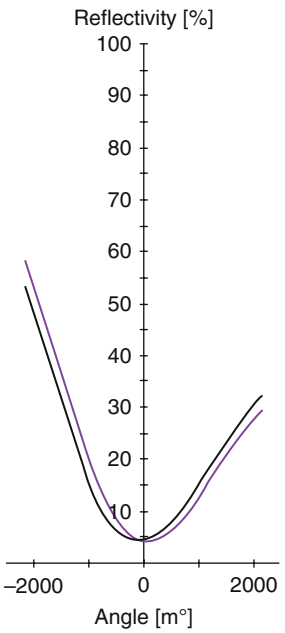

Fig. 1.3. SPR signal. The SPR signal, shown here as derived from an Autolab Esprit instrument, is measured as a dip in intensity of reflected light. The angle at which the reflection is minimal changes with the refractive index, which is very sensitive to mass changes near the gold surface. In Biacore instruments the SPR signal is expressed in RU, in Autolab Instruments (and some others) as a shift in angle in millidegree (m°).

incident light, and the angle of incidence (13). The angular position and shape of the curve is also very sensitive to the optical properties of the dielectric medium immediately near the metal surface. The application of SPR to characterize kinetics and binding of biomolecules is based on this sensitivity.

1.4. SPR Signal: Bulk Effects, Temperature Dependence, and Bound Mass

The SPR angle is characterized by a complex dielectric constant within the thin layer including the material attached to the metal surface. This dielectric constant includes the refractive index n and the extinction coefficient (13). This implies that every change in refractive index is sensed as a change in SPR signal. Even small differences in running buffer or the presence of protein in the bulk solution give rise to so-called bulk effects. An extreme example is shown in **Fig. 1.4**. Bulk effects are characterized by immediate changes in the SPR signal upon change of buffer, e.g., at the start of the association or dissociation phase. They are normally corrected by applying a reference surface, identically treated as the sample surface, but without the immobilized ligand (*see* **Fig. 1.4**).The SPR signal is extremely sensitive to temperature changes. As shown in **Fig. 1.4** the reference signal is indicative of temperature effects and deviations from thermal equilibrium. The sample signal corrected for the reference yields an apparently correct interaction curve, however, the reference signal indicates that in the initial phase of the association the system is not yet at thermal equilibrium. Therefore this part of the sensorgram may not be suitable for kinetic analysis. It is important that measurements occur under well-thermostated conditions. This is especially

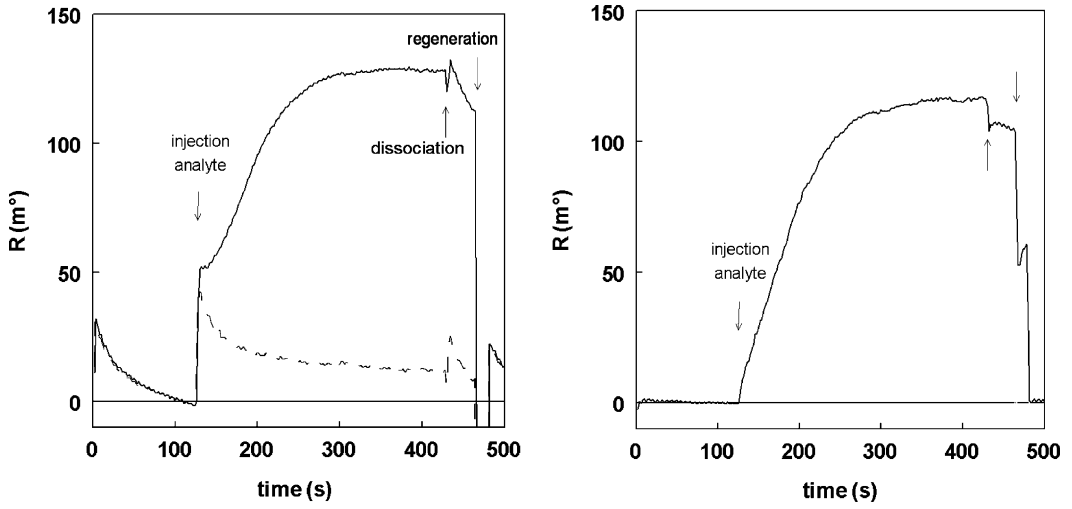

Fig. 1.4. Bulk effects in SPR sensorgrams. *Left* sensorgrams of sample (*solid line*) and reference (*broken line*) of an interaction at 40°C under poor thermostating conditions are shown. The SPR signal is extremely temperature sensitive. *Right* the sample signal corrected for the reference. The temperature effects on the bulk signals are well corrected for, but this does not mean that the system is at thermal equilibrium.

relevant when measuring at temperatures deviant from room temperature.

The change in SPR signal is basically a change in angle at which the minimum of reflection is observed (*see* **Fig. 1.3**). For Biacore instruments the SPR signal is expressed in RU units, with 1 RU unit corresponding to 1 pg/mm^2 of mass bound to the sensor surface, although this is not a fixed number (*see* **Note 1**). For some other instruments, e.g., Autolab, the SPR signal is directly expressed as the change in SPR angle in millidegrees (m°): 1 ng/mm^2 of mass bound to a sensor surface with an approximately 100 nm thick dextran hydrogel layer, such as, e.g., in Biacore CM5 chips, corresponds to 100 ± 10 m° (14). The contribution to the SPR signal due to variations in the extinction coefficient, which in principle also influences the change in SPR angle upon binding of a certain amount of mass to the surface, can be neglected in practice when dealing with biomolecules like proteins and nucleic acids. The relation between bound mass at the surface and shift in SPR angle is linear till 50 ng/mm^2 (14), corresponding to 50,000 RU or 5,000 m°.

1.5. The Strength of the SPR Signal Decays Rapidly with the Distance from the Metal Surface

As mentioned above, the oscillating electrons in the metal film generate an evanescent electromagnetic field directly at the metal–dielectric interface, penetrating into the dielectric medium in the direction opposite to that of the incident light. The amplitude of this evanescent field is strongest at the metal–dielectric interface and decays exponentially with increasing distance from the metal surface, becoming practically zero at 300 nm (*see* **Fig. 1.5**). As a consequence of this, the SPR signal is strongest immediately near the metal surface. The most frequently used type of SPR sensors have hydrogel (dextran-type) matrices attached to the gold surface of approximately 100 nm thickness (e.g., the CM5 chip of GE Biacore). Within this distance the strength of the evanescent field is already considerably decreased. Molecules bound to easily accessible binding sites at the outside of the sensor matrix will contribute less to the signal than molecules penetrated deeper into the sensor matrix. This could even lead to sigmoid types of association curves (*see* **Chapter 2** for more detail). For shorter brush-type sensors and sensors existing of lipid layers near the metal surface a relatively larger signal will be sensed. It should be kept in mind, however, that such thin surfaces will have a more limited binding capacity. A hydrogel matrix with a thickness of 100 nm is in many cases a good compromise between binding capacity and signal strength.

The limited penetration depth of the evanescent field complicates quantitative detection of binding to larger objects such as complete immobilized cells, which generally have dimensions larger than 10,000 nm. In such situation binding may be

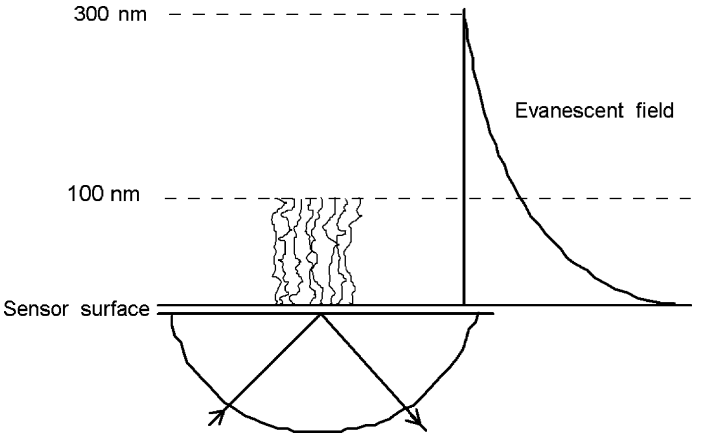

Fig. 1.5. Limited range of sensitivity for the SPR effect. The SPR effect is sensed only in the evanescent field coupled to surface plasmon resonance waves. The strength of this field decays exponentially with the distance from the surface and has a limited range of around 300 nm. A 100 nm thick hydrogel is a good compromise between signal sensitivity and binding capacity.

observed, but it will be impossible to relate the SPR signal to bound mass.

2. Mass Transport

2.1. Model to Estimate Extent of Mass Transport Limitation

A frequently occurring condition in kinetic SPR analysis is that the apparent association and dissociation rate of a molecular interaction does not correspond to the physical on-rates and off-rates. The origin of this lies in the fact that in certain cases the reaction flux is larger than the transport flux. In other words, the on-rate is so high that diffusion of analyte from the bulk into the sensor matrix becomes rate limiting, and that as a consequence the concentration of analyte near the sensor matrix is lower than in the bulk. For the dissociation phase a high on-rate implies that a dissociated analyte can rebind to an empty binding site, before it diffuses from the matrix environment. In such case, the observed dissociation rate is slower than the physical off-rate. It is important to realize that if mass transport limitation (MTL) is involved, the association as well as dissociation phase is influenced.

In **Chapter 2**, a more in-depth description is given of MTL and how to deal with it. Here we would like to describe a practical approach to estimate the extent of MTL, based on the transport flux of analyte from the bulk to the sensor matrix, and the reaction flux due to binding, as originally presented by Christensen (15). As described below, a quantitative description of the extent of MTL gives insight into the parameters contributing to MTL and

can help to decide whether it is possible to change these parameters to diminish/avoid MTL.

The transport and reaction fluxes are described by the transport coefficient L_m and the Onsager coefficient L_r for the reaction. The extent of MTL is described by **Equation [1]**

$$\mathrm{MTL} = \frac{L_r}{L_r + L_m} \qquad [1]$$

If the analyte transport is totally rate limiting ($L_r >> L_m$), the extent of MTL will approach 1. L_m is expressed in m s^{-1} and directly related to a parameter k_{tr} as defined by Peter Schuck (*see* **Chapter 2**, **Equations** [**5**], [**6**], and [**7**]). The value of k_{tr} can be readily obtained for a transport limited one-to-one interaction by global kinetic analysis using the two compartment reaction scheme given in Equation [**2**] with the programs CLAMP (2) or Scrubber (Biologic Software Pty. Ltd. Campbell, Australia).

$$\begin{aligned} A_0 &\underset{k_{tr}}{\overset{k_{tr}}{\rightleftharpoons}} A \\ A + B &\underset{k_{off}}{\overset{k_{on}}{\rightleftharpoons}} AB \end{aligned} \qquad [2]$$

Here A_0 is the analyte in the bulk, which diffuses to and from the sensor matrix with the same transport rate constant k_{tr}. A is the analyte near the sensor matrix and B is the immobilized ligand of which the concentration is expressed as RU or m°. The dimension of k_{tr} as obtained from the global kinetic analysis and the equations in **Chapter 2** is in RU s^{-1} l mol^{-1} or m° s^{-1} l mol^{-1} and should be converted to m s^{-1}, the unit for the coefficients L_m and L_r (*see* **Note 2**).

The Onsager coefficient for reaction flux (L_r) is given in **Equation [3]** (15):

$$L_r = k_{on}.[B] \qquad [3]$$

Here k_{on} is the on-rate obtained from global kinetic analysis (*see* **Equation [2]**) in M^{-1} s^{-1}, and [B] is the amount of immobilized ligand, which can be obtained in RU or m°. At the start of the interaction, [B] equals R_{max} the maximum binding capacity, which can be derived from a Langmuir-binding isotherm (*see* **Chapter 6**, **Equation [2]**) or global kinetic analysis. To get L_r in m s^{-1}, k_{on} must be expressed in m^3 mol^{-1} s^{-1} and [B] in mol m^{-2}. For k_{on} M^{-1} s^{-1} corresponds to 10^{-3} m^3 mol^{-1} s^{-1}. Using the same approach as outlined in **Note 2**, [B] (in m° or RU) is

expressed in mol m^{-2} using **Equations [4a]** and **[4b]**, respectively:

$$[B]_{m^\circ} = R_{max} x \frac{10^{-5}}{MW} \quad [4a]$$

$$[B]_{RU} = R_{max} x \frac{10^{-6}.}{MW} \quad [4b]$$

2.2. Application of the Model to Estimate Extent of MTL

Here, an example is given of application of the model to estimate the extent of MTL. We performed a global kinetic analysis of the binding of v-Src SH2 domain to an immobilized peptide derived from the hmT antigen using the model given in **Equation [2]** (4). The global fit returned values for k_{tr}, k_{on}, and R_{max}: k_{tr} is 4.49×10^6 m° s^{-1} l mol^{-1}, k_{on} is 2.67×10^6 M^{-1} s^{-1}, and R_{max} is 323 m°. The MW of the v-Src SH2 domain is 12.3 kD. Applying the conversion factors for k_{tr}, k_{on}, and R_{max} values for L_m and L_r are obtained; these are 3.65×10^{-6} and 7.01×10^{-4} m s^{-1}, respectively. Applying **Equation [1]**, the extent of MTL is then >0.99, which indicated a completely transport-limited interaction.

The assay of extent of MTL presented here also allows estimating whether it is possible to avoid MTL by changing experimental conditions. According to the model the extent of MTL can be reduced by lowering L_r or increasing L_m. According to **Equation [3]**, L_r can be decreased by lowering R_{max}, which means a lower amount of immobilized ligand on the surface. In this case, to significantly decrease MTL to, e.g., 0.5 ($L_r \approx L_m$), L_r has to be lowered 50-fold and R_{max} should be around 6 m°, which is too low for accurate measurements. Another strategy might be to increase the transport flux L_m by a higher flow rate, or more intense agitation in a cuvette-based instrument. In practice the increase in L_m will be rather limited due to hydrodynamics (stagnant layer) and the dimensions of the (flow) cell (*see* **Chapter 2**). In the case of this example it will not be possible to avoid MTL by increasing the flow. It is our experience that flow or cuvette design of the SPR instrument does not really matter for the occurrence and extent of MTL (16).

The model for extent of MTL also allows to estimate the range of k_{on} for which problems with MTL can be expected. For an analyte with a MW of 25 kD (Syk tandem SH2 domain) we observed a value for k_{tr} of 2.7×10^7 m° s^{-1} l mol^{-1} (*see* **Note 3**); the value for L_m will then be around 10^{-5} m s^{-1}. For a surface with R_{max} equal to 100 m° (corresponding to $\sim 4 \times 10^{-8}$ mol m^{-2}, *see* **Note 2**), it follows from **Equation [3]** that L_m will be equal to L_r if k_{on} is ~250 m^3 mol^{-1} s^{-1} or 2.5×10^5 M^{-1} s^{-1}. So the model indicates that in this case MTL occurs if k_{on} values are larger than around 10^5 M^{-1} s^{-1}, which indeed is generally

observed and used as a rule of thumb (*see* **Chapter 2**).This value will change somewhat with the MW of the analyte, heavier analytes will diffuse somewhat slower, giving rise to MTL at lower on-rates.

3. SPR Instrumentation and Surfaces

As already indicated Biacore AB (Uppsala, Sweden; today part of GE Healthcare) was the first to commercialize and upscale the SPR technique into an instrument that should benefit not only a large community of fundamental researchers, but also physicians and general practitioners. In the 1980s it was their intention to construct a machine that could routinely be used to study patient samples for drug–protein interactions, thereby creating the opportunity for a fast and reliable diagnosis tool. When the first machine appeared in 1990 the latter intention was not fully successful, nonetheless, Biacore instruments in a variety of versions are nowadays the most frequently used SPR equipment worldwide, used for a wide range of applications. However, meanwhile many other manufacturers have joined this competitive market. Over the years several adaptations of the basic technique have evolved. In **Table 1.1,** an overview of some of these manufacturers and their websites are given.

Differences between SPR equipments are not only seen in the construction of the machines with large variations in setup, degree of automation, and versatility, but also with respect to pricing. Instruments can be distinguished by fan-shaped, fixed angle, scanning angle, wavelength, and imaging types. There are also differences in the way the sensor is integrated into the machine and the analyte is exposed to the immobilized ligand on the sensor surface. Several methods have been applied to flow analyte along the sensing surface. The configuration shown in **Fig. 1.5** may be rotated upside down, such that the solution flow is above the surface or directly below. Biacore used the latter by pressing a microfluidics liquid-handling construct with very narrow and independent flow channels against the bottom of the gold surface. Others position cuvette-like cells on top of the sensor chip, in which solution either flows along the surface or is rapidly mixed by pumping devices. The cuvette design has advantages when long interaction times are needed to reach steady state (*see* **Fig. 1.1**), consuming much less analyte than in a flow. A disadvantage may be that analyte depletion occurs, for which corrections can be made (*see* **Chapter 6**). The best of both worlds is to be able to switch between flow and mixing conditions, e.g., mixing during (long) association and flow with running buffer in the dissociation phase.

Table 1.1
Manufacturers of SPR instruments

Manufacturer	Instrument	Website
Biacore	Biacore A100, Flexchip, 3000, T100, X100, C	http://www.biacore.com
Metrohm Autolab	Autolab ESPRIT, Springle	http://www.ecochemie.nl
ICX Technologies	SensiQ, Pioneer, Discovery	http://www.icxt.com
Reichert	SR 7000	http://www.reichertai.com
DKK-TOA Corporation	SPR-20	http://www.dkktoa.net
Biosensing instrument	BI-SPR1000, 2000, 3000	http://www.biosensingusa.com
Bio-Rad	ProteOn XPR36	http://www.bio-rad.com
Thermo Electron Corporation	SPR 100	http://www.thermo.com
Analytical μ-Systems	BIOSUPLAR 6	http://www.biosuplar.de
IBIS Technologies	IBIS-iSPR	http://www.ibis-spr.nl

A new emerging development is array-based SPR equipment. With this approach an array of peptide, proteins, or oligonucleotide ligands (varying in concentration and/or type) is "spotted" on the sensor surface, and the SPR signal can be registrated for every spot. The first commercial available platforms for array SPR have come to the market, e.g., Biacore's FLEXchip system and the IBIS-iSPR (IBIS Technologies, The Netherlands). In this volume we did not focus on array SPR, as these platforms are strongly in development now. However, they may find wide application in high-throughput environments, e.g., in drug discovery and proteomics.

Another exciting development in the SPR field is to integrate SPR and mass spectrometry (MS) analysis. SPR is used for affinity quantification and MS for structural characterization of the analyte. Now these analyses occur regularly off line, with separate steps to make the captured analyte available for MS analysis. This volume contains two chapters on SPR-MS (*see* **Chapter 18 and 19**).

Not only the equipment varies in its ways to detect changes in plasmon generation but also the sensor surface itself has evolved over the years, resulting in a large number of available different sensor chips. Besides homemade sensor chips or those that are dependent on the type of machine, companies

like Xantec (www.xantec.com) produce chips with a large variety of hydrophilic and hydrophobic surfaces. In a biological context, membrane environments are extremely relevant. This volume contains an overview of the preparation of lipid membrane surfaces (*see* **Chapter 12**) and several applications of membrane environments in the SPR field (*see* **Chapter 13**, **14**, **15**, **16**, **and 17**).

In summary, it is now possible to choose an instrument and a sensor surface or optimize your own surface, suitable for a wide variety of fundamental or practical research problems in this highly exciting field of interaction analysis.

4. Notes

1. As explained in **Section 1.5** it matters whether an analyte is bound deep in the matrix near the metal film of the sensor, or more at the outside. The numbers given here apply to the usually applied dextran sensors like the CM5 chip of Biacore with a layer thickness of approximately 100 nm. Presumably, for lipid bilayer surfaces or extreme short brush-type sensors the SPR signal per amount of bound mass per mm^2 may be larger.
2. To convert k_{tr} from RU s^{-1} l mol^{-1} or m° s^{-1} l mol^{-1} to L_m in m s^{-1}, two conversions have to be applied: (1) from RU or millidegree (m°) to mol m^{-2} and (2) from l mol^{-1} to m^3 mol^{-1}.
   1. The SPR signal expressed as RU (Biacore) corresponds to 1 RU, is 1 pg mm^{-2}, and when expressed as m° to 1 ng mm^{-2} is 100 m°. The conversion of RU to m° can be readily made as 10 RU corresponds to 1 m°. 1 ng mm^{-2} is 10^{-3} g m^{-2}; taking into account the MW (in Dalton) of the analyte, 1 m° corresponds to $\frac{10^{-5}}{MW}$ mol m^{-2}.
   2. 1 l mol^{-1} is 1 dm^3 mol^{-1}, this corresponds to 10^{-3} m^3 mol^{-1}.

   Combining (1) and (2) the conversion factor for 1 m° s^{-1} l mol^{-1} to get L_m, is $\frac{10^{-8}}{MW}$ m s^{-1}. For RU units, 1 m° corresponds to 10 RU, and the conversion factor becomes 1 RU s^{-1} l mol^{-1} equal to $\frac{10^{-9}}{MW}$ m s^{-1}.
3. The value of k_{tr} depends on the flow rate or agitation speed and the type of sensor chip used. It is our experience that it can also fluctuate between chips of the same type and even during the lifetime of a certain chip. Short brush-type sensor matrices are expected to show an increased value for k_{tr}.

References

1. Rich, R. L., and Myszka, D. G. (2008) Survey of the year 2007 commercial optical biosensor literature. *J. Mol. Recognit.* **21**, 355–400.
2. Morton, T. A., and Myszka, D. G. (1998) Kinetic analysis of macromolecular interactions using surface plasmon resonance biosensors. *Methods Enzymol.* **295**, 268–94.
3. Tummino, P. J., and Copeland, R. A. (2008) Residence time of receptor-ligand complexes and its effect on biological function. *Biochemistry* **47**, 5481–92.
4. de Mol, N. J., Dekker, F. J., Broutin, I., Fischer, M. J. E., and Liskamp, R. M. (2005) Surface plasmon resonance thermodynamic and kinetic analysis as a strategic tool in drug design. Distinct ways for phosphopeptides to plug into Src- and Grb2 SH2 domains. *J. Med. Chem.* **48**, 753–63.
5. de Mol, N. J., Catalina, M. I., Dekker, F. J., Fischer, M. J. E., Heck, A. J., and Liskamp, R. M. (2005) Protein flexibility and ligand rigidity: a thermodynamic and kinetic study of ITAM-based ligand binding to Syk tandem SH2. *Chembiochem* **6**, 2261–70.
6. Mayer, B. J. (2001) SH3 domains: complexity in moderation. *J. Cell Sci.* **114**, 1253–63.
7. Ohlson, S. (2008) Designing transient binding drugs: a new concept for drug discovery. *Drug Discov. Today* **13**, 433–39.
8. Wood, R. W. (1902) On a remarkable case of uneven distribution of light in a diffraction grating spectrum. *Phil. Magm.* **4**, 396–402.
9. Kretschmann, E., and Raether, H. (1968) Radiative decay of non-radiative surface plasmons excited by light. *Z. Naturforsch.* **23A**, 2135–36.
10. Otto, A. (1968) Excitation of surface plasma waves in silver by the method of frustrated total reflection. *Z. Physik.* **216**, 398–410.
11. Liedberg, B., Nylander, C., and Lundstrom, I. (1995) Biosensing with surface plasmon resonance – how it all started. *Biosens. Bioelectron.* **10**, i–ix.
12. Kooyman, R. P. H. (2008) Physics of surface plasmon resonance. In Schasfoort, R. B. M., and Tudos, A. J., (Eds.) *"Handbook of Surface Plasmon Resonance"*. pp. 15–34, The Royal Society of Chemistry, Cambridge, UK.
13. Salamon, Z., Macleod, H. A., and Tollin, G. (1997) Surface plasmon resonance spectroscopy as a tool for investigating the biochemical and biophysical properties of membrane protein systems. I: theoretical principles. *Biochim. Biophys. Acta* **1331**, 117–29.
14. Stenberg, E., Persson, B., Roos, H., and Urbaniczky, C. (1991) Quantitative determination of surface concentration of protein with surface plasmon resonance using radiolabeled proteins. *J. Coll. Interface Sci.* **143**, 513–26.
15. Christensen, L. L. (1997) Theoretical analysis of protein concentration determination using biosensor technology under conditions of partial mass transport limitation. *Anal. Biochem.* **249**, 153–64.
16. de Mol, N. J., and Fischer, M. J. E. (2008) Kinetic and thermodynamic analysis of ligand-receptor interactions: SPR applications in drug development. In Schasfoort, R. B. M., and Tudos, A. J., (Eds.) *"Handbook of Surface Plasmon Resonance"*. pp. 123–172, The Royal Society of Chemistry, Cambridge, UK.

Chapter 2

The Role of Mass Transport Limitation and Surface Heterogeneity in the Biophysical Characterization of Macromolecular Binding Processes by SPR Biosensing

Peter Schuck and Huaying Zhao

Abstract

This chapter presents an introduction to the kinetic analysis of SPR biosensor data for the determination of affinity and kinetic rate constants of biomolecular interactions between an immobilized and a soluble binding partner. The need to be aware of and critically test the assumptions underlying the analysis models is emphasized and the consequences for the experimental design are discussed. The two most common sources of deviation in SPR surface binding kinetics from the ideal pseudo-first-order binding kinetics of bimolecular reactions are mass transport limitations and the heterogeneity of the surface sites. These problems are intrinsic to the use of a biosensor surface for characterizing interactions. The effect of these factors on the observed binding kinetics, and strategies to account for them are reviewed, both in the context of mathematical data analysis, as well as the design of the experiments and controls.

Key words: Binding kinetics, affinity distribution, thermodynamics, mass transport limitation, surface binding, optical biosensor, Tikhonov regularization.

1. Introduction

Since the introduction of SPR biosensing in the early 1990s as a biophysical technique for studying molecular interactions, it has gained great popularity and has been used very successfully in a broad range of applications (1–5). The methodology has undergone a significant evolution, especially with regard to our understanding of the physical processes taking place at the sensor

N.J. de Mol, M.J.E. Fischer (eds.), *Surface Plasmon Resonance*, Methods in Molecular Biology 627,
DOI 10.1007/978-1-60761-670-2_2,

surface and in the immobilization matrix. Despite the numerous pitfalls that were encountered and exhaustively explored when SPR biosensors were first commercially introduced, many sophisticated SRP studies in the literature since then have established that SPR technology can be used as a reliable biophysical research tool, if carefully controlled.

The use of optical biosensors for the characterization of macromolecular interactions has specific advantages that can be unique and very powerful.

First, by adjusting the number of immobilized surface sites the binding signal can be chosen independent of the affinity of the interaction. This is in contrast to solution methods, which, in order to ensure the population of all binding partners both free and in complex, have to be conducted at very low concentrations for high-affinity systems. The SPR signal relies on refractive index changes in the evanescent field at the surface, and because the refractive index increment of biomacromolecules is typically small, relatively high surface concentrations of the immobilized binding partner are required to achieve good signal-to-noise levels. However, because the surface concentration is (ideally) not imposing constraints on the type or strength of interaction that is to be studied, the label-free study of high-affinity interactions is possible.

Second, the configuration of one binding partner immobilized in the detection volume, and a second binding partner (the "analyte") initially being essentially undetected in the bulk solution but becoming visible when bound to the surface, allows the real-time observation of the progress of complex formation. If a precise, timed control of the bulk analyte concentration is possible in the SPR instrument, such as provided for by an efficient flow system or a well-stirred cuvette system, the quantitative interpretation of the kinetics of the binding progress is possible. Besides the potential for measuring kinetic rate constants, this may allow estimating equilibrium constants for very slowly equilibrating systems without reaching equilibrium.

Third, the biosensor surface is essentially a miniaturized affinity chromatography purification system. This has several advantages. It opens the possibility for a wide variety of configurations for studying multi-protein complexes, a topic of increasing interest (6). Also, at least for small analytes, the elution of material from the SPR surface lends itself to mass spectrometric identification (7–11) (*see* also **Chapter 18 and 19**). Finally, the binding experiment is tolerant to nonreacting contaminants in the sample preparations.

For these features to be exploited, some difficulties inherent to biosensing must be overcome. Obviously, there is the need for one binding partner to be stably attached to the surface. This raises questions regarding the best strategy of attachment such

that the binding epitopes are presented in their native state with unimpeded access for the soluble analyte. This is not trivial, and goes beyond the question of the choice of immobilization chemistry; we have to consider the influence of the whole sensor surface on the immobilized macromolecule. In fact, as will be outlined below, we should expect in most cases an ensemble of surface sites with a spectrum of binding properties to arise from immobilization. In addition to artifactual low-affinity sites resulting from partial protein degradation, this can also include microheterogeneity. Similarly, the surface itself can present low-affinity "nonspecific" binding sites for the analyte even in the absence of the immobilized binding partner. Further, for some interacting bimolecular systems the surface itself may constitute a third component promoting or suppressing the complex formation.

Another fundamental problem introduced by the physical separation of immobilized sites at the surface and the analyte in the bulk solution is the need to establish efficient mass transfer between the bulk and the surface. Otherwise the analyte concentration near the surface will be different from the bulk concentration, exhibiting either a local depletion zone or retention zone, respectively (dependent on the phase of the experiment), and characteristic deviations in the binding progress ensue. For understanding the importance of this effect it is crucial to appreciate that binding and diffusion are coupled phenomena on two levels. Macroscopically, the more surface sites there are, the more effective the mass transport needs to be in order to replenish the analyte drawn to the surface. Microscopically, analyte molecules can only diffuse while they are not bound, and therefore the effective diffusion through an array of surface sites proceeds slower than the diffusion in the bulk. This difference can be of many orders of magnitude, dependent again on the density and binding parameters of the surface sites. Therefore, despite the deceptively short distances across the sensor surface, analyte concentration gradients may exist and mass transport may be associated with long-lived moving front phenomena (12, 13). The presence of low-affinity "nonspecific" surface sites, even if nonspecific and clearly distinct from the sites of interest, will therefore impact the mass transfer.

Thus, in order to interpret the observed time-course of the binding signal as if it directly reflects the properties of the interacting molecules of interest, rather than the physical properties of the particular surface/flow configuration, or just an average of an ensemble of proteins with a range of surface-induced conformations, we need to closely examine the physical binding process taking place. This can be a challenging proposition since we do not have microscopic knowledge of the surface site distribution and the local parameters of the physical environment, and we can only infer indirectly the nature of the process we observe from the

evolution of a single signal. It is crucial to keep in mind this fundamental problem of SPR biosensing. Unfortunately, the history of SPR kinetic analysis exposes a long series of silent or explicit assumptions about key aspects of the observed binding process which were implemented in various analysis approaches, but turned out to be convenient, yet invalid simplifications. Therefore, one achieving a correct and reliable interpretation of the data requires the art of recognizing the silent (or occasionally explicit) assumptions underlying the different analysis ideas and to critically question and experimentally test them whenever possible.

A variety of experimental design tools and methods for the stringent comparison of the measured data with the predictions from different models are available. This chapter is not meant to be a formal review, but rather an introduction to highlight experimental limitations intrinsic to optical biosensing fundamentally arising both from the need of mass transport to the sensor surface and from the immobilization of a binding partner to the surface. We discuss strategies to detect these problems and to experimentally minimize their influence on the estimation of the molecular interaction parameters of interest. We recapitulate robust and realistic approaches to account for their influence during the data analysis stage, as well as the limitations of the analytical descriptions. Accordingly, the chapter is structured in three main sections. We start with the ideal pseudo-first-order binding model, establishing some of its characteristic features and requirements for a sensible analysis of such binding data. Next, mass transport limited surface binding processes are examined in detail, followed by the description of surface heterogeneity and a discussion of the relationship between these sources or artifacts. Finally, we draw conclusions for experimental and data analysis strategy.

2. The First Goal– Establishing Ideal Pseudo-first-Order Binding Kinetics (or How the Data Deviate from this Model)

2.1. Basic Features of Ideal Surface Binding

It is nontrivial to ascertain that binding is taking place with ideal pseudo-first-order binding kinetics. In this paragraph, we will discuss criteria that should be applied to probe the data for their consistency with this model. From the experience with data

collected in our own laboratory as well as from the examination of the literature, we find that, in fact, it is rarely observed (2, 14, 15). Nevertheless, this process serves as a methodological reference point as it represents the simplest bimolecular surface binding reaction. Therefore, it is important to establish its hallmarks and the requirements for its rigorous analysis. Further, it can be quite informative to discern the specific features of the data that deviate from the pseudo-first-order predictions. This will help to diagnose the process that most likely takes place at the surface.

The pseudo-first-order kinetics describes the surface binding process where we have a concentration of free analyte, c, held constant either by replenishing the surface-bound molecules through the flow across the surface or because of the negligible number of surface-bound molecules relative to the total number of analyte molecules in the reservoir above. The binding progress $s(t)$ then follows the rate equation:

$$\frac{ds}{dt} = k_{\text{on}}c(s_{\text{max}} - s) - k_{\text{off}}s \qquad [1]$$

The first term accounts for the binding reaction to previously unoccupied surface sites (a subset of the total number of surface sites s_{max}) with the rate constant k_{on}, and the second term accounts for the continuous dissociation of analyte with the rate constant k_{off} due to the finite lifetime of the complex ($\tau = k_{\text{off}}^{-1}$). As the binding proceeds and the surface sites fill up, the dissociation term becomes increasingly more important, until it matches the association term and an equilibrium or steady state is attained. The overall time-course is a single-exponential approach of a steady-state signal. If we apply the analyte starting at the time t_0 for a total contact time t_c, we can integrate the rate equation and obtain the binding progress in the association phase

$$s_{\text{a}}(c,t) = s_{\text{eq}}(c)\left(1 - e^{-(k_{\text{on}}c + k_{\text{off}})(t - t_0)}\right) \qquad [2]$$

asymptotically approaching the steady-state response

$$s_{\text{eq}}(c) = \frac{s_{\text{max}}}{1 + (K_{\text{A}}c)^{-1}} \qquad [3]$$

which depends only on the equilibrium constant $K_{\text{A}} = k_{\text{on}}/k_{\text{off}}$ (or $K_{\text{D}} = k_{\text{off}}/k_{\text{on}}$) (16). After the analyte is removed, we see only the dissociation of bound analyte from the surface sites, which causes a single-exponential decay of the signal

$$s_{\text{d}}(c,t) = s_{\text{a}}(c,t_{\text{c}})e^{-k_{\text{off}}(t - t_{\text{c}})} \qquad [4]$$

An example for the shape of the kinetic binding signal *s(c,t)* and the equilibrium isotherm $s_{eq}(c)$ at different concentrations is given in **Fig. 2.1**.

2.2. Least-Squares Fitting the Pseudo-first-Order Reaction Model to Experimental Data

This model should be fit globally to the data acquired at different analyte concentrations or flow cells to test whether or not it is consistent with the data. For this test to be meaningful, not only must all data points (that are free of experimental artifacts) be included, but also the experiment must be carried out such that the experimental data actually contain the required information.

Obviously, the most important parameter is the signal-to-noise ratio, which we recommend to be at least on the order of ~100. For much smaller signals, such as those proposed in (17), the data may be fit with certain models (possibly even generating acceptable statistical error intervals for the question under study) but the validity of the models cannot be tested with confidence, as shown in (18, 19). In the extreme case, any model will fit in reasonably well to data that have amplitudes not much higher than the noise.

Regarding the quality of fit, there has been some uncertainty in the SPR field about what constitutes an acceptable fit. This is not unexpected for a new technique, since we have to make some allowance for unavoidable systematic errors, such as baseline drifts, injection artifacts from buffer changes, temperature and pressure fluctuations, and only experimental experience allows us to make these unavoidable judgments. However, experimental SPR technology has matured, and it has become clear that SPR data are usually highly reproducible, and one should apply the same stringent requirements as is custom in most other biophysical disciplines: When looking at the residuals (i.e., the difference between the fit and the data), they should be distributed uniformly and have a magnitude on the order of the noise of the data acquisition. We have shown recently that after accounting for surface site heterogeneity, kinetic SPR data can in fact usually be modeled to that level of detail (see below). An example is shown in **Fig. 2.2**.

If the model does not fit, especially if the deviations appear nonrandom, we have to conclude that the model used does not correctly capture the process observed in the experiment. From common sense, it seems that very small deviations would affect mostly the details of the analysis and perhaps widen the error intervals or slightly bias the parameter estimates, whereas substantial deviations should be expected to render the derived "best-fit" parameters entirely meaningless. Unfortunately, this judgment is difficult to quantify mathematically or statistically.

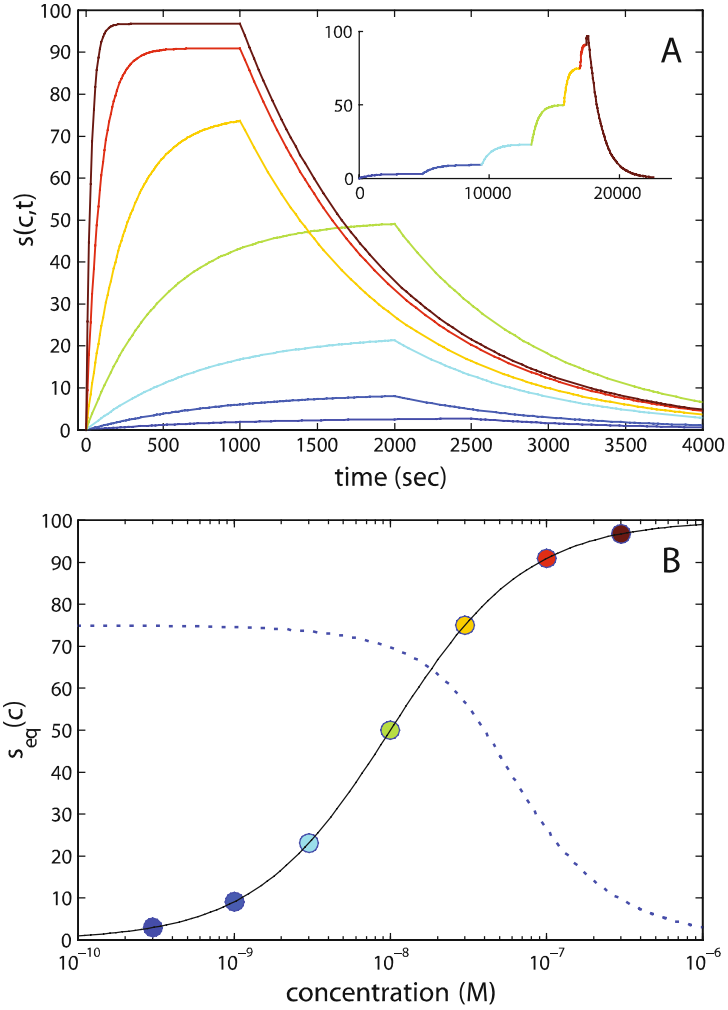

Fig. 2.1. Surface plasmon resonance biosensor signal ideally expected for a simple 1:1 interaction with pseudo-first-order kinetics, in different experimental configurations: (**a**) This is a superposition of sensorgrams in the kinetic configuration most commonly used, where the association/dissociation cycles at different concentrations are separated by regeneration steps. The data shown are generated for the binding of molecules with a K_D of 10 nM ($k_{on} = 1.0 \times 10^5$ $M^{-1}s^{-1}$ and $k_{off} = 1.0 \times 10^{-3}$ s^{-1}) probed with a range of analyte concentrations (0.3 nM *navy*, 1 nM *blue*, 3 nM *cyan*, 10 nM *green*, 30 nM *orange*, 100 nM *red*, and 300 nM *dark red*). In order to approach more closely the equilibrium signal at the lower concentrations, the contact time for the lowest concentration cycles is increased. The inset shows an alternative kinetic titration configuration in which the signal from bound material is continuously accumulated by applying a stepwise increased analyte concentrations, followed by only a single dissociation phase. This has the advantage of not requiring a regeneration step, but at the cost of lower information content (see text). The colors of the *curve* depict the equivalent concentrations as the main plot. (**b**). The equilibrium binding constant can be determined independent of the kinetics, by evaluating the extrapolated steady-state signals as a function of concentration (filled *circles*), using the same color scheme as in (**a**), which follows a Langmuir isotherm (*solid line*). The *dotted line* presents an isotherm from a solution competition assay, in which the sample solution contains analyte at a constant concentration (at $2 \times K_D$) mixed with a varying concentration of soluble ligand competing for the surface sites (*see* **Chapter 6**). This strategy utilizes the SPR surface sites to report on the remaining free analyte in solution for the different mixtures applied in the flow and yields binding constants for the interaction in solution. It can be combined with an empirically constructed calibration curve of SPR binding signal vs. free analyte concentration. In this latter configuration, no assumptions on the property of the surface binding sites are necessary.

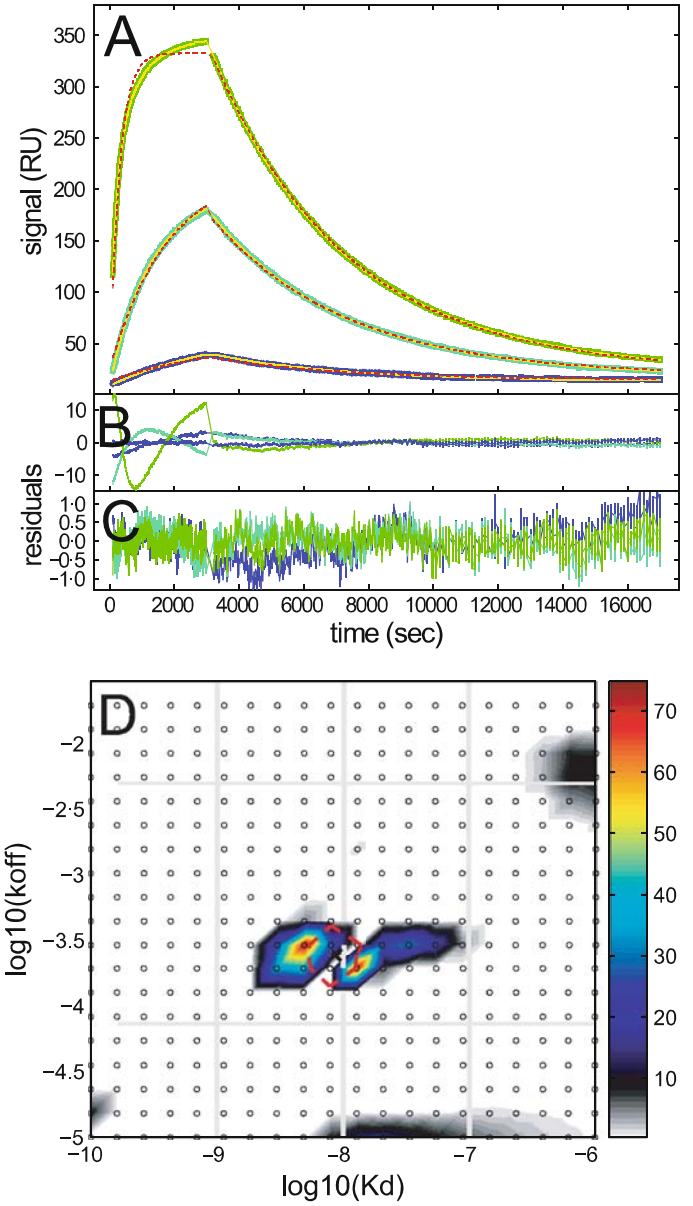

Fig. 2.2. Typical example for the inability of single-site model in describing the surface binding data, due to the presence of heterogeneity of binding sites on the surface. This is binding of an antigen to its monoclonal antibody immobilized on a short-chain carboxymethyl dextran surface. For details, *see* (19). (**a**) Experimental binding traces at analyte concentrations of 1 (*navy*), 10 (*blue*), and 100 nM (*green*), best-fit traces using the surface site distribution model (*solid yellow line*), and best-fit curves from a single-site model (*dashed red line*). (**b**) Residuals of the fit from the single-site model, with an rmsd of 3.42 RU. (**c**) Residuals of the fit from the Bayesian distribution model shown in (**d**), with an rmsd of 0.31 RU. (**d**) Affinity and rate constant distribution calculated using the Bayesian analysis to obtain the distribution closest to a single class of sites with average parameters (encircled by the *red dashed line*). The distribution is depicted as a color temperature contour plot, with the colors indicating the signal values shown in the color bar at the right. Also shown in the distribution plot are the concentrations applied in the experiment (*vertical gray lines*), and the rate constants that could be well characterized within the experimental dissociation time (*horizontal gray lines*).

2.3. Qualitative Features of Pseudo-first-Order Binding Kinetics and Consequences for Conducting Experiments

There are qualitative requirements the data must fulfill in order to satisfy convincingly the test for pseudo-first-order binding (and to allow a global fit with the pseudo-first-order binding model). These are related to certain characteristic features of pseudo-first-order binding kinetics, some of which can be tested quite easily even by visual inspection or back-of-the-envelope calculations (20). They may help us gain confidence in the overall interpretation.

First, both the association and the dissociation processes are single exponentials. Apparent multi-exponential behavior in both is an unequivocal sign of more complex binding reactions involving multiple sites or multiple states, or of mass transport limitation (see below). In order to establish that the data are single exponential and to enable us measuring the exponent (i.e., the rate constants), it is essential that the data exhibit curvature. Generally, one could say that it is the curvature in the data that contains most information for the analysis with most models. For an exponential process to be well defined, the observation time should be on the order of several-fold the characteristic decay time (or lifetime) τ, which is here $\tau = (k_{on}c + k_{off})^{-1}$ for the association phase and $\tau = k_{off}^{-1}$ for the dissociation phase. This may not always be possible in practice, especially for slowly dissociating complexes. However, this should be kept in mind as a goal in the experimental design, and as a caveat in the data interpretation of shorter experiments. Truncations of the data set beyond the regions of artifacts from buffer changes destroy information and should be avoided. An example for how a poorly designed, arbitrarily truncated data acquisition time can lead to a misinterpreted binding process is shown in **Fig. 2.3**.

As can be recognized from **Eq. [2]**, the association attains steady state with a rate constant that is dependent on concentration, following $k_{obs}(c) = k_{on}c + k_{off}$. Consistency with this linear concentration behavior will be apparent in the global least-squares fit of the data. Linearization of **Eq. [2]** and separate analysis of $k_{obs}(c)$ and k_{off} can lead to significant errors and frequently rather arbitrary results (in particular when combined with short data acquisition or data truncation). Since the association proceeds to steady state more slowly at lower concentrations, it is advisable to extend the experimental contact time for the association/dissociation cycles with these concentrations (**Fig. 2.1**). This not only improves the kinetic information content of the lower concentration data, but also allows to better determine the steady-state response (see below).

The dissociation phase is characterized by a single dissociation rate constant, independent of the analyte concentration that was applied in the preceding association phase. This is due to the fact that the binding sites and complexes have no memory of their

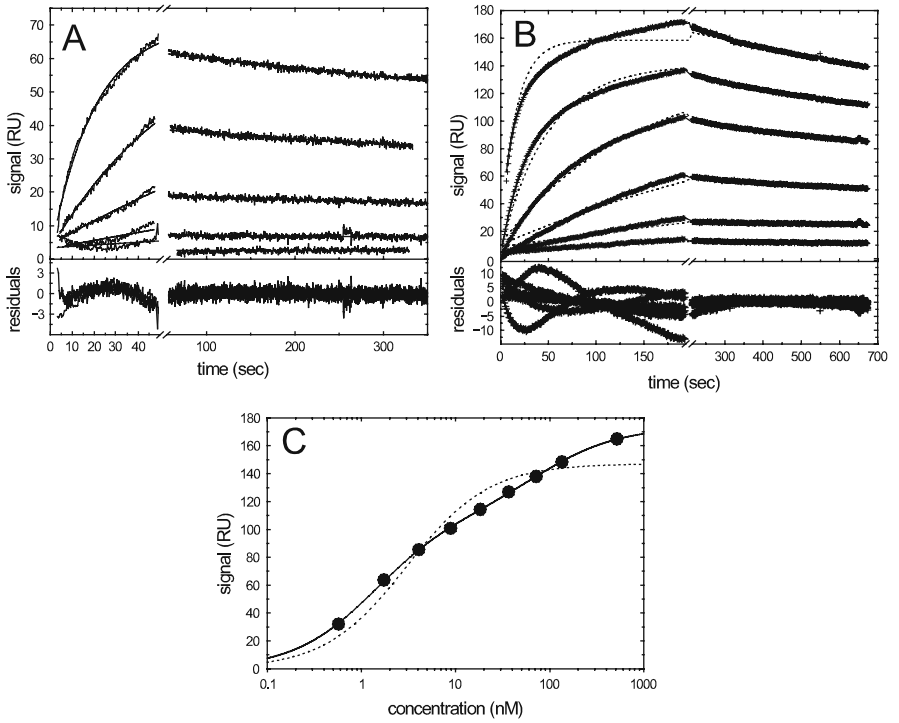

Fig. 2.3. Demonstration of how the arbitrary truncation of the data acquisition can lead to qualitative misinterpretation of the binding kinetics. Shown are kinetic binding signals of myoglobin binding to immobilized antibody. (**a**) Roden and Myszka (58) used this model system in their study aimed at demonstrating that SPR surface binding data follow simple bimolecular binding to a single class of sites, without complications arising from factors such as the immobilization matrix and mass transport. They developed an experimental design that uses analyte at four concentrations and is restricted to acquire association data for only 42 s. The data shown in (**a**) are very similar to those presented by Roden and Myszka, and lead to binding rate constants of $k_{on} = 1.9 \times 10^5$ $M^{-1}s^{-1}$, $k_{off} = 3.98 \times 10^{-4}$ s^{-1}, very close to those reported by Roden and Myszka of $k_{on} = 1.94 \times 10^5$ $M^{-1}s^{-1}$, $k_{off} = 4.70 \times 10^{-4}$ s^{-1}. Indeed, a good fit is achieved with this model. However, the low degree of curvature in the kinetic traces severely limits the information content. (**b**) Binding data using a more informative experimental design that features a considerably longer association phase and an extended range of analyte concentrations. Here, the global kinetic analysis using the pseudo-first-order model (*dotted line*) does not lead to an acceptable fit, as it is unable to describe the slower binding phase that becomes apparent at contact times >50 s. Since the data are from the same surface, it clearly shows that the restricted data collection in (**a**) led to the gross misinterpretation of the data. (**c**) An equilibrium binding isotherm using the equilibrium titration method described in (21) and obtained from the same surface reveals a biphasic isotherm, which cannot be explained on the basis of a single class of sites (*dotted line*), but can be modeled well with two classes of sites (*solid line*). Best-fit parameters are $K_{D,1} =$ 1.4 nM (63%) and $K_{D,2} = 79$ nM (37%). For details, *see* (21).

history. Therefore, the overlay of the dissociation traces, when adjusted for baseline offsets and aligned at the start of the dissociation phase, should lead to curves that do not intersect. For the same reason, experiments conducted at different contact times for the analyte during the association phase should be followed by dissociation phases exhibiting the same dissociation rate, independent of contact time.

Finally, the steady-state values that are asymptotically attained at long association times, to the extent that they can be estimated

from the experimental data, should follow an isotherm as indicated in **Fig. 2.1b**. Half-saturation is obtained at $c = K_D$, and 10 and 90% saturation at 0.1-fold and 10-fold K_D, respectively, and naturally, the K_D estimate from this isotherm should be identical to the ratio k_{off}/k_{on} from the analysis of the binding kinetics. These are checks for self-consistency which frequently can be applied quickly (20). Again, a global least-squares fit will constrain the model to be internally consistent.

For both the binding isotherm analysis as well as the analysis of the binding kinetics, it is highly desirable that a range of analyte concentrations be used, starting from well below K_D up to 10-fold K_D. Clearly, if the concentration range that produces saturation of the surface sites is not accessed experimentally, the estimated saturation signal will be correlated with the K_D estimate in the data analysis. Further, at concentrations below K_D, many kinetic processes other than pseudo-first-order binding will exhibit traces very similar to the expected single-exponential asymptotic attainment of a steady state, and the incorporation of higher concentration data will enable better discrimination of the binding process. If the steady-state binding data cover a wide enough concentration range, the equilibrium constant may be determined without reference to the binding kinetics, which may be helpful if no simple model explaining the binding kinetics can be found. Experiments at a single concentration will neither reveal good estimates of kinetic rate or equilibrium constants, nor allow conclusions on the type of binding process observed, nor allow us to diagnose the presence of artifacts.

Many of the historic methods proposed when SPR technology was first introduced to the study of macromolecular interactions did not require or were in conflict with some of the above criteria. Nevertheless they generally implied a priori assumptions that the binding process is a pseudo-first-order reaction. However, with the overwhelming evidence accumulating that most experimental SPR kinetic data do not actually follow this model, the need has become obvious to demonstrate that the binding model actually applies. Only in this case can one verify that the numbers obtained are meaningful in that they really reflect molecular parameters of interest. On the other hand, if the data are collected and analyzed according to these criteria, this will not only help establishing that a simple first-order binding kinetics takes place, but also help in the characterization of binding processes that are more complicated.

Alternative experimental configurations have been proposed, including the continuous accumulation of bound material obtained in a stepwise increased analyte concentration, followed by only a single dissociation phase (**Fig. 2.1a** inset). This idea was first introduced by us in the context of equilibrium titration with circulating sample (21). One obvious advantage is that of saving

time (since no dissociation takes place in between the application of different analyte concentrations, and due to the slightly shorter association phases needed during the application of each but the first concentration). In the conventional linear flow configuration, the total analyte amounts required can be reduced slightly, although the saving can be more substantial in the configuration with circulating (21) or oscillating sample (22). The biggest practical advantage in most cases is certainly the absence of a surface regeneration step in between the association phases.

A disadvantage of this configuration is the loss of information in the association kinetics: It is easy to see that with small concentration increments, the approach to the new steady-state level will be close to exponential even in highly mass transport limited cases. In contrast, in the conventional configuration of multiple association/dissociation cycles, the application of concentrations greater than K_D can exhibit the linear initial association kinetics so characteristic for mass transport limited binding (see below). The dissociation phase, unfortunately, is not as discriminatory, since in mass transport limited cases it will resemble a double-exponential, which could be caused by many processes. The loss of information will be compounded when the individual steps do not lead to close attainment of steady state, as in the variation of the titration method proposed by Karlsson and coworkers (23). In this case characteristic information on the nature of the association phase kinetics as well as on the equilibrium constants may be destroyed by the experimental design.

2.4. Deviations from the Pseudo-first-Order Model

As mentioned above, it is rare that the SPR surface binding data of protein–protein interactions actually meet the criteria for pseudo-first-order binding. The most commonly observed deviation from the ideal pseudo-first-order binding includes a slow signal increase in what should ideally be a steady-state signal at high analyte concentrations. This can arise, for example, from heterogeneity of the surface sites or heterogeneity of the analyte. Another widespread feature is the lack of saturation of the steady-state response as a function of concentration, which points to the existence of weaker, possibly nonspecific binding sites. Finally, partially linear association signals are frequently observed, a signature of mass transport limitation.

Some experimental factors can introduce systematic errors, such as baseline drifts and the need to subtract signals from bulk effects measured on reference surfaces (24, 25). The magnitude of these effects needs to be experimentally assessed for the surface under study in the reaction conditions, and the experimental design and the data to be analyzed should be chosen such as to minimize these effects.

Before proceeding to review methods to address surface site heterogeneity and mass transport limited binding, we also have to

assume in the following that we can rule out multivalent surface attachment of analyte. Multivalent surface attachment could be caused, for example, by small populations of analyte oligomers, or by the presence of more than one binding epitope on the analyte molecule capable of binding simultaneously to the immobilized binding partner at the surface. In these cases, a fraction of surface-bound molecules may undergo a second binding event with a nearby binding site. This subpopulation will experience a dramatically different dissociation kinetics, since now both attachments have to be severed simultaneously in order for the analyte to become free. In many cases, this makes the binding virtually irreversible on the timescale of the experiment, and consequently this analyte fraction will continuously accumulate at the surface and may be substantially overrepresented among the surface-bound analyte relative to its abundance in the bulk analyte flow. Unfortunately, since there is no knowledge of the distribution of surface sites and their local mobility in the immobilization matrix, which would govern the likelihood for multivalent attachment, it is impossible to realistically interpret such binding kinetics (26, 27). (Although one can write more or less sophisticated binding equations, they have to rely on detailed knowledge of the physical properties of the surface and the immobilization matrix, requiring parameters that are not known at all, or not with any degree of confidence. Alternatively, they are so oversimplified to yield, in our opinion, essentially meaningless best-fit parameters.)

In principle, multivalent surface attachment can be minimized experimentally, for example, by chromatographic removal of the analyte oligomers that are present at least in trace amounts in many or even most protein preparations (28–30) and/or by verifying analytically the absence of oligomers by sedimentation velocity analytical ultracentrifugation (31). More difficult are cases where the analyte exhibits reversible self-association, either free in solution, or promoted by the high local macromolecular concentration inside the immobilization matrix (if used). If there is any known tendency for the analyte to exhibit such oligomerization, it cannot be used in quantitative kinetic SPR experiments as the mobile binding partner, and the role of mobile and immobilized binding partner should be reversed. If both binding partners exhibit the potential for multimerization, SPR surface binding cannot be used to assess quantitatively the molecular binding parameters, and instead solution binding assays are required (*see* **Note 1**).

If the above criteria for data collection have been fulfilled, fortunately, the binding of (partially) multivalent analyte should not be correlated much with the binding kinetics to multiple independent surface sites, and with mass transport limited binding. The unrecognized presence of multivalent analyte will degrade the quality of fit with the latter models, or vice versa, an excellent

fit with the surface heterogeneity and/or mass transport limited model (to suitable data sets) suggests the absence of multivalent analyte.

If the kinetic surface binding data deviate from the pseudo-first-order binding, which is the case in the overwhelming majority of protein–protein interactions encountered in our laboratory and in the literature, one possible way to proceed is the postulation of more complex chemical interaction schemes, such as conformational change or multisite models. We believe that most experimental data sets that have a concentration-dependent, monotonically increasing signal in the association phase and a monotonically decreasing signal in the dissociation phase can be force-fitted with one or more sufficiently complex reaction schemes (32), simply because the shape of the experimental binding progress curves is not very rich in information. However, whether or not these models reflect correct process taking place cannot be answered easily. Following the principle of Occam's razor – which recommends us to interpret the data with the simplest possible model – would lead us not to invoke complex reaction schemes, but to probe first whether common surface-induced artifacts can explain the shape of the data and whether a model accounting for these effects can yield estimates for the binding parameters for pseudo-first-order chemical reactions. Further confidence can be gained with the application of experimental tools that can establish qualitatively the key aspects of the model, such as the variation of the analyte contact time in the association phase, the variation of flow parameters, immobilization protocols, and different competition assays (33).

The surface site heterogeneity and the mass transport limitation model will be described in the following with respect to their potential and limitation for estimating molecular binding parameters, and with their corresponding experimental tools.

3. The Influence of Mass Transport on the Binding Kinetics

3.1. Physical Picture

Mass transport limitation (MTL) is caused fundamentally by the analyte and the surface sites initially being located physically at different points. In any surface binding experiment, this brings about the necessity to transport the analyte to the surface in the association phase, and to transport it away from the surface in the dissociation phase. As we will see, MTL problems in the association and dissociation phases are of the same magnitude,

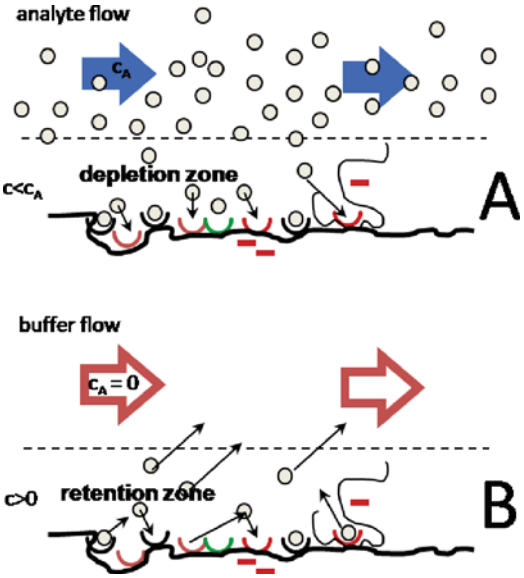

Fig. 2.4. Cartoon depicting the effect of limited mass transport on the analyte concentration. (**a**) In the association phase, limited mass transport causes the analyte close to the surface to be bound more quickly than it can be resupplied by the bulk analyte flow. This creates a depletion zone of analyte at the surface, resulting in c (concentration of analyte close to the surface) lower than c_A (concentration of analyte in the bulk). (**b**) In the dissociation phase, limited mass transport leads to the retention of analyte close to the surface, whereby analyte rebinding to empty surface sites occurs before it can migrate to the bulk flow.

even though they show in different ways. Under MTL conditions, in the association phase a depletion zone will be caused ($c_s < c_0$) where the local concentration is lower than the target in the bulk (**Fig. 2.4a**), whereas in the dissociation phase a retention zone is present close to the surface sites ($c_s > 0$), that allows dissociated analyte molecules to rebind to empty surface sites before they can escape into the bulk flow (**Fig. 2.4b**). These concentration gradients (relative from surface to bulk) diminish continuously with time as steady state is attained. Unless the lifetime of these gradients is much faster than the timescale of the chemical kinetics, they will have profound influence on the observed binding kinetics.

One can distinguish MTL on different length scales, and each can be the rate-limiting step causing MTL (2) (**Fig. 2.5**). First, there is the macroscopic transport, which may be accomplished, for example, by a conventional pressure-driven flow system, a stirred cuvette system, a manual pipette-type probe, or other more sophisticated configurations, such as exploiting electro-osmotic flow (34). Since the pressure-driven laminar flow system is the most commonly employed, such a system will be assumed in the following. Our macroscopic experience suggests that in order

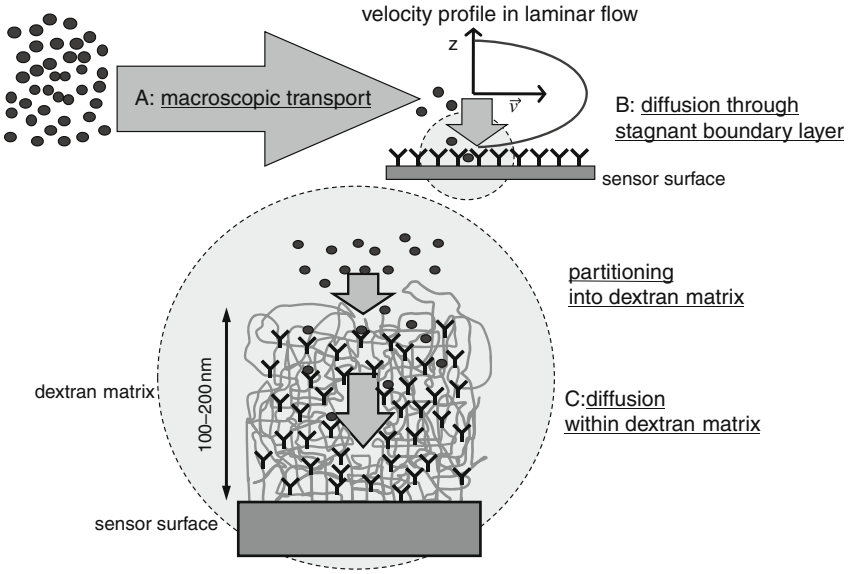

Fig. 2.5. Schematics depicting the different possible physical origin of mass transport limitation (2). (**a**) The first macroscopic step is the transport through the microfluidic system and is dependent on the bulk flow rate. (**b**) The diffusion through the non-stirred boundary layer in laminar flow depends on the bulk flow rate, flow cell geometry, and the diffusion coefficient of the analyte in the bulk solution. If a polymer support, such as the common dextran matrix, is applied, the analyte partitions into this matrix. This depends on the size and chemical properties of analyte and polymer matrix. (This step is not a transport step per se, but reduces the analyte concentrations and concentration gradients in the matrix, leading to lower transport.) (**c**) The diffusion through the immobilization matrix depends on the size and charge of the analyte, thickness and density of the dextran matrix, the diffusion coefficient of the reactant in polymer solution and close to surfaces, the spatial distribution of surface binding sites, and on nonspecific binding properties.

to adjust the analyte concentration in the flow-cell volume to a certain target concentration c_0, we should ensure that it be rinsed with at least several times its volume. As examined by (35, 36), this imposes minimal flow velocities for the observation of binding reactions with high k_{off}.

Second, we can consider the properties of the laminar flow across the surface. The ordinary nonslip boundary conditions will cause a non-stirred liquid layer through which the analyte must transport by diffusion (37). Laminar flow-assisted transport to a reacting surface has been well studied in hydrodynamics and chemical kinetics, and simple approximate expressions for the effective molecular transport rate dependent on the flow geometry and the molecular diffusion coefficient are available (38). Most importantly, they show that the transport rate constant changes with the cube root of the flow velocity, i.e., in order to double the transport rate through the stagnant layer an eightfold increase in flow velocity is necessary.

Finally, the perhaps most intriguing transport step is the microscopic transport through the sensing volume itself. Most commonly, a hydrophilic polymer matrix is employed as immobilization support and for suppressing nonspecific binding,

often consisting of several hundred kDa carboxymethyl dextran randomly attached to the surface (39). The thickness of such a matrix is estimated variously to be only on the order of 100–400 nm (40, 41). We have shown experimentally and theoretically that it also can be the rate-limiting step of transport, dependent on the surface properties and the properties of the interacting macromolecules (12). Key to the propagation of free analyte in the matrix is the recognition that it does not proceed with bulk diffusion coefficients, but instead has to be regarded as a coupled reaction/diffusion process (42). Mass transport limited binding and binding limited mass transport are two sides of the same physical phenomenon. Since analyte molecules can only diffuse during the time they are not bound to the surface sites (be it the specific sites of interest or other, perhaps, nonspecific sites) we can estimate the order of magnitude of an "effective diffusion constant D_{eff}", that is, the bulk diffusion constant D_0 reduced by a factor $\tau_{\text{free}}/\tau_{\text{bound}}$ reflecting the time-average state the analyte is unbound. We can estimate the order of magnitude of this factor from the steady-state condition via the ergodic theorem, and approximate this factor as the ratio of the population average of free and bound $c_{\text{free}}/c_{\text{bound}}$ analyte states in the matrix. Since typical SPR signals of 100×10^{-6} refractive index units (~100 RU) require on the order of ~1 mg/mL concentrations in a ~100 nm thick matrix, the number of surface sites in the detection volume is very high, for example, ~100 μM for a 10 kDa protein. When studying high-affinity reactions with $K_D < 10$ nM, analyte molecules will spend most of the time in the bound state, and therefore the effective diffusion coefficient can be lowered easily by a factor 10^4, which brings the diffusion time through the detection volume from the fraction of a millisecond in free solution to in the order of seconds in the presence of surface sites. Any transient binding will delay diffusion, not only binding to specific sites; nonspecific interactions can likewise significantly exacerbate this effect and further reduce diffusion (15) (*see* **Note 2**). Matrix-mediated transient interactions should be strongly dependent on the macromolecules of interest, as well as pH and ionic strength of the buffer.

Further, besides the fundamental problem of diffusion through an array of sites, if a polymeric immobilization matrix is used, the physical properties of the matrix itself hamper the mobility of the analyte. There is partitioning of analyte into the matrix, which will reduce the concentrations and diffusion fluxes (although not the equilibrium response due to the proportionally higher analyte chemical activity) and restricted diffusion due to the presence of the carbohydrate chains and immobilized proteins (43). (It seems possible that under some circumstances the immobilization of proteins into the matrix by random chemistries may lead to its cross-linking.)

Because the detection volume extends quite some distance in transverse direction parallel to the flow, a problem of the surface binding reaction coupling to diffusion will exist in a similar form for a flat, truly two-dimensional surface, here reducing the effective transverse diffusion in the stagnant boundary layer. Finally, it has been shown that near a surface the basic hydrodynamics of macromolecular diffusion is altered, resulting in reduced mobility irrespective of the presence of a matrix (44).

As a consequence, when considering this microscopic step, we have to take into account the full three-dimensional distribution of the surface sites and the density distribution of the matrix, which is most certainly not uniformly perpendicular to the surface (45) and also dependent on electrostatic and steric interactions (46) that may change with buffer conditions. Unfortunately, the complexity of the matrix and the level of detail needed on the distribution of the immobilized surface sites make an analytical model very difficult. However, this does not preclude us from making theoretical predictions for certain plausible parameters and to study the features of MTL for simplified model systems.

Given all the unknowns and their paramount influence on the extent of MTL, it is very difficult to predict a priori the chemical on-rate constants where MTL will become relevant. From practical experience, one should consider the possibility of MTL for reactions with k_{on} greater than 10^5/Ms, although even slower chemical kinetics may be mass transport limited under unfavorable conditions. One problem with this assessment is, however, that generally the chemical rate constants are not known independently, and obviously the apparent rate constant estimates obtained from the SPR biosensing themselves cannot be trusted since under MTL conditions they may be significantly too low (see below).

3.2. Effect on the Observed Binding Kinetics

At the most basic conceptual level, we can use a two-compartment model to account for the fact that there are different regions in space with different analyte concentrations, and that there can be transport between these regions (47). More specifically, we can postulate that there is a region "close to the surface" with analyte concentration c_{surf} and the region "far from the surface" where the analyte concentration is that of the bulk, and that the transport is governed by a rate constant k_{tr}. Binding then proceeds locally as indicated in **Eq. [1]**, but at the surface analyte concentration c_{surf}. This leads to a combined rate equation for compartment-like transport and binding:

$$\begin{aligned} \frac{dc_{surf}}{dt} &= k_{tr}(c - c_{surf}) - \frac{ds}{dt} \\ \frac{ds}{dt} &= k_{on}c_{surf}(s_{max} - s) - k_{off}s \end{aligned} \qquad [5]$$

(*see* **Note 3**). It is important to realize that this model only provides a limited view of mass transport effects because each compartment is assumed to be instantaneously well-mixed (see below). However, the two-compartment model is useful as a first-order approximation, to the extent that we could always "discretize" an existing small concentration gradient into two homogeneous regions separated by a single concentration step (and analogously, *n*-compartment models could model the concentration gradients with $(n-1)$ steps (13)).

This approximation allows us to predict some of the essential features of MTL. As illustrated in **Fig. 2.6**, MTL causes both the association phase and the dissociation phase to exhibit slower kinetics. In the association phase, the binding progress deviates from the exponential toward an initially more linear approach of steady state. In contrast, the dissociation phase shows greater curvature at signals close to saturation, mimicking the existence of a fast phase and a slow phase. We emphasize that this is, here, not due to the presence of a second class of sites, but purely a consequence of mass transport limited binding. If the binding level is less than approximately half-saturation, qualitatively only a slow phase seems to appear.

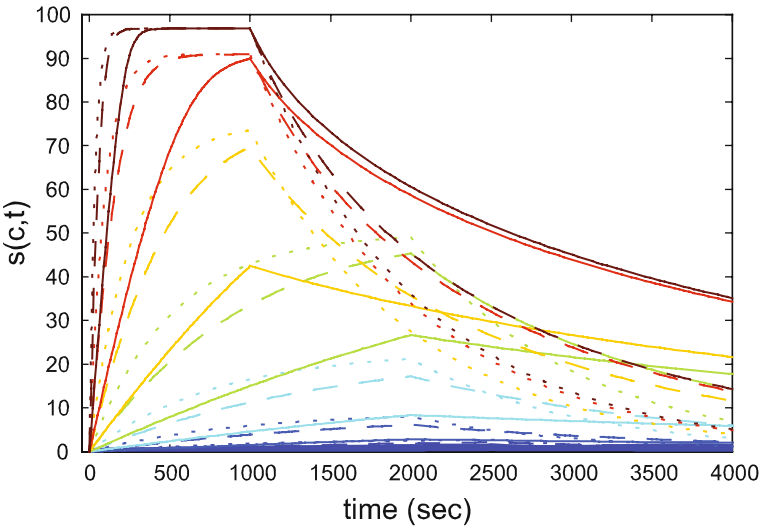

Fig. 2.6. The effect of limited mass transport on the surface binding kinetics. Mass transport limitation is gradually added to the same theoretical model system as shown in **Fig. 2.1**: $\log10(k_{tr}) = 8.48$ (*dotted lines*), $\log10(k_{tr}) = 7.0$ (*dashed lines*), and $\log10(k_{tr}) = 6.30$ (*solid lines*). With increasing mass transport limitation (lower transport rate constant k_{tr}), both the association and dissociation phases exhibit slower kinetics. In the association phase, due to the local depletion zone at the surface, slower and more convex binding progress curves are expected. In the dissociation phase, when the rate of dissociation is higher than the transport rate, a nonvanishing concentration of analyte in the vicinity of the sensor surface allows rebinding to empty surface sites. The retention effect results in a slower overall dissociation from the surface and to apparent biphasic decays, in particular when the dissociation is started from close to saturation.

On a more quantitative level, the so-called steady-state approximation yields further insights. Since the surface concentration will quickly assume a steady state with dc_{surf}/dt being approximately zero (i.e., all materials arriving in the surface compartment from bulk will be used up for new binding events), we can insert this in **Eq. [5]** and arrive at the picture of apparent rate constants

$$\frac{ds}{dt} = k_{on}^{(app)} c_0 (s_{max} - s(t)) - k_{off}^{(app)} s(t)$$
$$\frac{k_{on}^{(app)}}{k_{on}} = \frac{k_{off}^{(app)}}{k_{off}} = \frac{1}{1 + \frac{[k_{on}(s_{max} - s(t))]}{k_{tr}}} \quad [6]$$

Although **Eq. [6]** formally looks like the ideal rate **Eq. [1]**, both rate constants are reduced by a factor that grows with $k_{on}\left(s_{max} - s(t)\right)/k_{tr}$, i.e., is dependent on the occupation of the surface sites and changes with time. We can interpret $k_{on}\left(s_{max} - s(t)\right)/k_{tr}$ as the probability of analyte binding to the empty surface sites relative to the probability of transport. In the dissociation phase, this can immediately be reconciled with the picture (**Fig. 2.4b**) showing the retention of analyte close to the surface due to rebinding before the analyte can escape. Analogously, in the association phase the same factor describes the magnitude by which the surface sites themselves represent sinks for analyte preventing c_{surf} to be raised uniformly to the level of c_0. Thus, the magnitude of the effect of MTL on the apparent on-rate constant and the apparent off-rate constant is the same, although the effect on the shapes of the profiles is different (*see* **Note 4**). The compartment model can be extended to models with multiple compartments and multiple surface sites, and we have shown that under steady-state conditions more general equations analogous to **Eq. [6]** can be derived.

We can see from **Eq. [6]** also that, under conditions of virtual saturation of all sites, the binding process evolves with rates close to the true chemical rate constants (*see* **Note 5**). This is consistent, again, with the picture introduced above of binding (to open sites) limiting the transport, therefore causing MTL or rather limited mass transport. On the other hand, for experimental configurations that include only concentrations lower than K_D, the fractional saturation will never exceed 50%, such that the ratio $k_{on}\left(s_{max} - s(t)\right)/k_{tr}$ will not change during the course of the binding experiment by more than a factor of 2 (although the influence of MTL could be arbitrarily large). Therefore, the MTL binding processes take on shapes more similar to the ideal pseudo-first-order model **Eq. [1]**. For this reason, the shape of the binding signal itself is not sufficient to rule out the influence of MTL. (This also highlights again the need for analyte concentrations far above K_D.)

It also follows from **Eq. [6]** that $k_{on}^{(app)} < k_{tr}\left(s_{max} - s(t)\right)^{-1}$, which means that the fractional saturation reached in the experiment and the transport rate constant impose an absolute upper limit on the apparent rate constant that can possibly be observed in SPR biosensing, irrespective of the true chemical rate constant (*see* **Note 6**).

As useful as they are, it is important to recognize that the use of compartment models is highly oversimplifying the physical situation. As mentioned above, if we equate the compartment with physical regions, the spatial parameters within these regions are ignored, since the compartments are well-mixed within. As a consequence, compartment models are not applicable, for example, where the microscopic step of the transport creates significant concentration gradients within the sensing volume, which will occur in the more severely transport-influenced binding processes. In fact, due to the very nature of a coupled reaction/diffusion processes, the formation of concentration gradients propagating as moving fronts is a hallmark of the binding process. Such moving fronts of saturation would violate the steady-state assumptions going into the approximation of **Eq. [6]** (even in more refined multi-compartment models).

That moving fronts of saturation can be present in SPR surface binding has been experimentally verified in three different ways. The first exploits that across the sensing volume the sensitivity of the SPR biosensor is not uniform: laterally it is determined by the shape of the spot being optically interrogated, and perpendicular to the surface it is governed by the evanescent field exponentially decreasing with increasing distance from the surface. Thus, if a moving front of saturation occurs during the association phase, as it moves from the outer regions to the more sensitive inner regions (either laterally or perpendicular to the surface), it will create binding signals with increasing slopes. These have been widely observed (**Fig. 2.7**) (12, 13), and are difficult to explain with chemical kinetics, even with cooperative binding models. Second, in the experiment we can stop this front of saturation by shutting off the analyte supply and switching to the dissociation phase. If this is done at a point in time when the front is located at a steep gradient of sensitivity, the slow effective diffusion within the matrix of binding sites will transport some analyte from the saturated front into the array of empty sites located ahead in the more sensitive regions, thereby creating an increasing signal component during the dissociation phase – i.e., without net introduction of new analyte to the sensor surface! Simulations of this effect showed that this signal increase can even match or be larger than the loss of signal from the effective dissociation rate (which is slowed due to retention from rebinding) (12). This causes a signature of highly MTL influenced dissociation with slowly decreasing signals following high saturation, but

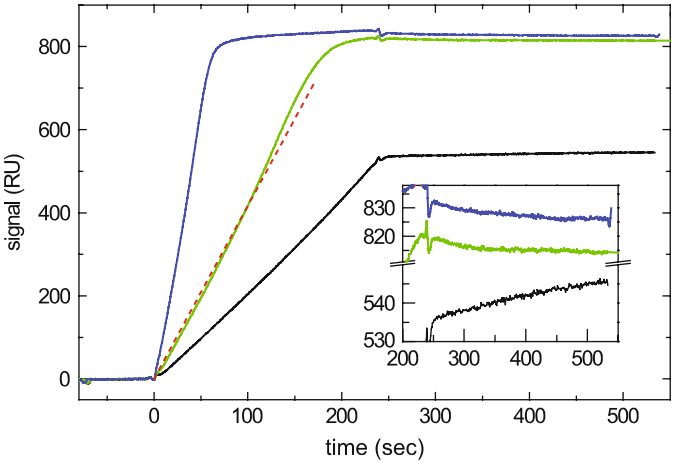

Fig. 2.7. Illustration of spatial concentration gradients in the sensing volume during mass transportation limitation influencing the surface binding kinetics by creating characteristic, counterintuitive artifacts (13). HyHel-10 mAb is immobilized to a long-chain carboxymethyl dextran matrix (CM5 chip), and binding of 10, 20, and 60 nM (*bottom to top*) soluble antigen (hen egg lysozyme) is observed at a flow rate of 5 μL/min. To highlight the sigmoid-shaped binding curve with increasing slope that arises when a moving front of saturation enters more sensitive regions, a straight (*dotted*) is plotted for comparison. The inset shows the dissociation traces after incomplete association in enlarged scale. The increasing signal in the dissociation following the application of the 10 nM sample stems from the slow decay of concentration gradients within the inhomogeneous sensing volume.

increasing signals following partial saturation. Typical experimental profiles can be found in the literature (12), and an example studied in our laboratory is shown in **Fig. 2.7**. Third, the formation of moving fronts of saturation during the electrostatic preconcentration of BSA during the immobilization process has been directly observed with two-color SPR (48), which allows to probe the binding progress in different zones perpendicular to the surface by virtue of the different penetration depths of the evanescent fields of the different wavelengths.

It is important to realize that for severely mass transport limited binding processes with moving fronts the density distribution of surface sites relative to the sensitivity profile of the detection will have a paramount influence on the observed binding profiles. For example, if a majority of sites are at locations of low sensitivity and easily accessible (such as at the top of the immobilization matrix), and a minority of sites are at locations of high sensitivity but require significant additional analyte transport time (such as in the interior of the immobilization matrix), kinetic binding traces may arise under MTL conditions that deviate from the linear initial phase in the association and instead exhibit more convex shapes in the association phase with some similarity to biphasic exponential binding (15).

3.3. Probing Experimentally for Mass Transport Limitation

As indicated above, the extent of MTL is difficult to predict a priori for any given system, since it will depend so much on matrix (or surface)/analyte interactions that are hard to quantify, in addition to the true intrinsic binding rate constants that are generally unknown. Therefore, experimental tools are of critical importance for the detection and moderation of MTL.

An obvious but not very effective way to detect MTL is the variation of the flow rate (*see*, for example, **Fig. 2.8**). If a change in the analyte and buffer flow rate in the different experiment phases, respectively, results in differences in the observed surface binding kinetics, MTL is unequivocally demonstrated. Unfortunately, the reverse is not true. As mentioned above, the effective transport rate k_{tr} in the laminar flow depends only on the cube root of the flow rate, which requires very large changes in the flow rate and concomitantly very large increases in the applied volumes (which may be a limiting factor). Further exacerbating this problem is that, as shown in **Eq. [6]**, except for completely mass transport limited cases, we should not expect a change in $k_{on}^{(app)}$ or $k_{off}^{(app)}$ to be proportional to k_{tr}, but to exhibit a weaker influence. Finally, if the microscopic transport step in the matrix is the rate-limiting one, the flow rate across the matrix may not show a significant influence on the binding progress.

Nevertheless, it is certainly a good practice to use the highest possible flow rate in order to minimize this transport step. In order to keep the option open to quantitatively analyze the mass transport-influenced binding kinetics, it is useful to apply the same flow rate in the association and the dissociation phase of the experiment. The oscillating flow technique can help to strongly reduce the amount of sample required, independently of the flow rate (22).

An alternative approach to probe for the presence of MTL in the laminar flow is the change of the solvent viscosity, for example, by adding glycerol to the buffer (49, 50). Again, an influence on the observed binding kinetics suggests the presence of MTL. (In principle, there may be some undesired side effects through differences of protein solvation, as well as the hydration of the immobilization matrix.)

Clearly, the total number of surface sites is an important factor that directly determines the magnitude of MTL, as is reflected in **Eq. [6]** of the two-compartment model. This led to the approach of comparing the signal from analyte binding to surfaces with different densities of the immobilized binding partner (or, more precisely, different total binding capacities). If the time-course of the analyte binding signal of each surface is normalized relative to the total surface site density, superimposable curves should ideally be obtained in the absence of MTL, whereas in the presence of MTL slower kinetics should be obtained for the higher density

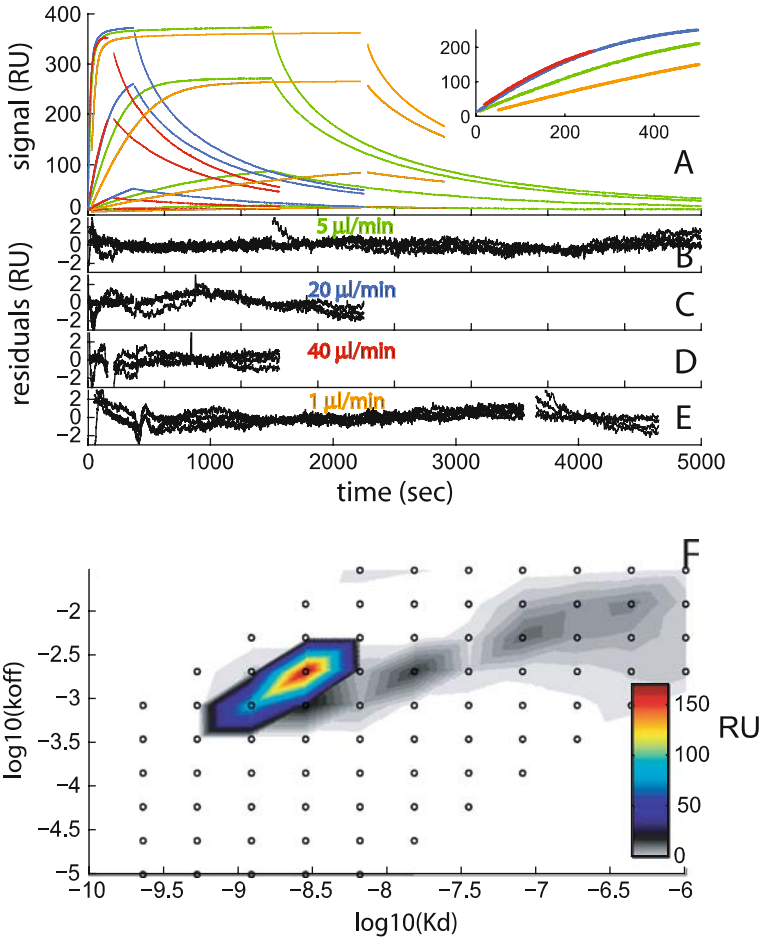

Fig. 2.8. The effect of flow rate on the surface binding kinetics for mass transport limited binding (13). Shown are surface binding data acquired from the same surface at flow rates of 1, 5, 20, and 40 µL/min, and the global fit with a model for transport-influenced binding to a distribution of surface sites allowing for different transport rate constants at the different flow rates. (**a**) Experimental data at 1 (*orange*), 5 (*green*), 20 (*blue*), and 40 (*red*) µL/min for analyte concentrations of 0.1, 1, 10, and 100 nM (no 0.1 nM data available at 20 µL/min). The inset expands the initial association data at an analyte concentration of 10 nM for all flow rates. The results of the global fit are at 5 µL/min: $\log10(k_{tr}) = 7.91$ with an rmsd of 0.53 RU (**b**), at 20 µL/min: $\log10(k_{tr}) = 8.18$ with an rmsd of 0.79 RU (**c**), at 40 µL/min: $\log10(k_{tr}) = 8.21$ with an rmsd of 0.66 RU (**d**). (**e**) Given the distribution from the fit of the three high flow rates, we applied the distribution as a constant prior knowledge to the data at 1 µL/min, here optimizing solely the transport rate constant, resulting in $\log10(k_{tr}) = 7.62$ with an rmsd of 0.74 RU. (**f**) Best-fit distribution from the global fit of all data.

surfaces (37). The advantage of this approach is that it will allow equally the detection of MTL arising from the laminar flow as well as from the microscopic step of diffusion within the matrix. However, a caveat is that this presumes the surface sites exhibiting equal intrinsic binding properties on all surfaces. Unfortunately, this assumption may not always be fulfilled, as we have recently

observed in the context of studying the affinity distributions of the ensemble of surface sites (19) (see below).

To minimize the potential influence of MTL it is prudent to aim for low surface site densities, although not to the extent of sacrificing reasonable signal-to-noise ratio (see above). Similarly, in our experience it can be advantageous to use thin immobilization matrices, which usually accommodate sufficient numbers of molecules to generate adequate signal levels.

In many cases perhaps the best strategy to diagnose the presence of MTL is the use of a soluble competitor in the dissociation phase, which binds to the analyte once dissociated and prevents it from rebinding to the empty surface sites (51). If the binding reaction under study is mass transport limited, the competitor can dramatically increase the dissociation rate, in particular, when applied at a point in time when half or more of the surface sites are already (or still) unoccupied. There can be potential concern with very large competitors that may not be able to penetrate the matrix well and not diffuse well into the rebinding zone. A significant advantage of this approach is that it can allow to estimate the intrinsic chemical off-rate constant, provided the concentration of the competitor should be sufficiently high to lead to essentially stoichiometric capture of all analyte molecules as they are released from the surface sites (2). This may be combined with the equilibrium constant from the analysis of the steady-state surface binding isotherm to provide an estimate of the true on-rate constant.

Ideally, we recommend the use of all or a combination of several of these techniques to diagnose the presence of MTL in the measured binding kinetics.

3.4. Incorporating Mass Transport Influence into the Model of the Binding Kinetics

Unfortunately, given the complexity of the physicochemical phenomena at the sensor surface and in the immobilization matrix, it seems highly unrealistic to even establish a complete physical model for the transport process that incorporates all the relevant processes, not to speak of determining all the necessary parameters. This becomes evident considering only the problem that we would need to know the spatial distribution of the immobilized surface sites. Making assumptions about these parameters is an important and valid tool to explore their possible influence, but it would lead to unreliable and to a high degree arbitrary results when used for the analysis of MTL data.

Some authors have studied the mass transport problem confining their attention to the laminar flow, which is a simpler problem and more tractable, and suggested it would be possible to predict the mass transport rate constant on the basis of the known geometry of the flow and the analyte diffusion constant (52). However, as we have demonstrated elsewhere using a commonly available antibody/antigen system, the experimental transport rate constants can be far off the predicted values dependent on the immobilization matrix used (13).

Due to these difficulties, it seems reasonable only to attempt the application of the simplest phenomenological compartment model for transport and to restrict the usage of this model to just the onset of mass transport limitation where the spatial concentration gradients are small, and the approximation of the spatial geometry by a simple division into two regions is tolerable to serve as a first approximation. Alternatively, it may be applied in the limit of the approach to steady state in the association phase, where existing gradients have decayed (49). Since there are several physical processes affecting the transport with unknown relative importance (dependent on the interacting system and the matrix properties), we can use an effective overall transport rate constant $k_{tr}^{(app)}$, which will arise as a harmonic mean of effective transport rate constants of many different sequential transport steps (13). Because we cannot predict the value of $k_{tr}^{(app)}$ without making assumptions of uncertain validity, it needs to be incorporated as an adjustable parameter into the data analysis.

At low influence of MTL, i.e., in the reaction limited regime, the value of $k_{tr}^{(app)}$ will not be well determined by the data, except that we can establish a lower limit of $k_{tr}^{(app)}$. However, the rate constants of the chemical reaction of interest are well determined. Vice versa, in the limit of high influence of MTL, the value of $k_{tr}^{(app)}$ may be well determined by the data, but we can only estimate a lower limit of the chemical on-rate constant.

In practice, **Eq. [5]** can be fit directly globally to the set of association/dissociation phases from a single-site model. The two-compartment transport step outlined in **Eq. [5]** may also be combined with other, more complex models for the chemical binding step. For more strongly MTL surface binding reactions, we observed in a computer model of transport within the immobilization matrix that the spatial gradients in the dissociation phase are smaller than in the association phase. This suggests that the application of **Eq. [6]** to the set of dissociation phases, which leads to the compact form

$$\frac{ds(t)}{dt} = \frac{-k_{off}s(t)}{1 + \frac{k_{on}}{k_{tr}}\left(s_{max} - s(t)\right)} \qquad [7]$$

may be a more robust approach (*see*, e.g., (49, 50)) to estimate the chemical off-rate constant. This could be combined with the equilibrium constant derived from the steady-state isotherm to provide estimates for the chemical on-rate constant.

It should be noted that for the analysis of MTL binding traces, the data reporting on the kinetics under the condition of high site occupancy are the most informative. Therefore, **Eqs. [5]** or **[7]** are applied best to data sets that include concentrations far above K_D.

4. Heterogeneity of the Surface Sites

4.1. Physical Origin

The need to immobilize one of the binding partners of the interaction to be studied raises another problem fundamental to biosensing. Obviously, we want to assume (and if possible verify) that the immobilization itself does not significantly influence the molecular binding parameters. This may not always be trivial, considering general experience with labeling of proteins, the SPR surface being nothing less than a macroscopic-sized label. In addition, however, a less obvious but equally important assumption is that all immobilized sites are uniformly active (and a fraction may be completely inactive, respectively, which would not contribute to the binding signal). Considering the physical microheterogeneity of any SPR surface on a molecular scale (even without polymer matrices), the different local chemical properties of the surface, the possible geometric configurations of the immobilized sites relative to the surface and relative to the molecules comprising the immobilization matrix, possible heterogeneity in the protein conformations, in addition to the common chemical heterogeneity in the covalent attachment, it seems actually a very daunting task to achieve uniformity in the binding properties of the immobilized macromolecules. This is true even for preparations that in solution exhibit properties consistent with a single class of sites.

Although there are strategies to avoid some sources of heterogeneity, such as the surface attachment by site-directed chemistries or capture techniques, these cannot address other problems arising from the physical and chemical microheterogeneity of the surface itself as well as the immobilization matrix (if used) (**Fig. 2.9**).

As a consequence, it seems a much more sensible assumption that the immobilized surface sites could present a distribution exhibiting a continuum of binding energies. This naturally incorporates the possibility for partially active sites, nonspecific sites, as well as multiple independent sites on the immobilized molecules.

4.2. Description of Analyte Binding to an Ensemble of Surface Sites with a Distribution of Rate and Affinity Constants

We can express the idea that the observed binding signal is the sum of signals from sites that could have different dissociation equilibrium constants and different off-rate constants as an integral equation:

$$s_{\mathrm{tot}}(c,t) = \int_{K_{\mathrm{D,min}}}^{K_{\mathrm{D,max}}} \int_{k_{\mathrm{off,min}}}^{k_{\mathrm{off,max}}} s_1(k_{\mathrm{off}}, K_{\mathrm{D}}, c, t) P(k_{\mathrm{off}}, K_{\mathrm{D}}) dk_{\mathrm{off}} dK_{\mathrm{D}} \quad [8]$$

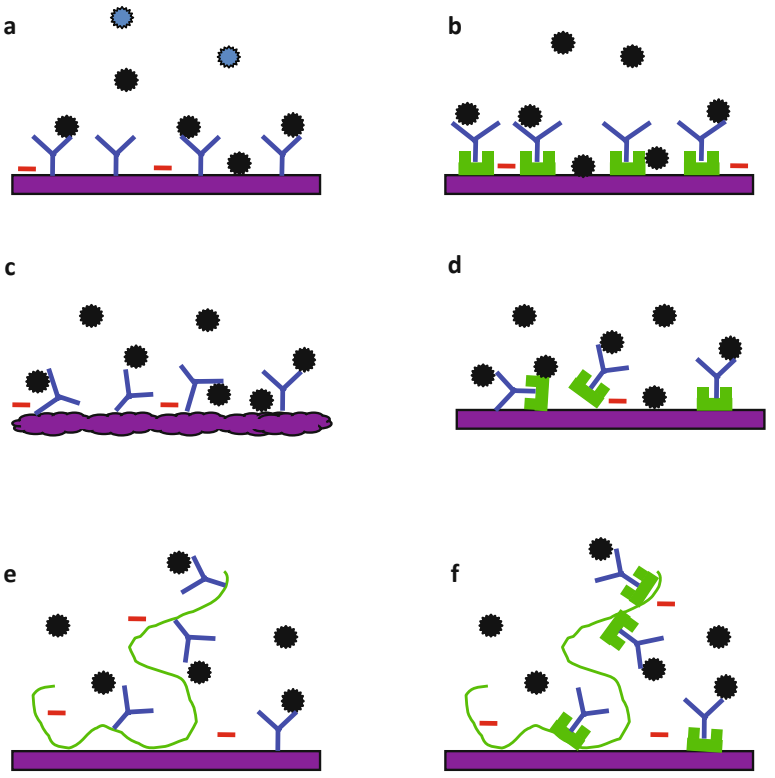

Fig. 2.9. Cartoon illustrating different sources of heterogeneity of surface binding sites. *Filled circles* depict the analyte molecules, and "Y" depicts the macromolecular binding partner to be immobilized and serve as surface binding site. (**a**) Surface site heterogeneity may occur fundamentally from nonspecific binding to the surface. (**b**) The same is true in the presence of a capturing protein (e.g., an antibody or streptavidin) for the macromolecule of interest. In addition, the capturing molecules may contribute to the available "nonspecific" surface sites. (**c**) The surface is heterogeneous on a molecular scale both with respect to surface rugosity, as well as surface charges and local pH. (**d**) The same is true for a capturing protein, which itself may not be oriented uniformly and expose the analyte to different microenvironments. (**e**) If a polymeric immobilization matrix is used, immobilization to different regions can give rise to different extent of steric hindrance and heterogeneous microenvironment from spatial and chemical nonuniformity of the matrix. (**f**) The same effects occur when using a capturing protein, possibly exacerbated due to the overall higher degree of functionalization of the immobilization matrix (higher total protein concentration at the surface).

where $s_1(k^*_{\mathrm{off}},K^*_{\mathrm{D}},c,t)$ is the binding signal we would observe for a site with equilibrium constant K^*_D and off-rate constant k^*_{off} at a unit binding capacity of $s_{\max}(k^*_{\mathrm{off}},K^*_D)=1$, following **Eqs. [2], [3], and [4]** and where $P(k_{\mathrm{off}},K_D)$ is the two-dimensional distribution of affinity and rate constants (53). This model, with the features described below, has been implemented in the software EVILFIT and is available from the authors on request.

It is well known that the decomposition of experimental data into a distribution of exponentials is an ill-posed problem (54), and the analysis of SPR surface binding data is no exception.

This is because within a given level of noise, single exponentials, for example, are poorly distinguishable from a combination of two exponentials of lower and higher exponents. In practice, this leads to the amplification of noise in the data to the extent that it can govern the overall distribution. As a consequence, if **Eq. [8]** were fitted directly to experimental data, the best-fit distribution would likely be a series of poorly reproducible spikes, which would present much more detailed features than information really contained in the original data. A very powerful modern approach to address this problem, termed "regularization," follows the principle of Occam's razor, which suggests that the simplest possible interpretation of the data is most likely the right one. It is implemented by defining a mathematical measure of information content of the final distribution and aims at minimizing this information content as much as possible without decreasing the quality of fit to the raw data (as judged by statistical analysis of the residuals). It results in the simplest or broadest distribution consistent with the experimental data.

This provides a very convenient way to assess the information content of the experimental SPR data (19, 53): For example, when applied to data consisting of a single association/dissociation trace, data at concentrations $<<K_D$, data at very low signal-to-noise ratio, or otherwise poorly designed experiments, the distribution of affinity and off-rate constants shows broad peaks reflecting the limited conclusions that can be drawn from the experiment. In contrast, when applied to data from a better designed experiment, the peaks in the distribution become sharp and allow more detailed insight into the surface binding process. This is illustrated in **Fig. 2.10**, which shows the affinity and rate constant distribution for the interaction of the same analyte to an identical surface, once with very short association and dissociation times (left) and once with a larger analyte concentration range and longer observation times in both the association and dissociation phases.

When applied to suitable data, the level of detail that can be observed on the functional distribution of surface binding sites is high, and, as shown in (19), the distributions are quite reproducible. It is possible to clearly distinguish the high-affinity sites of interest from subpopulations of sites with impaired affinity, which possibly reflect protein immobilized in altered conformations and/or in poorly accessible locations on the surface in the immobilization matrix, and from low-affinity sites, which may be intrinsic to the surface (nonspecific binding of analyte to the surface) or reflect residual weak interactions with denatured proteins. By discriminating between the different populations, it is possible to focus on the interaction of interest and to obtain binding parameter estimates that are not skewed by subpopulations of partially inactive or nonspecific surface sites. If there is a doubt

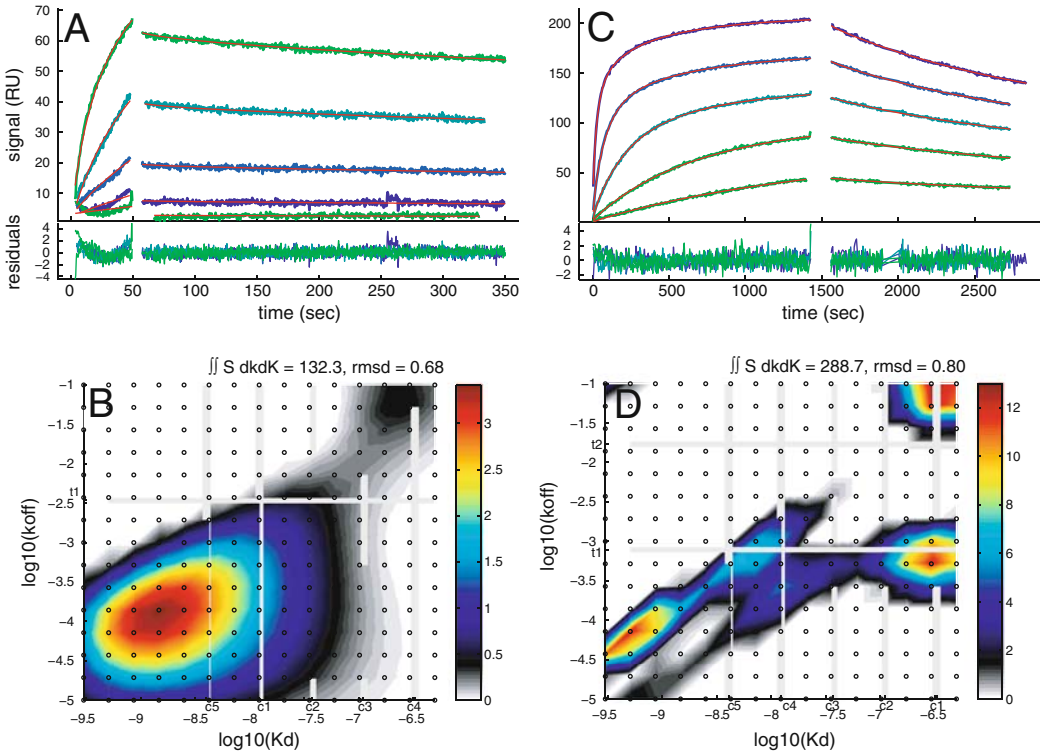

Fig. 2.10. Comparison of affinity and kinetic rate constant distribution obtained from the same surface from binding experiments with different design. This is the distribution analysis of the same data sets as shown in **Fig. 2.3**. Excellent fits are achieved for both experimental designs, but the regularization in the distribution analysis exposes different information content. (**a**) and (**b**) Arbitrarily truncated data and analysis with short association and dissociation times and a small analyte concentration range. The resulting distribution exhibits only broad features, suggesting not more than the order of magnitude of both the kinetic and affinity binding constants. (**c**) and (**d**) Experimental binding data and analysis of longer contact times and larger analyte concentration range. The resulting distribution is very detailed, resolving multiple classes of surface sites. For details, *see* (53).

about which of the peaks reflects the "native" interaction, we recommend to conduct solution competition assays to measure the affinity constant in solution (21, 33) (*see* also **Chapter 6**).

Since the standard regularization causes peaks to be as broad as consistent within the signal-to-noise level of the experimental data, it is not immediately clear whether a single species model would be consistent with the data. To this end, a Bayesian approach can be taken to reshape the regularization profile toward favoring distributions consistent with prior knowledge (or prior hypothesis) (19). To examine to what degree given data are consistent with a single-site model, suitable prior knowledge may be bootstrapped from experimental data by performing a preliminary analysis with conventional regularization, followed by integration over the distribution region in question (which possibly may represent a single species) and assigning the prior knowledge for the following Bayesian analysis to be a sharp peak with

the signal-average binding constants from the relevant region. The result will be the affinity and rate constant distribution that resembles as close as possible a single-site model, given the experimental data. In contrast to the direct application of **Eqs. [1], [2], [3], and [4]** that would strictly constrain the fit to a single-site model and cause (in virtually all cases when applied to meaningful data) a statistically unacceptable fit, this Bayesian approach will not diminish the quality of fit from the best possible fit with the full distribution model and instead add features to the putative single species model that are essential to explain the actually observed data. These additional features may be populations of low-affinity sites or poorly reversible sites.

The Bayesian approach was applied with the EVILFIT software (standalone Windows executables and MATLAB scripts are freely available from the authors on request), for example, to the data in **Fig. 2.2** in order to test for the homogeneity of the surface sites. The result clearly shows that the hypothesis of a single homogeneous binding site for the main peak cannot be accommodated in the fit of the experimental data. Instead, the distribution highlights that there must be microheterogeneity of the surface sites. This validates the physical picture sketched in **Fig. 2.9** where microheterogeneity in the local, physical, and chemical environment of the immobilized molecules, as well as chemical and/or conformational heterogeneity from surface attachment create polydispersity of the binding energies and therefore subpopulations of different affinity and rate constants for analyte binding. For the data shown in **Fig. 2.10**, this – in addition to trace populations of low-affinity sites and poorly reversible sites – explains the deviation of the binding progress curves from the single exponential ideally expected.

Independent of the interpretation of the resulting distribution, another important observation from the distribution model is the high quality of fit. This is consistent with the generally excellent stability and reproducibility of SPR biosensor data. From our experience applying this model to many systems, it is possible to routinely (but not always) achieve fits with residuals satisfactorily within the noise of the data acquisition. This is very significant in that it on one hand suggests the validity of the model and its underlying assumptions (provided the data set is collected with meaningful design) and on the other hand sets the bar for a satisfactory data interpretation back to the same criteria used in most other biophysical disciplines, where systematic deviations between data and fit are simply taken to reject the model. The same rational conclusion can and should be drawn when analyzing SPR data. We do believe that when the best-fit is significantly worse, one should conclude that the model does not reflect the binding process actually taking place. This may require the combination with MTL corrections, as described below, or reflect the fact that the

assumption of independent parallel 1:1 binding events of uniform analyte molecules does not apply.

5. Relationship Between Mass Transport and Surface Heterogeneity

We have discussed above the two most common sources of deviation from ideal single-exponential pseudo-first-order surface binding. In practice, MTL and surface heterogeneity are related problems, since both are governed by the density, spatial distribution, and detailed local properties of the immobilized surface sites.

Any of the surface sites, whether reflecting the "native" binding properties or artificial low-affinity or "nonspecific" sites, will contribute to the depletion and retention, respectively, of analyte in the vicinity of the sensor surface, and thereby diminish the effective transport rate and increase MTL. This causes the surface binding to the different surface sites be a coupled process: Analyte molecules dissociating from one class of sites may rebind to another site with different affinity and kinetic constants.

Fortunately, the effect of MTL and surface heterogeneity on the shape of the observed surface binding traces is opposite: MTL often causes less convex binding kinetics (more linear) in the association phase, whereas surface heterogeneity typically causes more convex traces in the association phase. The effect on the shape of the dissociation phase is similar in that both appear multiphasic, but with different concentration dependence. For this reason, MTL and surface heterogeneity do not correlate much and can be distinguished in the analysis of experimental data.

Mathematically, the combined effects of surface heterogeneity and MTL can be expressed with the system of rate equations

$$\begin{aligned} \frac{dc_{\text{surf}}}{dt} &= k_{\text{tr}}(c - c_{\text{surf}}) - \frac{ds}{dt} \\ \frac{ds_i}{dt} &= k_{\text{on},i}c_{\text{surf}}(P_i(k_{\text{off},i},K_{\text{D},i}) - s_i) - k_{\text{off}}s_i \end{aligned} \qquad [9]$$

where the sum of all binding signals to each population i is the total measured signal, $s(c,t) = \sum_i s_i(c,t)$, and the population $P_i(k_{\text{off},i},K_{\text{D},i})$ of each site gives a discretized representation of the affinity and kinetic rate constant distribution (13). Such a model was applied, for example, for the global analysis of the data shown in **Fig. 2.8**. This model assumes a single transport rate constant for binding to all sites. This may strictly not always be fulfilled, for example, to account for binding inside or outside the immobilization matrix. Unfortunately, accounting for such an effect seems to exceed current computational capabilities in the data analysis

and likely the information content of experimental surface binding data.

Since MTL depends strongly on the total number of surface sites, a popular approach to diagnose the presence of and to quantitatively account for MTL has been the comparison of analyte binding kinetics to surfaces at different total immobilization density (or rather different binding capacity). However, this is based on the silent assumption that the binding properties of the surface sites do not change for the different surfaces. With the availability of the surface site distribution analysis it is possible to test this assumption. **Figure 2.11** shows the functional surface site distribution for two different antibody–antigen systems. The system shown in panels A and B exhibits very similar affinity and kinetic distributions when immobilized at different levels. In

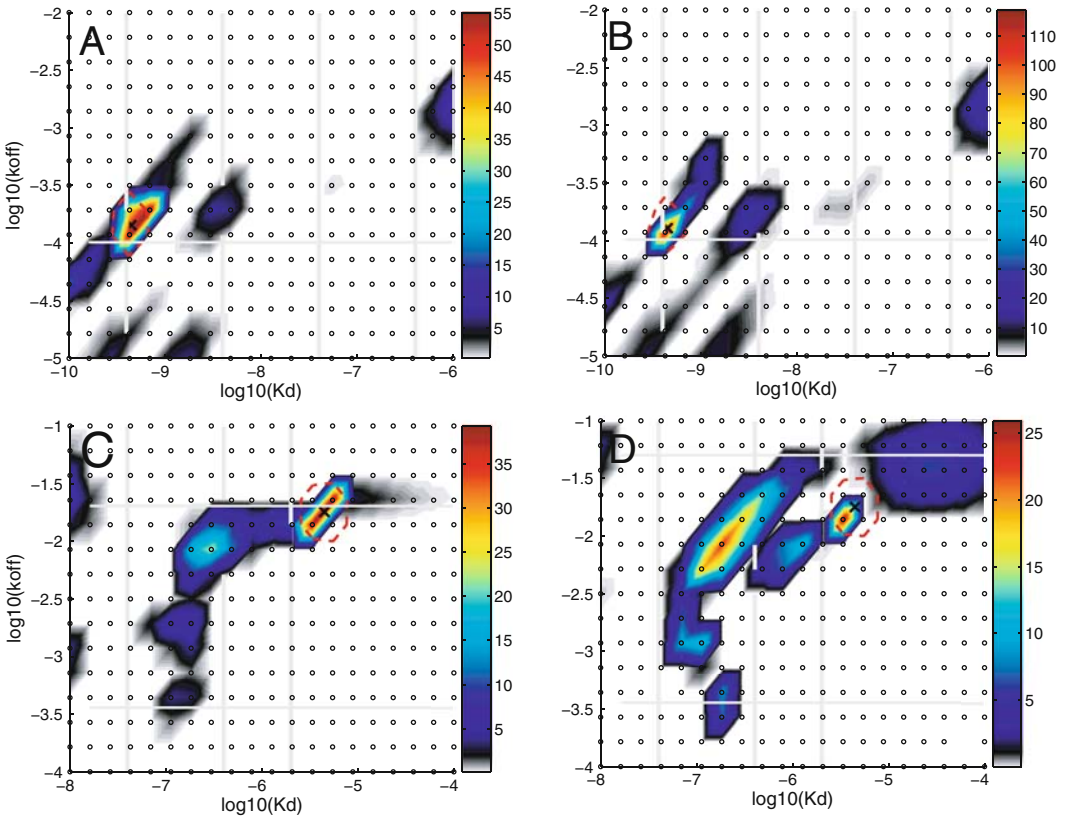

Fig. 2.11. Example for the affinity and kinetic rate constant distribution measured at surfaces with different immobilization levels. (**a**) and (**b**) Binding of a soluble monoclonal Fab to its immobilized antigen protein at a low surface density of 1,400 RU leading to a total binding capacity of ~340 RU (**a**) and high surface density of 3,800 RU leading to a total binding capacity of ~700 RU (**b**), respectively. For this molecule, the resulting functional surface site distributions are virtually the same, independent of immobilization level. (**c**) and (**d**) Binding of another soluble monoclonal Fab to its antigen protein immobilized at low surface density of 920 RU leading to a total binding capacity of 381 RU (**c**), and immobilized at a higher surface density (1,500 RU) leading to a total binding capacity of 464 RU (**d**). In this case, a significant increase in the fraction of higher affinity sites is observed at the higher density surface. For details, *see* (19).

contrast, the other system shown in panels C and D exhibits a significant shift toward a higher affinity population at the higher immobilization density. This highlights that the immobilization process, dependent on the macromolecular system under study, may indeed create different subpopulations of sites at different stages of the immobilization process.

This could be related to the intrinsic heterogeneity of the surface, in particular when using an immobilization matrix, and the fact that the immobilization process itself is a kinetic process requiring mass transport, likely being mass transport limited itself. One could easily imagine that the resulting spatial distribution of the immobilized surface sites will not be uniform and therefore create different amounts of subpopulation in different microenvironments with different binding properties.

Another possible mechanism for a dependence of the affinity distribution on the total immobilization density could involve the oligomerization of the immobilized macromolecules. Contributing factors for oligomerization are the high local concentrations (routinely in the 1–10 mg/mL range or higher inside the matrix) and the increased propensity of protein oligomerization in the presence of a surface (55) as well as volume-excluding polymers (56). In particular for proteins undergoing self-association in solution, this may be a likely scenario.

In practice, concerns of MTL and surface heterogeneity must both be kept in mind and may have to be balanced when deciding on the strategy of surface immobilization. For example, the use of proteins for site-specific capture of the binding partner of interest, such as antibodies or streptavidin, may improve the chemical homogeneity of the surface sites, but at the same time make the surface more sticky and dense, and thereby hamper diffusion and create stronger MTL. Conversely, the use of no or very short polymer supports for immobilization matrices can eliminate longer diffusion distances and improve MTL, but may not screen as well nonspecific binding sites (e.g., driven by hydrophobic interactions) directly at the surface, and thereby increase the heterogeneity of the measured affinity distribution.

This is not to suggest that both could not be minimized simultaneously, but just to highlight how they are interrelated fundamentally due to the need for immobilization to the surface of one of the binding partners to be characterized. If the initial rate or the steady-state signal of SPR surface binding is only taken as an empirically calibrated signal reporting on the concentration of free analyte, and this surface binding assay is used to probe the solution equilibrium constant in the presence of soluble competitors to the surface sites, both problems of MTL and surface heterogeneity become irrelevant.

6. Conclusions

The present chapter was meant as an introduction to the strategies for the kinetic analysis of SPR surface binding data, and two major problems arising in the surface binding format. The brief history of SPR biosensing in the biomedical sciences cautions us that the correct interpretation of kinetic surface binding traces as reflecting molecular parameters, rather than merely being a reflection of the often complex properties of the particular surface generated, is not trivial at all. The most important requirements for a reliable characterization of molecular parameters are the following: (1) the design of experiments that will provide meaningful information on the desired parameters and allows us to discriminate between chemical binding of interest and artifact (2), the application of stringent tests of the consistency of the model and the data (3), the critical awareness of the assumptions made in the analysis, and (4) the design and application of experimental controls to test these assumptions.

This is especially important when the binding traces do not follow the simplest possible binding process, that of a single site with pseudo-first-order binding kinetics. Two simple reasons for deviations that are fundamentally related to SPR biosensing (rather than primarily the molecules of interest) are MTL and surface heterogeneity. We have introduced tools that help to address both problems and to obtain, despite their presence, estimates for the affinity and kinetic parameters of the molecular interaction to be studied. Using the model that accounts for surface heterogeneity, fits can often be achieved that describe the experimental data within the noise of data acquisition. This should be the goal of the kinetic analysis, and failure to meet this criterion should lead us to reject the hypothesis underlying the data analysis.

We have not discussed advanced questions of how to further improve the model if the consideration of the two most common surface-related problems cannot explain the data. Glaser and Hausdorf (32) have studied a model system exhibiting multiphasic binding and noted the difficulty that many different more complex binding models fitted the data equally well. This is exacerbated by the fact that the problems of surface heterogeneity and MTL will likely be superimposed to more complex chemical kinetics. The recently discovered apparently ubiquitous presence of surface site heterogeneity, in particular, would make the reliable identification of a complex reaction scheme much more difficult. Even if the reaction scheme is known from other techniques, the determination of its associated molecular binding parameters could be highly problematic. In such situations, it

seems more appealing to constrain the quantitative data analysis to the interpretation of the steady-state responses as a function of analyte concentration toward estimating equilibrium binding constants. Alternatively, the solution competition approach may provide solution affinity constants (*see* **Chapter 6**). In some cases of more complicated binding reactions between two or more molecules, it is also possible to use the SPR surface binding assay to at least answer qualitative questions about the binding scheme, presence of cooperativity, etc. (6). This is a very powerful aspect of the application of SPR surface binding which seems sometimes underappreciated, but can often provide reliable and critical information about the mechanism of protein interactions.

7. Notes

1. It should be noted that this is true irrespective of the fact that the molecules under study may include surface receptors that in the biological environment exist and act at a surface. Unless this exact biological surface can be used, e.g., by coating the SPR surface with actual cell membranes, the differences of the native and the artificial environment in the SPR sensing volume with respect to the precise physical environment and the surface site distribution will be the dominating factor for the observed surface binding kinetics, yielding parameters potentially many orders of magnitude different from those in the native environment.
2. For example, if an analyte of 100 kDa at a concentration of 10 nM leads to a signal from nonspecific binding on the level of 10^{-6} refractive index units (1 RU), which may be difficult to distinguish from a bulk shift, the ratio $c_{\mathrm{free}}/c_{\mathrm{bound}}$ only considering the nonspecific sites is 0.01, and this alone leads to an extra reduction of the analyte mobility by a factor 100.
3. In **Eq. [5]**, we have chosen to express the transport rate constant k_{tr} in signal units of RU $\times$ M^{-1} $\times$ s^{-1}. For the geometry of the Biacore instruments, typical numerical values are 10^{7}–10^{12}, and they are best thought of on a logarithmic scale. If a number of assumptions are made, among them the neglect of transport through the immobilization matrix, k_{tr} can be theoretically related to a macromolecular diffusion coefficient. However, in a careful study we have not obtained reasonable values for the diffusion coefficients with this approach in practice (13), raising doubts on the utility of the underlying assumptions.

4. Because of the latter it is not possible to use an ideal model **Eq. [1]** to fit data that are mass transport limited, and expect the ratio of the apparent rate constants to reflect the true equilibrium constant. The least-squares fit will be poor and biased differently in association and dissociation depending on the experimental configuration, such as length of association and dissociation phases and concentrations chosen.
5. This should not be misunderstood to mean that the binding progress close to reaching steady state is not mass transport influenced, as suggested by Karlsson et al. (57). It only vanishes close to saturation of all sites, not close to any steady-state.
6. Therefore, as indicated above, the estimates for $k_{on}^{(app)}$, if derived from an empirical application of a pseudo-first-order model, cannot be taken as a measure for estimating the possible extent of MTL, since the latter would require knowledge of the true k_{on}, which may be much higher especially in the presence of MTL.

Acknowledgment

This research was supported by the Intramural Research Program of the National Institute of Bioengineering and Physical Science, National Institutes of Health.

References

1. Fägerstam, L. G., Frostell, Å., Karlsson, R., et al. (1990) Detection of antigen-antibody interactions by surface plasmon resonance. Application to epitope mapping. *J. Mol. Recogn.* **3**, 208–14.
2. Schuck, P. (1997) Use of surface plasmon resonance to probe the equilibrium and dynamic aspects of interactions between biological macromolecules. *Ann. Rev. Biophys. Biomol. Struct.* **26**, 541–66.
3. Cooper, M. A. (2002) Optical biosensors in drug discovery. *Nat. Rev. Drug Discov.* **1**, 515–28.
4. Pattnaik, P. (2005) Surface plasmon resonance: applications in understanding receptor-ligand interaction. *Appl. Biochem. Biotechnol.* **126**, 79–92.
5. Schasfoort, R. B. M., and Tudos, A. J. (2008) *Handbook of Surface Plasmon Resonance.* RSC Publishing, Cambridge, UK.
6. Sundberg, E. J., Andersen, P. S., Gorshkova, I. I., and Schuck, P. (2007) Surface plasmon resonance biosensing in the study of ternary systems of interacting proteins. In Schuck P. (Ed.) *Protein Interactions: Biophysical Approaches for the Study of Complex Reversible Systems.* Vol. 5, pp. 97–141, Springer, New York.
7. Krone, J. R., Nelson, R. W., Dogruel, D., Williams, P., and Granzow, R. (1997) BIA/MS: interfacing biomolecular interaction analysis with mass spectrometry. *Anal. Biochem.* **244**, 124–32.
8. Sonksen, C. P., Nordhoff, E., Jansson, O., Malmqvist, M., and Roepstorff, P. (1998)

Combining MALDI mass spectrometry and biomolecular interaction analysis using a biomolecular interaction analysis instrument. *Anal. Chem.* **70**, 2731–36.
9. Natsume, T., Nakayama, H., Jansson, O., Isobe, T., Takio, K., and Mikoshiba, K. (2000) Combination of biomolecular interaction analysis and mass spectrometric amino acid sequencing. *Anal. Chem.* **72**, 4193–98.
10. Gilligan, J. J., Schuck, P., and Yergey, A. L. (2002) Mass spectrometry after capture and small-volume elution of analyte from a surface plasmon resonance biosensor. *Anal. Chem.* **74**, 2041–47.
11. Mehlmann, M., Garvin, A. M., Steinwand, M., and Gauglitz, G. (2005) Reflectometric interference spectroscopy combined with MALDI-TOF mass spectrometry to determine quantitative and qualitative binding of mixtures of vancomycin derivatives. *Anal. Bioanal. Chem.* **382**, 1942–48.
12. Schuck, P. (1996) Kinetics of ligand binding to receptor immobilized in a polymer matrix, as detected with an evanescent wave biosensor. I. A computer simulation of the influence of mass transport. *Biophys. J.* **70**, 1230–49.
13. Svitel, J., Boukari, H., Van Ryk, D., Willson, R. C., and Schuck, P. (2007) Probing the functional heterogeneity of surface binding sites by analysis of experimental binding traces and the effect of mass transport limitation. *Biophys. J.* **92**, 1742–58.
14. Karlsson, R. (1994) Real-time competitive kinetic analysis of interactions between low-molecular-weight ligands in solution and surface-immobilized receptors. *Anal. Biochem.* **221**, 142–51.
15. Schuck, P. (1997) Reliable determination of binding affinity and kinetics using surface plasmon resonance biosensors. *Curr. Opin. Biotechnol.* **8**, 498–502.
16. Langmuir, I. (1918) The adsorption of gases on plane surfaces of glass, mica and platinum. *J. Am. Chem. Soc.* **40**, 1361–403.
17. Myszka, D. G. (1999) Improving biosensor analysis. *J. Mol. Recognit.* **12**, 279–84.
18. Ober, R. J., and Ward, E. S. (1999) The influence of signal noise on the accuracy of kinetic constants measured by surface plasmon resonance experiments. *Anal. Biochem.* **273**, 49–59.
19. Gorshkova, I. I., Svitel, J., Razjouyan, F., and Schuck, P. (2008) Bayesian analysis of heterogeneity in the distribution of binding properties of immobilized surface sites. *Langmuir* **24**, 11577–86.
20. Schuck, P., and Minton, A. P. (1996) Minimal requirements for internal consistency of the analysis of surface plasmon resonance biosensor data. *Trends Biochem. Sci.* **252**, 458–60.
21. Schuck, P., Millar, D. B., and Kortt, A. A. (1998) Determination of binding constants by equilibrium titration with circulating sample in a surface plasmon resonance biosensor. *Anal. Biochem.* **265**, 79–91.
22. Abrantes, M., Magone, M. T., Boyd, L. F., and Schuck, P. (2001) Adaptation of the Biacore X surface plasmon resonance biosensor for use with small sample volumes and long contact times. *Anal. Chem.* **73**, 2828–35.
23. Karlsson, R., Katsamba, P. S., Nordin, H., Pol, E., and Myszka, D. G. (2006) Analyzing a kinetic titration series using affinity biosensors. *Anal. Biochem.* **349**, 136–47.
24. Ober, R. J., and Ward, E. S. (1999) The choice of reference cell in the analysis of kinetic data using BIACORE. *Anal. Biochem.* **271**, 70–80.
25. Karp, N. A., Edwards, P. R., and Leatherbarrow, R. J. (2005) Analysis of calibration methodologies for solvent effects in drug discovery studies using evanescent wave biosensors. *Biosens. Bioelectron.* **21**, 128–34.
26. Ladbury, J. E., Lemmon, M. A., Zhou, M., Green, J., Botfield, M. C., and Schlesinger, J. (1995) Measurement of the binding of tyrosyl phosphopepdites to SH2 domains: a reappraisal. *Proc. Natl. Acad. Sci. USA* **92**, 3199–203.
27. Muller, K. M., Arndt, K. M., and Pluckthun, A. (1998) Model and simulation of multivalent binding to fixed ligands. *Anal. Biochem.* **261**, 149–58.
28. Davis, S. J., Ikemizu, S., and Wild, M. K., van der Merwe, P. A. (1998) CD2 and the nature of protein interactions mediating cell-cell recognition. *Immunol. Rev.* **163**, 217–36.
29. Andersen, P. S., Lavoie, P. M., Sekaly, R. P., et al. (1999) Role of the T cell receptor alpha chain in stabilizing TCR-superantigen-MHC class II complexes. *Immunity* **10**, 473–83.
30. Schuck, P., Boyd, L. F., and Andersen, P. S. (1999) Measuring protein interactions by optical biosensors. In Coligan, J. E., Dunn, B. M., Ploegh, H. L., Speicher, D. W., and Wingfield, P. T. (Eds.) *Current Protocols in Protein Science*. Vol. 2, 20.2.1–20.2.21, John Wiley & Sons, New York.
31. Brown, P. H., Balbo, A., and Schuck, P. (2008) A Bayesian approach for quantifying trace amounts of antibody aggregates by sedimentation velocity analytical ultracentrifugation. *AAPS J.* **10**, 481–93.

32. Glaser, R. W., and Hausdorf, G. (1996) Binding kinetics of an antibody against HIV p24 core protein measured with real-time biomolecular interaction analysis suggest a slow conformational change in antigen p24. *J. Immunol. Methods* **189**, 1–14.
33. Nieba, L., Krebber, A., and Pluckthun, A. (1996) Competition BIAcore for measuring true affinities: large differences from values determined from binding kinetics. *Anal. Biochem.* **234**, 155–65.
34. Krishnamoorthy, G., Carlen, E. T., Kohlheyer, D., Schasfoort, R. B., and van den Berg, A. (2009) Integrated electrokinetic sample focusing and surface plasmon resonance imaging system for measuring biomolecular interactions. *Anal. Chem.* **87**, 1957–63.
35. van der Merwe, P. A., Barclay, A. N., Mason, D. W., et al. (1994) Human cell-adhesion molecule CD2 binds CD58 (LFA-3) with a very low affinity and an extremely fast dissociation rate but does not bind CD48 or CD59. *Biochemistry* **33**, 10149–60.
36. Hall, D. R., Cann, J. R., and Winzor, D. J. (1996) Demonstration of an upper limit to the range of association rate constants amenable to study by biosensor technology based on surface plasmon resonance. *Anal. Biochem.* **235**, 175–84.
37. Glaser, R. W. (1993) Antigen-antibody binding and mass transport by convection and diffusion to a surface: a two-dimensional computer model of binding and dissociation kinetics. *Anal. Biochem.* **213**, 152–61.
38. Lok, B. K., Cheng, Y.-L., and Robertson, C. R. (1983) Protein adsorption on crosslinked polydimethylsiloxane using total internal reflection fluorescence. *J. Coll. Interface Sci.* **91**, 104–16.
39. Gedig, E. (2008) Surface chemistry in SPR technology. In Schasfoort, R. B. M., and Tudos, A. J. (Eds.) *Handbook of Surface Plasmon Resonance*. pp. 173–220, The Royal Society of Chemistry, Cambridge.
40. Stenberg, E., Persson, B., Roos, H., and Urbaniczky, C. (1991) Quantitative determination of surface concentration of protein with surface plasmon resonance using radiolabeled proteins. *J. Coll. Interface Sci.* **143**, 513–26.
41. Yeung, D., Gill, A., Maule, C. H., and Davies, R. J. (1995) Detection and quantification of biomolecular interactions with optical biosensors. *Trends Anal. Chem.* **14**, 49–56.
42. Crank, J. (1975) *The Mathematics of Diffusion*. Clarendon Press, Oxford.
43. Yarmush, M. L., Patankar, D. B., and Yarmush, D. M. (1996) An analysis of transport resistances in the operation of BIAcore; Implications for kinetic studies of biospecific interactions. *Mol. Immunol.* **33**, 1203–14.
44. Pero, J. K., Haas, E. M., and Thompson, N. L. (2006) Size dependence of protein diffusion very close to membrane surfaces: measurement by total internal reflection with fluorescence correlation spectroscopy. *J. Phys. Chem. B Condens. Matter Mater. Surf. Interfaces Biophys.* **110**, 10910–18.
45. de Gennes, P. G. (1980) Conformation of polymers attached to an interface. *Macromolecules* **13**, 1069–75.
46. Xu, F., Persson, B., Lofas, S., and Knoll, W. (2006) Surface plasmon optical studies of carboxymethyl dextran brushes versus networks. *Langmuir* **22**, 3352–57.
47. Balgi, G., Leckband, D. E., and Nitsche, J. M. (1995) Transport effects on the kinetics of protein-surface binding. *Biophys. J.* **68**, 2251–60.
48. Zacher, T., and Wischerhoff, E. (2002) Real-time two-wavelength surface plasmon resonance as a tool for the vertical resolution of binding processes in biosensing hydrogels. *Langmuir* **18**, 1748–59.
49. Schuck, P., and Minton, A. P. (1996) Analysis of mass transport limited binding kinetics in evanescent wave biosensors. *Anal. Biochem.* **240**, 262–72.
50. de Mol, N. J., Plomp, E., Fischer, M. J. E., and Ruijtenbeek, R. (2000) Kinetic analysis of the mass transport limited interaction between the tyrosine kinase lck SH2 domain and a phosphorylated peptide studied by a new cuvette-based surface plasmon resonance instrument. *Anal. Biochem.* **279**, 61–70.
51. DeLisi, C. (1980) The biophysics of ligand-receptor interactions. *Q. Rev. Biophys.* **13**, 201–30.
52. Myszka, D. G., He, X., Dembo, M., Morton, T. A., and Goldstein, B. (1998) Extending the range of rate constants available from BIACORE: interpreting mass transport-influenced binding data. *Biophys. J.* **75**, 583–94.
53. Svitel, J., Balbo, A., Mariuzza, R. A., Gonzales, N. R., and Schuck, P. (2003) Combined affinity and rate constant distributions of analyte or ligand populations from experimental surface binding and kinetics and equilibria. *Biophys. J.* **84**, 4062–77.
54. Provencher, S. W. (1979) Inverse problems in polymer characterization: direct analysis of polydispersity with photon

correlation spectroscopy. *Makromol. Chem.* **180**, 201–09.
55. Minton, A. P. (2001) Effects of excluded surface area and adsorbate clustering on surface adsorption of proteins. II. Kinetic models. *Biophys. J.* **80**, 1641–48.
56. Zimmerman, S. B., and Minton, A. P. (1993) Macromolecular crowding: biochemical, biophysical, and physiological consequences. *Annu. Rev. Biophys. Biomol. Struct.* **22**, 27–65.
57. Karlsson, R., Michaelsson, A., and Mattson, L. (1991) Kinetic analysis of monoclonal antibody-antigen interactions with a new biosensor based analytical system. *J. Immunol. Methods* **145**, 229–40.
58. Roden, L. D., and Myszka, D. G. (1996) Global analysis of a macromolecular interaction measured on BIAcore. *Biochem. Biophys. Res. Commun.* **225**, 1073–77.

Chapter 3

Amine Coupling Through EDC/NHS: A Practical Approach

Marcel J.E. Fischer

Abstract

Surface plasmon resonance (SPR) is one of the leading tools in biomedical research. The challenge in its use is the controlled positioning of one of the components of an interaction on a carefully designed surface. Many attempts in interaction analysis fail due to the non-functional or unsuccessful immobilization of a reactant onto the complex matrix of that surface. The most common technique for linking ligands covalently to a hydrophilic solid surface is amine coupling via reactive esters. In this chapter detailed methods and problem discussions will be given to assist in fast decision analysis to optimize immobilization and regeneration. Topics in focus are different coupling techniques for small and large molecules, streptavidin–biotin sandwich immobilization, and optimizing regeneration conditions.

Key words: SPR, amine coupling, small molecule, streptavidin–biotin, immobilization, regeneration.

1. Introduction

1.1. General Introduction

Surface plasmon resonance (SPR) is a very sensitive tool for measuring interactions between biomolecules with label-free detection and is performed on a special gold coated chip or disk surface (1, 2). In order to detect binding phenomena near the gold layer of this surface it is necessary to immobilize one of the molecules (the ligand) involved in the interaction onto the surface. An interaction can then be measured by adding the binding compound (analyte) in solution. This chapter is focused on the most frequently used technique to immobilize ligands: the amine coupling method. Although many methods for covalent coupling have been developed, due to its ease of use the amine coupling is the preferred choice (in over 80% of cases). Although the method

N.J. de Mol, M.J.E. Fischer (eds.), *Surface Plasmon Resonance*, Methods in Molecular Biology 627,
DOI 10.1007/978-1-60761-670-2_3,

is straightforward, often problems arise with the procedure. These problems are usually related with either the type of surface, the pH of the buffer, the molecular properties of ligand or analyte, or the effectiveness of the regeneration after binding. Also the stability of either ligand or analyte, or steric problems related to the interaction at the surface may cause serious problems. Methods will be presented for the preparation of the sensor surface prior to immobilization and to help in choosing the correct coupling conditions. Immobilization procedures for ligands with primary amines or containing an aldehyde group are presented, as well as a method for immobilization of small molecules with a highly negative charge, which is more difficult. A sophisticated example of a complex protocol is the multilayered streptavidin–biotin interaction often used in ELISA. Regeneration of the chip surface between measurements is a prerequisite for good quality data and long stability. A method is added for optimization of regeneration conditions. The methods are given in a format adaptable to various types of SPR instruments, and may need fine-tuning depending on the specifications of the equipment. For a better understanding of the methods a short introduction to the problems at hand will be given, combined with some prior considerations.

1.2. Choice of Sensor Surface

Many types of sensor surfaces are available nowadays, from bare gold to lipid bilayers. However, in biological interaction analysis a water environment is crucial and therefore the surface is usually coated with a hydrophilic three-dimensional non-cross-linked carboxymethylated polymer (the hydrogel). The ligand can be covalently linked to the carboxyl group of this polymer, positioning it close to the gold surface. The refractive index-related SPR signal is generated on top of the gold layer in the first 300 nm in a decaying evanescent field (**Fig. 3.1**). The most sensitive interaction signals are generated closest to the gold. A typical hydrogel has a three-dimensional structure with a certain density and length of the polymer chains (**Fig. 3.2**). Variation in polymer density or length offers the manufacturers control on the nanostructure of the surface matrix and its molecular characteristics. For many types of applications different sensor surfaces exist (3, 4; *see*, e.g., www.biacore.com and www.xantec.com). In general, for protein interactions whether or not with small molecules, a 50–100 nm thick linear carboxymethylated dextran or polycarboxylate layer with a medium to high chain density is used (e.g., BIAcore, Xantec) (*see* **Note 1** and **Chapter 2**). The thickness influences the diffusion rate of molecules into the matrix. The density controls the immobilization capacity, however, too dense matrices may block partitioning of larger molecules. For small molecules high densities should be chosen. Another advantage of hydrogels

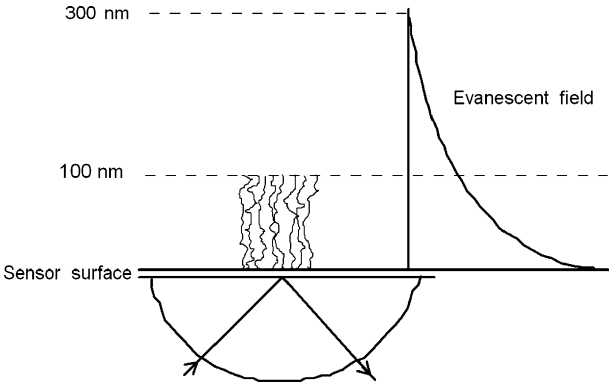

Fig. 3.1. Schematic view of a sensor surface with dextran layer and exponential decay of the evanescent field, sensing changes in refractive index.

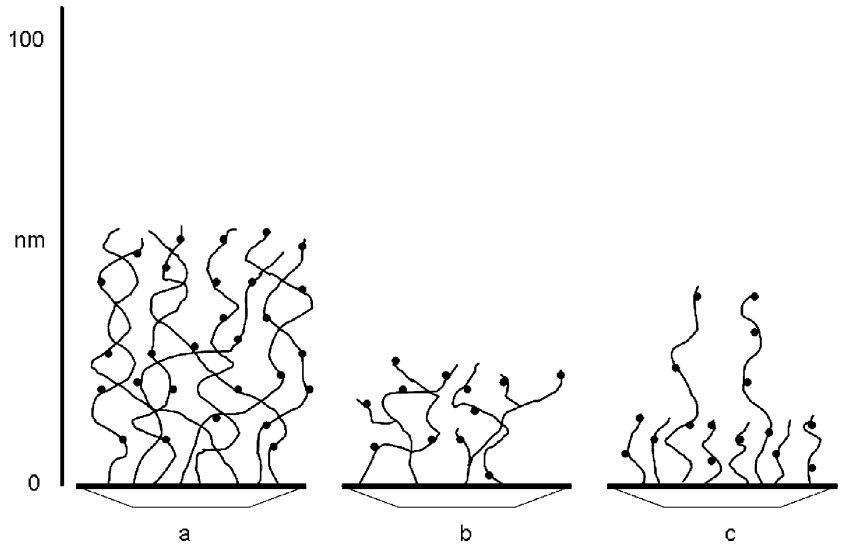

Fig. 3.2. Overview of the hydrogel matrix on top of a gold sensor surface. The carboxylated (•) dextran chains can be dense (**a**), or less dense and with different thicknesses (from 20 to 500 nm) and even be branched (**b**), or be composed of mixed polymer thicknesses known as self-assembled monolayers (**c**).

is the low level of non-specific binding, either with buffer or sample components. The surface matrix can have many properties that influence the interaction in a noncontrolled way (*see* **Chapter 2**). Moreover, surface choice also depends on molecular restrictions or properties of the molecules involved in the interaction as indicated below (*see* **Section 1.4**).

1.3. Role of Buffer pH

The pH plays two important roles in the immobilization procedure. For the reaction with the activated ester to occur (step 2 of the reaction scheme in **Fig. 3.3**) the ligand has to be uncharged and brought in close proximity of the surface by a process called

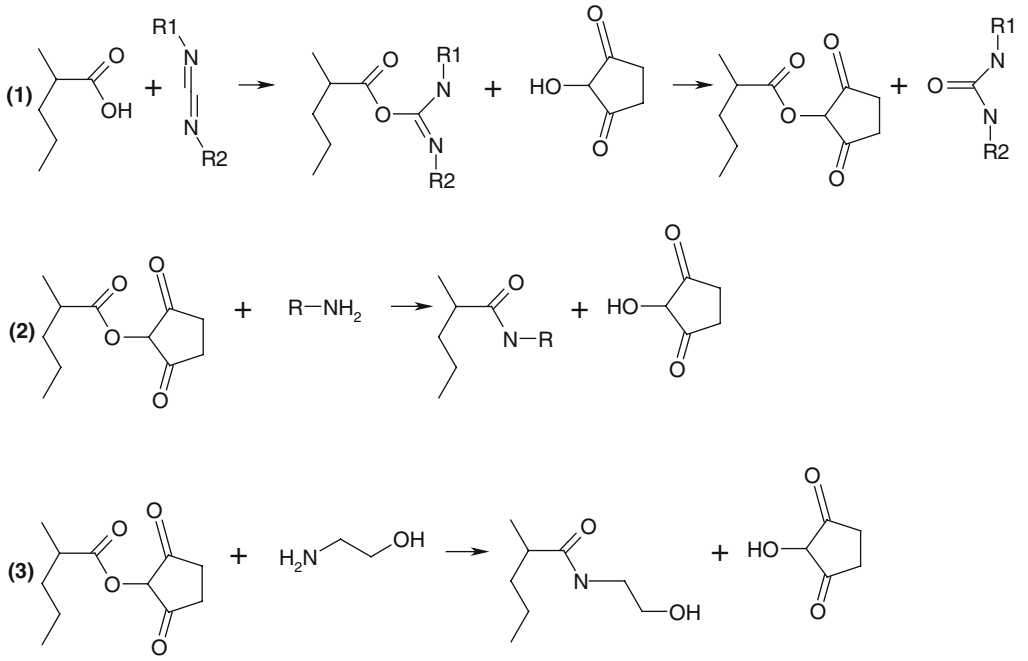

Fig. 3.3. The chemical reaction scheme for the coupling of a ligand to the surface of a sensor disk. The carboxylgroup is activated with EDC/NHS (*step 1*) followed by covalent attachment of the ligand by its primary amine (*step 2*). The remaining esters are deactivated with ethanolamine (*step 3*). In this scheme R stands for a protein or a small molecule like a peptide or a drug. The side group R1 is $–CH_2CH_3$ and R2 is $-(CH_2)_3N^+H(CH_3)_2Cl^-$.

preconcentration. This surface matrix-linked process is achieved by electrostatic attraction between the oppositely charged remaining surface carboxyls and the amino group of the ligand (*see* **Note 2**). The second role the pH is involved in is optimal reaction pH (*see* **Note 3**).

1.4. Influence of Physicochemical Properties of Ligand or Analyte

A decision has to be made on which of the two interacting molecules will be immobilized on the surface. This choice depends on a number of molecular conditions: size (drug or peptide versus protein) (*see* **Note 4**), stability (*see* **Note 5**), solubility, availability of an immobilizable functional group like an amine or a lysine that is located distant from the binding site, or the presence of lysine groups near the binding site of the ligand (*see* **Note 6**). It must be emphasized that immobilization should be as uniform as possible. Finally, the overall charge of the ligand is an important factor for immobilization (*see* **Note 2**).

1.5. Regeneration Properties

To maintain integrity of the immobilized ligand in the regeneration cycle the bound analyte should be removed under as mild as possible conditions. Breaking up high-affinity interactions is not always easy and requires often physically powerful reagents.

The ligand should be able to withstand these conditions. A stepwise protocol to inspect regeneration conditions is included (*see* **Section 3.7**).

1.6. Activity and Steric Properties

Affinity is a measure of a thermodynamic and reproducible binding constant and may be influenced by immobilization procedures. Processes like mass transport limitation (MTL) and rebinding (*see* **Chapter 2**) can be avoided/decreased by lowering the binding capacity of the surface or by increasing the flow rate (5) (*see* **Note 7**). Also the use of sensor chips with thin dextran layers will lower mass transport. The interaction may be sensitive to another effect. Relatively small ligand molecules should maintain some distance from the surface polymer to prevent steric hindrance during binding with the analyte. Distance can be introduced by, e.g., attaching a linker (e.g., a 6-aminohexanoic acid or an oligoethylene glycol spacer) to the ligand (5).

Not rarely the ligand contains more primary amines that are sensitive to the EDC/NHS reaction. In peptides and proteins these usually are lysines. Coupling of ligands with different groups leads to heterogeneous surfaces. There is even a (small) chance of cross-linking the dextran chains by multivalent coupling (*see* **Note 8**). In either case the ligand will be facing the analyte from different directions, which may influence the binding constant. Indications for such an effect may be present in the kinetic profile of the sensorgram. Peter Schuck shows an approach to analyze heterogeneous surfaces (*see* **Chapter 2**).

2. Materials

2.1. Buffers

1. Coupling buffer 1: Dependent on the isoelectric point of the ligand either formic acid (pH 3.0–4.5), acetic acid (pH 4.0–5.5), or maleic acid (pH 5.5–7.0) is diluted in water at 5–10 mM, and adjusted to proper pH with NaOH. Store at 4°C.
2. Running buffer: HEPES buffered saline (HBS) is a solution of 10 mM HEPES, 3 mM EDTA, and 150 mM NaCl, and is set to pH 7.4 with NaOH, after which the solution is filtered over a 0.2 μm filter to degas and remove particles. Finally, Tween 20 is added at 0.005% (*see* **Note 9**) and carefully dissolved with gentle rotation preventing reuptake of air.
3. Coupling buffer 2: This buffer is used for negatively charged small ligands. Prepare a buffer with 100 mM boric acid and 1 M NaCl and set at pH 8.3 with NaOH.

4. Buffer 3: Sodium acetate 100 mM is adjusted to pH 5.5 with NaOH.
5. Buffer 4: Sodium acetate 100 mM is adjusted to pH 4.0 with NaOH.
6. Sodium metaperiodate 50 mM in buffer 3.
7. Hydrazine or carbohydrazide at 5 mM.
8. Sodium cyanoborohydride at 0.1 M in buffer 4.

2.2. Coupling Reagents

1. EDC (*N*-(3-dimethylaminopropyl)-*N'*-ethylcarbodiimide hydrochloride) of high quality (e.g., GE Healthcare, BR-1000-50) is rapidly weighed in and dissolved in water at 0.4 M, divided into small aliquots, and stored at −20°C (*see* **Note 10**). Solid EDC is hygroscopic and labile and must be kept under dry gas.
2. NHS (*N*-hydroxysuccinimide) is dissolved in water at 0.1 M, divided into small aliquots, and stored at −20°C.
3. Ethanolamine hydrochloric acid is dissolved in water at 1 M and pH adjusted to 8.5 with HCl, subsequently divided into small aliquots and stored at −20°C.
4. Desalting column (e.g., GE Healthcare, PD-10).

2.3. Regeneration Reagents

1. Basic regeneration solutions are indicated in **Table 3.1**.
2. The six stock solutions A, B, I, U, D, and C given below can be used in the protocol described in **Section 3.7**.

   Solution A. Acidic: Mix equal volumes of 0.15 M solutions of oxalic acid, phosphoric acid, malonic acid, and formic acid and bring to pH 5.0 with NaOH.

   Solution B. Basic: Mix equal volumes of 0.20 M solutions of ethanolamine, piperazine, glycine, and Na_3PO_4 and bring to pH 9.0 with HCl.

   Solution I. Ionic: Combine solutions of KSCN (0.46 M), urea (0.92 M), guanidine–HCl (1.83 M), and $MgCl_2$ (1.83 M).

   Solution U. Nonpolar water soluble solvents: Prepare a solution of equal volumes of DMSO, formamide, 1-butanol, acetonitrile, and ethanol.

   Solution D. Detergents: Prepare a solution of 0.3% (w/w) CHAPS, 0.3% (w/w) zwittergent 3–12, 0.3% (v/v) Tween-80, 0.3% (v/v) Tween-20, and 0.3% (v/v) Triton X-100.

   Solution C. Chelating: Make a solution of 20 mM EDTA.

   All stock solutions should be filtered (0.2 μm).

Table 3.1
List of recommended regeneration solutions. Concentrations reported depend on chip manufacturer, type of surface, and stability of the immobilized ligand

Solution	Concentration	Properties
Acetonitrile	20%	Highly hydrophobic
Ethanol	10–100%	Risk of protein denaturation
Ethylene glycol	25–50%	Hydrophobic
Formic acid	1–20%	Alternative for HCl
Glycine-HCl	0.01–2 M (pH 2–3)	Mild; highly recommended
Glycine-NaOH	10 mM (pH 9–10)	Intermediate
Guanidine chloride	6 M	Strongly ionic
HEPES-NaOH	10 mM (pH < 9)	Weak
HCl	10–1,000 mM	Mild to strong; highly recommended
$MgCl_2$	2–4 M	Intermediate; ionic
NaOH	10–100 mM	Good; risk of denaturation
NaCl	1 M	Weak; ionic
Na_2CO_3	200 mM (pH 11.5)	Milder than NaOH
Phosphoric acid	0–1,000 mM	Strong acid
SDS	0.01–20%	Good in combination with HCl or NaOH
Urea	8 M	For high affinity prot–prot interactions

3. Methods

For coupling of proteins and peptides a diversity of chemical methods exist. More specifically two of the most frequently used will be presented in this section. The standard amine coupling includes a three-step reaction with EDC/NHS chemistry (**Fig. 3.3**). The immobilization via aldehyde groups and reductive amination is shown in **Fig. 3.4**. This method can also be used for ligands containing sialic groups or *cis*-diols. Both methods can be applied with several types of SPR machines (*see* **Note 11**). Many small molecules like drugs can be chemically modified to include amine or aldehyde functionality. A few exceptions to these coupling procedures exist: neutral molecules and highly negatively charged molecules. Because coupling of such compounds often gives rise to problems (*see* **Section 1.4**) an example of an adapted method will be given for highly negatively charged molecules. In cases where

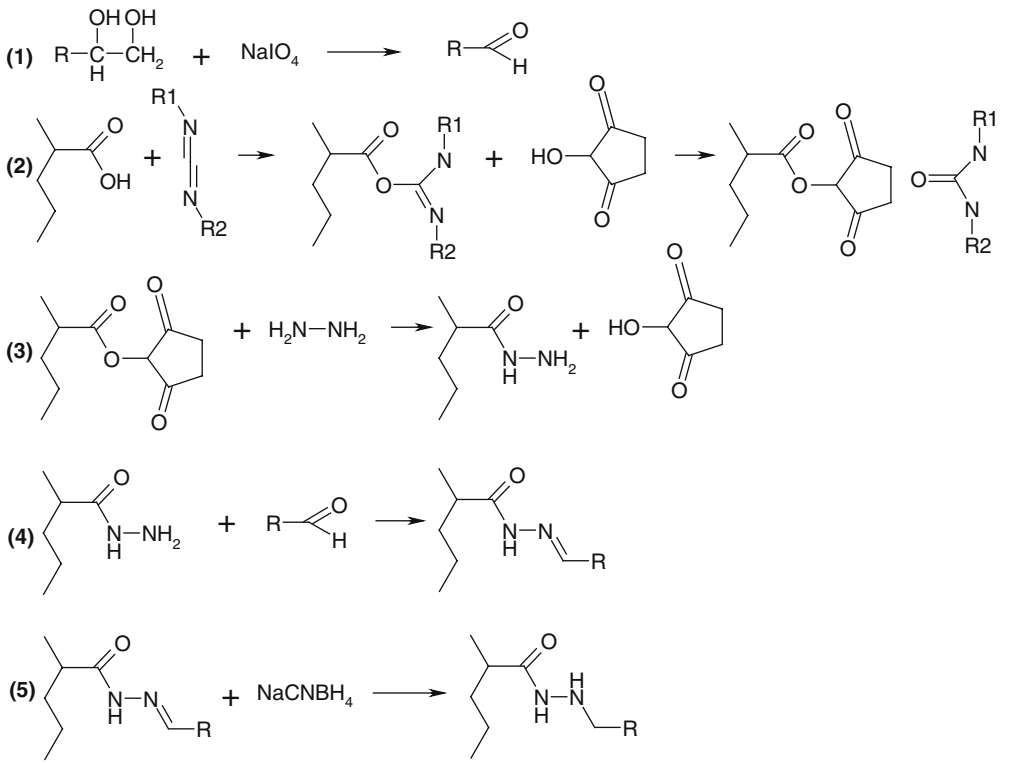

Fig. 3.4. Reaction scheme for reductive amination via aldehyde groups. Ligands already containing an aldehyde group can directly be coupled to the surface. Ligands containing *cis*-diols are oxidized with sodium metaperiodate to the aldehyde form (*step 1*). The carboxymethylated surface is activated with EDC/NHS (*step 2*) followed by reaction with hydrazine (*step 3*). After blocking of unreacted activated esters with ethanolamine, the ligand with an aldehyde group is immobilized in *step 4*. The newly formed covalent bond is stabilized with cyanoborohydride (*step 5*).

compounds can be biotinylated, a sandwich coupling technique with streptavidin may be used. This method makes use of the very strong binding affinity of streptavidin–biotin of 10^{-15} M. The biotinylation procedure itself is not subject in this chapter; however, many protocols are available in literature (e.g. Invitrogen or Thermo Scientific) and suitable surfaces with streptavidin are commercially available. The last protocol will focus on the regeneration process after coupling. Finding a suitable reagent to regenerate a high affinity or otherwise vulnerable surface is not always easy. This protocol developed by Andersson et al. (6). will help in picking the best condition for a given experiment.

3.1. Preparation of a Chip Surface

1. New chip surfaces have to be primed to remove preservatives, particles and to rewet the dry polymer layer. This presoaking is essential for reliable and reproducible coupling and stable baselines. Use quality reagents and solutions filtered over a 0.2 μm filter. After fitting the chip into the SPR equipment (*see* **Notes 1** and **12**) run the system with

running buffer and provide in 10-min intervals short 1-min pulses with 50 mM HCl until the baseline becomes stable. Make sure that the system and liquids are free of proteins as these will adsorb to the surface.

2. A more intense way of priming the system is achieved by subsequent 1 min pulses of 0.5% SDS, 6 M urea, 1% acetic acid, and 0.2 M $NaHCO_3$ each followed by water, and close with running buffer until a stable baseline is established (7) (*see* **Note 13**). Alternatively, use 0.1% SDS (1 min), 50 mM glycine-HCl pH 2.2 (10 min), 2 M NaCl (10 min), and 10 mM NaOH (10 min) (3).
3. From this point leave the buffer system running at a low flow rate when the instrument is idle (*see* **Note 14**). If the system goes in standby mode, always restart by washing a few times with regeneration solution to remove salt build-up from the running buffer. Some types of sensor chips can be removed from the machine, stored at 4°C, and may be reused.

3.2. Finding the Correct Coupling Conditions for Macromolecules

1. At this point the surface should be cleaned and is negatively charged at the pH of the running buffer. Prior to immobilization, the ligand and/or analyte should be tested for their ability to bind non-specifically to the surface. Example of basic proteins could show a high degree of electrostatic surface binding. If the analyte shows this tendency, problems during later experiments can be expected. In case of non-specific binding try to increase the ionic strength of the running buffer or use a different chip surface. Consider to couple the molecule that shows the highest level of non-specific binding.
2. Coupling buffers should be made of sodium formate, acetate, or maleate with a low ionic strength (5–10 mM) and a pH between 4 and 8 (*see* **Section 2.1**). The buffers must not contain primary amines or detergents. The correct coupling pH is verified by observing preconcentration. Use purified ligands, containing no preservatives like azide as these preservatives may bind strongly to the surface. Check ionic strength of the ligand solution and microdialyze against coupling buffer, if necessary. If the p*I* of the ligand is not known make a series of coupling buffers with 0.5 pH increments between pH 4 and 8. Run the SPR system with coupling buffer 1 (pH 8) and introduce the ligand in this buffer to the surface at 50 μg/mL. The SPR signal will increase when ligand preconcentration occurs (*e.g.*, *see* **Fig. 3.5**), if not repeat the experiment at a lower pH. This test works for proteins and not for small molecules (<1 kDa) as the refractive index change is too small to observe preconcentration. A separate p*I* measurement or

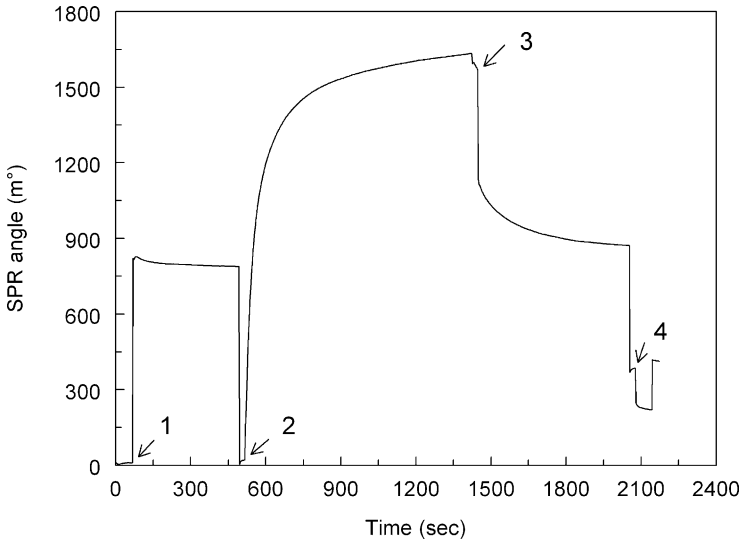

Fig. 3.5. Example of a full immobilization of an arbitrary protein on an Autolab ESPRIT SPR system (Metrohm-Autolab, The Netherlands). For clarity the reference signal has been left out. Steps include activation with EDC/NHS (*1*), preconcentration and coupling of the protein (*2*), deactivation (*3*), and regeneration (*4*).

calculation (www.chemaxon.com) should be performed for small molecules. Finally, use the pH at approximately 80% of maximal ligand preconcentration, which is about 0.5 pH units below pI. If no electrostatic ligand preconcentration is apparent, aim at a different coupling technique or use **Section 3.5**.

3. Remove any electrostatically bound ligand from the surface with running buffer and a pulse of 50 mM HCl.

3.3. Coupling of a Protein Through EDC/NHS

1. During all steps record the SPR signal in real time. Always include a reference surface (*see* **Note 15**).
2. Wash the prepared surface with coupling buffer 1.
3. Defrost vials of EDC, NHS, and ethanolamine. Mix EDC and NHS 1:1 immediately for use. The fresh mixture of EDC–NHS can only be used for one activation round.
4. Immediately activate both, sample and reference surface with the EDC/NHS mixture in 5–10 min (*see* **Note 16**). Activation time can be used to regulate the amount of immobilized ligand.
5. Wash quickly but thoroughly with coupling buffer 1.
6. Introduce the ligand to the sample surface for 5–15 min (*see* **Note 17**) in a concentration of 10–200 μg/mL in coupling buffer 1, which will eventually present an analyte response as low, but accurate and reproducible, as possible (*see* **Notes 18**

and 19). The ligand concentration has to be established experimentally as the coupling efficiency is very dependent on its properties. A reasonable starting concentration is 10–50 μg/mL dependent on the size of the molecule. Large molecules (>100 kDa) will not penetrate very deep into the matrix and need a higher concentration.

7. Wash with coupling buffer 1.
8. The remaining NHS–ester groups are blocked with a primary amine like ethanolamine at slightly alkaline pH for 7 min (*see* **Note 20**).
9. Immediately after coupling, wash with a mild acidic regeneration fluid like 50–100 mM HCl. A complete coupling procedure can be seen in **Fig. 3.5** .
10. Switch the system to running buffer and introduce the analyte. Check the equilibrium signal level. If the binding capacity is too low repeat the coupling procedure with a higher concentration of ligand, and if too high load a new chip under milder conditions.
11. Perform interaction experiments with series of analyte concentrations in running buffer with the appropriate regeneration condition (*see* **Section 3.6**) (*see* **Notes 14, 21, and 22**). If the baseline after regeneration increases or analyte signal changes in subsequent binding experiments try another regeneration agent (*see* **Table 3.1** and **Note 23**).

3.4. Protein Coupling Through Reductive Amination Using the Aldehyde Group

1. Aldehyde coupling is an alternative procedure when amine or thiol coupling is insufficient (**Fig. 3.4**). Moreover, the procedure can be used with ligands containing sialic groups or *cis*-diols that can be easily oxidized to aldehydes with sodium metaperiodate.
2. Introduction of aldehydes in *cis*-diol-containing ligands. Make a cold solution of 1 mg/mL ligand in buffer 3. Add 10 mM sodium metaperiodate from a 50 mM fresh stock in previous buffer, or if a sialic acid needs oxidation use metaperiodate at 1 mM. To regulate the amount of aldehydes formed, the periodate concentration, the temperature, and contact time may be varied.
3. Keep on ice for 20 min.
4. Introduce on a desalting column and elute with buffer 4.
5. The level of oxidation should be checked on a hydrazide-activated surface (*see* below).
6. Prime the chip (*see* **Section 3.1**).
7. Activate both sample and reference surface with a 1:1 mixture of EDC/NHS for 3 min.

8. Wash with coupling buffer 1.
9. Add hydrazine or carbohydrazide in water at 5 mM for 7 min.
10. Wash with coupling buffer 1.
11. Deactivate both sample and reference surfaces with ethanolamine for 7 min.
12. Add 20–50 μg/mL ligand-containing aldehyde groups in coupling buffer 1 on the sample surface for 7 min (*see* **Note 18**).
13. Wash with coupling buffer 1.
14. Reduce excess aldehydes on both reference and sample surface by addition of 0.1 M sodium cyanoborohydride in buffer 4 for 20 min.
15. Wash with 50 mM HCl regeneration fluid.
16. Switch to running buffer and introduce the analyte. Check the binding capacity. If the signal is too low repeat the coupling procedure with a higher concentration of ligand, and in case of a too high signal, restart with a new chip under milder conditions.
17. Perform interaction experiments with series of analyte concentrations in running buffer with the appropriate regeneration condition (*see* **Section 3.6**) (*see* **Notes 14, 21, and 22**). If the baseline after regeneration increases or analyte signal changes in subsequent binding experiments try another regeneration agent (*see* **Table 3.1** and **Note 23**).

3.5. Coupling of a Small Molecule with Negative Charge

1. In this method the molecule to be immobilized is small and negatively charged and will not preconcentrate on the negative surface. To overcome the repulsion a high ionic strength can be used. Furthermore, the concentration of the ligand should be much higher (up to 5 mM), and the immobilization pH for the reaction with the ester must be increased to the optimal value of pH 8.0–8.3.
2. Wash the prepared surface with coupling buffer 2 (*see* **Section 2.1**).
3. Defrost vials of EDC, NHS, and ethanolamine. Mix EDC and NHS 1:1 immediately before use.
4. Immediately activate both sample and reference surfaces with the EDC/NHS mixture in 5–10 min.
5. Wash quickly but thoroughly with coupling buffer 2.
6. Add the ligand in coupling buffer 2 to the sample surface for 1–15 min in a concentration of 1–5 mM (*see* **Note 18**). The concentration and reaction time have to be established experimentally for each ligand. Start as low as possible.

7. Wash with coupling buffer 2.
8. Deactivate the remaining NHS esters on both sample and reference surfaces with ethanolamine for 7 min.
9. Wash with 50 mM HCl regeneration fluid.
10. Return to running buffer and introduce the analyte. Check the equilibrium response. If the signal is too low repeat the coupling procedure with a higher concentration of ligand, and if too high fit a new chip and restart under milder conditions.
11. Perform interaction experiments with series of analyte concentrations in running buffer with the appropriate regeneration condition (*see* **Section 3.6**) (*see* **Notes 14, 21, and 22**). If the baseline after regeneration increases or analyte signal changes in subsequent binding experiments try another regeneration agent (*see* **Table 3.1** and **Note 23**).

3.6. Sandwich Coupling: Streptavidin–Biotin Immobilization

1. Sandwich coupling is a type of indirect immobilization through site-specific capture molecules on the surface. Usually this method is preferred when the ligand is difficult to immobilize as a result of charge or activity. Of the possible methods the very strong interaction between streptavidin and a biotinylated molecule is preferred. Prior to immobilization the ligand of interest must be biotinylated. Commercial kits are sufficiently available. Be aware that the biotinylated ligand should be thoroughly purified from free non-reacted biotin. Use streptavidin-coated chips or prepare the surface as indicated below. An interesting application is given in **Chapter 4.**
2. Purchase streptavidin or avidin with a sufficiently high p*I* value. Establish preconcentration conditions (*see* step 2 of **Section 3.2**). Couple 20–200 μg/mL of streptavidin or avidin in low ionic coupling buffer (*see* **Section 3.3**), deactivate with ethanolamine, and regenerate the surface.
3. Prepare a 1–20 μg/mL solution of biotinylated ligand in a buffer. This buffer is non-critical as biotin interacts with streptavidin with a very high affinity. Bring this solution in contact with the surface for 1–30 min. Change contact time and concentration to control level of binding. Depending on the stoichiometry one or more binding sites will be occupied by the ligand. It is nearly impossible to break the interaction by regeneration.
4. Return to running buffer and introduce the analyte. Check the equilibrium response. If this is too low repeat the coupling procedure with a higher concentration of streptavidin, or use a new chip. If this also fails a commercial but more expensive streptavidin chip can be used.

5. Switch to interaction experiments with series of analyte concentrations in running buffer with the appropriate regeneration condition (*see* **Section 3.6**) (*see* **Notes 14, 21, and 22**). If the baseline after regeneration increases or analyte signal changes in subsequent binding experiments try another regeneration agent (*see* **Table 3.1** in **Section 2** and **Note 23**). Be aware that some harsh regeneration fluids may even break the streptavidin–biotin interaction (*see* **Section 3.7**).
6. Too harsh regeneration conditions may lower baseline levels and binding response due to a gradual loss of biotinylated ligand. A restoration of signal can be achieved by repeating step 3.

3.7. Optimizing the Regeneration Conditions

1. Most reversible interactions on a surface can be broken with standard regeneration solutions as indicated in **Table 3.1**. However, there are high-affinity interactions, sometimes consisting of additional multiple interactions of which some can be non-specific, that need more harsh conditions. The idea is to attack multiple binding forces with a cocktail of chemicals. Six stock solutions are prepared (*see* step 2 of **Section 2.3**).
2. After binding of a saturating amount of analyte the regeneration effect of one of the cocktails (**Table 3.2**) is measured (30 s pulse) and expressed as a percentage of maximal regeneration. This effect is noted as a change in baseline before and after a full analysis run. If the effect is poor try another cocktail. After the first series of tests the system can be optimized.
3. Compare the best three cocktails and their composition. Based on that evaluation take three of the best performing stock solutions and prepare from them new cocktails. If necessary, increase the levels of the best performing stock solution. Repeat the binding and regeneration cycles until the best solution is found. Check regularly for the integrity of the sensor surface.

4. Notes

1. Three choices for chip surfaces will be specified. The cheapest way is to build-up the surface on bare gold yourselves using proper chemical techniques. Biacore has a product line of carboxymethylated dextran surfaces of which the CM5 type is most commonly used (www.biacore.com).

Table 3.2
Several cocktail mixtures composed of regeneration solutions allowing to trace effectivity of surface regeneration (6). The mixtures consist of three equal volumes of stock solution(s) (*see* Section 2.3) and/or water. The capital letter indicates one volume of a regeneration stock solution, the letter w stands for a volume of water. Not all mixtures in the last two columns are considered optimal (precipitation or to aggressive)

Cocktail of different regeneration solutions				
Aww	BAw	IDw	ABI	AID
Bww	BDw	ICw	ABU	AIC
Iww	BCw	DUw	ABD	AUD
Uww	AIw	DCw	ABC	AUC
Dww	AUw	UCw	AIU	ADC
Cww	ADw			
	ACw			

Xantec manufactures a great number of different types of surfaces that are primarily used in cuvette-based instruments (www.xantec.com). These chips are larger, cheaper, and when properly refitted they can be activated several times, using different spots on the surface.

2. To get positive charges on the amino groups of the ligand the pH has to be 0.5–1 units below the isoelectric point of the ligand. To preserve the negative charge of the carboxyl groups on the sensor matrix, this pH should be above 4. The protein with the highest p*I* is the best choice for immobilization. Highly negatively charged ligands (p$I < 4$) cannot preconcentrate and need an adapted protocol (*see* **Section 3.5**).
3. The optimal reaction rate of the EDC/NHS chemistry proceeds around pH 8.5. Below pH 3.5 no reaction will take place. Due to this controversy between optimal reaction pH and required preconcentration, some molecules may be less effective to immobilize.
4. If sensitivity of the SPR instrument plays a role the largest molecule is preferred as the analyte. If however the ligand is a large protein, it is possible that only the most accessible activated esters at the outside of the matrix can be reached. In this case only a two-dimensional surface of proteins, or a heterogeneous surface is formed after immobilization

that downsizes the ultimate interaction response (*see* **Chapter 2**). For large ligands a low density surface is required.

5. Because often harsh regeneration conditions are required always couple the most stable compound on the chip.
6. The presence of lysine groups inside or in the vicinity of the binding pocket of the protein makes it unsuitable for coupling. There is a large chance that the binding site will be blocked or hampered, thus influencing binding constants. In those cases an alternative coupling procedure or the streptavidin–biotin system (*see* **Section 3.6**) is recommended. If that fails a chemical modification of the ligand should be considered. Many chemical applications (e.g., Invitrogen, Thermo Scientific) are available for coupling ligands specifically to compounds that have a group linkable to the surface. Examples are biotinylation, ABH (*p*-Azidobenzoyl hydrazide) for oxidized carbohydrates or APDP (*N*-[4-(*p*-Azidosalicylamido)butyl]-3'-(2'-pyridyldithio)propionamide) for sulfhydryl groups and introduction of a spacer arm.
7. MTL is not always avoidable. If for an interaction the association rate constant k_a is smaller than $\sim 10^5\ M^{-1}s^{-1}$, a lowering of the binding capacity may lead to an acceptable level of MTL and rebinding.
8. The possibility of cross-linking polymer chains via multiple lysines in protein ligands forming polymerized gels is minimized by low protein immobilization concentrations.
9. When considerable non-specific binding is observed use 0.05% Tween 20. Both salt and detergent assist in preventing non-specific binding. HEPES or MES buffers in 10–50 mM concentration are an excellent option, but phosphate or tris buffers may also be used. In special cases non-specific binding can be prevented by higher salt concentrations.
10. After priming the crucial factor is the activation with EDC. This water soluble hydrochloric salt is both hygroscopic and labile, and its instability is frequently the cause of a failed immobilization. Stock solutions of EDC should be immediately stored in small aliquots at –20°C and after defrosting rapidly 1:1 mixed with a NHS stock solution and instantly used for activation. In frozen condition EDC in water is reasonably stable, however, decomposition will rapidly increase at higher temperatures. In special tough coupling reactions which require higher EDC concentrations, freshly weighed dry material should be used. Store the supply of EDC under dry gas.

11. The type of available SPR instrument like that using a flow or a cuvette design may affect methods and conditions. Be sure that the methods specified here are suitable for your equipment. Not all systems have similar sensitivities. Use a machine with high enough sensitivity. In some machines small molecules can be used as analyte, in others a molecular weight of at least 5,000 Da is required. Long coupling or interaction times in some flow systems may consume a lot of (sometimes) valuable ligand or analyte, certainly when high concentrations are needed.
12. One should be aware of leakage from the measuring chamber into the surrounding apparatus. Leakage could seriously damage your system as a result of the high salt levels or other aggressive solutions. And by leakage your interaction responses may alter undetected leading to false binding data. In general, follow the advised procedures of the manufacturer.
13. SDS may be used in priming of the surface. The disadvantage of this choice is that SDS changes the constitution of the matrix by swelling. SDS is strongly adsorbed, is highly negatively charged, and the molecules are difficult to remove. Thus SDS influences preconcentration and coupling of the ligand to the surface carboxyls. Use maximal 0.5% and preferably in a short pulse of 10–15 s followed by a thorough wash with 50 mM glycine-HCl pH 8.5 for 10 min. In contrast, the use of 0.2% SDS in regeneration is mild but effective and maintains stable baselines during many cycles.
14. In standby periods leave the machine running in refreshment mode or with a low flow of running buffer. Consider that also in idle time between experiments, molecular build-up of buffer molecules will slowly increase baseline levels. This non-specific bound aggregate needs to be removed by regeneration before a new series of experiments can be started.
15. Always include a reference surface for immediate correction of artifacts like bulk refractive index changes, matrix and temperature effects, non-specific binding, and baseline drift. Only analyze reference subtracted responses.
16. The activation of the amine to an active ester takes place in approximately 10–30% efficiency. The deactivated esters cannot be reactivated anymore, but the remaining carboxyl groups may be reused for another round of immobilization. Up to three attempts can be made to activate the remaining free carboxyl groups on the surface, although with lower efficiency. Be aware that if the ligand contains

carboxyl groups the already immobilized ligand will participate in subsequent coupling reactions, which might affect affinity measurements and kinetics.

17. Ligand contact time varies with pH: at lower pH the reaction time is longer. Rarely more than 15 min are needed.
18. Depending on the sensitivity of the SPR instrument different levels of ligand should be immobilized. For good kinetic experiments the ligand capacity on the surface should be as low as possible to minimize mass transport, cross-linking, overcrowding, or aggregation. Low signal data with random noise can still be analyzed sufficiently accurate by global kinetic analysis (8; Scrubber 2, BioLogic Software).
19. Amine coupling takes place at primary amines. In proteins this usually is the N-terminal amino group; however, also the less active lysine groups are sensitive to the chemistry. If more amine groups are present, immobilization is a random process, which might affect affinity behavior of part of the attached ligand molecules (surface heterogeneity).
20. Not all active NHS esters react with a ligand and it is therefore crucial to eliminate unreacted esters by deactivation, else they could attack amino groups in buffer or analyte during the interaction experiment. The deactivation step with a high concentration of ethanolamine changes the active ester into an inactive hydroxyethyl amide (*see* step 3 of **Fig. 3.4**).
21. Immediately after coupling, perform a number of test runs with the analyte in a single concentration to check for quality and reproducibility of the SPR-binding responses. Always conduct control experiments at regular time intervals during analyte analysis. Check for baseline drift. Check regularly for the reproducibility of the maximal binding capacity. As a rule the maximum binding capacity gradually decreases during multiple cycles. Apply replicates in randomized order. Include a blank running buffer measurement.
22. Immediately after coupling at least five regeneration cycles with the regeneration solution of choice are pivotal to equilibrate the surface. From that point measurements will yield more consistent binding constants.
23. Regeneration effectiveness depends highly on the stability and physicochemical properties of the coupled ligand, however, a good first approach is to follow the next steps: increase acidity (to 100 mM HCl), add glycine (0.01–0.1 M) or a mild base (from 10 to 50 mM NaOH), or add 0.2–0.5% of a detergent like SDS (sodium

dodecyl sulfate) to the acid or base solutions. SDS changes the swelling of the matrix and thus the baseline, but is a good interaction breaker. Stronger agents can be tested if this fails. Utilize all regeneration reagents in short pulses of 10–60 s, followed by washes with running buffer. Depending on the effectiveness of the regeneration and the stability of the ligand, complete binding cycles may be repeated at least over 200 times.

References

1. de Mol, N. J., Fischer, M. J. E., Castrop, J., and Frelink, T. (2006) Determination by surface plasmon resonance of the binding characteristics of a kinase and its substrates. *Biomol. Interactions* **18**, 19–22.
2. Cooper, M. A. (2003) Label-free screening of bio-molecular interactions. *Anal. Bioanal. Chem.* **377**, 834–42.
3. Gedig, E. T. (2008) Surface chemistry in SPR technology. In Schasfoort R. B. M. and Tudos A. J. (Eds.) *Handbook of Surface Plasmon Resonance*. pp. 173–220, RSC Publishing, Cambridge.
4. Rich, R. L., and Myszka, D. G. (2000) Advances in surface plasmon resonance biosensor analysis. *Curr. Opin. Biotech.* **11**, 54–61.
5. de Mol, N. J., Plomp, E., Fischer, M. J. E., and Ruijtenbeek, R. (2000) Kinetic analysis of the mass transport limited interaction between the tyrosine kinase lck SH2 domain and a phosphorylated peptide studied by a new cuvette based surface Plasmon resonance instrument. *Anal. Biochem.* **279**, 61–70.
6. Andersson, K., Areskoug, D., and Hardenborg, E. (1999) Exploring buffer space for molecular interactions. *J. Mol. Recognit.* **12**, 310–15.
7. Myszka, D. G. (1999) Improving biosensor analysis. *J. Mol. Recognit.* **12**, 279–84.
8. Myszka, D. G., and Morton, T. A. (1998) Clamp: a biosensor kinetic data analysis program. *TIBS* **23**, 149–150.

Chapter 4

High-Affinity Immobilization of Proteins Using Biotin- and GST-Based Coupling Strategies

Stephanie Q. Hutsell, Randall J. Kimple, David P. Siderovski, Francis S. Willard, and Adam J. Kimple

Abstract

Surface plasmon resonance (SPR) is a highly sensitive method for the detection of molecular interactions. One interacting partner is immobilized on the sensor chip surface while the other is injected across the sensor surface. This chapter focuses on high-affinity immobilization of protein substrates for affinity and kinetic analyses using biotin/streptavidin interaction and GST/anti-GST-antibody interaction.

Key words: BIAcore 3000, biotin, streptavidin, GST, high-affinity immobilization, SPR.

1. Introduction

By immobilizing a protein on a sensor chip surface, one can take advantage of the optical phenomenon known as surface plasmon resonance (SPR) to observe molecular interactions in real time. Accordingly, SPR can be used to determine rate and affinity constants for interactions involving proteins, nucleic acids, carbohydrates, lipids, or small molecules (1–3). This chapter will focus on the high-affinity immobilization of protein and peptide ligands to a sensor chip surface. This can be accomplished by a number of different approaches including direct amine coupling, antibody capture, and biotin/streptavidin affinity among others (4–7). The semiautomated nature of SPR biosensor operations, the low consumption of reagents, and the capacity to produce quantitative data about macromolecular interactions make this method

N.J. de Mol, M.J.E. Fischer (eds.), *Surface Plasmon Resonance*, Methods in Molecular Biology 627,
DOI 10.1007/978-1-60761-670-2_4,

preferable to traditional approaches like pulldown assays, analytical chromatography, or isothermal titration calorimetry (ITC) (*see* **Note 1**).

One approach to high-affinity immobilization is the covalent linkage of an anti-glutathione *S*-transferase (GST) antibody to the sensor chip surface (**Fig. 4.1**). Recombinant proteins fused with GST are readily immobilized on a sensor chip surface through the GST/anti-GST antibody interaction (**Figs. 4.2 and 4.3**). Cloning, expression, and purification of GST chimeric proteins are relatively straightforward. Commercial vectors available for the expression of GST-fusion proteins include pGEX (GE Healthcare), pAB-GST (AB Vector), and pAcG (BD Bioscience). The advantage of this approach is that the antibody serves as a universal adapter, permitting the capture of all GST-fusion proteins on the sensor chip surface. As the antibody is covalently bound to the sensor chip, the anti-GST surface can be regenerated many times and coated with different GST-fusion constructs. Regeneration is accomplished by injecting a glycine-HCl solution at pH 2.2 over the sensor chip surface. As the antibody is covalently bound to the surface, it does not dissociate upon exposure to glycine-HCl pH 2.2 solution, but the GST/anti-GST antibody interaction is disrupted, and thus the chip can be subsequently loaded with a new GST-fusion protein. While the overall output signal strength is lower than other protein immobilization techniques, the anti-GST sensor chip surface can be regenerated upward of

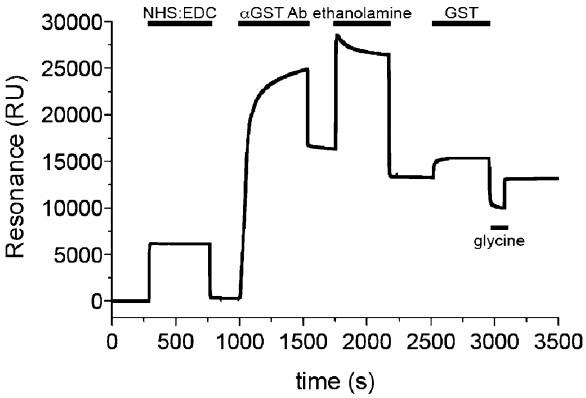

Fig. 4.1. A typical single flow cell sensorgram generated during the loading of anti-GST antibody. The flow cell surface was activated for direct amine coupling of the anti-GST antibody (αGST-Ab) by injecting the coupling solution (40 μL NHS/EDC at 5 μL/min flow rate with EXTRACLEAN command). Anti-GST antibody was then diluted to 30 μg/mL in immobilization buffer and 45 μL were injected at 5 μL/min flow rate, omitting the EXTRACLEAN command. To deactivate esters on the sensor chip surface, ethanolamine was injected (35 μL at 5 μL/min flow rate with EXTRACLEAN command). To test the binding surface, supplied recombinant GST protein was diluted to 5 μg/mL and 100 μL were injected over the sensor chip at 20 μL/min flow rate. To remove GST from the binding surface, 40 μL of glycine-HCl pH 2.2 was injected at 20 μL/min flow rate.

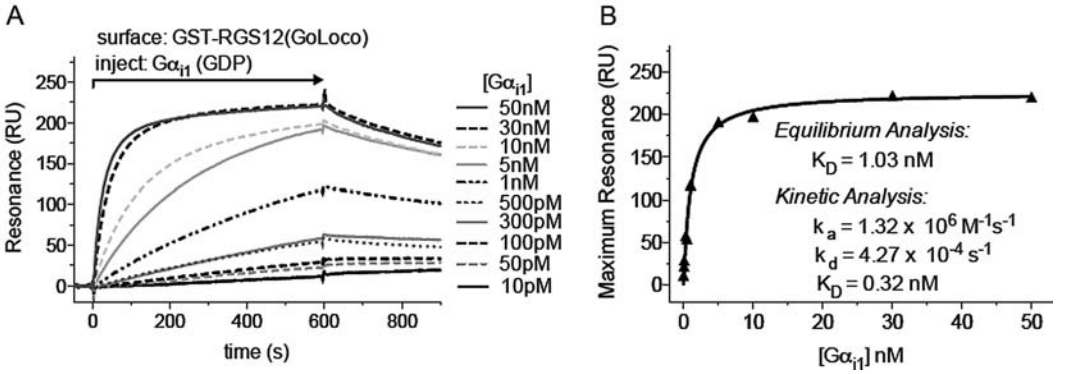

Fig. 4.2. Affinity and kinetic measurements using an anti-GST antibody CM5 sensor chip. (**a**) Flow cells 1 and 2 were loaded with 1,000 RUs of GST and GST-RGS12GoLoco proteins, respectively. Increasing concentrations of $G\alpha_{i1}$ were injected using the KINJECT command (300 μL injections with a 200 s dissociation phase at 20 μL/min flow rate). Specific binding was determined by subtracting nonspecific binding to a GST control flow cell from the GST-RGS12GoLoco response curve. (**b**) Binding affinities were determined by plotting the maximum response attained at each concentration of $G\alpha_{i1}$ versus the concentration of the $G\alpha_{i1}$, then by fitting to a Langmuir binding isotherm using GraphPad Prism 5.0 (GraphPad Software, La Jolla, CA) to determine dissociation constant (K_D). Kinetic analyses of the association (k_a) and dissociation (k_d) rates were also used to determine K_D using the simultaneous k_a/k_d (1:1 Langmuir) model (BIAevaluation). Differences in K_D determination between kinetic and equilibrium analyses are likely to reflect mass transport and/or rebinding limitations to binding assay execution, as indicated by large k_a values, nearly linear initial association seen on sensorgrams, and/or greatly slowed dissociation (*see* **Chapter 2** by Peter Schuck and Huaying Zhao, this volume for further information).

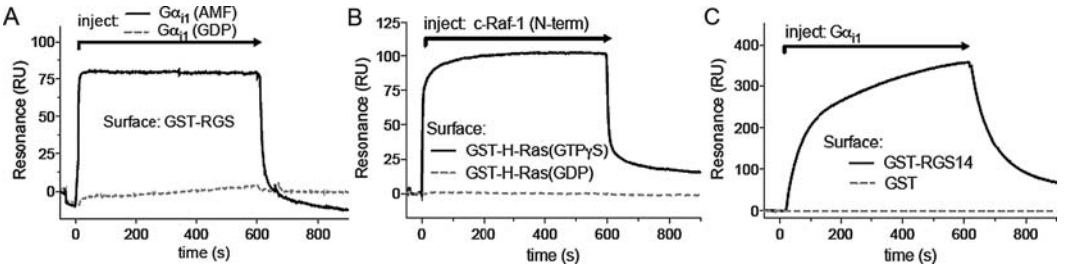

Fig. 4.3. Diverse applications of an anti-GST CM5 sensor chip. (**a**) A GST-RGS fusion protein was immobilized on the surface of flow cell 1 and GST was immobilized on the surface of flow cell 2 (the latter surface is used to subtract sensorgram changes in resonance due to buffer shifts). $G\alpha_{i1}$ pre-incubated with either GDP or GDP+Mg^{2+}+AlF_4^- (AMF), a transition-state mimetic form known to bind avidly to RGS proteins, was injected over the sensor surface. GST-RGS bound to the $G\alpha_{i1}$(AMF) but not $G\alpha_{i1}$(GDP) as expected. (**b**) GST-H-Ras loaded with a non-hydrolyzable GTP analogue, GTPγS, was loaded in flow cell 1, GST-H-Ras loaded with GDP was loaded in flow cell 2, and GST control was loaded in flow cell 3. An N-terminal construct of c-Raf-1, a known H-Ras-binding partner, was injected across the sensor chip surface. The data show the nucleotide state selectivity of the H-Ras/c-Raf-1 interaction. (**c**) GST-RGS14 was loaded in flow cell 1 and GST was loaded in flow cell 2. $G\alpha_{i1}$ was injected in GDP+Mg^{2+}+AlF_4^- (AMF) running buffer over the sensor chip surface and a $G\alpha_{i1}$/RGS14-specific interaction was detected. Specific binding for all injections was determined by subtracting the nonspecific binding observed from a GST control flow cell from the experiment containing flow cells.

200 times with different GST-fused proteins, facilitating multiple types of experiments on a single anti-GST antibody-derivatized chip.

The biotin/streptavidin interaction is another high-affinity, non-covalent (8, 9) method to immobilize substrate to the sensor chip surface. Because of the low dissociation constant associated with the interaction (approximately 10^{-15} M (10)), biotinylated substrates are almost irreversibly bound to the sensor chip surface. Protein biotinylation can be performed in vivo or in vitro and can be verified by western blot (**Fig. 4.4**). Biotinylation can occur concomitantly with protein expression in bacteria by co-transfection of biotin ligase and a vector construct coding for the protein of interest fused to a biotin ligase substrate sequence (G L N D I F E A Q K I E W H E) (11). Alternatively, purified recombinant protein from bacterial, insect, or mammalian expression, with a biotin ligase substrate sequence, can be biotinylated post-purification by incubation with biotin ligase in vitro (Avidity, Aurora, CO) (6, 12). Biotinylated proteins can be directly

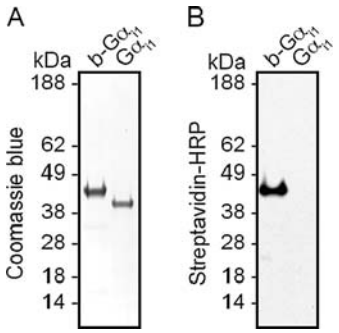

Fig. 4.4. Confirmation of biotinylated protein production. (**a**) SDS-PAGE gel stained with Coomassie blue dye reveals the migration of biotinylated Gα_{i1}, designated b-Gα_{i1}, and unlabeled Gα_{i1}. (**b**) Immunoblot of SDS-PAGE gel transferred to nitrocellulose using streptavidin horseradish peroxidase antibody to detect biotinylated protein.

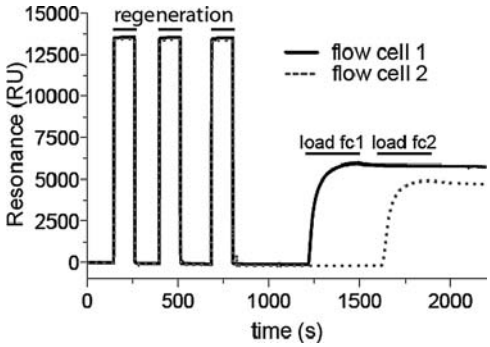

Fig. 4.5. Loading Streptavidin (SA) Sensor Chip. A typical sensorgram generated during the loading of biotinylated protein to flow cells 1 and 2. The flow cell surface was stabilized with 3 $\times$ 20 μL injections of regeneration buffer before loading of biotinylated Gα_{i1} (260 nM final concentration, as diluted in biotin-conjugate immobilization buffer), one flow cell at a time, until saturation is observed (note plateau in sensorgram *curves*).

immobilized on commercially available streptavidin-coated sensor chips (**Fig. 4.5**). To further facilitate the study of molecular interactions, biotinylated peptides can be synthesized (4, 5). Protein/nucleic acid interactions can also be probed using SPR when biotinylated oligonucleotides are immobilized on the sensor chip surface (13) (most oligonucleotide vendors offer biotin as a modification). Advantages of this approach include the assurance that all immobilized molecules will be in the same orientation and that a high substrate density can be achieved using commercially available streptavidin sensor chips. Additionally

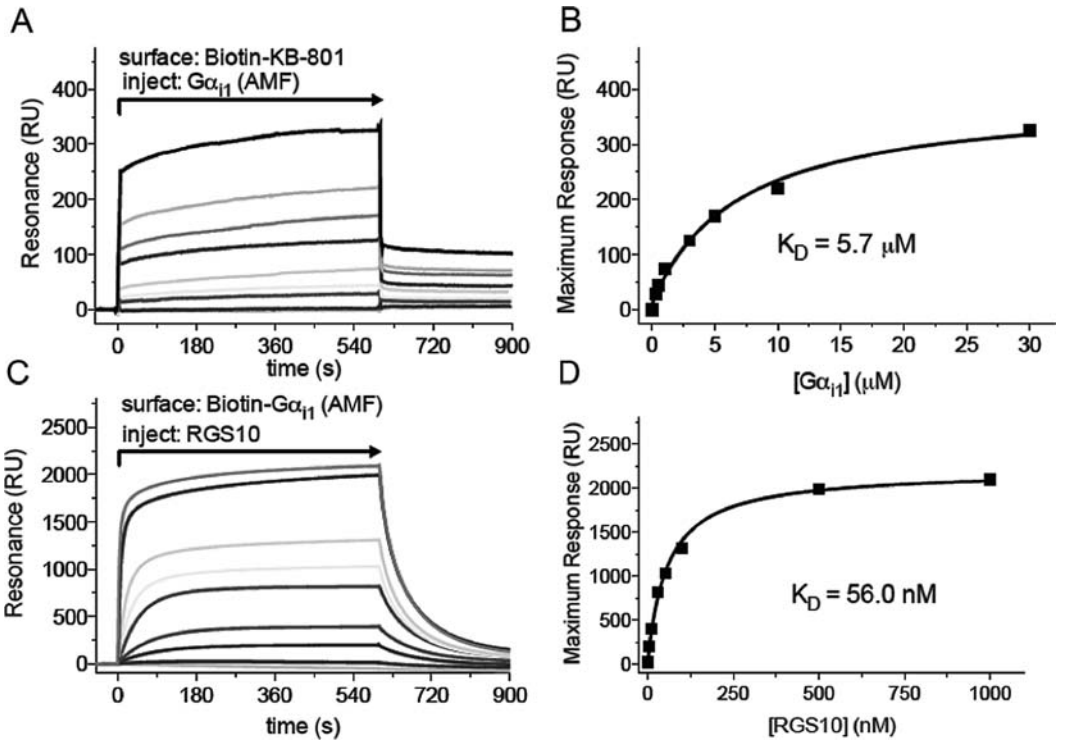

Fig. 4.6. Affinity measurements using a SA sensor chip. (**a**) Flow cell 1 was loaded with 450 RUs of biotin-KB-801 peptide, and flow cell 2 was loaded with 350 RUs mNotch peptide as a control. Increasing concentrations of $G\alpha_{i1}$ in $GDP+Mg^{2+}+AlF_4^-$ (AMF) buffer, the transition-state mimetic form, were injected over the sensor surface as indicated, using the KINJECT command (300 μL injections with a 200 s dissociation phase at 20 μL/min flow rate). *Binding curves* were obtained by subtracting nonspecific binding to a noninteracting biotinylated peptide from all experiment-containing flow cells. (**b**) Binding affinities were determined by plotting the maximum response attained at each concentration of $G\alpha_{i1}$ versus the concentration of the $G\alpha_{i1}$, then by fitting to a rectangular hyperbola to determine K_D using GraphPad Prism 5.0 (Graphpad Software, La Jolla, CA). (**c**) Flow cell 1 was loaded with 450 RUs of biotin-$G\alpha_{i1}$, and flow cell 2 was loaded with an equivalent RU signal of denatured biotin-$G\alpha_{i1}$. Varying concentrations of RGS10 in $GDP+Mg^{2+}+AlF_4^-$ (AMF) buffer were injected over the sensor surface as indicated, using the KINJECT command (300 μL injections with a 200 s dissociation phase at 20 μL/min flow rate). Specific binding was determined by subtracting nonspecific binding from a flow cell containing denatured biotin-$G\alpha_{i1}$. (**d**) Binding affinities were determined by plotting the maximum response attained at each concentration of RGS10 versus the concentration of the RGS10, then by fitting to a rectangular hyperbola to determine K_D using GraphPad Prism 5.0 (GraphPad Software, La Jolla, CA). These final panels were reproduced from Soundararajan et al. (7). Copyright (c) 2008 National Academy of Sciences, USA.

use of biotin/streptavidin immobilization offers the ability to use harsher regeneration conditions (e.g., 1 M urea) than the GST/anti-GST antibody surfaces – so long as the biotinylated moiety (protein, peptide, DNA oligo, etc.) also survives the regeneration without losing its capacity for binding to analyte.

We have used both of these methods with great success in a number of protein–protein interaction studies (*see* **Note 2**) (4–7, 12, 14) (**Figs. 4.2, 4.3, and 4.6**).

2. Materials

2.1. GST-Fusion Protein Production

1. 6 × 1 L Luria broth prepared and autoclaved in baffled 2,800-mL flasks, then supplemented with ampicillin (50 μg/mL final concentration).
2. 6 mL 1 M IPTG (isopropyl-beta-D-thiogalactopyranoside) stock solution (Arcos Organics, New Jersey).
3. 200 mL of a BL21(DE3) *Escherichia coli* overnight culture transformed with desired vector construct (GeneChoice, Frederick, MD).
4. Beckman J-6 Centrifuge.
5. Beckman LM-8 Ultracentrifuge.
6. High-pressure homogenizer (Emulsiflex, Avestin).
7. Akta FPLC (GE Healthcare).
8. HiTrap Glutathione Sepharose-4B Fast Flow (GSTrap) column (GE Healthcare).
9. Sephacryl S200 HR column (GE Healthcare).
10. Vivaspin 20 ultrafiltration spin column (Sartorius Stedim Biotech, Goettingen Germany) with an appropriate molecular weight cutoff for retention of desired protein during filtration/concentration.

2.2. GST-Protein Immobilization via Antibody

1. Running buffer: 10 mM HEPES pH 7.5, 150 mM NaCl, 3 mM EDTA, 0.0005% (v/v) NP-40 alternative (Calbiochem, La Jolla, CA). Filtered with 0.2 μm polystyrene bottle-top filter and degassed by allowing the vacuum to continue for 10 min after filtering is complete. Agitation may be required to release air bubbles from vessel walls.
2. 10 mM Glycine-HCl pH 2.2 (included in GST Capture Kit).
3. Buffer A: 50 mM Tris-HCl pH 7.5, 100 mM NaCl, 1 mM dithiothreitol, 5% (w/v) glycerol.

4. Buffer B: 50 mM Tris-HCl pH 7.5, 100 mM NaCl, 10 mM reduced glutathione, 1 mM dithiothreitol, 5% (w/v) glycerol.
5. S200 buffer: 50 mM Tris-HCl pH 8.0, 250 mM NaCl, 5 mM dithiothreitol, 2.5% (w/v) glycerol.
6. GST Capture Kit (GE Healthcare (15)): goat anti-GST antibody 0.8 mg/mL in 0.15 M NaCl, recombinant GST 0.2 mg/mL in 10 mM HEPES pH 7.4, 0.15 M NaCl, 3 mM EDTA, 0.005% Surfactant P20, immobilization buffer (10 mM sodium acetate pH 5.0), regeneration solution (10 mM glycine-HCl pH 2.2).
7. Sensor Chip CM5 (GE Heathcare).
8. Amine Coupling Kit (GE Healthcare): 750 mg 1-ethyl-3-(3 dimethylaminopropyl)carbodiimide hydrochloride (EDC) resuspended in water to 0.2 M concentration, 115 mg *N*-hydroxysuccinimide (NHS) resuspended in water to 0.05 M, 10.5 mL 1.0 M ethanolamine-HCl pH 8.5.

2.3. Binding Assay

1. GST-fusion protein (*see* **Section 2.1**).
2. 10 mM Glycine-HCl pH 2.2 (included in GST Capture Kit).

2.4. Biotin-Conjugated Protein Production

1. 6 × 1 L Luria broth prepared and autoclaved in baffled 2,800-mL flasks, then supplemented with ampicillin (50 μg/mL) and chloramphenicol (10 μg/mL final concentration).
2. 6 ml of 1 M IPTG (isopropyl-beta-D-thiogalactopyranoside) stock solution (Arcos Organics, New Jersey).
3. 50 mM D-Biotin (Sigma) dissolved in ethanol. Add 1 mL to each flask for a 50 μM final concentration.
4. B strain *(hsdR, lon11, sulA1) E. coli* transformed with chloramphenicol-resistance plasmid expressing biotin ligase BirA (Avidity, Aurora, Colorado).
5. Beckman J-6 Centrifuge.
6. Beckman LM-8 Ultracentrifuge.
7. High-pressure homogenizer (Emulsiflex, Avestin).
8. Akta FPLC (GE Healthcare).
9. Buffer N1: 50 mM HEPES pH 7.5, 400 mM NaCl, 30 mM imidazole, 5% (w/v) glycerol.
10. Buffer N2: 50 mM HEPES pH 7.5, 400 mM NaCl, 1 M imidazole, 5% (w/v) glycerol.

11. S200 Buffer: 10 mM HEPES pH 7.5, 300 mM NaCl, 5 mM dithiothreitol, 5% (w/v) glycerol.
12. HisTrap Fast Flow column (GE Healthcare).
13. Sephacryl S200 HR column (GE Healthcare).
14. Vivaspin 20 ultrafiltration spin column (Sartorius Stedim Biotech, Goettingen Germany) with an appropriate molecular weight cutoff for desired protein.

2.5. Biotinylation Verification

1. Laemmli loading buffer (2×) (Sigma).
2. TBS-T buffer – Tris buffered saline (Sigma) with 0.1% v/v Tween 20 (Fisher).
3. Blocking buffer – 5% w/v powdered non-fat milk in TBS-T.
4. 1:10,000 dilution (in blocking buffer) of stock streptavidin horseradish peroxidase (SA-HRP; GE Healthcare).
5. Polyacrylamide denaturing gel. We routinely use NuPAGE Bis-Tris 4–12% gradient gels (Invitrogen).
6. Polyacrylamide gel electrophoresis apparatus and Coomassie stain.
7. MES buffer for electrophoresis: (50 mM Tris base, 50 mM 3–(*N*–Morpholino)propanesulfonic acid, 1 mM EDTA, 0.01% SDS at pH 7.3).
8. See Blue molecular weight marker (Invitrogen).
9. Western blot transfer apparatus (homemade).
10. ECL Plus Chemiluminescence Detection Kit (GE Healthcare).

2.6. Streptavidin Immobilization and Binding Assay

1. Biotin-conjugate immobilization buffer: 10 mM HEPES pH 7.5, 150 mM NaCl, 3 mM EDTA, 0.0005% (v/v) NP-40 alternative (Calbiochem La Jolla, CA). Filtered with 0.2 μm polystyrene bottle-top filter and degassed by allowing the vacuum to continue for 10 min after filtering is complete. Agitation may be required to release air bubbles from vessel walls.
2. Regeneration buffer: 1 M NaCl, 50 mM NaOH.
3. Sensor Chip SA (GE Healthcare).
4. Running buffer: 10 mM HEPES pH 7.4, 150 mM NaCl, 50 μM EDTA, 100 μM GDP, 0.0005% (v/v) NP-40 alternative (Calbiochem) (*see* **Note 3**). Filtered with 0.2 μm polystyrene bottle-top filter and degassed by allowing the vacuum to continue for 10 min after filtering is complete. Agitation may be required to release air bubbles from vessel walls.

3. Methods

The carboxymethylated dextran surface is highly negatively charged, and it is therefore difficult to immobilize proteins with a significant negative charge. CM4 sensor chips with a lower degree of carboxymethylation are available, and are better suited for the immobilization of such proteins. Quantitative analysis of binding data using saturation binding or kinetic methods requires specific binding to be measured. To determine specific binding, we usually perform background subtraction with an appropriate control for nonspecific binding. For biotin–streptavidin experiments, we usually use denatured protein or an irrelevant biotinylated peptide. For GST experiments, we use GST alone or an irrelevant GST-fusion protein. As controls for protein–protein interaction specificity, we often employ the use of proteins with loss-of-function mutations. This can provide definitive supporting evidence as to the specificity of molecular interactions being tested (16, 17) (*see* **Note 4**).

3.1. GST-Fusion Protein Production

1. Inoculate 6 × 1 L Luria broth (containing antibiotic) with *E. coli* transformed with protein expression construct.
2. Culture at 37°C while shaking at 210 rpm.
3. Reduce temperature to 20°C after the optical density of the culture OD600 reaches 1.0.
4. Induce protein expression with IPTG (500 μM final concentration) and culture 14 h at 20°C while shaking at 210 rpm.
5. Harvest cells by centrifugation at 10,000*g* for 10 min and resuspend in 25 mL buffer A.
6. Lyse cells using a high-pressure homogenizer at 10,000 psi.
7. Clarify lysate by ultracentrifugation for 45 min at 160,000*g*.
8. Purify by GST affinity chromatography. We use an Akta FPLC. Load clarified lysate onto 5 mL GSTrap column. Unbound protein is washed through the column with five column volumes of buffer A. GST-fusion protein is eluted from the column with five column volumes of buffer B. Fractions containing GST-fusion protein are pooled and subjected to size exclusion chromatography using a Sephacryl S200 HR column. Monodisperse protein is eluted in S200 buffer, concentrated using a VivaSpin 20 ultrafiltration spin column at 4°C 3,000*g*, and stored at –80°C.

3.2. GST Immobilization via Antibody

Based on BIAcore GST Capture Kit Instructions for Use (15).

1. Dock CM5 sensor chip.
2. PRIME system with running buffer.

3. Start sensorgram flow cells 1–4.
4. Mix 100 μL of 0.05 M *N*-hydroxysuccinimide (NHS) from Amine Coupling Kit with 100 μL of 0.2 M 1-ethyl-3-[3-dimethylaminopropyl]carbodiimide hydrochloride (EDC) from Amine Coupling Kit and INJECT 40 μL of resultant mixture with EXTRACLEAN at 5 μL/min flow rate.
5. Dilute anti-GST antibody (from GST Capture Kit) (*see* **Note 5**) in immobilization buffer, also from kit, to 30 μg/mL. We dilute 3 μL of antibody in 70 μL immobilization buffer. INJECT 45 μL at 5 μL/min, as this is sufficient antibody to derive all four flow cells. Do not select the EXTRACLEAN command **(***see* **Note 6).**
6. INJECT (with EXTRACLEAN) 35 μL ethanolamine from Amine Coupling Kit at 5 μL/min flow rate.
7. Flow running buffer at 20 μL/min.

To check the capacity of the newly created anti-GST antibody chip to bind GST, perform the following steps:

1. Dilute recombinant GST (from the GST Capture Kit) to 5 μg/mL in running buffer.
2. INJECT 100 μL of diluted GST over the anti-GST antibody surface at 20 μL/min flow rate across all flow cells. The equilibrium saturation value provides a measure of the surface capacity of individual flow cells chip. A freshly prepared sensor chip surface will load ~2,000 RUs of GST (**Fig. 4.1**) (*see* **Note 7**).
3. Regenerate surface with a 40 μL glycine-HCl pH 2.2 injection at a flow rate of 20 μL/min across all flow cells.

3.3. Immobilized GST-Fusion Protein-Based Binding Assay

1. Load sensor chip surface by using MANUAL INJECT command to inject GST-fusion protein over desired flow cell(s). 500 nM is a good starting concentration for the gradual loading of protein to the sensor chip surface; using the MANUAL INJECT command will allow for repeating stopping and restarting of protein injection until desired level of binding is achieved.
2. If loading flow cells independently, load the same molar amounts of protein to the surface of each flow cell; if the proteins are of a similar molecular weight, this will result in loading the same number of RUs to each flow cell.
3. The surface is now ready for the injection of analyte. This should be done using the KINJECT command. Begin with an injection of buffer as a control, then proceed with increasingly more concentrated injections of analyte. (*See*

Note 8 for considerations about when regeneration might be required) (**Figs. 4.2 and 4.3**).

4. To dissociate GST-fusion proteins from the antibody surface, inject 40 μL glycine-HCl pH 2.2 at flow rate of 20 μL/min across all flow cells. As the anti-GST antibody is covalently attached, this regeneration procedure does not negatively affect the ability to bind another round of injected GST-fusion proteins.

3.4. Biotin-Conjugated Protein Production

1. Inoculate 6 × 1 L of sterile Luria broth containing ampicillin (50 μg/mL final concentration) and chloramphenicol (10 μg/mL final concentration) with *E. coli* transformed with BirA and protein expression construct sub-cloned with a biotin ligase targeting sequence.
2. Culture at 37°C while shaking at 210 rpm.
3. Reduce temperature to 20°C when the culture attains an optical density OD600 of 1.0.
4. Induce protein expression with IPTG (500 μM final concentration), add D-biotin solution (50 μM final concentration), and culture for 14 h at 20°C while shaking at 210 rpm.
5. Harvest cells by centrifugation at 10,000*g* for 10 min and resuspend in 25 mL buffer N1.
6. Lyse cells using a high-pressure homogenizer at 10,000 psi.
7. Clarify lysate by ultracentrifugation for 45 min at 160,000*g*.
8. Purify by affinity chromatography. Our expression vectors for biotinylating proteins also contain an N-terminal hexahistidine tag, which demonstrates affinity for charged nickel, and thus the biotinylated proteins are purified by a nickel chelating column (HisTrap). We use an Akta FPLC (GE Healthcare). Load lysate onto a 5 ml HisTrap column. Unbound protein is washed through the column with five column volumes of buffer N1. His-fusion protein is eluted from the column with sequential steps of 3% then 30% buffer N2 in five column volumes each. Fractions containing His-fusion protein are pooled and subjected to size exclusion chromatography using a Sephacryl S200 HR column. Monodisperse protein is eluted in S200 buffer concentrated using a VivaSpin 20 ultrafiltration spin column at 4°C and 3,000*g*, and stored in aliquots at –80°C.

3.5. Biotinylation Verification

1. In separate tubes, add 2 μg of biotinylated protein and 2 μg of a non-biotinylated control protein to 40 μL of 2X Laemelli loading buffer and boil for 5 min.
2. Load a 12-well denaturing gel as follows: lane 1 – markers, lane 2 – biotin-protein, lane 3 – control protein, lanes 4–5

blank, lane 6 – markers, lane 7 – biotin-protein, lane 8 – control protein, lanes 9–12 blank.

3. Following completion of gel electrophoresis, cut the gel vertically along lane 5.
4. Stain lanes 1–5 with Coomassie brilliant blue dye. This is a positive control to verify equivalent protein loading.
5. Transfer the lanes 5–12 onto a nitrocellulose membrane using a standard electroblotting transfer technique.
6. After the completion of the transfer, wash the nitrocellulose membrane three times in TBS-T.
7. At room temperature, soak the membrane in blocking buffer with gentle rocking for 1 h.
8. Wash 3X with TBS-T.
9. Dilute enough SA-HRP in TBS-T/milk solution (1 μL SA-HRP to 2.5 mL TBS-T/milk solution) to cover the entire blot and incubate with rocking for 1 h at room temperature.
10. Wash 3X with TBS-T
11. Detect the presence of SA-HRP using chemiluminescence (**Fig. 4.4**).

3.6. Streptavidin Immobilization and Binding Assay

1. Stabilize the sensor chip surface with multiple injections (usually three or more) of regeneration buffer at a flow rate of 20 μL/min (*see* **Note 9**).
2. Maintain a 5 μL/min flow rate and, one flow cell at a time using the MANUAL INJECT command, inject biotinylated protein (**Fig. 4.5**, *see* **Note 10**).
3. The negative control used to subtract buffer shifts should be a biotinylated protein/peptide relevant to the experiment. For Gα subunits, we often use a biotinylated Gα that is denatured on the surface by performing 4 × 20 μL injections of regeneration buffer post-immobilization.
4. Once the binding surface has been established, multiple rounds of injections of analyte can be performed (**Fig. 4.6**, *see* **Note 11**). These injections can be automated as follows (GST-fusion protein is used as an example).

4. Notes

1. We have frequently observed that protein–protein interactions described in the literature using affinity-pulldowns with purified proteins cannot be reproduced using SPR. A

Command	Explanation
DEFINE APROG galpha	//a unique name for this block
PARAM %position	//defines "position" is the only variable
FLOW 20	//sets the flow rate (units μL/min)
FLOWPATH 1,2,3,4	//can be modified to inject only two flow cells
KINJECT %position 200 300	//performs a stabilized injection, 200 μL volume and 300 s dissociation time
END	
DEFINE APROG loadGST	//specifies what to load to sensor chip surface
FLOW 5	
FLOWPATH 1,2	//specifies flow cells to load
INJECT R2F3 15	//specifies position to retrieve GST from stock tube and amount (in μL)
EXTRACLEAN	
END	
DEFINE APROG loadGSTfusion	//specifies what to load to sensor chip
FLOW 5	
FLOWPATH 3,4	
INJECT R2F4 20	//specifies position to retrieve GST-fusion protein and amount (in μL)
EXTRACLEAN	
END	
DEFINE APROG glycine	//specifies removal of GST/GST-fusion from antibody surface
FLOW 20	
FLOWPATH 1,2,3,4	
INJECT R2F6 40	
EXTRACLEAN	
END	
MAIN	
RACK 1 THERMO_C	//specifies which thermal block is to be found in the rack positions
RACK 2 THERMO_A	
RACK R Reag_A	
DETECTION 1,2,3,4	
APROG loadGST	//loads a GST control
APROG loadGSTfusion	//loads the experiment
APROG galpha R2A1	//injection of 200 μL of the sample in rack position R2A1
APROG glycine	//regenerates the binding surface
APPEND Standby	
END	//puts the machine in standby mode

major reason for this discrepancy is that artifactual binding interactions are observed in affinity-pulldown experiments when impure and aggregated protein preparations are used,

and nonquantitative analysis is performed. Thus it is most effective to do experiments with homogenous purified protein samples. Moreover, investigators should not be overly discouraged at their inability to replicate published literature based on affinity-pulldown experiments.

2. From our experience, the BIAcore 3000 does not provide reproducible data in the presence of moderate to high concentrations of DMSO (>0.1%). Therefore, this system does not provide a robust approach to determine the effects on protein–protein interactions of low affinity (K_D > 1 μM) small molecule inhibitors that are often dissolved in DMSO.
3. The addition of GDP is specific to studying heterotrimeric Gα subunits and may not be needed for studying other protein families.
4. A large component of observed resonance changes upon analyte injection can be due to "buffer shifts." This is due to altering the refractive index of the liquid at the sensor surface (18) and should not be misconstrued as specific binding. If identical running and analyte buffers are used, no "buffer shift" is observed. Buffer shift is typically removed by background subtraction as described in **Section 3**. To avoid buffer shift, we advise preparing analytes directly in the running buffer for the experiment, or at high enough stock concentrations that dilution removes the majority of "buffer shift."
5. We have attempted to use other GST-antibodies from other vendors and have found them to not be amenable to multiple regenerations.
6. For high-quality data, do not use the EXTRACLEAN feature when using the KINJECT command. This often results in additional noise immediately before the injection begins.
7. When generating anti-GST sensor surfaces, we typically observe differential immobilization of antibody on the four flow cells. This is due to the serial nature of the sensor chip fluidic system. Injected solutions flow from Fc1 to Fc2 then to Fc3 and finally to Fc4. Thus Fc4 can have significantly lower amounts of immobilized ligand than Fc1 due to depletion of ligand in the flowing injection stream. To overcome this problem, differential flow cell loading by multiple, independent injections can be performed to equalize immobilization levels across all four flow cells. Alternatively, to account for this phenomenon, we routinely switch the flow cells on which ligands are immobilized.

8. The binding surface of the anti-GST-coated sensor chip requires regeneration under two circumstances:
   a. One wishes to change the immobilized GST-fusion protein prior to the next analyte injection.
   b. One observes a slow dissociation of the binding partner, such that the sensorgram does not return to baseline in a given time interval after the injection of analyte is complete. For accurate binding data in this case, it is necessary to reload the GST-fusion protein after each round of analyte binding.
9. Regeneration buffer is injected in repeated, sequential 20 μL amounts until the sensorgram baseline returns to less than 10 RUs from the pre-injection baseline.
10. When using biotinylated protein, we usually saturate the surface. However, when using biotinylated peptides, we usually try not to saturate the surface and load approximately 100–500 RUs to the surface. If mass transport is a concern, we load multiple flow cells with varying amounts of biotinylated peptides to make sure our measurements are not affected by mass transport effects.
11. Full-length biotinylated proteins immobilized on sensor chips are often not stable when undocked; these sensor chips are likely not to function if reinserted into the BIAcore apparatus. In contrast, streptavidin-bound biotinylated peptide and anti-GST antibody sensor chips are more stable and can be undocked, stored at 4°C inside a 50 mL polypropylene capped tube filled with running buffer for months at a time, then redocked, and additional binding experiments conducted.

References

1. Malmqvist, M., and Karlsson, R. (1997) Biomolecular interaction analysis: affinity biosensor technologies for functional analysis of proteins. *Curr. Opin. Chem. Biol.* **1**, 378–83.
2. Jason-Moller, L., Murphy, M., and Bruno, J. (2006) Overview of Biacore systems and their applications. *Curr. Protoc. Protein Sci.* **Chapter 19**, Unit 19.13.
3. Majka, J., and Speck, C. (2007) Analysis of protein-DNA interactions using surface plasmon resonance. *Adv. Biochem. Eng. Biotechnol.* **104**, 13–36.
4. Johnston, C. A., Afshar, K., Snyder, J. T., Tall, G. G., Gonczy, P., Siderovski, D. P., and Willard, F. S. (2008) Structural determinants underlying the temperature-sensitive nature of a Galpha mutant in asymmetric cell division of Caenorhabditis elegans. *J. Biol. Chem.* **283**, 21550–58.
5. Johnston, C. A., Lobanova, E. S., Shavkunov, A. S., Low, J., Ramer, J. K., Blaesius, R., Fredericks, Z., Willard, F. S., Kuhlman, B., Arshavsky, V. Y., and Siderovski, D. P. (2006) Minimal determinants for binding activated G alpha from the structure of a G alpha(i1)-peptide dimer. *Biochemistry* **45**, 11390–400.
6. Kimple, A. J., Willard, F. S., Giguere, P. M., Johnston, C. A., Mocanu, V., and Siderovski, D. P. (2007) The RGS protein inhibitor CCG-4986 is a covalent modifier of the RGS4 Galpha-interaction face. *Biochim. Biophys. Acta* **1774**, 1213–20.
7. Soundararajan, M., Willard, F. S., Kimple, A. J., Turnbull, A. P., Ball, L. J., Schoch,

G. A., Gileadi, C., Fedorov, O. Y., Dowler, E. F., Higman, V. A., Hutsell, S. Q., Sundstrom, M., Doyle, D. A., and Siderovski, D. P. (2008) Structural diversity in the RGS domain and its interaction with heterotrimeric G protein alpha-subunits. *Proc. Natl. Acad. Sci. USA* **105**, 6457–62.

8. Green, N. M. (1963) Avidin. 1. The use of (14-C)Biotin for kinetic studies and for assay. *Biochem. J.* **89**, 585–91.
9. Melamed, M. D., and Green, N. M. (1963) Avidin. 2. Purification and composition. *Biochem. J.* **89**, 591–99.
10. Haun, M., and Wasi, S. (1990) Biotinylated antibodies bound to streptavidin beads: a versatile solid matrix for immunoassays. *Anal. Biochem.* **191**, 337–42.
11. Beckett, D., Kovaleva, E., and Schatz, P. J. (1999) A minimal peptide substrate in biotin holoenzyme synthetase-catalyzed biotinylation. *Protein Sci.* **8**, 921–29.
12. Willard, F. S., Low, A. B., McCudden, C. R., and Siderovski, D. P. (2007) Differential G-alpha interaction capacities of the GoLoco motifs in Rap GTPase activating proteins. *Cell Signal.* **19**, 428–38.
13. Webster, C. I., Cooper, M. A., Packman, L. C., Williams, D. H., and Gray, J. C. (2000) Kinetic analysis of high-mobility-group proteins HMG-1 and HMG-I/Y binding to cholesterol-tagged DNA on a supported lipid monolayer. *Nucleic Acids Res.* **28**, 1618–24.
14. Willard, F. S., and Siderovski, D. P. (2006) Covalent immobilization of histidine-tagged proteins for surface plasmon resonance. *Anal. Biochem.* **353**, 147–49.
15. BIAcore (2005) GST Capture Kit Instructions for Use GE Healthcare.
16. Willard, F. S., Kimple, A. J., Johnston, C. A., and Siderovski, D. P. (2005) A direct fluorescence-based assay for RGS domain GTPase accelerating activity. *Anal. Biochem.* **340**, 341–51.
17. Willard, F. S., Zheng, Z., Guo, J., Digby, G. J., Kimple, A. J., Conley, J. M., Johnston, C. A., Bosch, D., Willard, M. D., Watts, V. J., Lambert, N. A., Ikeda, S. R., Du, Q., and Siderovski, D. P. (2008) A point mutation to Galpha i selectively blocks GoLoco motif binding: direct evidence for Galpha/GoLoco complexes in mitotic spindle dynamics. *J. Biol. Chem.* **283**, 36698–710.
18. Decker, J., and Reischl, U. (2004) *Molecular Diagnosis of Infectious Diseases.* Humana Press, Totowa, NJ.

Chapter 5

A Capture Coupling Method for the Covalent Immobilization of Hexahistidine Tagged Proteins for Surface Plasmon Resonance

Adam J. Kimple, Robin E. Muller, David P. Siderovski, and Francis S. Willard

Abstract

Surface plasmon resonance (SPR) is a robust method to detect and quantify macromolecular interactions; however, to measure binding interactions, one component must be immobilized on a sensor surface. This is typically achieved using covalent immobilization via free amines or thiols, or noncovalent immobilization using high-affinity interactions such as biotin/streptavidin or antibody/antigen. In this chapter we describe a robust method to covalently immobilize His_6 fusion proteins on the sensor surface for SPR analysis.

Key words: Biacore, SPR, capture coupling, immobilization, hexahistidine, his-tag.

1. Introduction

Detection of protein–protein or protein–ligand interactions using surface plasmon resonance (SPR) is possible because the refractive index of a gold–fluid interface fluctuates as molecules interact with the surface and change the apparent molecular mass of the surface (1, 2). This change in the refractive index is directly related to the total mass of interacting molecules at the surface; thus, by immobilizing a protein analyte on the chip surface using high-affinity interactions (i.e., antibody capture or streptavidin/biotin (1–3)) or covalently using amine coupling

N.J. de Mol, M.J.E. Fischer (eds.), *Surface Plasmon Resonance*, Methods in Molecular Biology 627,
DOI 10.1007/978-1-60761-670-2_5,

(4, 5), one can directly observe the binding of a ligand (protein or small molecule) to the immobilized component. The kinetic nature of these measurements allows for real-time observation and quantification of molecular interactions. This data can be used to determine on-rates and off-rates and affinity constants. Once protocols are established for immobilizing a particular analyte on a sensor surface, determination of binding affinities and screening for interaction partners can be performed in an automated manner for tens to hundreds of ligands per day (6); however, in our experience, identifying an optimal way to immobilize protein analytes resulting in a stable surface with high binding capacity can be tedious.

The availability of commercial nitrilotriacetic acid (NTA) sensor chips allows for repeated immobilization, stripping, and regeneration of His_6-tagged proteins; however, this method of immobilization has multiple deficiencies that prevent its widespread use. First, while the NTA–His_6 interaction is robust, slow and continuous dissociation of immobilized components is common (7–9). The decaying surface can be corrected *post hoc* using computational methods (10); however, this solution is less than ideal and would prove daunting even to aficionados of SPR. The second commonly encountered problem with NTA sensor chips is the idiosyncratic drift of flow cells (*see* **Note 1**). If equivalent drifts occur across all flow cells, double referencing can be used to correct systematic deviations across all flow cells (11); however, we have frequently encountered deviations that only occur on individual flow cells, which cannot be corrected for using this method. While this problem is often attributed to contaminating cation interaction with the sensor surface, in our hands it is often found to be random and apparently independent of routine maintenance or buffer composition and can sometimes be resolved by simply redocking a chip or using a new sensor chip. We have developed a capture coupling method for His_6 fusion proteins that results in the capture of a His_6-fusion protein in a nonrandom orientation by the His_6 epitope prior to direct amine coupling. This method, referred to as "capture coupling," is superior to Ni^{2+}·NTA/His_6 or amine coupling alone because there is no loss of surface over time and the protein is immobilized initially by the His_6-tag. This method more reproducibly generates a high specific activity, functional SPR surface. We have used this approach to investigate protein–protein interactions in heterotrimeric G-protein biology (2, 9) (*see* **Note 2**) and other groups have also used our method to look at a diverse array of protein–protein interactions (12–14).

2. Materials

2.1. Buffers

1. Running buffer: 10 mM HEPES pH 7.4, 150 mM NaCl, 50 μM EDTA, 0.005% (v/v) NP-40. NP-40 is no longer commercially available; thus, we use "NP-40 Alternative" available from Calbiochem (La Jolla, CA) or Surfactant P20 available from GE Healthcare.
2. Dispenser buffer: 10 mM HEPES pH 7.4, 150 mM NaCl, 3 mM EDTA, 0.005% (v/v) NP-40.
3. Regeneration buffer: running buffer containing 350 mM EDTA.
4. Nickel sulfate solution: running buffer containing 500 μM $NiSO_4$.
   Note: The addition of guanine nucleotides, $MgCl_2$, NaF, and $AlCl_3$, is specific to the application of this method for studying heterotrimeric Gα subunits and are not needed for the study of other protein families.
5. Ground state running buffer: running buffer with an additional 100 μM GDP.
6. Active state running buffer: running buffer with 5 mM $MgCl_2$ and 100 μM GTPγS.
7. Transition state running buffer: running buffer with 5 mM $MgCl_2$, 100 μM GDP, 20 mM NaF, 30 μM $AlCl_3$.

2.2. Biacore 3000 Supplies

1. NTA Sensor Chip (GE Healthcare)
2. Amine Coupling Kit (GE Healthcare) (*see* **Note 3**)

3. Methods

1. Twenty four hours prior to use, run a Desorb and "Super Clean" (*see* **Note 4**) and inspect pumps for corrosion (*see* **Note 5**).
2. Prepare all buffers fresh and filter using bottle top or syringe filters (0.22 μm or smaller pore size). If using syringe filters, be sure to degas all buffers as microbubbles accumulate along the fluidics and can be deleterious to the sensor chip surface.
3. Undock maintenance chip and dock new NTA Sensor Chip.

4. Prime with the right pump in dispenser buffer and the left pump in running buffer. To verify which tube is connected to each pump, the panel that separates the rack area from the buffer storage area can be removed by undoing two thumb screws. Follow each tube to the originating pump (*see* **Fig. 5.1** for details).
5. Start a new sensorgram.
6. Direct flow path to a single flow cell with a flow rate of 20 μL/min.
7. Inject 20 μL of regeneration buffer using the Extraclean feature.
8. Wash needle (in addition to the Extraclean injection in step #7).
9. Inject 40 μL of nickel sulfate solution using the Extraclean feature.
10. Wash needle.
11. Set flow rate to 5 μL/min.
12. Make up 100 μL of coupling solution (a 1:1 (v/v) mixture of NHS/EDC (*N*-hydroxysuccinimide/*N*-ethyl-*N* ′-(3-diethylaminopropyl)carbodiimide) (included in the Amine Coupling Kit)).
13. Inject 30 μL of coupling solution.

Fig. 5.1. Identification of *left* and *right* pump inlets on Biacore 3000. Loosen the two screws (*white circles/arrows*) on the panel to remove the cover. This allows the user to trace each inlet back to the *right* and *left* pump. The Biacore Running Buffer should be placed in the inlet corresponding to the *left* pump while the *right* pumps inlet should be submerged in Dispenser Buffer.

14. Dilute His_6-fusion protein in running buffer (*see* **Note 6**).
15. Inject 66 μL of the His_6-fusion protein.
16. Inject 35 μL of 1 M ethanolamine (included in the Amine Coupling Kit) (*see* **Note 7**).
17. Set flow rate to 20 μL/min.
18. Inject 20 μL of regeneration buffer using the Extraclean feature.
19. Repeat steps 6–16 to load as many flow cells as desired.
20. Start a new sensorgram over all flow cells to be used with both inlets in the appropriate running buffer.
21. Once the immobilized protein surface has been generated, multiple rounds of analyte injection (*see* **Note 8**) can be automated as follows:

    Note: comments located after "//" should not be included

```
! ---
! This method was generated from ...   //stamp indicating this program was
! Timestamp:    03-Nov-08 14:28        //created from the command queue
! Software:     BIACORE 3000 ...
! Version:      3.2
! Configuration: IFC6
! ---
DEFINE APROG CommandQueue              //defining program name
 FLOW 20                               //setting flow to 20 μL/min
 INJECT R2A1 20                        //injecting 20 μL of regeneration buffer
 EXTRACLEAN                            //with Extraclean (from position R2A1)
 WASH n                                //washing needle
 INJECT R2A2 40                        //injecting 40 μL of NiSO4 with
 EXTRACLEAN                            //Extraclean from position R2A2
 WASH n                                //washing needle
 FLOW 5                                //set flow to 5 μL/min
 INJECT R2A3 30                        //injecting 30 μL of NHS/EDC
 INJECT R2A4 66                        //injecting 66 μL of His-fusion protein
 INJECT R2A5 35                        //injecting 35 μL of ethanolamine
 FLOW 20                               //set flow to 20 μL/min
 INJECT R2A1 20                        //inject regeneration buffer with
 EXTRACLEAN                            //Extraclean
END
MAIN
 RACK 1 THERMO_C                       //setting up racks
 RACK 2 THERMO_A
 RACK R REAG_A
 DETECTION 2                           //Change 2 to any flow cell (1–4) to
 APROG CommandQueue                    //perform this method on a different flow
 APPEND Standby                        //cell
END                                    //machine will be left in standby
```

After you have generated one flow cell using the command queue, go to the "File" menu in the command queue window and select "Generate Method." This will save a *.blm file that generates a surface exactly as indicated in the command queue. This script can easily be edited to generate a surface on a different flow cell by manually changing the "DETECTION 2" command (in our example) to DETECTION X, where X is any flow cell you want to generate (flow cell 1–4). The reagents must be in the same positions that were used while using the command queue initially.

4. Notes

1. The capture coupling method of immobilizing fusion proteins eliminates the possibility of the immobilized component dissociating from the sensor chip surface; however, it is not uncommon to encounter drifting baselines that are not consistent between flow cells. These are idiosyncratic and are difficult to correct. One method we use to account for buffer shifts is to use multiple negative controls for background subtraction. We often use a flow cell with no protein attached, which has been treated with a 20 μL injection of regeneration buffer at 20 μL/min. If experimental conditions allow, it is also helpful to have an additional negative control flow cell with a His_6-fusion protein that will not interact with the analyte (*see* **Fig. 5.3** for representative data).
2. In this chapter, we describe the use of this method for the immobilization of a novel RGS protein (**Figs. 5.2 and 5.3**). Similarly, we have used this method to immobilize $G\alpha_q$ (2) and $G\beta\gamma$ subunits (2, 9). We anticipate that this method will be applicable to the analysis of a wide variety of molecular interactions. Other representative examples of the use of this methodology from other groups include refs. (13, 14).
3. We typically purchase an Amine Coupling Kit from GE Healthcare (GE Healthcare, BR-1000-50) and make separate 100 μL aliquots of NHS and EDC. These aliquots must be stored at –20°C. If poor covalent coupling is observed, it is likely that the NHS/EDC reagents have lost activity.
4. In addition to regularly performing the Desorb procedure, we also recommend performing a "Super Clean" procedure before performing capture coupling. This automated procedure can be accessed under the "Tools" menu, "Service Tools" option, and then selecting "Super Clean." This

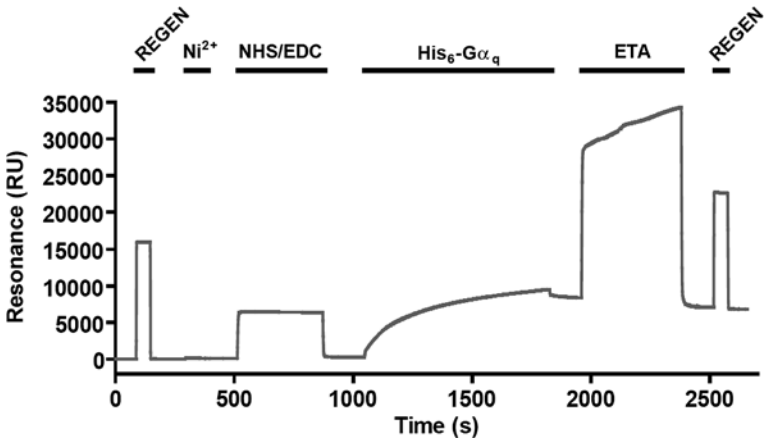

Fig. 5.2. Loading – A typical sensorgram generated during the production of a single flow cell using the capture coupling method. The flow cell surface was stabilized by the injection of regeneration buffer (20 μL regeneration buffer at 20 μL/min) followed by binding of nickel to the surface (40 μL nickel sulfate solution at 20 μL/min). The surface was then activated for primary amine coupling by the injection of coupling solution (30 μL EDC/NHS at 5 μL/min). His_6-Gα fusion protein in pH 7.4 running buffer was then injected over the surface (66 μL of 1 μM His_6-Gα at 5 μL/min). To block uncoupled primary amines on the sensor surface, ethanolamine was injected over the surface (35 μL ethanolamine at 5 μL/min). To prevent further immobilization of His_6-fusion proteins and to remove non-covalently coupled His_6-Gα, EDTA-containing regeneration buffer was injected (20 μL at 20 μL/min).

procedure will require 4 mL aliquots of H_2O, 1% (v/v) acetic acid, 0.2 M $NaHCO_3$, 6 M guanidine HCl, and 10 mM HCl. It is essential to filter and degas all solutions.

5. In the past several years, we have observed a corrosive build-up on the shaft of the Hamilton syringe pumps. We recommend an extensive visual inspection before performing any experiment but this is of special importance when conducting covalent capture techniques employing NTA-based immobilization. If rust/oxidation is observed, we recommend replacing the syringe (GE Healthcare, BR-1000-84). The new syringe can be easily replaced by the user by following the instruction found under the "Tools" menu, "Service Tools" option, and then selecting "Syringe/Tip (Right/Left)." Standard cleaning procedures such as Desorb and Super Clean do not vigorously clean the syringes, so we recommend performing a Sanitize procedure several times a year using the Sanitize command in the "Working Tools" menu. The Sanitize procedure will require BIA disinfectant solution (1% sodium hypochlorite) which can be purchased as part of a Biacore Maintenance Kit (GE Healthcare, BR-1006-66, BR-1006-67, BR-1006-51).

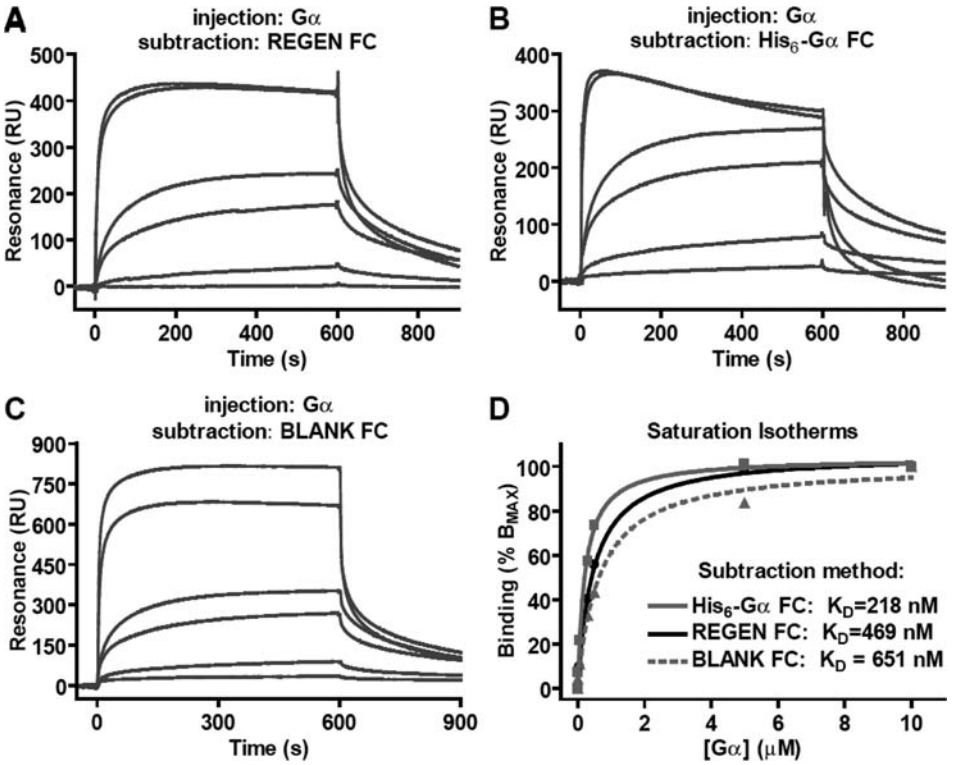

Fig. 5.3. Curves – Capture coupling was used to generate a sensor surface with a novel His_6-RGS protein. Four flow cells were prepared: FC1 ("REGEN FC") – a blank surface that had 20 μL of regeneration buffer injected over it; FC2 ("BLANK FC") – a non-treated NTA surface that only had experimental injections; FC3 ("His_6-Gα FC") – ~6000 RUs of His_6-Gα were immobilized; FC4 – ~6000 RUs of a novel His_6-RGS protein. Varying concentrations of His_6-Gα were injected over all four flow cells, in the presence of transition state running buffer, using the KINJECT command (200 μL injections with a 300 s dissociation phase at 20 μL/min). Specific binding of the injected Gα was only seen to His_6-RGS as would be expected (2); however, the qualitative appearance of the curves changed depending on the flow cell used to subtract nonspecific binding and changes in the refractive index upon injection of buffers. **(a)** Specific binding was determined by subtracting nonspecific binding to flow cell 1 (REGEN FC) that had 20 μL of regeneration buffer injected over it prior to injections. **(b)** Nonspecific binding was subtracted by using a flow cell loaded with a non-interacting protein immobilized on the surface (i.e., Gα does not dimerize). **(c)** An otherwise untreated flow cell (BLANK FC) was used to subtract nonspecific binding and changes in refractive index. **(d)** Using equilibrium saturation analysis, dissociation constants (K_d values) for the Gα/RGS protein–protein interaction were determined to be 469 (95% CI 426–512) nM, 218 (95% CI 149–288) nM, and 651 (95% CI 389–917) nM using background subtraction to a regenerated blank flow cell, an immobilized His_6-Gα flow cell, and a blank flow cell, respectively.

6. We currently have not identified a quantitative method for determining the amount/concentration of protein to covalently couple to the sensor surface. To empirically determine a useful protein concentration, we start with a 50 μL injection at a flow rate of 5 μL/min using 1 μM of the His_6 fusion protein. In general with His_6 capture coupling, we saturate the flow surface in the shortest amount of time possible; however, if excess protein is injected, a significant loss of protein from the surface will be observed when the

injection is stopped and protein may bind through conventional amine coupling, thereby immobilizing protein in a random orientation. If too little protein is injected, a linear increase in protein loading will be occurring even when the injection ends. An additional consideration that must be noted is the likelihood of observing mass transport effects if excess protein loaded on the surface or flow rates are too slow (15–17; *see* also **Chapter 2**).

7. An analogous method to the one presented in this chapter has been described in (15) although, in this particular method, amine coupling reagents are added after NTA immobilization has occurred. We have tested this method with His_6-Gβγ subunits and found it ineffective in generating a functional surface.
8. To increase the probability of experimental success, it is critical to use a homogenous protein sample. We highly recommend a multiple step chromatographic approach starting with affinity purification and ending with gel exclusion chromatography to ensure that the protein samples are homogenous and non-aggregated. For more information regarding protein purification, we recommend the Protein Purification Handbook which can be downloaded for free from the GE Healthcare website under product number 18-1142-75.

References

1. Kimple, A. J., Willard, F. S., Giguere, P. M., Johnston, C. A., Mocanu, V., and Siderovski, D. P. (2007) The RGS protein inhibitor CCG-4986 is a covalent modifier of the RGS4 Galpha-interaction face. *Biochim. Biophys. Acta* **1774**, 1213–20.
2. Soundararajan, M., Willard, F. S., Kimple, A. J., Turnbull, A. P., Ball, L. J., Schoch, G. A., Gileadi, C., Fedorov, O. Y., Dowler, E. F., Higman, V. A., Hutsell, S. Q., Sundstrom, M., Doyle, D. A., and Siderovski, D. P. (2008) Structural diversity in the RGS domain and its interaction with heterotrimeric G protein alpha-subunits. *Proc. Natl. Acad. Sci. USA* **105**, 6457–62.
3. Johnston, C. A., Kimple, A. J., Giguere, P. M., and Siderovski, D. P. (2008) Structure of the parathyroid hormone receptor C terminus bound to the G-protein dimer Gbeta1gamma2. *Structure* **16**, 1086–94.
4. Johnsson, B., Lofas, S., and Lindquist, G. (1991) Immobilization of proteins to a carboxymethyldextran-modified gold surface for biospecific interaction analysis in surface plasmon resonance sensors. *Anal. Biochem.* **198**, 268–77.
5. Ferner-Ortner, J., Mader, C., Ilk, N., Sleytr, U. B., and Egelseer, E. M. (2007) High-affinity interaction between the S-layer protein SbsC and the secondary cell wall polymer of Geobacillus stearothermophilus ATCC 12980 determined by surface plasmon resonance technology. *J. Bacteriol.* **189**, 7154–58.
6. Kimple, A. J., Yasgar, A., Hughes, M., Jadhav, A., Willard, F. S., Muller, R. E., Austin, C. P., Inglese, J., Ibeanu, G. C., Siderovski, D. P., and Simeonov, A. (2008) A high throughput fluorescence polarization assay for inhibitors of the GoLoco Motif/G-alpha interaction. *Comb. Chem. High Throughput Screen.* **11**, 396–409.
7. Clow, F., Fraser, J. D., and Proft, T. (2008) Immobilization of proteins to Biacore sensor chips using Staphylococcus aureus sortase A. *Biotechnol. Lett.* **30**, 1603–07.
8. Nieba, L., Nieba-Axmann, S. E., Persson, A., Hamalainen, M., Edebratt, F., Hansson, A., Lidholm, J., Magnusson, K., Karlsson, A. F.,

and Pluckthun, A. (1997) BIACORE analysis of histidine-tagged proteins using a chelating NTA sensor chip. *Anal. Biochem.* **252**, 217–28.
9. Willard, F. S., and Siderovski, D. P. (2006) Covalent immobilization of histidine-tagged proteins for surface plasmon resonance. *Anal. Biochem.* **353**, 147–49.
10. Joss, L., Morton, T. A., Doyle, M. L., and Myszka, D. G. (1998) Interpreting kinetic rate constants from optical biosensor data recorded on a decaying surface. *Anal. Biochem.* **261**, 203–10.
11. Myszka, D. G. (1999) Improving biosensor analysis. *J. Mol. Recognit.* **12**, 279–84.
12. Diskar, M., Zenn, H. M., Kaupisch, A., Prinz, A., and Herberg, F. W. (2007) Molecular basis for isoform-specific autoregulation of protein kinase A. *Cell Signal.* **19**, 2024–34.
13. Jomain, J. B., Tallet, E., Broutin, I., Hoos, S., van Agthoven, J., Ducruix, A., Kelly, P. A., Kragelund, B. B., England, P., and Goffin, V. (2007) Structural and thermodynamic bases for the design of pure prolactin receptor antagonists: X-ray structure of Del1-9-G129R-hPRL. *J. Biol. Chem.* **282**, 33118–31.
14. Koehnke, J., Jin, X., Trbovic, N., Katsamba, P. S., Brasch, J., Ahlsen, G., Scheiffele, P., Honig, B., Palmer, A. G. 3rd, and Shapiro, L. (2008) Crystal structures of beta-neurexin 1 and beta-neurexin 2 ectodomains and dynamics of splice insertion sequence 4. *Structure* **16**, 410–21.
15. Wear, M. A., and Walkinshaw, M. D. (2007) Determination of the rate constants for the FK506 binding protein/rapamycin interaction using surface plasmon resonance: an alternative sensor surface for Ni2+-nitrilotriacetic acid immobilization of His-tagged proteins. *Anal. Biochem.* **371**, 250–52.
16. Karlsson, R. (1999) Affinity analysis of non-steady-state data obtained under mass transport limited conditions using BIAcore technology. *J. Mol. Recognit.* **12**, 285–92.
17. Myszka, D. G., Morton, T. A., Doyle, M. L., and Chaiken, I. M. (1997) Kinetic analysis of a protein antigen-antibody interaction limited by mass transport on an optical biosensor. *Biophys. Chem.* **64**, 127–37.

Chapter 6

Affinity Constants for Small Molecules from SPR Competition Experiments

Nico J. de Mol

Abstract

Direct assay of small molecules by SPR in general is troublesome and at least tedious procedures have to be applied. Competition experiments offer an attractive alternative. A small ligand known to bind to the analyte is immobilized on an SPR sensor surface, and the binding of the larger analyte in the presence of compounds under investigation in a concentration range is assayed. The resulting inhibition curves of the equilibrium SPR signal as function of the compound concentration can be analyzed to yield thermodynamic binding constants for the interaction *in solution* between analyte and the compounds under investigation. An additional advantage of this method is that series of compounds can be analyzed using the same sensor surface, so there is no immobilization needed for each compound. An adaptation of the method to analyze interactions with bivalent analytes (e.g., antibodies) is also included. Some observed different affinities in solution compared to that on the SPR surface are discussed.

Key words: Surface plasmon resonance (SPR), binding constant, competition experiments, antibodies, low molecular weight compounds, solution affinity.

1. Introduction

In many situations affinity data are needed for ligands with low molecular weight (~ <2,000 kDa). For example in drug development according to Lipinski rules "drug-like" molecules preferably have molecular weights smaller than 500 kDa (1). It can be troublesome to measure affinity data for such small analytes directly by SPR, because the SPR signal is directly related to the change in mass at the SPR surface. With sensitive instrumentation and careful laborious experimental design reliable affinity data have been assayed for small analytes (2). An attractive alternative is to

N.J. de Mol, M.J.E. Fischer (eds.), *Surface Plasmon Resonance*, Methods in Molecular Biology 627,
DOI 10.1007/978-1-60761-670-2_6,

perform a competition experiment in which an analyte, e.g., a protein (high MW!), is bound to an immobilized ligand at the surface. By competition upon binding of investigational ligands in solution, the analyte is displaced from the surface leading to a decrease in SPR signal (*see* **Fig. 6.1**).

Here it is derived that such competition experiments can yield thermodynamic binding constants for the affinity in solution (K_S), which in some cases might deviate from the affinity to immobilized ligands on the SPR surface (K_C). Another advantage of this approach is that with the same surface and the same immobilized ligand the affinity of numerous ligands in solution can be assayed, which is very useful when screening compound libraries, a common practice in drug development.

The approach presented here is versatile and can be applied to many situations. The emphasis in this chapter is on the basics of the derivation of K_S, the best conditions for the experiments, and some examples validating the approach are presented. It is assumed that an immobilization strategy is available for the ligand to be immobilized. Further steps in the competition experiments

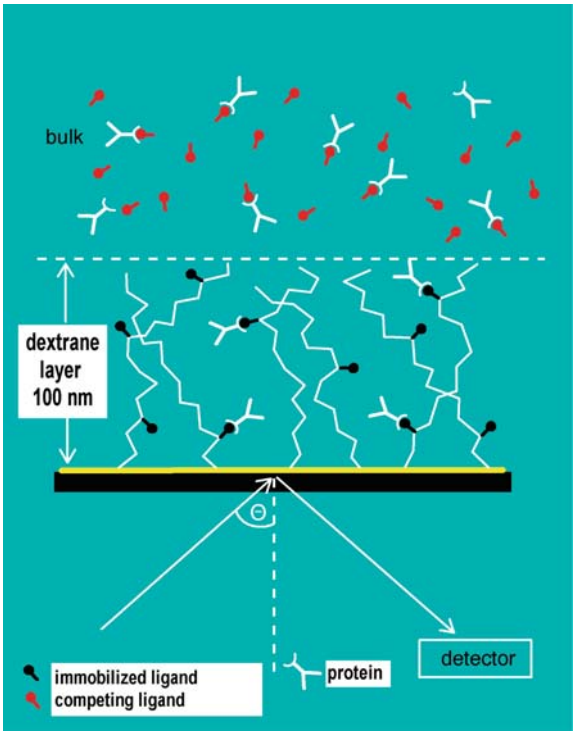

Fig. 6.1. Schematic representation of the competition assay. A ligand is immobilized on the carboxylated methyl dextran chains of the sensor chip. The analyte binds to this ligand with dissociation constant K_C. Upon addition of a competitive binding ligand to the bulk solution, the equilibrium binding of analyte to the sensor surface is shifted toward lower binding. A model is derived, describing the shift in binding as function of the amount of ligand in the bulk (**Eq. [4]**). From this K_S, the thermodynamic dissociation constant in solution, is obtained.

are assumed to be standard SPR experiments. Where needed additional considerations are presented.

2. Assay of the Analyte Affinity to Immobilized Ligand on the Sensor Chip (K_C)

In order to assay the affinity in solution, first the affinity of the analyte (high molecular weight biomolecule) to the immobilized ligand must be known. For this we used standard CM5 chips from GE-Biacore or CMD chips from XanTec bioanalytics GmbH (Düsseldorf, Germany). These chips contain a carboxymethylated dextran hydrogel layer, mimicking a hydrophilic environment. The carboxyl groups can be activated for covalent immobilization of the ligand. For an overview of immobilization strategies *see* **Chapter 3** and various immobilization protocols are described in other chapters in this volume, e.g., **Chapters 4** and **5** (*see* **Note 1**). In general it is better not to have too high binding capacity on the sensor chips to avoid all kinds of artifacts in the binding process. A value of 1000 RU (Biacore instruments) corresponding to 100 m° (Autolab Esprit, Eco Chemie) is generally excellent.

After immobilization of the ligand the surface is ready for K_C assay by performing binding assays of a series of analyte concentrations. These concentrations are chosen around the (estimated) K_C value for the binding of analyte to the immobilized ligand, e.g., from 0.5 to 5 times K_C. In our experiments we used an Esprit Autolab SPR instrument (Eco Chemie, Utrecht, The Netherlands). This instrument is based on a double channel cuvette. One channel (the sample channel) is used for immobilization of the ligand, the other channel is treated similarly without ligand and is the reference channel. The SPR signal of the reference channel is subtracted from that of the sample channel. The cuvette design has advantages and disadvantages compared to the flow design as found in the instruments of market leader Biacore (*see* also **Chapter 1**).

Here it is relevant that we prefer to use the equilibrium signal (R_{eq}) to assay K_C and K_S. In the cuvette it is no problem to extend the assay time till equilibrium is reached; however, under flow conditions considerable amounts of often precious analyte can be consumed before equilibrium is reached (*see* **Note 2**). A problem with cuvette design might be that the original added analyte concentration does no longer correspond to the free concentration in the cuvette, by depletion due to binding of analyte to the surface. In the assay of K_C, correction for depletion can be performed (*see* **Note 3**).

To assay K_C we prefer nonlinear fitting of R_{eq} as function of the free ligand concentration $[L]$ with a Langmuir binding isotherm (**Eq. [1]**, *see* also **Fig. 6.2a**) in which R_{max} is the

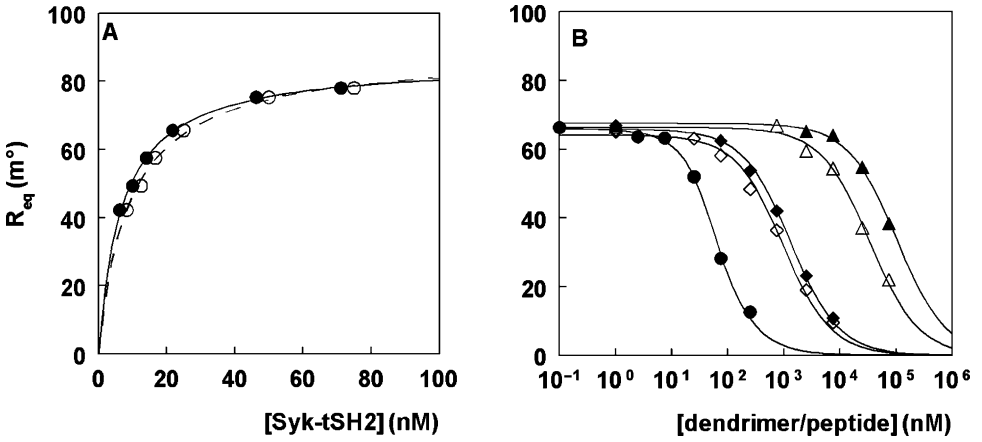

Fig. 6.2. K_C assay and competition experiments with various ligands. (**a**) K_C assay of the bivalent interaction of Syk tandem SH2 domain (Syk-tSH2) to immobilized diphosphorylated γ-ITAM-peptide. The uncorrected data (*open circles*) and data corrected for binding to the surface (depletion correction, *closed circles*) are shown, see text. K_C obtained from this assay with depletion correction is 6.9 ± 0.4 nM, and R_{max} is 85.9 ± 1.3 m°. The uncorrected data yield values of 9.3 ± 0.5 nM and 88.6 ± 1.3 m°, respectively. (**b**) Competition experiments on the same surface with various dendrimeric constructs functionalized to different degrees (1–8) with monovalent γ-ITAM phosphopeptides. The [Syk-tSH2] in this experiment was 25 nM. The *lines* are fits with **Eq. [4]**.

binding capacity, the maximum SPR signal upon saturation of all binding sites:

$$R_{eq} = \left(\frac{[L]}{[L] + K_C}\right) \times R_{max} \qquad [1]$$

Linearization as in Scatchard plots can introduce large errors upon transforming the data (3).

As presented here it is assumed in first approach that both at the sensor surface and in solution the binding can be described by a one-site model. However, the assay can also be adapted for binding of antibodies, that may bind bivalently to the surface, and with mono or bivalent binding in solution (*see* **Section 4**)

3. Assay of Affinity Between Analyte and Ligands in Solution (K_S) from Competition Experiments

The setup of these experiments is simple: For a fixed amount of analyte, R_{eq} is assayed in the presence of various concentrations of the ligand under investigation. It is important to assay K_C and K_S on the same surface, preferably within a short time interval especially on less stable surfaces.

The analyte concentration could best be chosen as around twice the observed K_C value. The concentration range for the

ligand depends on the affinity. In a first experiment, concentrations in a broad range, e.g., from 10^{-4} to 10^{-9} M, with 10-fold concentration steps can be explored. In a second experiment, the assay can be refined by using 5–6 data points in a smaller concentration range around the concentration at which the amount of binding is half of that without competitor, choosing 3-fold concentration steps.

To obtain K_S the concentration of the ligand in solution is plotted on the X-axis on a log scale and R_{eq} on the Y-axis (**Fig. 6.2b**). The data are fitted with an equation that is derived for a simple one-site binding model, yielding the parameters R_{max} and K_S (**Eq. [4]**, *see* **Section 3.1**). Note that R_{max} is not the R_{eq} value in the absence of competing ligand as generally the concentration of analyte is not chosen to be under saturation conditions of all binding sites on the SPR surface, rather R_{max} is the SPR signal when all binding sites on the surface are occupied (compare **Figs. 6.2a, b**). R_{max} from the fits of **Eq. [4]** should be in agreement with the value obtained from the K_C analysis.

3.1. Derivation of the Model to Obtain Thermodynamic Binding Constants in Solution (K_S)

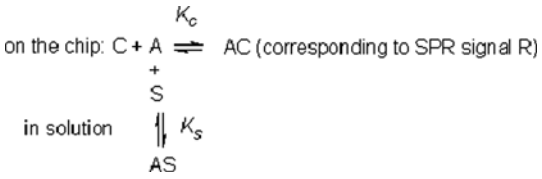

The derivation presented here is an extension of that presented by Morelock et al. (4). The abbreviations used in the derivation are $[A]_T$ and $[S]_T$ for the total amount of analyte A and competitor S, respectively. R_{max} is the binding capacity of the SPR surface at saturation of all binding sites. K_C and K_S are the dissociation constants for binding of A to immobilized ligand on the sensor surface, and with S in solution, respectively. $[AS]$ is the amount of A bound to S.

In the presence of competitor S in solution, the SPR signal at equilibrium (R_{eq}) is obtained from **Eq. [1]**, correcting $[A]_T$ for the amount bound by S in solution ($[AS]$), as given by **Eq. [2]**:

$$R_{eq} = \left(\frac{[A]_T - [AS]}{K_C + [A]_T - [AS]} \right) R_{max} \qquad [2]$$

$[AS]$ is defined by K_S as a thermodynamic binding constant in solution:

$$K_S = \frac{[A][S]}{[AS]} = \frac{([A]_T - [AS])([S]_T - [AS])}{[AS]}$$

From this it follows that

$[AS]^2 - ([A]_T + [S]_T + K_S)[AS] + [A]_T.[S]_T = 0$, this is a quadratic equation of type $ax^2 + bx + c = 0$ with solution $x = \frac{-b \pm \sqrt{b^2 - 4ac}}{2a}$. So,

$$[AS] = \frac{[A]_T + [S]_T + K_S - \sqrt{([A]_T + [S]_T + K_S)^2 - 4[A]_T[S]_T}}{2} \quad [3]$$

This expression can be substituted into **Eq. [2]** yielding **Eq. [4]**:

$$R_{eq} = \left(\frac{[A]_T - \frac{[A]_T+[S]_T+K_S-\sqrt{([A]_T+[S]_T+K_S)^2-4[A]_T[S]_T}}{2}}{K_C + [A]_T - \frac{[A]_T+[S]_T+K_S-\sqrt{([A]_T+[S]_T+K_S)^2-4[A]_T[S]_T}}{2}} \right) R_{max} \quad [4]$$

The known values for $[A]_T$, $[S]_T$, and K_C can be inserted into the equation and it can then be readily fitted with any nonlinear fitting program yielding the parameters K_S and R_{max}.

Alternatively, K_S could be derived from a single point of the inhibition curve by assaying $[S]_T$ at $0.5 \times R_{max}$ (4). K_S for this situation is then given by **Eq. [5]**:

$$K_S = \frac{[S]_T - [A]_T + K_C}{\frac{[A]_T}{K_C} - 1} \quad [5]$$

For use in this equation the value of $[S]_T$ is read on the X-axis of the plot for the competition assay. Note that $0.5 \times R_{max}$ is not the IC_{50} value of the competition plot but R_{eq} at half the maximum binding capacity as explained above. This method may be less accurate than a fit of all data points. Furthermore, from the fit according to **Eq. [4]** R_{max} is obtained, and this value can be validated with that from the K_C assay. Upon application of **Eq. [5]** the value of $0.5 \times R_{max}$ is derived from the value of R_{max} from the K_C experiment.

3.2. Applications of K_S Assays

Depletion correction for cuvette-based SPR instruments (see above) is not fully feasible in the competition experiments using **Eq. [4]** (*see* **Note 4**). Therefore, when using cuvette design instruments problems may arise especially with interactions of high affinity in combination with surfaces with high binding capacity (R_{max}). In such case it is advised to choose conditions for which depletion correction is minimal: low R_{max} and not too high ligand concentrations in solution to avoid large differences in binding to the surface. In general, R_{eq} values in a range from 100 to 50% of the observed maximum R_{eq}, with depletion corrections <10%, are sufficient for a reliable fit of **Eq. [4]**. Alternatively, in case of a strong analyte depletion effect one might use depletion correction using **Eq. [5]** to assay K_S (*see* **Note 4**).

An application of assay of K_S is shown in **Fig. 6.2**. In **Table 6.1** some experimental K_S and K_C values for various interactions are presented. In general for analytes with one binding site, the affinity in solution agrees with that at the sensor surface. However, exceptions may occur (*see* **Note 5**). When the analyte is a dimer, e.g., when expressed as a GST-fusion protein (5), or the Grb2 SH2 domain under certain conditions (6), the affinity at the sensor surface may be much higher due to the avidity effect caused by binding to the SPR matrix with both binding sites simultaneously (*see* **Table 6.1**). In such cases the K_S value will in general be representative of the affinity of a ligand for the analyte in solution. Antibodies are also analytes possessing *two identical binding sites*, giving rise to bivalent binding at a sensor surface. For such cases the model derived in **Section 3.1** can be adapted as described in **Section 4**.

Table 6.1
Comparison of affinity at the sensor surface (K_C) and in solution (K_S), as assayed from fits of competition experiments with Eq. [4]

Protein + peptide	K_C (nM)	K_S (nM)
v-Src SH2 + hmT-peptide	220	234
Syk tSH2 + γ-ITAM-peptide (bivalent interaction)	5.4	5.7
MN12H2 antibody + GT(norL)DTNNNL-peptide	19.7	1,040[a]
Lck-SH2 GST-fusion protein[b] +hmT-peptide	6	60
Grb2-SH2 GST-fusion protein + pYVNV-peptide	7.9	260
Grb2-SH2 not heated[c] + pYVNV-peptide	134	1,800
Grb2-SH2 heated + pYVNV-peptide	220	255
Full-length Grb2 protein + pYVNV-peptide	790	230

[a]Derived from fit with **Eq. [9]**
[b]If explicitly indicated the dimer forming GST moiety is present
[c]Heating to 50°C converts the Grb2-SH2 dimer irreversibly to the monomer (6)

4. Assay of K_S for Antibodies

The K_S assay described above can be extended for application to binding of antibodies and analytes with two identical binding sites. The assay of K_C is identical to that described in **Section 2**. However, in solution now several bound species have to be taken into account: unbound, single bound, and double bound species. Of these only unbound and single bound species are able to bind to the SPR surface. A derivation of a model to obtain K_S for an antibody as analyte is given in **Section 4.1**. The K_C value

appearing in **Eq. [9]** can again be obtained from a separate experiment, assaying the affinity of the antibody for the immobilized ligand on the SPR surface. K_C will be much smaller than K_S due to the above-described avidity effect of the bivalent binding antibody at the sensor surface (*see* **Table 6.1**). An example of measuring a series of antibody ligands with fits according to **Eq. [9]** is shown in **Fig. 6.3**.

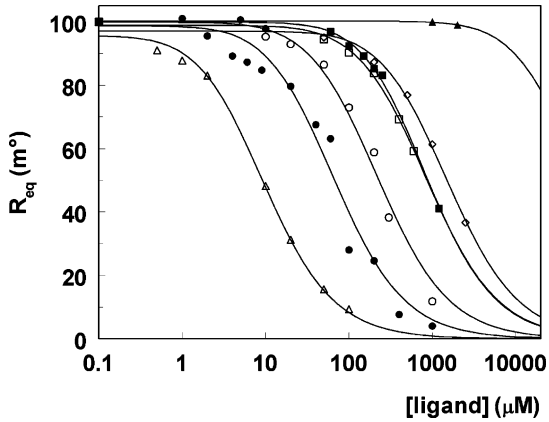

Fig. 6.3. Competition experiments with ligands for the MN12H2 antibody. K_C of antibody for immobilized GTXDTNNNL-NH2 peptide was 19.7 nM (X is norLeu). Competition experiments were with 60 nM MN12H2, investigating ligands with various amino acid substitutions for X. The lines are the fits according to the antibody model (**Eq. [9]**). Reprinted from ref. (8), Copyright (2001), with permission from Elsevier.

4.1. Derivation of the Model to Obtain Thermodynamic Binding Constants in Solution (K_S) for a Ligand Binding to an Antibody

For an antibody with two identical binding sites, the thermodynamic binding constant K_S is defined as

$$K_S = \frac{2[A][S]}{[AS]}$$

Here $[A]$ is the free antibody (analyte) concentration (with $2[A]$ binding sites) and $[S]$ the free concentration of ligand S in solution. If f is the fraction of binding sites of A that are occupied, then K_S can be transformed into

$$K_S = \frac{(2[A]_T - 2f[A]_T)([S]_T - 2f[A]_T)}{2f[A]_T}$$

Here $[A]_T$ and $[S]_T$ are the total concentrations of A and S, respectively. From this a quadratic expression for f, as function of $[A]_T$ and $[S]_T$, can be derived of the form $af^2 + bf + c = 0$, which has as (a physiological relevant) solution

$$f = K_s + B - \frac{\sqrt{(K_s + B)^2 - C}}{4[A]_T} \qquad [6]$$

Here B and C are constants in a given experimental setup: $B = 2[A]_T + [S]_T$ and $C = 8[A]_T[S]_T$.

Now we have to take into account that when fraction f of the binding sites A in solution is bound, there is a binomial distribution over double, single, and non-bound antibody of which only single and unbound antibody can bind to the SPR surface. The fraction double bound is $(1-f)^2$, the fraction single bound is $2f(1-f)$, and the fraction unbound antibody is $f^2(7)$. Therefore the effective concentration of antibodies available for binding to the SPR surface is$(1-f^2)[A]_T$. Substituting f(**Eq. [6]**) yields

$$\left(1-f^2\right)[A]_T = \frac{[A]_T^2 - \frac{1}{16}\left(K_S + B - \sqrt{(K_S+B)^2 - C}\right)^2}{[A]_T} \quad [7]$$

For binding to the SPR surface the equivalent for **Eq. [2]** in **Section 3.1** for antibody binding is

$$R_{eq} = \left(\frac{(1-f^2)[A]_T}{K_C + (1-f^2)[A]_T}\right) R_{max} \quad [8]$$

Substitution of $(1-f^2)[A]_T$(**Eq. [7]**) in **Eq. [8]** and replacing terms B and C yields

$$R_{eq} = \left(\frac{[A]_T^2 - \frac{1}{16}\left(K_S + 2[A]_T + [S]_T - \sqrt{(K_S + 2[A]_T + [S]_T)^2 - 8[A]_T[S]_T}\right)^2}{K_C[A]_T + [A]_T^2 - \frac{1}{16}\left(K_S + 2[A]_T + [S]_T - \sqrt{(K_S + 2[A]_T + [S]_T)^2 - 8[A]_T[S]_T}\right)^2}\right) R_{max} \quad [9]$$

The equation can be readily used in a nonlinear fitting program. The values of $[A]_T$ and K_C are known and filled in to fit the data of a plot of R_{eq} vs. $[S]_T$, yielding the unknown parameters K_S and R_{max}. The value of R_{max} should agree with the value obtained from the K_C assay.

5. Notes

1. To allow enough space for binding of the analyte to the immobilized ligand we standard incorporate a spacer in the ligand, so that the distance between the binding epitope of the ligand and the matrix of the SPR chip is increased. This permits also analytes with deep binding pockets to bind without crowding effects between analyte and SPR sensor matrix. In our peptide and peptidomimetic ligands we generally apply H_2N-$CH_2CH_2OCH_2CH_2OCH_2$-C(=O)OH as a building block for the spacer.

2. Assay of affinity based only on the kinetic phases of the interaction can lead to large errors, in spite of nice fits of the association and dissociation phases (*see* also **Chapter 2**). Only if one can be sure that no transport limitation (MTL) occurs, and a one-site binding model applies, such fits can generate valuable affinity data. Analysis of equilibrium signals can avoid these errors.
3. Depletion correction can especially be needed when analyzing high-affinity interactions. In this case low concentrations of analyte are used (around K_C), and depletion will have a larger effect on low concentrations. The amount of bound analyte is proportional to R_{eq} (in millidegree (m°) for Autolab/Esprit instruments) and the sensor surface S (in mm^2). Furthermore, the conversion factor for SPR signal and bound mass is needed: 1 ng/mm^2 corresponds with an SPR signal of 100 m° (or 1,000 RU for Biacore instruments). To calculate the effect of bound mass on the free analyte concentration the molecular weight (MW) of the analyte and volume of the bulk solution (V_{bulk}) in the cuvette is needed. The effect of depletion on the original analyte concentration $[A]_o$ when the SPR signal is expressed in m° is

$$[A]_{corr} = [A]_o - \frac{R_{eq} \times S \times 10^{-11}}{MW \times V_{bulk}} \qquad [10]$$

With fixed values for MW, S, and V_{bulk} for a given experimental setup, corrections as a function of R_{eq} can readily be made in a spreadsheet.

4. In the competition experiment using **Eq. [4]**, depletion correction is not simply feasible. The model assumes a constant analyte concentration ($[A]_T$) and this does not apply when $[A]_T$ is severely effected by depletion, where the correction will vary with R_{eq} (*see* **Note 3**). When the depletion correction is less than 5–10%, reliable fits with **Eq. [4]** can be made without depletion correction. For high-affinity interactions with a considerable depletion correction, assay of K_S using **Eq. [5]**, with $[S]_T$ at $R_{eq} = 0.5 \times R_{max}$, can be applied. In this case $[A]_T$ can be corrected for depletion using **Eq. [10]** with $0.5 \times R_{max}$ as R_{eq}.
5. Next to the avidity effect of multivalent analytes, mentioned in the text, differences between K_S and K_C may occur for different reasons. For example, for very large ligands it may be difficult to partition into the sensor matrix, leading to differences in effective concentration at the sensor surface. Also the surface might be heterogeneous due to nonuniform coupling of proteins/ligands to the sensor (*see* **Chapter 2**). The

immobilized binding epitope may be sterically hindered by the SPR matrix (*see* **Note 1**). It is also feasible that positively charged analytes have additional electrostatic interactions with free carboxyl groups of the sensor matrix.

References

1. Lipinski, C. A. (2004) Lead- and drug-like compounds: the rule-of-five revolution. *Drug Disc. Today Technol.* **1**, 337–41.
2. Markgren, P. O., Hamalainen, M., and Danielson, U. H. (2000) Kinetic analysis of the interaction between HIV-1 protease and inhibitors using optical biosensor technology. *Anal. Biochem.* **279**, 71–78.
3. Pliska, V. (1997) Thermodynamic parameters of ligand-receptor interactions: computation and error margins. *J. Recept. Signal Transduct. Res.* **17**, 495–510.
4. Morelock, M. M., Ingraham, R. H., Betageri, R., and Jakes, S. (1995) Determination of receptor-ligand kinetic and equilibrium binding constants using surface plasmon resonance: application to the lck SH2 domain and phosphotyrosyl peptides. *J. Med. Chem.* **38**, 1309–18.
5. Ji, X., Zhang, P., Armstrong, R. N., and Gilliland, G. L. (1992) The three-dimensional structure of a glutathione S-transferase from the mu gene class. Structural analysis of the binary complex of isoenzyme 3-3 and glutathione at 2.2-Å resolution. *Biochemistry* **31**, 10169–84.
6. Schiering, N., Casale, E., Caccia, P., Giordano, P., et al. (2000) Dimer formation through domain swapping in the crystal structure of the Grb2-SH2-Ac-pYVNV complex. *Biochemistry* **39**, 13376–82.
7. Stevens, F. J. (1987) Modification of an ELISA-based procedure for affinity determination: correction necessary for use with bivalent antibody. *Mol. Immunol.* **24**, 1055–60.
8. Fischer, M. J. E., Kuipers, C., Hofkes, R. P., Hofmeyer, L. J., Moret, E. E., and de Mol, N. J. (2001) Exploring computational lead optimisation with affinity constants obtained by surface plasmon resonance for the interaction of PorA epitope peptides with antibody against Neisseria meningitides. *Biochim. Biophys. Acta* **1568**, 205–15.

Chapter 7

Surface Plasmon Resonance Signal Enhancement for Immunoassay of Small Molecules

John S. Mitchell and Yinqiu Wu

Abstract

Sensitive detection of small molecules using surface plasmon resonance (SPR) presents significant challenges as the antigen cannot serve as a signal generator because of its low mass; efficient binding of the target requires the binding event to be spaced from the sensor surface through a specialist linker conjugation. Competitive immunoassay of steroid hormones can be performed by conjugation through a rationally designed linker system at positions distant from existing antigenic functional groups. The binding signal from the primary antibody can then be further enhanced by sequential addition of secondary antibody or conjugated gold nanoparticles which can produce 13-fold signal enhancements through both their mass and co-operative plasmon coupling.

Key words: Gold nanoparticle, SPR, small molecule, immunoassay, linker, conjugation, steroid, signal enhancement.

1. Introduction

Immunoassays using SPR transduction have found wide application in the detection of proteins and oligonucleotides where the large mass of the antigen or its antibody acts as the signal generator (1, 2). Small molecule sensing, however, requires the antigen to be immobilized on the sensor surface or tagged with a high mass label in competitive assay formats (3). This requires careful consideration of the spatial environment of the antigen to ensure minimal steric hindrance to antibody binding and maximal specificity through conjugation at sites distant from existing functional groups (4, 5). Intermediate linkers can be used to provide optimal antigen presentation in flow-through assay formats. For steroid

N.J. de Mol, M.J.E. Fischer (eds.), *Surface Plasmon Resonance*, Methods in Molecular Biology 627,
DOI 10.1007/978-1-60761-670-2_7,

hormones, conjugation at the A-ring 4-position of the steroids has been shown to offer excellent antibody recognition and a linker length of 18 atoms is optimal (5). When tailored polar oligoethylene glycol (OEG) linkers are used the antigen can be projected into the polar mobile phase (6) with low non-specific binding to the non-immunogenic linker chain (7). By using a covalent conjugation to a dextran sensor chip surface, very high stability can be attained even in the face of harsh regeneration conditions and such surfaces are known to last more than 1,100 binding and regeneration cycles (6). Traditionally small molecule SPR immunoassays have suffered from poor sensitivity arising from a lack of signal resolution at low antigen concentrations. Sequential binding of secondary antibody provides signal enhancements of 8- to 9.5-fold, much more than is suggested by simple 1:1 binding (6, 8). When this is combined with conjugated gold

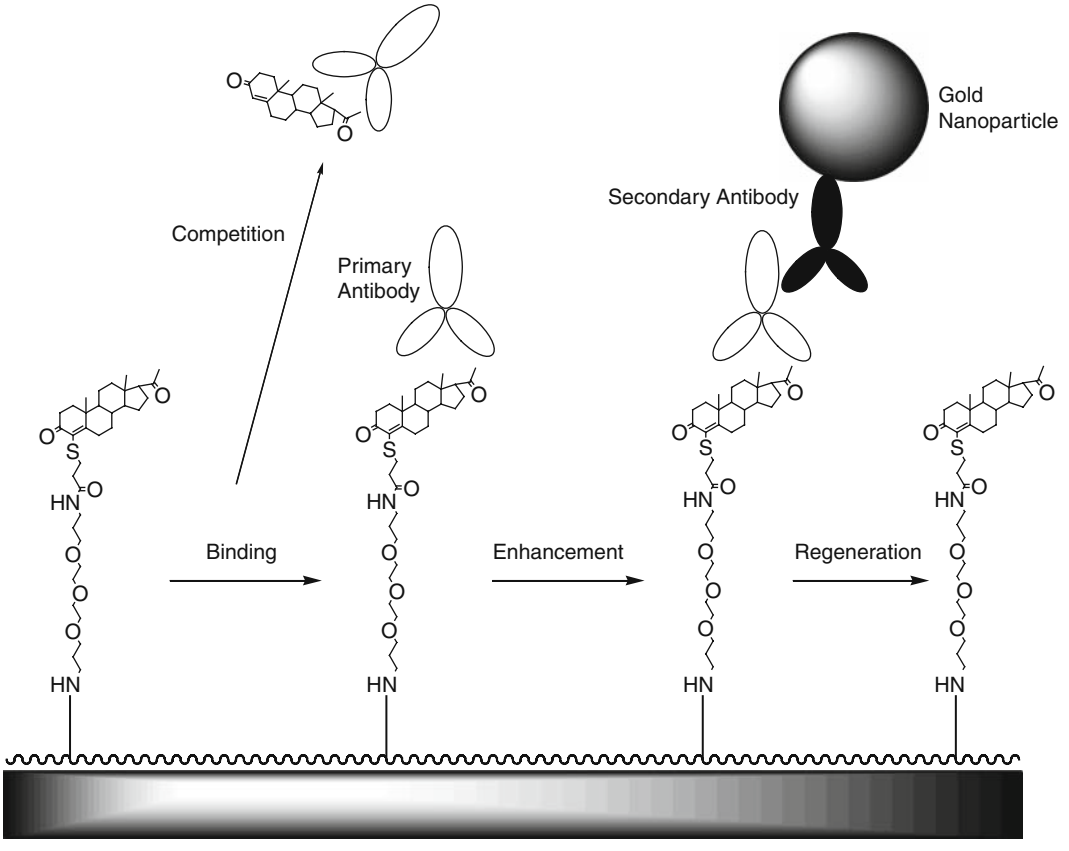

Fig. 7.1. A schematic of the SPR biosensor format for detection of progesterone, showing competitive immunoassay binding of primary antibody to the progesterone-functionalized surface followed by signal enhancement with gold nanoparticle-labeled secondary antibody and then regeneration to return the surface to its original state for the next assay cycle.

nanoparticles of 25 nm diameter, signal enhancements can be further boosted to 13-fold (6) by mass labeling and co-operative plasmon coupling (9) with the gold sensor surface. Limits of detection (LOD) of 8.6 pg/mL can be obtained for steroids compared with 1 ng/mL for more traditional approaches. A schematic of the assay format with nanoparticle enhancement is given in **Fig. 7.1**. The linkers are also crucial in minimizing steric hindrance to conjugated nano-gold and can be applied to other plasmonic platforms such as nanohole arrays (10).

2. Materials

2.1. Steroid-Linker Conjugation

1. Progesterone-4-thiopropionic acid (compound **1A**, *see* **Fig. 7.2**) and estradiol-4-thiopropionic acid (compound **1B**) must be synthesized from the parent steroid. Limited quantities can be sourced from HortResearch, New Zealand.
2. Progesterone-11α-hemisuccinate (P_4-11-HS) (Fitzgerald Industries, MA), β-estradiol-6-one 6-(*O*-carboxymethyloxime) (E_2-6-CMO) (Sigma) (*see* **Note 1**).
3. 1 g (4.58 mmol) di-*tert*-butyl dicarbonate (DBDC) (Fluka) in 10 mL methanol (dried over molecular sieves).
4. 1.9 g (8.60 mmol) 4,7,10-trioxa-1,13-tridecanediamine (OEG) (Fluka) in 20 mL methanol (dried over molecular sieves).
5. Triethylamine.
6. Silica gel 60 (grade 9385, 230–400 mesh) (Merck) used for flash chromatography.
7. Solvents: Analytical grade chloroform ($CHCl_3$), methanol (MeOH), acetic acid (AcOH), dichloromethane (CH_2Cl_2), dimethylformamide (DMF), and formic acid.
8. 1,3-Dicyclohexylcarbodiimide (DCC) (2.35 mmol) in 1.5 mL dry DMF. *N*-Hydroxy-succinimide (NHS) (2.35 mmol) in 1.5 mL dry DMF.

2.2. Immobilization

1. Immobilization buffer: 10 mM phosphate-buffered saline (PBS) consisting of 0.05% v/v Tween-20, 10 mM Na_2HPO_4, 1.8 mM KH_2PO_4, 138 mM NaCl, and 2.7 mM KCl; adjusted to pH 9 with 0.1 M NaOH.
2. Compounds **4A**, **4B**, and **7** or P_4-11-HS and E_2-6-CMO OEG-NH_2 analogs (prepare a 100 mg/mL stock in DMF, then dilute to a 1 mg/mL solution in PBS, pH 9) (*see* **Note 2**). The DMF stock can be kept for up to 1 week at

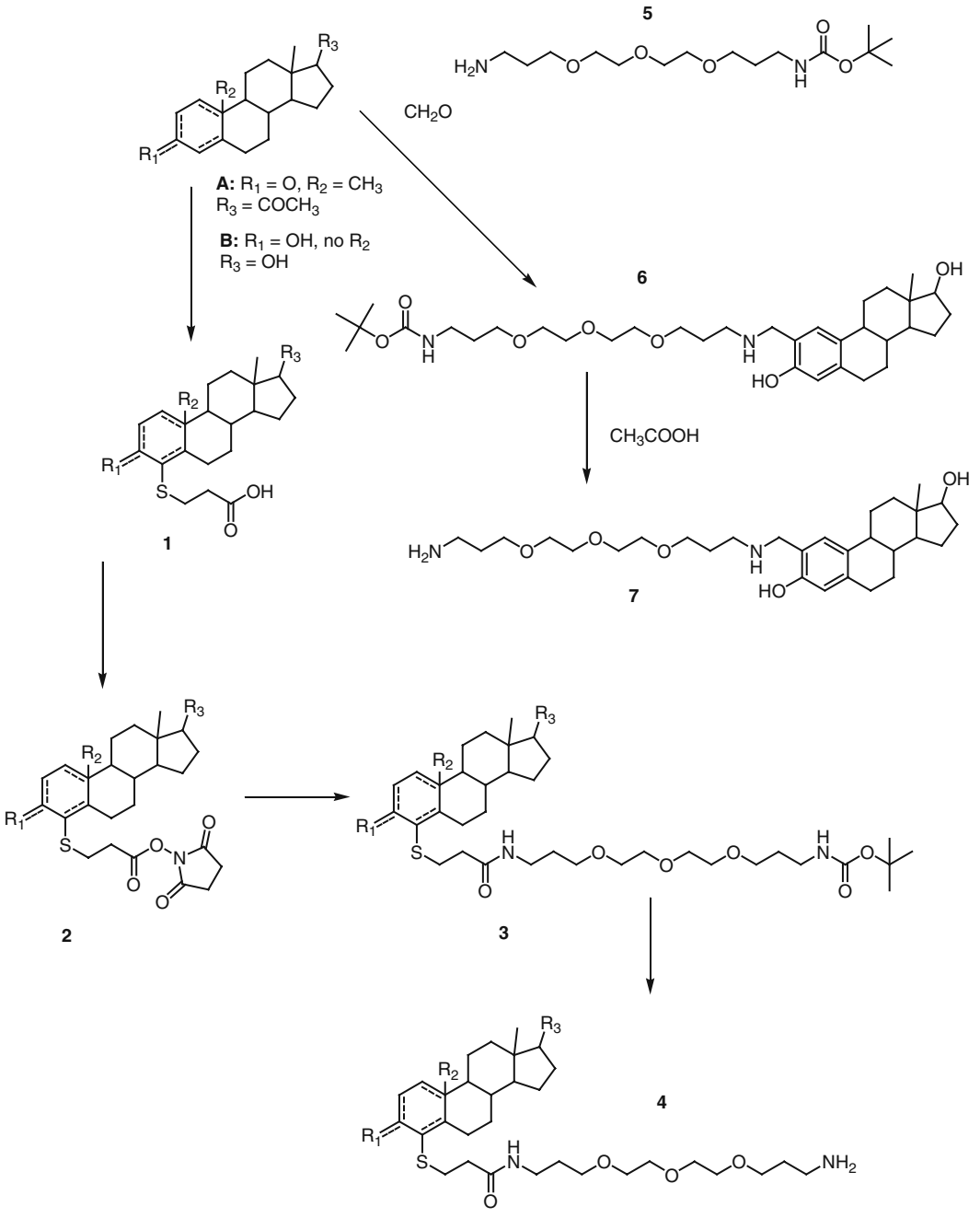

Fig. 7.2. The chemical reaction scheme for the synthesis of the steroid-linker derivatives for immobilization in the SPR biosensor. Functional group combination **A** is progesterone and combination **B** is 17β-estradiol with an aromatic A-ring. The linker attachment can proceed by either conjugation through a carboxylic acid derivative (compound **1** or commercially available alternatives) or through a Mannich reaction of the estradiol to give compound **6**. The acid derivatives are activated with NHS to give compound **2** or analog and then an oligoethylene glycol linker is attached to give compound **3**. Compounds **3** and **6** can then be de-protected when needed to produce compounds **4** and **7**, respectively. Once prepared, one batch of conjugate can be used to immobilize a large number of chip flow cells.

4°C, the diluted stock should be used within 1 day. Unused compound can be recovered by vacuum evaporation of the DMF stock.

3. A BIAcore 2000 or 3000 SPR instrument (BIAcore, Uppsala, Sweden) equipped with reference flow cell subtraction (*see* **Note 3**).
4. BIAcore CM5 dextran-coated chip (BIAcore, Research Grade BR-1000-14) (*see* **Note 4**). Store at 4°C wrapped in laboratory film when not in use.
5. Running buffer: Dissolve 0.95 g HEPES, 3.51 g NaCl, 0.44 g ethylene diamine tetraacetic acid (EDTA), and 0.2 mL P-20 surfactant in 400 mL of deionized water and adjust pH to 7.4 with 0.1 M NaOH. All water used must be deionized to a resistivity of 18 MΩ cm. Running buffer should be filtered through 0.4-μm nylon membrane and degassed under vacuum.
6. 400 mM *N*-ethyl-*N*-(3-dimethylaminopropyl) carbodiimide (EDC) and 100 mM *N*-hydroxy-succinimide (NHS) coupling solutions (BIAcore) are aliquoted and frozen. Thaw aliquots as needed, transfer to plastic BIAcore vials and use within 6 h.
7. Deactivation solution: 1.0 M ethanolamine–HCl, pH 8.5.

2.3. Gold Nanoparticle Production and Conjugation

1. $HAuCl_4 \cdot 3H_2O$ (Acros) (5.8 mg) is dissolved in 50 mL of water (0.01% w/v of $HAuCl_4$) (*see* **Note 5**).
2. Trisodium citrate (Aldrich, 99% pure). Dissolve in water to make a 1% w/v solution.
3. Polyethylene glycol (PEG)-400 (Prolabo). Used at 3% v/v in the gold colloid for centrifugally concentrating nanoparticles.
4. Secondary antibody solution: Anti-rat IgG (whole molecule, raised in rabbit, Sigma) 8 mg/mL in water with pH adjusted to 8.5. Use immediately after preparation.
5. Blocking solution: 20% w/v bovine serum albumin (BSA) in water with pH adjusted to 8.5. Use within 1 h.

2.4. SPR Immunoassay with Secondary Antibody Enhancement

1. Primary antibody solutions: Anti-progesterone monoclonal antibody (mAb) (Sigma, raised to progesterone-7-BSA) 6 μg/mL (*see* **Note 6**) in running buffer or anti-estradiol mAb (US Biologicals, raised to estradiol-6-CMO-BSA) 50 ng/mL in running buffer. Upon receipt of antibody stock solutions, aliquot and freeze; we do not add glycerol. Thawed aliquots can be used for up to 1 month when stored at 4°C, without significant decay. Use dilutions within 2 days of preparation.

2. Progesterone standards: Prepare a stock solution of progesterone (Sigma; >99%) in DMF at 10 mg/mL. Visually inspect the solution to ensure all solid is dissolved, use vigorous vortex mixing. Dilute to 100 μg/mL in running buffer (*see* **Note 7**) and then again to 1 μg/mL. The DMF stock can be kept for up to 2 months and the others for up to 2 weeks at 4°C. Serially dilute from 1 μg/mL to produce standards at 0.1, 1, 5, 10, 50, and 100 pg/mL and 1, 10, and 50 ng/mL in running buffer (*see* **Note 8**). Running buffer can serve as the blank in all cases. Prepare the serial dilution fresh for each new assay. Do the same for estradiol (ICN) but serially dilute to 0.5, 1, 5, 10, 50, 100, and 500 pg/mL and 1 and 5 ng/mL.
3. Secondary antibody solutions: Anti-rat IgG (whole molecule, Sigma) dilute to 400 μg/mL in running buffer. Anti-mouse IgG (whole molecule, Sigma) dilute to 200 μg/mL in running buffer.
4. Regeneration cocktail: 200 mM NaOH, 20% v/v acetonitrile for progesterone assay, 50 mM NaOH, 10% v/v acetonitrile for estradiol assay.

2.5. SPR Immunoassay with Secondary Antibody-Gold Enhancement

1. Progesterone mAb solution: 3 μg/mL in running buffer.
2. Progesterone standards: Prepare as above but at 1, 10, 50, and 100 pg/mL and 1 and 10 ng/mL.
3. Secondary antibody-25 nm gold conjugate (*see* **Section 3.3**): Dilute to 50% v/v in 1% v/v PEG-400 solution in water.
4. Regeneration cocktail: 200 mM NaOH, 20% v/v acetonitrile.

3. Methods

The challenges in obtaining ultrasensitive immunoassays of small molecules can be effectively overcome by combining gold nanoparticle labeling with linker conjugation that allows binding to take place with minimal steric hindrance (6). It is important therefore to first conjugate the antigen of interest to a spacer linker, and this can be performed from appropriate carboxylic acid derivatives at points distant from existing functional groups through simple active ester formation and amide coupling, **Fig. 7.2**. The amine terminus on the linker chains is protected with a *t*-butoxide group (11) that can be easily removed when ready for immobilization and the protected compound will be stable for months – years with storage at 4°C.

Immobilization is achieved by simply flowing the steroid-linker derivative (6, 8) over a carboxymethylated (CM) dextran surface bearing carboxylic acid groups (12) activated with EDC/NHS under alkaline conditions in situ within the biosensor. Competitive immunoassay is then possible by pre-mixing antibody and antigen and then injecting after brief incubation in a microtiter plate. The signal from bound primary antibody will be greatly enhanced through use of secondary antibody binding either with or without gold nanolabels, depending upon how low an LOD is required (*see* **Fig. 7.1**). Gold colloids for labeling can be produced by citrate reduction (13, 14). Simple addition of PEG to the gold colloid prevents settling of the colloid (15) and helps to reduce non-specific binding. Surfaces can be simply and completely regenerated despite high bound mass without damaging the surface; chips once immobilized can be used for many assays of the target antigen. The secondary antibody-conjugated gold nanoparticles have the potential for multivalent interactions with the primary antibody bound on the sensor surface which would result in higher affinity interactions and may contribute to improved immunoassay sensitivity in addition to the effects of a high bound mass and co-operative plasmon coupling.

3.1. Steroid-Linker Conjugation

1. Add OEG stock solution to a 50-mL round bottom flask and set stirring vigorously using a magnetic stirrer bar. Add triethylamine (1 mL). Place a rubber septum over the mouth of the flask and using a glass-barreled syringe inject dropwise the DBDC stock and stir for 16 h. All chemical reactions are illustrated in **Fig. 7.2**.
2. Remove solvent using a vacuum line and purify by silica gel flash chromatography using successively 4:1 CH_2Cl_2:MeOH, 32:8:1 CH_2Cl_2:MeOH:AcOH, and 16:4:1 CH_2Cl_2:MeOH:AcOH as eluant. To perform the chromatography, mix silica gel (*see* **Section 2.1**) with the starting eluant (4:1 CH_2Cl_2:MeOH) to form a slurry and then pour into a glass chromatography column (500 × 20 mm) with a sintered glass panel and tap. Run off excess solvent and allow the silica gel bed to settle to its final volume whilst ensuring that no part of the silica is dry. Compressed air can be used to speed the flow. Pack to 75% full or less for smaller quantities of sample. Dissolve the sample in the minimum of eluant solvent and carefully apply to the top of the silica gel. Allow the solvent to run through and then run solvents in the order indicated as eluants and collect fractions into separate vials. The compound can be identified by thin-layer chromatography (TLC) of the column fractions using the 16:4:1 mobile phase. On silica gel 60 F_{254} plates the retention factor (R_f) is 0.85 for

compound **5**. Combine the relevant fractions and remove the solvent under vacuum (*see* **Note 9**).

3. Dissolve the steroid-4-propionic acid derivative (compound **1A** or **1B** or alternatives listed above, 2.14 mmol) in dry DMF (3 mL) (*see* **Note 10**) in a glass-stoppered small flask and stir with a magnetic stirrer bar. Add the DCC stock solution (1.5 mL) dropwise using a glass Pasteur pipette followed by the NHS stock (1.5 mL) likewise. A white solid should precipitate from the solution within 5 min (this is dicyclohexylurea byproduct).
4. Stir in the dark for 16 h and then remove the precipitate by filtering with a small sintered glass filter funnel. At this point the product can be purified further by flash chromatography if desired (*see* **Note 11**).
5. Place the steroid solution (compounds **2A**, **2B**, or analogs) in a small clean flask and stir as above. Add compound **5** (1.371 g, 4.27 mmol) dropwise (*see* **Note 12**) to the stirring solution. Add triethylamine (2 mL) and stir for 60 h in the dark.
6. Remove the solvent using a vacuum line and purify by flash chromatography using 15:1 $CHCl_3$:MeOH eluant to yield the product (compounds **3A** and **3B** or analogs) as yellow oil. The compound can be identified by TLC of the column fractions using the same running phase. On silica gel 60 F_{254} TLC plates the R_f is 0.36 for compound **3A** and 0.50 for compound **3B** (*see* **Note 13**).
7. To produce compound **6**, dissolve 17β-estradiol (100 mg, 0.367 mmol) in absolute ethanol (10 mL) in a 50-mL round bottom flask with quick-fit attachment and stir with a magnetic stirrer bar. Add compound **5** (236 mg, 0.734 mmol in 4:1 ethanol:water, 5 mL) gradually.
8. Add 37% v/v formaldehyde solution (222 μL, 8.06 mmol) and anti-bumping granules and then attach a water-jacketed condenser to the flask and heat the flask in a heating mantle until the solution boils. Heat under reflux for 6 h. Cool and then remove solvent under vacuum.
9. Reconstitute in $CHCl_3$ and purify by flash chromatography with $CHCl_3$, 15:1 $CHCl_3$:MeOH, 10:1 $CHCl_3$:MeOH as successive eluants to yield compound **6** as clear colorless oil. The product can be identified by TLC, R_f is 0.33 using 15:1 $CHCl_3$:MeOH eluant.
10. To remove the Boc protecting groups from compounds **3A**, **3B**, and **6**, dissolve the required amount of purified steroid derivative in formic acid (20 mg/mL) in a glass round bottom flask and stir in the dark for 3–4 h. Remove

the solvent under vacuum being sure to allow plenty of time for the formic acid to evaporate. Store compounds **4A**, **4B**, and 7 in a freezer when not in use and use within 1 week (*see* **Note 14**).

3.2. Immobilization

1. Dock a fresh CM5 dextran chip into the BIAcore instrument by following the software "wizard" prompts.
2. Prime the system twice with running buffer and start a data file with a flow rate of 20 μL/min on flow cell 2 only.
3. Place separate vials of EDC, NHS, the steroid-linker stock solution, and ethanolamine and an empty vial in the BIAcore rack. Using BIAcore commands, transfer 150 μL of EDC to the empty vial followed by the same volume of NHS. Mix with a mix volume of 200 μL (*see* **Note 15**). Inject from the mix vial 50 μL at 5 μL/min.
4. Without delay, inject 100 μL of the stock steroid solution at 5 μL/min (*see* **Note 16**). Follow this with an injection of the ethanolamine solution (50 μL, 5 μL/min). Stop the recording of data (*see* **Note 17**).
5. Open a new data file set to flow cell 1 only. Perform the transfer, mix, and injection sequences as above but omit the steroid-linker injection. Flow cell 1 will serve as a blank reference flow cell.
6. Clean the surfaces with three injections of 50 mM NaOH (15 μL each at 5 μL/min) to remove contaminants not covalently bound.

3.3. Gold Nanoparticle Production and Conjugation

1. Assemble a quick-fit 100-mL round bottom flask, a water-jacketed condenser, and any necessary adaptors ensuring the glassware is totally clean, dry, and free of any traces of organic matter or metals (*see* **Note 18**).
2. Place 50 mL of the $HAuCl_4$ solution into the flask and bring to boil by heating in a mantle with the condenser fitted and supplied with cooling water.
3. Carefully, while hot, remove the condenser and quickly dispense 900 μL of the trisodium citrate solution into the flask using a pipette. Replace the condenser promptly and allow boiling for a further 10 min before cooling to room temperature (adapted from (13)). The solution will change color from pale orange to black and then to "claret" red (13).
4. Measure the volume of the colloid once cooled and top up to 50 mL as required compensating for any slight evaporative losses. Store the colloid at room temperature in the dark and use within 1 week. Do not freeze as the unprotected colloid will aggregate.

5. When ready to conjugate, determine the volume of final gold conjugate required and take five times that volume of gold colloid and add PEG-400 (sufficient for it to be 3% v/v of the total) and centrifuge at 14,000*g* for 30 min. Remove the supernatant from the pellet and reconstitute in one-fifth of the initial gold colloid volume with water, sonicating as required to reconstitute the colloid.
6. Adjust the pH of the concentrated colloid to pH 8.5 with dilute NaOH (*see* **Note 19**) in a plastic centrifuge tube. Cover the top of the tube with laboratory film and vortex mix to create a strong vortex up the inside of the tube. Inject the secondary antibody stock at a loading of 10% v/v to the colloid through the film covering while vortex mixing and seal with another piece of film. Mix for 30 s longer and then cap and shake for 5 min at 400 rpm. Store it overnight at 4°C.
7. Using the same technique as for the secondary antibody conjugation, add the blocking solution at a loading of 1% v/v to the conjugated colloid. After shaking, store at 4°C for a minimum of 4 h before use.

3.4. SPR Immunoassay with Secondary Antibody Enhancement

1. Dock the pre-immobilized CM5 dextran chip and prime the system twice with running buffer.
2. Start a new BIAcore "wizard" program. Program the following series of commands: set keyword = From_ID, set flow to 20 μL/min, transfer 70 μL of "Antibody" to Mix_ID, transfer 70 μL of From_ID to Mix_ID. Mix the Mix_ID using automix, wait 300 s, inject 60 μL of Mix_ID with a baseline reference point 60 s before the injection. Change the flow rate to 10 μL/min, perform a "Quickinject" of 60 μL of "IgG," change the flow back to 20 μL/min, wait 30 s, and then Quickinject 20 μL of "Regen" with a response reference point inserted 20 s before regeneration injection.
3. "From_ID" refers to the standards and/or samples being analyzed and will vary from one cycle to the next. "Mix_ID" refers to the vials in which the standard or sample is mixed with the primary antibody and from which injections are made. "Antibody" is the primary antibody vial, "IgG" is the secondary antibody vial, and "Regen" is the vial for the regeneration cocktail. When prompted select reference subtraction of flow cell 1 from all immobilized cells. Enter in the standard and sample identities into the sample table and the number of replicates of each (this should be 3–5 replicates).
4. Arrange the sampling positions for the autosampler such that mixing takes place in a microtiter plate (all "Mix_ID" positions should be in this plate). Arrange the vials such that

larger 4 mL vials are allocated for primary and secondary antibodies and regeneration as these solutions must be used in every cycle.

5. Place all the needed vials in the sampling rack according to the positions you have allocated in the wizard program. This includes a set of vials for the standards, buffer blanks, and any samples, vials for the primary antibody solution, secondary antibody solution, and regeneration cocktail. Check for air bubbles in all vials, especially those with beveled bottoms. Be sure to double check vial positions as once the assay has begun, the instrument door locks and changes cannot be made without aborting the assay.
6. Select the "start" assay option with a prime before the assay and standby flow after the assay. The assay will now run automatically but it is sensible to check the progress of the assay at least for the first cycle to ensure no errors in the sampling commands. Assay sensorgram data can be accessed whilst the assay is in progress by opening another instance of the software. All immunoassays are run at 25°C.
7. At the conclusion of the assay, tabulate the total response values in refractive index units (RU) provided by the response point just before the regeneration pulse. Compute mean and standard deviation data for the replicates and fit the standards to a four-parameter logistic curve using standard graphing or statistics software such as SigmaPlot™. Display the assay curve as a plot of response vs. steroid concentration, with the concentration on a log scale. If your assay standard curve data is asymmetric, then you may need to fit to a five-parameter logistic curve instead. The equation for the curve fitting is then re-arranged to enable calculation of concentrations from response values in RU. The LOD of the assay may be computed by taking the blank response, subtracting 2× the standard deviation in the blank response, and translating this into the corresponding concentration using the curve-fitting equation. Examples of the sorts of binding responses, standard curves, and curve fittings one can expect are given in **Figs. 7.3a, b** and **7.4a** for 17β-estradiol and progesterone.

3.5. SPR Immunoassay with Secondary Antibody-Gold Enhancement

1. This assay is constructed using the same transfer, mix, wait, and injection sequence as in **Section 3.4**. Use a primary antibody concentration of 3 μg/mL in the vial. Replace the secondary antibody with the secondary antibody-25 nm gold conjugate prepared in **Section 3.3** at a 0.5 dilution in water with 1% v/v PEG-400. Use serially diluted steroid standards at concentrations of 0, 10, 50, and 100 pg/mL and 1 and 10 ng/mL and run in triplicate. Data processing and

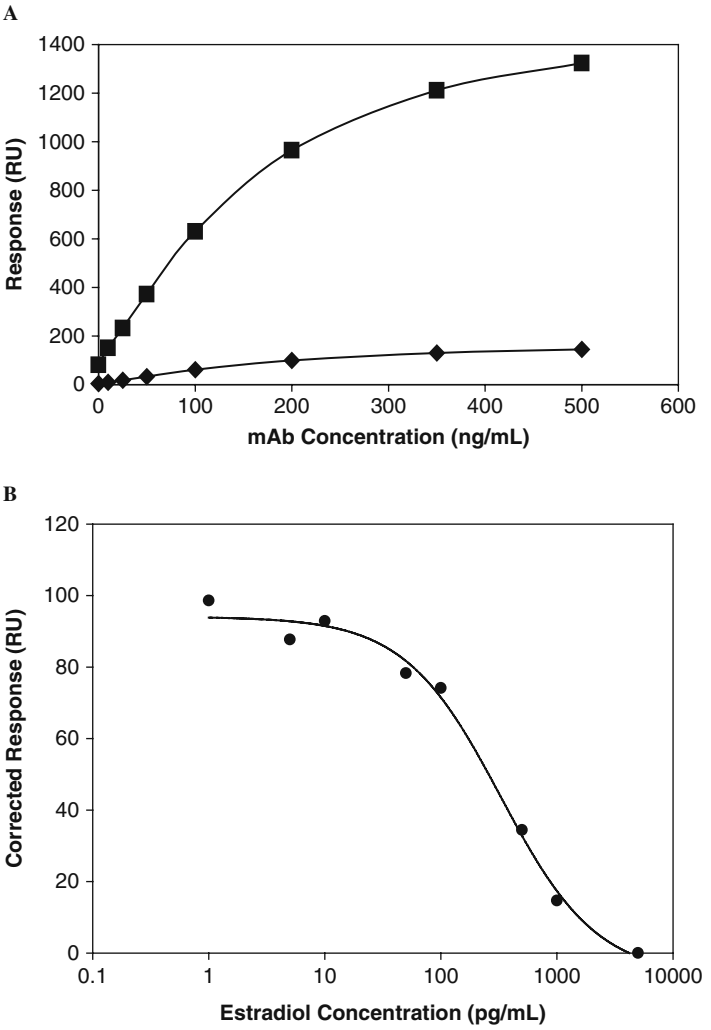

Fig. 7.3. The enhanced immunoassay system applied to biosensing of 17β-estradiol. (**a**) A plot of response (RU) vs. primary antibody concentration (ng/mL) for estradiol sensing. The plot shows both the primary antibody-only response (♦) and the secondary antibody-enhanced signal (■). At higher loadings of the primary antibody, saturation binding to the surface takes place and the response levels out. A fully linear portion of the plots can be seen between 0 and 100 ng/mL. The slope of the enhanced line is 9.5-fold that of the primary antibody, indicating a high level of enhancement beyond that expected from 1:1 binding. (**b**) Assay standard curve with 4-parameter logistic fitting for ultrasensitive immunoassay of estradiol using secondary antibody enhancement. (Both graphs reprinted from (8), with permission from Elsevier.)

instrument setup are as described in **Section 3.4**. An example of the sort of assay curve performance expected vs. an un-enhanced format for progesterone is given in **Fig. 7.4b**.

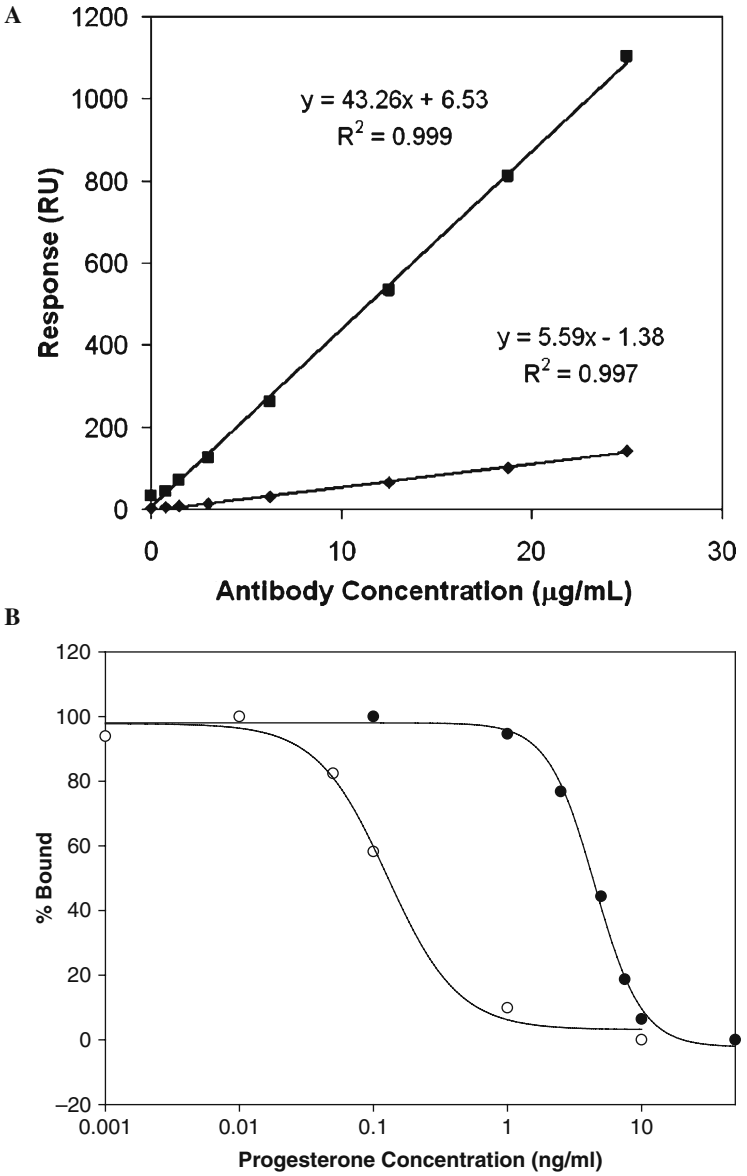

Fig. 7.4. The enhanced immunoassay system applied to ultrasensitive measurement of progesterone. (a) An antibody binding plot showing response from both primary antibody (♦) and secondary antibody-enhanced binding (■) demonstrating linearity of response and a 7.7-fold signal enhancement. Despite the high concentration, the non-specific binding is low (only 6.5 RU). (b) The effect of gold nanoparticle enhancement on assay standard curves and their limits of detection. Standard curves for both a sequential binding secondary antibody-25 nm gold-enhanced assay (○) and an unenhanced assay using a progesterone-protein conjugate (●) are compared. The curve shifts about two orders of magnitude upon nanoparticle enhancement allowing detection at much lower concentrations which are typically found in many biological fluids. LOD with enhancement is 8.6 pg/mL compared with >1 ng/mL without enhancement. (Both graphs reprinted from (6), with permission from Elsevier.)

2. At the conclusion of the assay the immobilized chip should be undocked and the instrument should be cleaned using the "Desorb" program of the BIAcore with the maintenance chip docked. This is especially important to ensure that no gold residues are left in the integrated microfluidics cartridge where they could impregnate into the plastic.
3. Perform data analysis as for the secondary antibody-enhanced assay. The assay signal responses of the system at high analyte concentrations will not reach zero response units because of residual non-specific binding from the gold conjugate. It is advisable therefore to include a high-concentration standard and subtract its response from all the other responses to correct for non-specific binding.
4. Non-specific binding from the gold-secondary antibody conjugate can be reduced by centrifugally purifying the colloid to remove unbound secondary antibody but this procedure reduces enhancement to about 40% of that obtained without purification. Purification can be achieved by leaving the blocked conjugate for at least 4 h at 4°C before centrifuging (13,000*g*, 30 min), removing supernatant with a Pasteur pipette, reconstituting in water, and then repeating once more.
5. The 25-nm colloid size was chosen as larger colloids have a greater risk of aggregation and settling over the time course of the assay whilst smaller colloids lack sufficient surface area for conjugation, reducing the number of antibody residues that can attach. If any signal response drift issues are seen, then the stability of the colloid should be examined. The colloid should not settle onto the bottom of its vial. Doing so indicates that the colloid size is too large, which can be caused by unclean glassware at the nanoparticle production stage or colloid that has been left unblocked for extended periods. Minor signal drift can be corrected for adequately through subtraction of non-specific binding as explained above.
6. The PEG loading used in the diluent of the gold conjugate will both minimize gold settling through charge repulsion and reduce non-specific binding of the gold nanoparticle surfaces to the dextran polymer.
7. To determine the assay sensitivity, create a plot of response vs. concentration for standards in the mid range of the assay standard curve and perform a linear data fitting. The magnitude of the slope of this line is the sensitivity in units of RU mL/ng. The sensitivity using nano-gold enhancement should be above 300 RU mL/ng.

4. Notes

1. The compounds listed are commercially available alternatives to the thiopropionic acid derivatives and can be used in subsequent reactions at the same molarity as the propionic acid compounds and their linker analogs. The 4-position for progesterone and the 2- and 4-positions for 17β-estradiol have been found to offer the best performance in flow-through immunoassays. The derivatives at the 11- and 6-positions may not perform as well but should still generate acceptable assay standard curves for applications requiring only higher LOD. The reactions can be scaled up or down depending upon the amounts of compound required.
2. Dissolve the steroid in a small flask or vial as not much DMF is needed. Make sure that the solvent passes over the entire steroid in the flask. When diluting in PBS there may be some slight solid formation, mix thoroughly until the solution clears.
3. Other types of SPR equipment can also be applied, with appropriate adaptations according to the user manual.
4. Once immobilized, these chips will last much longer than the expiry date on the pack as long as they are stored at 4°C when not in use. To ensure proper alignment of flow cells, only use a chip on the same instrument that it was immobilized with.
5. The gold salt must be weighed and dissolved quickly as it is very hygroscopic. Use only plastic spatulas and weigh boats as it may form a black insoluble solid if left for long in contact with metal. The percentage of loading is calculated from the $HAuCl_4$ only. As you are weighing the trihydrate, the water of hydration must be compensated for.
6. To determine protein concentration of the antibody stock, perform bincinchoninic acid (BCA) assay (Pierce) as stock concentrations given with the product can be inaccurate.
7. Upon dilution, the DMF may cause salts in the buffer to temporarily precipitate. They will re-dissolve upon vigorous mixing.
8. Always serially dilute the standards, i.e., prepare each standard by dilution from the one before it in the concentration series. This prevents dilution inconsistencies. Take care to avoid any cross-contamination of high- and low-concentration standards.

9. At this point we usually wash the linker derivative by adding a solution of sodium bicarbonate in water to the combined fractions in a separating funnel, allowing the layers to settle and then running off the organic phase (lower layer) and removing the solvent under vacuum. This returns the compound to the free amine form.
10. DMF can be dried by placing molecular sieves (type 4A, 4–8 mesh) in the stock bottle of DMF. Be careful not to pipette the fines from the bottom of the bottle.
11. For flash chromatography, use eluant of 15:1 chloroform:methanol, $R_f = 0.95$ for compound **2A** and 0.96 for compound **2B**. Purification here can make purification of compound **3** easier though it should be done promptly to ensure minimal degradation of the active ester.
12. Compound **5** is a viscous liquid. Adding 1 mL of dry DMF can make it easier to pipette.
13. Once the fractions have been spotted and TLC plates run and dried, the spots can be visualized by simply viewing under a short-wave UV lamp.
14. The primary amine can oxidize to a nitro group with time and so should be stored at low temperature and in the dark.
15. The mix volume is the amount of solution the needle takes up to mix the sample. This should usually be set at 0.65–0.75 of the total volume in the vial.
16. The surface, once activated, is prone to hydrolysis of the active esters so the amine should be exposed to the surface as soon as possible after activation. A high steroid concentration and slow flow rate ensures high efficiency of coupling and allows saturation immobilization.
17. Flow cells 3 and 4 can be immobilized in the same way as for flow cell 2 enabling detection of up to three steroids from the same chip.
18. Organic and metal traces can provide nucleation points that disrupt the growth of the colloid and can cause aggregation or a colloid with multimodal particle size distributions.
19. Adjust pH with 0.01 M NaOH carefully. If the pH becomes too alkaline, discard the colloid and begin again. Adding acid to reduce the pH generates salt which will cause colloid aggregation.

Acknowledgments

The authors would like to thank Associate Professor Lyndsay Main and Dr. Christian Cook for their advice and encouragement. This work was funded by the New Zealand Foundation for Research Science and Technology.

References

1. Homola, J. (2008) Surface plasmon resonance sensors for detection of chemical and biological species. *Chem. Rev.* **108**, 462–93.
2. He, L., Musick, M. D., Nicewarner, S. R., Salinas, F. G., Benkovic, S. J., Natan, M. J., and Keating, C. D. (2000) Colloidal Au-enhanced surface plasmon resonance for ultrasensitive detection of DNA hybridization. *J. Am. Chem. Soc.* **122**, 9071–77.
3. Kim, S. J., Gobi, K. V., Iwasaka, H., Tanaka, H., and Miura, N. (2007) Novel miniature SPR immunosensor equipped with all-in-one multi-microchannel sensor chip for detecting low-molecular-weight analytes. *Biosens. Bioelectron.* **23**, 701–07.
4. Bieniarz, C., Husain, M., Barnes, G., King, C. A., and Welch, C. J. (1996) Extended length heterobifunctional coupling agents for protein conjugations. *Bioconjug. Chem.* **7**, 88–95.
5. Wu, Y., Mitchell, J. S., Cook, C. J., and Main, L. (2002) Evaluation of progesterone-ovalbumin conjugates with different length linkers in enzyme-linked immunosorbent assay and surface plasmon resonance-based immunoassay. *Steroids* **67**, 565–72.
6. Mitchell, J. S., Wu, Y., Cook, C. J., and Main, L. (2005) Sensitivity enhancement of surface plasmon resonance biosensing of small molecules. *Anal. Biochem.* **343**, 125–35.
7. Otsuka, H., Nagasaki, K., and Kataoka, K. (2003) PEGylated nanoparticles for biological and pharmaceutical applications. *Adv. Drug Deliv. Rev.* **55**, 403–19.
8. Mitchell, J. S., Wu, Y., Cook, C. J., and Main, L. (2006) Estrogen conjugation and antibody binding interactions in surface plasmon resonance biosensing. *Steroids* **71**, 618–31.
9. Lyon, L. A., Musick, M. D., and Natan, M. J. (1998) Colloidal Au-enhanced surface plasmon resonance immunosensing. *Anal. Chem.* **70**, 5177–83.
10. Sharpe, J. C., Mitchell, J. S., Lin, L., Sedoglavich, N., and Blaikie, R. (2008) Gold nanohole array substrates as immunobiosensors. *Anal. Chem.* **80**, 2244–49.
11. Robertson, J. (2000) *Protecting Group Chemistry.* Oxford, New York.
12. Johnsson, B., Löfås, S., and Lindquist, G. (1991) Immobilization of proteins to a carboxymethyldextran-modified gold surface for biospecific interaction analysis in surface plasmon resonance sensors. *Anal. Biochem.* **198**, 268–77.
13. Frens, G. (1973) Controlled nucleation for the regulation of the particle size in monodisperse gold suspensions. *Nature.* **241**, 20–22.
14. Oliver, C. (1999) Preparation of colloidal gold. *Methods Mol. Biol.* **115**, 327–30.
15. Takae, S., Akiyama, Y., Otsuka, H., Nakamura, T., Nagasaki, Y., and Kataoka, K. (2005) Ligand density effect on biorecognition by PEGylated gold nanoparticles: regulated interaction of RCA_{120} lectin with lactose installed to the distal end of tethered PEG strands on gold surface. *Biomacromolecules* **6**, 818–24.

Chapter 8

High-Throughput Kinase Assay Based on Surface Plasmon Resonance

Hiroyuki Takeda, Naoki Goshima, and Nobuo Nomura

Abstract

We have designed a novel high-throughput (HTP) kinase assay using an array-based surface plasmon resonance (SPR) apparatus. For high flexibility and performance, the kinase assay procedure is divided into an in vitro phosphorylation part and a phospho-detection part on a sensor chip. Not only biotinylated peptides but also recombinant proteins fused with FLAG-GST tandem tag can be used as native substrates. The substrate is selectively captured by a capture antibody immobilized on a sensor chip, and phospho-tyrosine (pTyr) residues are detected by an anti-pTyr antibody. The level of tyrosine phosphorylation is calculated from the capture level of the substrates and the binding level of the anti-pTyr antibody monitored by SPR. A wide dynamic range and real-time monitoring of SPR contribute to improved data reliability, and optimization of the procedure for an array-based apparatus achieved multiple sample processing (1,000 samples/day).

Key words: Tyrosine phosphorylation, capture method, recombinant protein, in vitro kinase assay, Gateway technology, wheat germ cell-free protein expression, Biacore A100.

1. Introduction

Protein phosphorylation plays important roles in cellular processes. Phosphorylation analysis is conducted strenuously for studying signal transduction or exploring potential drug targets, and a highly sensitive, fast, and reliable kinase assay method is required (1, 2). Here, we introduce an in vitro high-throughput tyrosine kinase assay method using surface plasmon resonance (HTP-SPR method) (3).

The advantages of utilizing an SPR biosensor are the ability to detect analytes quantitatively with high sensitivity and

N.J. de Mol, M.J.E. Fischer (eds.), *Surface Plasmon Resonance*, Methods in Molecular Biology 627,
DOI 10.1007/978-1-60761-670-2_8,

wide dynamic range, reliability from real-time sampling, and handiness with automated processing. Recently, manufacturers have improved the throughput of SPR biosensors for large-scale screening assays (4). Biacore A100 is an array-based apparatus based on S51 technology, providing both high sensitivity and high throughput. In order to process as many samples as possible, the present protocol is designed based on a "capture method." In the HTP-SPR method, the phosphorylation step is conducted efficiently in a microtiter plate, apart from the phospho-detection step by SPR (**Fig. 8.1**). Capturing and purification of phosphorylated substrates and monitoring of anti-phospho-tyrosine (anti-pTyr) antibody binding toward phosphorylated substrates are conducted automatically by an SPR apparatus. Finally, captured substrates and an anti-pTyr antibody are washed away, and the sensor chips can be reused for hundreds of cycles. Approximately 1,000 samples can be processed per day using the present method. The separation of phosphorylation reactions from the detection step contributes not only to the efficiency of assay processes but also to the reliability of the obtained data. Since the kinase reaction is performed in solution, it guarantees accessibility of a kinase to substrates and theoretically prevents denaturation of proteins.

This chapter also introduces high-throughput preparation of substrate proteins for the capture method using an in vitro translation system. Improvements in the construction of proteome-scale cDNA libraries (5, 6), Gateway recombinant technology, and protein expression technology (7) have made it possible to provide a variety of fresh recombinant proteins with required tags in the short term. In particular, a wheat germ cell-free expression system provides high performance and stable expression in vitro and is suitable for protein production in a small-scale 96/384-well format (8); it may contribute to supplying a large number of fresh and active recombinant proteins for the assay.

This method is applicable to a variety of purposes, such as for a kinase catalytic study, substrate analysis, and inhibitor screening using both native proteins and peptides as the substrate. The present method may collaborate well with existing methods, such as mass spectrometry or in vivo assay, and can be a powerful tool for exploring candidates of phosphorylation targets.

Fig. 8.1. (continued) for spot *3*. Spots *1* and *5* are used for capturing samples and spots *2–4* are used as references. *Step 1*: a kinase reaction mix is injected into spot *1* and a substrate protein is selectively captured by the anti-FLAG antibody. Auto-phosphorylated tyrosine kinase is washed out. *Step 2*: another kinase reaction mixture is injected into spot *5*. *Step 3*: the anti-pTyr antibody is injected throughout the flow cell, and pTyr residues on the captured substrates are detected. *Step 4*: the sensor chip is regenerated by washing with 10 mM NaOH.

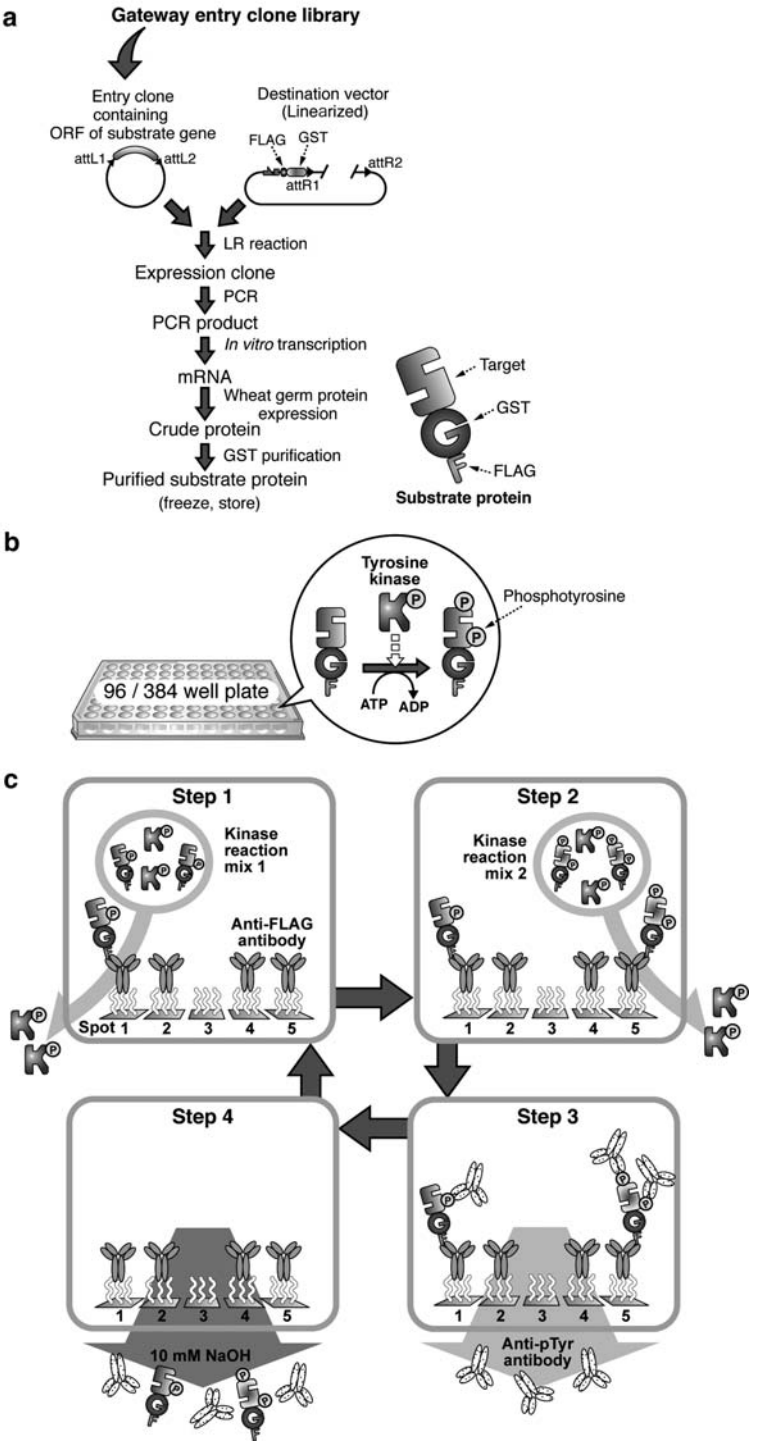

Fig. 8.1. Experimental overview. (**a**) Preparation of substrate proteins. All procedures may be performed in a 96-well format. (**b**) In vitro kinase reaction. (**c**) Phosphotyrosine detection using Biacore A100. Biacore A100 has four flow cells in total with 20 detection spots on the sensor chip, and the figure illustrates the events in a flow cell. The anti-FLAG antibody is pre-immobilized on each detection spot by amine coupling except

2. Materials

2.1. Preparation of Substrate Proteins

1. Gateway entry clone: Entry clones that contain the ORFs of target proteins are selected from the human Gateway entry clone sets (8). Plasmid is diluted to 1 ng/μL with TE buffer (10 mM Tris–HCl, 1 mM EDTA, pH 8.0).
2. Destination vector: pEW-5FG vector (8) contains SP6 promoter for transcription, omega sequence, FLAG-GST tandem tag, and *att* sites (**Fig. 8.1**). The plasmid vector should be linearized with a combination of *Xba*I (Toyobo, Osaka, Japan) and *Pst*I (Nippon Gene, Toyama, Japan) treatment. Linearized vector is diluted to 150 ng/μL with TE buffer.
3. Gateway LR clonase and LR reaction buffer (Invitrogen, Carlsbad, CA, USA). Store at −80°C.
4. Air incubators: ICB-10, NIB-10, and ICB-151AJN (Asahi Techno Glass, Chiba, Japan) and MIR-262 (Sanyo, Osaka, Japan).
5. Centrifuges: CT2Y and LX-140 with microplate racks (Hitachi Koki, Tokyo, Japan).
6. KOD Dash DNA polymerase (2.5 units/μL), 10× KOD Dash reaction buffer, and 2 mM dNTPs (Toyobo, Osaka, Japan).
7. Dimethyl sulfoxide (Wako Pure Chemical Industries, Osaka, Japan).
8. A set of primer pair for PCR is designed to amplify a region from the upstream of SP6 promoter to the 1.8 kb downstream of the *att*R2 sites (**Fig. 8.1**). Concentration is adjusted to 10 pmol/μL with water. The forward primer is 5′-ACATACGATTTAGGTGACACT-3′ and the reverse primer is 5′-GTCAGACCCCGTAGAAAAGA-3′.
9. Thermal cycler: DNA Engine PCT200 (MJ Research, now Bio-Rad, Hercules, CA, USA).
10. RNA polymerase (80 units/μL) (Promega, Madison, WI, USA).
11. RNase inhibitor (40 units/μL) (Promega).
12. Transcription buffer (5×): 400 mM HEPES–KOH, pH 7.8, 80 mM magnesium acetate, 10 mM spermidine, and 50 mM DTT are dissolved in GIBCO water. Store in aliquots at −30°C.
13. NTP mix solution: 25 mM of each nucleotide triphosphate (ATP, UTP, GTP, and CTP) is dissolved in GIBCO water. Store in aliquots at −30°C.

14. Water: GIBCO water distilled sterile (Invitrogen) (*see* **Note 1**).
15. Reagents for wheat germ expression: WEPRO 1240 wheat germ extract and SUB-AMIX translation buffer (40× stock solutions S1–S4) are from CellFree Sciences (Yokohama, Japan). Store in aliquots at −150°C.
16. Creatine kinase (Roche Diagnostics, IN, USA) is dissolved in GIBCO water at 20 mg/mL. Store as single-use aliquots at −150°C.
17. 96-Well plate, flat bottom, sterile (TPP, Trasadingen, Switzerland).
18. Plate seal (Invitrogen).
19. Wash buffer: 50 mM Tris–HCl (pH 7.4), 150 mM NaCl, and 1 mM DTT. Prepare just before use.
20. Elution buffer: 50 mM Tris–HCl (pH 8.0), 20 mM reduced glutathione, and 1 mM DTT. Store as single-use aliquots at −30°C.
21. Glutathione–Sepharose 4B obtained from GE Healthcare (Buckinghamshire, UK) is equilibrated with wash buffer and 10% slurry is prepared before use.
22. Storage buffer (2×): 50 mM Tris–HCl, pH 8.0, 1 mM DTT, 300 mM NaCl, 0.1% Brij35, 20% glycerol, and 2 mg/mL BSA. Store as single-use aliquots at −30°C.
23. 1 M DTT: Store in aliquots at −30°C (*see* **Note 2**).
24. Filter plate: MultiScreen, ø 0.45 μm, 96 wells (Millipore, Billerica, MA, USA).
25. Air bath plate shaker: MBR-024 (TAITEC, Saitama, Japan).
26. Liquid nitrogen.

2.2. Pre-immobilization of Anti-FLAG Antibody for Substrate Capturing

1. Biacore A100 optical biosensor is purchased from Biacore (now part of GE Healthcare, Uppsala, Sweden).
2. Series S sensor chip CM5 (certified) (Biacore).
3. Amine coupling kit type 2 (Biacore): EDC and NHS are dissolved in Milli-Q water according to the manufacturer's instruction. They are stored in aliquots at −80°C. 1 M ethanolamine is stored at 4°C.
4. FLAG M2 antibody (Sigma–Aldrich, St. Louis, MO, USA). Store at −30°C.
5. 10 mM sodium acetate (pH 4.5) (Biacore).
6. Biadissolve solutions 1 and 2 in Biacore maintenance kit type 2 (Biacore).

7. HBS-EP+buffer (10×): 10 mM HEPES–NaOH (pH 7.4), 150 mM NaCl, 0.05% (v/v) Tween 20, and 3 mM EDTA, filtered through sterile 0.45-μm filter. Store at 4°C. The buffer (100 mL) is diluted with 900 mL water before use (*see* **Note 3**).

2.3. In Vitro Kinase Reaction

1. Commercial protein tyrosine kinases are purchased from Millipore and Carna Biosciences (Kobe, Japan) (*see* **Note 4**).
2. Kinase reaction buffer (2×): Stock solutions (1 M HEPES–NaOH (pH 7.2), 1 M $MgCl_2$, and 1 M $MnCl_2$) are stored separately at room temperature. 2× buffer (40 mM HEPES–NaOH, 20 mM $MgCl_2$, and 6 mM $MnCl_2$) is prepared before use.
3. ATP solution: ATP is dissolved at 10 mM into a solution containing 20 mM HEPES–NaOH (pH 7.4) and 20 mM $MgCl_2$. Store as single-use aliquots at −80°C.
4. EDTA solution: 50 mL of 500 mM EDTA-Na (pH 8.0) is mixed with 450 mL of HBS-EP+buffer. Store at 4°C.
5. 96-Well round-bottom plates (BR-1005-05) and 384-well flat-bottom plates (BR-1005-03) are purchased from Biacore.
6. Microplate foils BR-1005-77 (384 wells) and BR-1005-78 (96 wells) are obtained from Biacore.

2.4. pTyr Detection by SPR

1. Anti-pTyr antibody: P-Tyr-100 is obtained from Cell Signaling Technology (Danvers, MA, USA). Lot 11 (1.5 mg/mL) was used in **Figs. 8.3** and **8.4**.
2. Regeneration solution: Freshly prepared 10 mM NaOH (*see* **Note 5**).
3. Reagent plates and foils are obtained from Biacore.

3. Methods

Figure 8.1 shows an outline of the sample preparation, kinase reaction, and pTyr detection. Substrate proteins are expressed as FLAG-GST tandem tag fusion proteins. The GST tag is used for pre-purification, and the FLAG tag is used for capturing onto a sensor chip. Capturing using a FLAG tag is suitable for wheat germ expression, that is, internal proteins in the wheat germ hardly bind to anti-FLAG antibody and do not interfere with the binding between FLAG-tag fusion proteins and the antibody (*see* **Note 6**). Furthermore, it is an advantage for large-scale assay that FLAG M2 antibody can be regenerated and reused for hundreds of cycles (*see* **Note 7**).

The advantage of wheat germ cell-free expression is its high speed and stable expression, and a variety of proteins may be expressed to some extent without requiring detailed optimization for each protein. Reaction volume can be easily decreased since it is an in vitro cell-free system. Therefore, the wheat germ expression system is a suitable expression system for the protein sample preparation of a screening assay that requires a small volume but a large number of samples. In addition, the wheat germ has no internal tyrosine kinase activity, and it reduces the background level to the minimum. Proteins expressed by other systems or peptides may be used as substrates (*see* **Notes 8** and **9**).

A quality control of protein samples is important for obtaining high-quality data. One of the key features of the method is the utilization of native proteins as substrates. When a substrate protein is denatured, it often causes artifacts. The present method is designed to minimize protein denaturation, for instance, by in solution kinase reaction or by controlling temperature during the kinase reaction and pTyr detection. Furthermore, scrupulous handling of protein samples in the purification steps and sample storage would be desirable.

3.1. Preparation of Substrate Proteins

1. Gateway LR reaction: A premix is prepared by mixing 0.5 μL of a linearized destination vector, 1 μL of LR reaction buffer, 1 μL of LR clonase, and 1.5 μL of TE buffer (*see* **Note 10**). The premix (4 μL) is dispensed into 96-well PCR plates and the entry clone (1 μL) is added. The plate is covered with a plate seal. The reaction mixture is mixed by tapping, spun down, and incubated at 25°C for 18 h. TE buffer (15 μL) is added to the resultant LR reaction mixture and stored at −80°C.
2. PCR amplification of templates for transcription: The DNA fragment in the entry clone is amplified as a template for in vitro transcription. A premix is prepared by mixing 5 μL of 10× KOD Dash reaction buffer, 5 μL of 2 mM dNTPs, 5 μL of dimethyl sulfoxide, 1 μL of each primer (0.2 μM), 0.25 μL of KOD Dash polymerase (2.5 units/μL), and 30.75 μL of water. The premix (48 μL) is dispensed into each well of a 96-well PCR plate and then LR reaction mixture (2 μL) is added. The plate is covered with a plate seal for PCR and the reaction mixture is mixed by tapping and spun down. The cycling parameters for the PCR are as follows: primary denaturation step (95°C, 1 min) and the following 30 cycles consisting of denaturing (94°C, 20 s), annealing (55°C, 5 s), and extension (74°C, 4 min). PCR products are stored at −80°C.
3. Preparation of mRNA: A premix is prepared by mixing 10 μL of 5× transcription buffer, 5 μL of NTP mix solution,

0.5 μL of 1 M DTT, 1 μL (40 units) of RNase inhibitor, 2 μL (160 units) of SP6 RNA polymerase, and 26.5 μL of water. The premix (45 μL) is dispensed into each well of a 96-well PCR plate and the PCR product (5 μL) is added. The plate is covered with a plate seal. The reaction mixture is mixed by tapping, spun down, and incubated at 37°C for 18 h. The resultant mRNA should be stored at −80°C (*see* **Notes 11** and **12**).

4. An upper layer solution for all samples is prepared in a single tube by diluting 3.5 μL of each SUB-AMIX translation buffer (S1–S4) with 126 μL of GIBCO water for each sample (totally 140 μL), then 136.4 μL of the buffer is dispensed into each well of a flat-bottom 96-well plate. For preparation of a lower layer solution, the wheat germ extract is placed on ice and thawed (*see* **Note 13**). The wheat germ extract (5 μL) is mixed with 0.7 μL of an RNase inhibitor and 0.4 μL of creatine kinase, then 6.1 μL of the mixture is dispensed into each well of another 96-well PCR plate. mRNA (7.5 μL) is added to the PCR plate and gently mixed by pipetting. The lower layer solution (13.6 μL) is transferred onto the bottom of the flat-bottom plate (total volume of 150 μL). The plate is covered with a plate seal and incubated at 26°C for 18 h.
5. After completing translation, expressed proteins should be purified immediately (*see* **Note 14**). The wash buffer and elution buffer are chilled on ice. Temperature in the centrifuge is kept at 4°C. A 10% Glutathione–Sepharose 4B slurry (30 μL) is added to each crude sample; the plate is covered with a plate seal and shaken vigorously (900 rpm) at 4°C for 3 h. The mixture is transferred to a filter plate and filtrated by centrifugation (50*g*) at 4°C for 1 min. The flow-through solution is discarded and then the resin is washed with 100 μL of ice-chilled wash buffer three times. The filter plate is placed on a new 96-well plate, and 30 μL of elution buffer is added to the resin. The plates are incubated at 4°C for 30 min and then purified proteins are collected by centrifugation (2,000*g*) at 4°C for 5 min. The same volume of storage buffer is added to the eluate. The solution is mixed by shaking at 900 rpm and 4°C for 5 min and then spun down. For short-term storage, the purified protein stocks are stored at 4°C. For long-term storage, the purified protein stocks should be divided into single-use aliquots and frozen immediately in liquid nitrogen. Frozen samples are stored at −80°C (*see* **Note 15**).

3.2. Pre-immobilization of Anti-FLAG Antibody for Substrate Capturing

1. The Series S sensor chip CM5 (certified) is mounted in the Biacore A100 biosensor (*see* **Note 16**).
2. The anti-FLAG M2 antibody, NHS, and EDC are thawed. The anti-FLAG M2 antibody is diluted with 10 mM sodium acetate (pH 4.5) to 20 μg/mL.
3. The anti-FLAG antibody is immobilized onto spots 1, 2, 4, and 5 of each flow cell using the standard amine coupling immobilization protocol for the capture method. HBS-EP+buffer is used as the running buffer and the flow rate is set to 10 μL/min. The surface of the sensor chip CM5 is activated by a 10-min injection of NHS–EDC. The anti-pTyr antibody is injected for 7 min. Residual reactive sites are blocked by ethanolamine injection (*see* **Note 17**).

3.3. In Vitro Kinase Reaction

1. Temperature in the air bath plate shaker is kept at 30°C. The 96/384-well microtiter plates are chilled on ice. Kinase, substrates, 2× reaction buffer, ATP solution, and Milli-Q water are prepared and then placed on ice.
2. A reaction premix consisting of 15 μL of 2× reaction buffer, 0.3 μL of 10 mM ATP, an arbitrary amount of kinase, and Milli-Q water (total volume of 24 μL) is prepared. At least one control sample in which the premix contains Milli-Q water instead of kinase should be prepared for each substrate in order to evaluate baseline. The substrates (6 μL) are dispensed into an ice-chilled 96/384-well plate (*see* **Note 18**). The kinase reaction is initiated by adding 24 μL of the premix. The plate is covered with a plate seal, placed in an air bath plate shaker, and the reaction is mixed by shaking at 900 rpm for 1 min. The plate is incubated for arbitrary period (from 20 min to 5 h) (*see* **Note 19**).
3. The kinase reaction is terminated by adding 80 μL of cold EDTA solution. The plate is covered with a microplate foil for the Biacore assay, inverted to mix, and spun down. The reaction plate is subjected to pTyr detection by Biacore immediately or kept at 4°C (*see* **Note 20**).

3.4. pTyr Detection by SPR

1. HBS-EP+ running buffer (1×) and Milli-Q water are prepared and their bottle is connected to Biacore A100. The anti-pTyr antibody is diluted with cold HBS-EP+ buffer to 1.5 μg/mL. The diluted anti-pTyr antibody and regeneration solution are dispensed into a reagent plate, and the

reagent plate is covered with a reagent plate foil. The temperature in the rack hotel of Biacore A100 is adjusted to around 4–6°C.

2. An assay cycle consists of four steps: (1) capturing FLAG-tagged substrates on spot 1 of each flow cell; (2) capturing substrates on spot 5; (3) injection of anti-pTyr antibody; and (4) regeneration. The flow rate is maintained at 10 μL/min. The times of capturing, anti-pTyr antibody binding, and regeneration are 150, 120, and 30 s, respectively. Prior to the assay cycles, five cycles of "start-up" cycles are performed.
3. The method file is opened, sample information is entered, and the assay program is executed. The microplate with the reaction mixture and reagent plate is inserted according to the instructions given by the program.

3.5. Data Processing

1. An example of sensorgrams is shown in **Fig. 8.2**. Spots 2 and 4 are references of spots 1 and 5, respectively, and reference-subtracted data is utilized. Values of relative responses at each report point, "capture_level^{-1}" (for spot 1), "capture_level_2" (for spot 5), and "stability_early" (**Fig. 8.2**), are measured to calculate the level of tyrosine phosphorylation (*see* **Notes 21** and **22**).

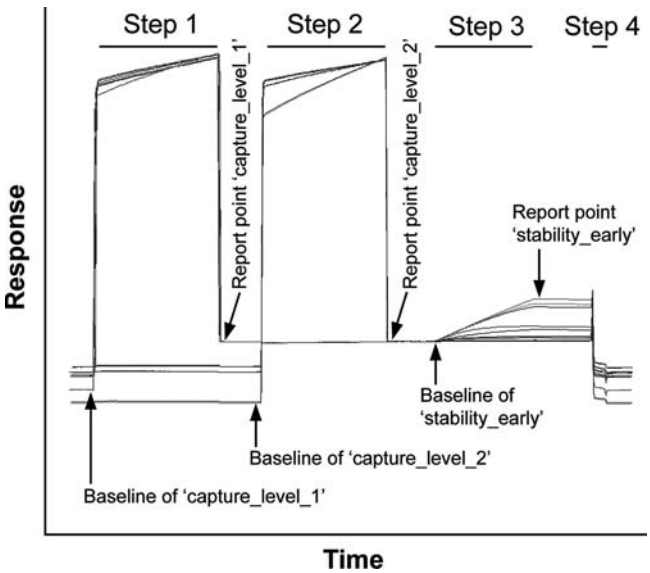

Fig. 8.2. Overlaid sensorgrams of the HTP-SPR method. Sensorgrams of spots 1 and 2 and spots 5 and 4 are shown. Injection events (*steps 1–4*) are described in step 2 of **Section 3.4** and **Fig. 8.1c**. Report points for the subsequent data processing are indicated.

2. Anti-pTyr antibody binding is normalized by the substrate capture level:
"Normalized anti-pTyr antibody binding" = "stability_early" × "capture_level^{-1}" × N,
where N is a coefficient (500 or 1,000 is suitable for protein substrate). Then baseline is subtracted and the level of tyrosine phosphorylation of the sample is deduced:
"Tyrosine phosphorylation" = "normalized anti-pTyr antibody binding$_{(\text{kinase-treated sample})}$" – "normalized anti-pTyr antibody binding$_{(\text{control})}$."

Examples of tyrosine kinase assay are shown in **Figs. 8.3** and **8.4**.

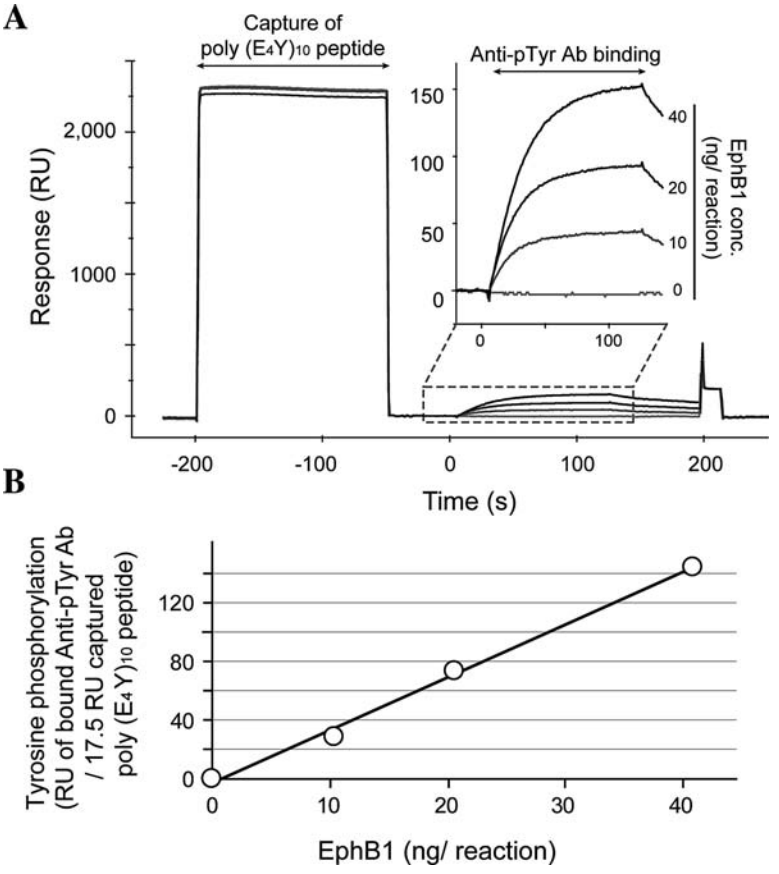

Fig. 8.3. Peptide phosphorylation. (**a**) Overlaid sensorgrams obtained from pTyr detection using a peptide substrate. Two micrograms of biotin-conjugated poly(Glu$_4$Tyr)$_{10}$ peptide in a 20 μL of reaction mixture was phosphorylated by different amounts of EphB1 kinase for 5 h. The substrate peptide was captured with an anti-biotin antibody, and anti-pTyr antibody binding toward a captured peptide was monitored. The binding curve of the anti-pTyr antibody (*dashed-line box*) is enlarged and shown in the *inset*. (**b**) Plot of EphB1 concentration against tyrosine phosphorylation of the substrate peptide. A good correlation between kinase activity and phosphorylation was observed ($R^2 = 0.996$). The tyrosine phosphorylation signal was proportional to EphB1 concentration, indicating that detection of pTyr phosphorylation by SPR was quantitative. (Reproduced from Takeda et al. (3), Elsevier Inc^R.)

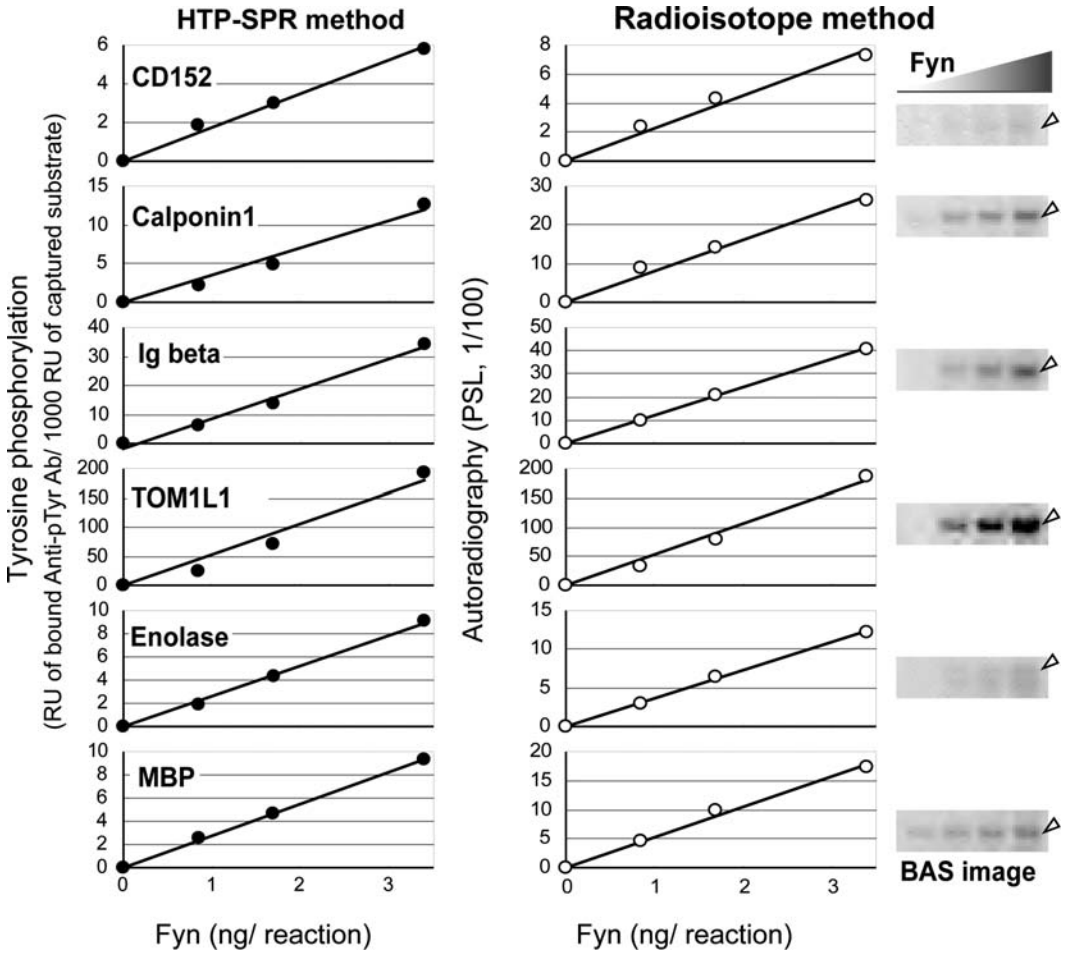

Fig. 8.4. Comparison between the HTP-SPR method and the RI method. Six protein substrates were phosphorylated by Fyn tyrosine kinase for 1 h under the same conditions and then phosphorylation on the substrates was detected by the HTP-SPR method and autoradiography. The *left* and *right* columns indicate the result of the HTP-SPR and RI methods, respectively. Photographs are autoradiographic images produced by FLA-5000 Fluoro Image Analyzer (Fuji, Tokyo, Japan); *white arrowheads* indicate the positions of corresponding substrate bands. The two detection methods provided similar results, strongly suggesting that the HTP-SPR method is quantitative and reliable. (Reproduced from Takeda et al. (3), Elsevier Inc^{R}.)

4. Notes

1. RNase-free water is used to prepare reagents for the transcription and translation steps.
2. Stock solutions are used for the preparation of buffers in the purification step.
3. When an SPR apparatus without a degasser (e.g., Biacore 3000) is used, degassing using an aspirator is required before use.

4. Any tyrosine kinase obtained from various expression systems (hosts) can be applied. The authors tested tyrosine kinases obtained from the *Escherichia coli*, insect cell, and wheat germ expression systems. The FLAG tag should not be fused to the enzymes (kinases) as far as the FLAG-tag capture method is applied.
5. The pH of NaOH solution may decrease by absorbing CO_2 after long-term storage. It may cause inefficient regeneration.
6. FLAG-tag fusion proteins tend to dissociate from the anti-FLAG antibody on a sensor chip after capturing. Dissociation, however, was scarcely observed when FLAG-GST tandem-tagged proteins were captured.
7. When TOM1L1 protein was captured (800 RU) and regenerated using 10 mM NaOH for 10 s, the anti-FLAG M2 antibody maintained approximately 60% of the original capturing ability after 200 cycles (unpublished data).
8. Substrates expressed by other expression systems are also applicable to this assay method. A substrate should be fused with a capture tag (FLAG) and purification tag (such as GST or His_6). Expression level of substrates and tyrosine phosphorylation by internal tyrosine kinase in the expression system should be considered. For example, the internal tyrosine kinase activity in the *E. coli* expression system does not need to be examined, since tyrosine kinase is absent in *E. coli* similar to the wheat germ. However, an inclusion body is often formed in the *E. coli* system, and thus the expression condition should be examined well in advance. On the other hand, insect cells have high expression efficiency, although the background level of tyrosine phosphorylation would be increased by internal kinases.
9. Peptide substrates are available for this assay method instead of a protein substrate (**Fig. 8.3**). The biotin-conjugated peptide substrate was captured by anti-biotin antibody (Vector Laboratories, Burlingame, CA, USA) on a sensor chip. When the biotin-conjugated poly(Glu_4 $Tyr)_{10}$ peptide ($GG[EEEEY]_{10}EE$, Upstate Biotechnology, Charlottesville, VA, USA) was utilized, 2 μg of a peptide was added to each reaction (3).
10. Numerals indicate volume per sample. A premix for all samples is prepared in a single 1.5-mL tube and then dispensed into each well of the plates.
11. In the transcription and translation steps, gloves and masks should be used to prevent contamination of RNase in the reaction.

12. A reaction mixture for the transcription step often has white precipitation after incubation, particularly apparent following freeze/thaw treatment. This precipitation should be mixed well with the reaction mixture by pipetting during the translation step because RNA is often trapped in this precipitation.
13. The wheat germ extract and buffers can be thawed rapidly under running water. The tubes should be placed on ice immediately after thawing.
14. Freezing of crude protein samples may damage the conformation of expressed proteins. Recombinant proteins should be purified after expression and used promptly or frozen in an appropriate storage solution using liquid nitrogen.
15. Freezing allows long-term storage of protein samples (from several weeks to months). Kinases can also be stored using the same procedure. For example, the activity of a tyrosine kinase can only be preserved for several days after storage at 4°C, but can be kept for more than 1 month after freezing.
16. Before exchanging a sensor chip, the flow pass in the SPR apparatus should be cleaned using a maintenance kit.
17. Typically, 10,000 RU of the anti-pTyr antibody is immobilized using the above condition.
18. The order of samples including the control samples should be considered. For example, when an extremely phosphorylated sample is captured on a sensor chip, it often increases the background level for more than 10 cycles. In order to evaluate baseline precisely, the control sample should be assayed first and then the kinase-treated samples sharing the same substrate are applied to the same detection spot.
19. With Fyn-phosphorylated TOM1L1 protein, phosphorylation on the substrate increased linearly in a time-dependent manner. However, long-term incubation may lower the specificity of phosphorylation in exchange for a higher signal intensity.
20. In the case of the plates being stored at 4°C before an SPR analysis, water often evaporates and condensation builds up on the inner side of the foil. This alters the total volume of a sample and causes air spikes. Do not freeze the reaction mixture; it decreases the capture level of a substrate.
21. Evaluation software of A100 conducts a quality check of the acquired data, automatic setting of report point, and statistical analysis. Here, default setting of report point for the capture method is used. After data approval, raw data

is exported to a file. The file extension of the exported file is changed to ".xls" and opened using MS Excel. Using filtering function, data of each report point can be copied to a new spreadsheet with information such as flow cell, spot, cycle, and sample name.

22. Detailed information on report points: Baseline of "capture_level," 10 s before capture molecule injection, 10 s average; "capture_level," 25 s after capture molecule injection, 5 s average; baseline of "stability_early," 10 s before anti-pTyr antibody injection, 10 s average; and "stability_early," 5 s after capture molecule injection, 5 s average.

Acknowledgments

We thank T. Yamamoto and T. Tezuka for technical guidance in the conduct of RI kinase assay. This work was supported by the grant "Functional Analysis of Human Proteins and Its Research Application" from the New Energy and Industrial Technology Development Organization (NEDO), Japan.

References

1. Johnson, S. A., and Hunter, T. (2005) Kinomics: methods for deciphering the kinome. *Nat. Methods* **2**, 17–25.
2. Ptacek, J., and Snyder, M. (2006) Charging it up: global analysis of protein phosphorylation. *Trends Genet.* **22**, 545–54.
3. Takeda, H., Fukumoto, A., Miura, A., Goshima, N., and Nomura, N. (2006) High-throughput kinase assay based on surface plasmon resonance suitable for native protein substrates. *Anal. Biochem.* **357**, 262–71.
4. Rich, R. L., and Myszka, D. G. (2007) Higher-throughput, label-free, real-time molecular interaction analysis. *Anal. Biochem.* **361**, 1–6.
5. Ota, T., et al. (2004) Complete sequencing and characterization of 21,243 full-length human cDNAs. *Nat. Genet.* **36**, 40–45.
6. Strausberg, R. L., et al. (2002) Generation and initial analysis of more than 15,000 full-length human and mouse cDNA sequences. *Proc. Natl. Acad. Sci. USA* **99**, 16899–903.
7. Sawasaki, T., Ogasawara, T., Morishita, R., and Endo, Y. (2002) A cell-free protein synthesis system for high-throughput proteomics. *Proc. Natl. Acad. Sci. USA* **99**, 14652–57.
8. Goshima, N., et al. (2008) Human protein factory for converting the transcriptome into an in vitro-expressed proteome. *Nat. Methods* **5**, 1011–17.

Chapter 9

SPR Biosensor as a Tool for Screening Prion Protein Binders as Potential Antiprion Leads

Beining Chen

Abstract

Prion diseases, also called transmissible spongiform encephalopathies (TSEs), are a group of neurodegenerative disorders affecting animals and humans. No effective treatments are currently available for the diseases, vCJD in particular. It is believed that the formation of protease-resistant insoluble prion protein (PrP^{Sc}), which is the main component of amyloidal deposits, from the cellular prion protein (PrP^{C}), is essential for the progression of the disease. Therefore, both PrP^{Sc} and PrP^{C} are currently being used as potential drug targets.

This protocol details an optimised experimental protocol to conduct an affinity screening of compound libraries by the immobilisation of PrP^{C} using an SPR-based instrument, Biacore 3000.

Key words: Prion protein, surface plasmon resonance, Biacore, affinity binding, drug screening, dissociation constant.

1. Introduction

Prion diseases, also called transmissible spongiform encephalopathies (TSEs), are a group of neurodegenerative disorders affecting animals and humans that include scrapie in sheep, bovine spongiform encephalopathy (BSE) in cattle, chronic wasting disease (CWD) in deer and elk, Gerstmann–Sträussler–Scheinker syndrome and Creutzfeldt–Jakob disease (CJD) in humans (1). Formation of amyloidal deposits in an affected brain is a hallmark of these diseases and the deposits are constituted mainly of aggregated prion protein in a misfolded state, hence the name of the disease. Prion diseases are also infective

N.J. de Mol, M.J.E. Fischer (eds.), *Surface Plasmon Resonance*, Methods in Molecular Biology 627,
DOI 10.1007/978-1-60761-670-2_9,

and can be transmitted via transplants, contaminated biological products from cadavers, blood transfusions, contaminated surgical instruments and ingestion of infected materials. The latter has been observed in humans after consumption of beef affected by BSE and has been termed variant CJD (vCJD). No effective treatments for CJDs, vCJD in particular, are currently available. It is believed that the formation of protease-resistant insoluble prion protein (PrP^{Sc}), which is the main component of amyloidal deposits, from the cellular prion protein (PrP^{C}), is essential for the progression of the disease. Therefore, both PrP^{Sc} and PrP^{C} are currently being studied as potential drug targets (2). However, PrP^{Sc} is insoluble and its structure is not known in detail, and it is technically impossible to produce sufficient quantities for in vitro screening. PrP^{Sc} is therefore mainly used as a biomarker in cellular assays to assess antiprion efficacy of compounds. Most of the affinity-screening assays use more widely available recombinant PrP^{C} as a target protein. The biological efficacy of the affinity binders is normally confirmed in cellular assays using PrP^{Sc} as a biomarker.

PrP^{C} is a membrane protein of unknown physiological function (3–5). It consists of an unstructured, flexible N-terminal domain (AA23–110) which contains five octarepeats (AA51–91); a globular C-terminal domain (AA111–230) which contains two glycosylation sites (Asn181, Asn197) (6); and a glycosylphosphatidylinositol (GPI) anchor (Ser230) (7). The SPR technique is easy to implement and it has medium sample throughput with automated sample handling. SPR has been reported as a binding assay for small drug-like molecules against other drug targets (8). Several groups have reported using SPR as an assay platform to screen compound libraries in order to discover leads which can bind to PrP^{C}, stabilise it and prevent its conformational change to PrP^{Sc} (9–11). For convenient and optimal throughput in drug screening for antiprion lead discovery, immobilising PrP^{C} on the surface and injecting a compound of interest to study their interactions would be ideal. This protocol details an optimised experimental method to conduct affinity screening of compound libraries through immobilised PrP^{C} using an SPR instrument, Biacore 3000. The recombinant full-length human PrP^{C} ($flhPrP^{C}$) is used to highlight the procedures involved.

2. Materials

2.1. Immobilisation of Recombinant Prion Protein PrP^{C}

1. An SPR instrument, Biacore 3000 (Biacore, Uppsala, Sweden) equipped with a CM5 sensor chip (*see* **Note 1**).
2. Immobilisation buffer: HBS-EP buffer consisting of 0.01 M HEPES, 0.15 M NaCl, 3 mM EDTA, 0.005% surfactant P20 at pH 7.4 (*see* **Note 2**).

3. Coupling reagents: 100 mM *N*-hydroxysuccinimide (NHS), 400 mM *N*-ethyl-*N*′-(3-diethylaminopropyl) carbodiimide hydrochloride (EDC) (*see* **Note 3**).
4. Recombinant PrP^Cs (human full length) are available from Prionics (Switzerland) or expressed in-house. It is diluted in 10 mM sodium acetate buffer pH 5.5 to the concentration required.
5. Blocking reagent: 1 M ethanolamine (*see* **Note 4**).
6. Regeneration solution 1 consisting of 25 mM NaOH, 1 M NaCl, 0.0005% SDS at pH 8.0.
7. Regeneration solution 2 consisting of 10 mM glycine–HCl at pH 3.0.
8. Running buffer: PBS buffer consisting of 10 mM Na_2HPO_4 – NaH_2PO_4, 0.15 M NaCl, 3 mM EDTA and 0.005% surfactant P20 at pH 7.4. The buffer needs to be degassed and filtered through nitrocellulose membrane with a pore size of 0.22 μm prior to use.

2.2. Screening of Small Molecule Compound Libraries

1. DMSO (Sigma-Aldrich).
2. Running buffer: the same as in 2.1.
3. Regeneration solutions 1 and 2: the same as in 2.1.
4. BIAdesorb and BIAdisinfectant solutions (Biacore).

3. Methods

It is well known that prion protein binds strongly to metal surfaces (12, 13). It may also bind to the carboxymethylated dextran (CM-dextran) on the gold surface because, structurally, CM-dextran resembles heparin, which is known to bind to prion proteins (14–16). It is important that an appropriate immobilisation protocol is developed and optimised so that the required immobilisation can be achieved.

On the other hand, drug-like compounds normally have a low molecular weight between 300 and 800 Da. To observe binding between a prion protein and those compounds it is essential to be able to immobilise prion proteins at a level between 3,000 and 10,000 RU and keep the baseline as stable as possible.

3.1. Immobilisation of Recombinant Prion Protein PrP^C

1. Two of the four flow cells are used in this assay (*see* **Note 5**). The CM-dextran on flow cells 1 and 2 of a CM5 sensor chip is washed and equilibrated with the running buffer. It is then activated by mixing equal volumes of 100 mM NHS and 400 mM EDC followed by injection of the mixture over

the sensor chip surface for 7 min at a flow rate of 5 μL/min (*see* **Note 6**).

2. The flhPrP^{c} to be immobilised is diluted in 10 mM sodium acetate buffer at pH 5.5 to a concentration of 2 μg/mL and is injected over the flow cell 2 (the test channel) for 7 min (*see* **Note 7**). The flow cell 1 (reference channel) is activated as described above but no protein is injected over the surface. The final immobilisation level of the PrP^{C} is around 4,000 RU on flow cell 2 (*see* **Fig. 9.1** and **Note 8**).
3. The unreacted sites on both flow cells of the sensor chip surface are blocked by the injection of 1 M ethanolamine pH 8.5 for 7 min (*see* **Note 9**).
4. The prepared flow cells on the sensor surface are washed thoroughly, immediately after the ethanolamine blocking step, by three consecutive injections of regeneration solution 1 at an interval of 8 s.
5. The surface is then equilibrated with the running buffer for 30 min prior to the injection of sample solutions.

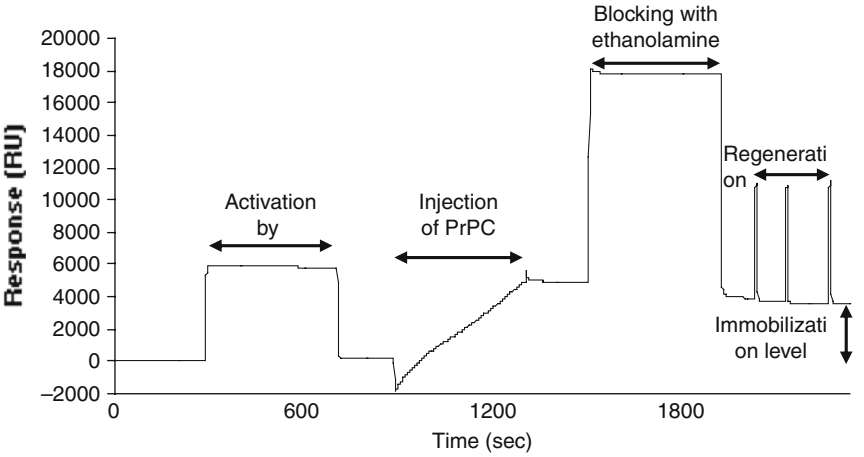

Fig. 9.1. Typical PrP^{C} immobilisation sensorgram (10). The difference between baseline at the start and end indicates the amount of immobilised protein in RU.

3.2. Screening of Small Molecule Compound Libraries

3.2.1. Sample Preparation

The compounds tested can be divided into two groups: water soluble and water insoluble.

1. 6.1 mM stock solutions of all water-soluble compounds are made using running buffer. Stock solutions are diluted to the required 40 μM concentration using the same running buffer prior to the screening.
2. Similarly, 6.1 mM stock solutions of all water-insoluble compounds are made in 100% DMSO. 10 μL of the stock solution is then added to 90 μL of DMSO to give a concentration of 610 μM. A final dilution is carried out by

mixing 65 μL of the second DMSO dilution solution with 935 μL of the running buffer to give a final compound concentration at 40 μM containing 6.5% (v/v) of DMSO. 6.5% DMSO is added to the running buffer.

3.2.2. Compound Screening

1. All assays are carried out at 25°C with a flow rate of 30 μL/min and a compound concentration of 40 μM, using phosphate buffer as the running buffer.
2. For water-soluble compounds, each analytical cycle consisted of running buffer for 1 min (stabilisation phase), a sample injection at 40 μM in running buffer for 1 min (association phase) and running buffer for 3 min (dissociation phase). Subsequent surface regeneration at a flow rate of 35 μL/min was carried out using the two regeneration solutions 1 and 2 sequentially at an interval of 8s. After regeneration the surface was allowed to stabilise for 1 min. The total run time was approximately 8 min/cycle. The sensor chip was usually discarded after 5 days.
3. For compounds using DMSO as a co-solvent, 6.5% DMSO is added to the running buffer and a DMSO calibration using buffer samples containing DMSO at concentrations of 5.5, 6, 6.5, 7 and 7.5% respectively was carried out at the beginning and the end of each block of 10 compounds to correct for solvent effects (*see* **Note 10**). Each screening cycle consists of one 10-injection buffer block, one 5-concentration DMSO calibration block, one 10-compound screening block and another 5-concentration DMSO calibration block (*see* **Note 11**).
4. The data is analysed and the binding is expressed as $\%RU_{max}$ (*see* **Note 12**). The binding strength of compounds can be ranked and compared.

3.2.3. Binding Affinity Study

The binding affinity of positive binders from initial screening in 3.2.2 can be further studied and quantified by the following protocols.

1. For aqueous soluble compounds the PrP^C surface is prepared using the optimal immobilisation procedure (*see* **Section 3.1**). A series of concentrations are injected at a flow rate of 30 μL/min over immobilised PrP^C, and the reference surface at 25°C. A single injection of each solution was carried out from the lowest to the highest concentration and sensorgrams were recorded for each injection (*see* **Fig. 9.2a**). The sensor surface is regenerated with a pulse of 25 mM NaOH/1 M NaCl between each injection. The detailed binding kinetics can be analysed using BIAevaluation software 4.1 (*see* **Note 13**).

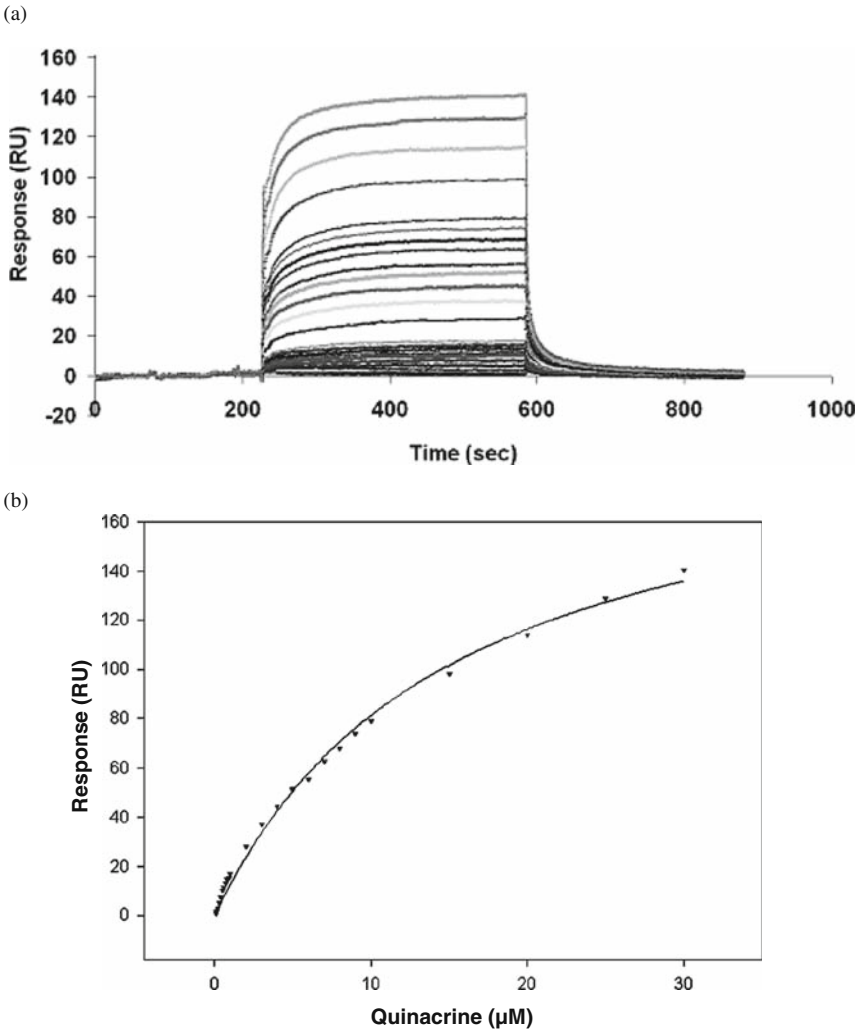

Fig. 9.2. Sensorgrams of quinacrine binding to huPrP^C (concentrations are from 0 to 30 μM) (**a**) and non-linear regression of kinetics data using Langmuir binding isotherm for 1:1 interaction (**b**) (K_d is estimated as 15 μM) (10).

2. For compounds requiring DMSO as a co-solvent, a series of concentrations were injected in triplicate, in ascending order, each containing 6.5% DMSO. DMSO calibration was performed over 2 min, instead of 1 min in the compound-screening protocol, and the equilibrium %RU_{max} calculated (*see* **Sections 3.2.2** and **3.2.3** for more details and **Note 11**). The sensorgrams were then overlaid, and the RU response obtained at the end of the association time was plotted against the concentration and analysed using Excel by non-linear regression and Langmuir 1:1 isotherm binding mode to give the affinity constant (K_d) for each compound (*see* **Fig. 9.2b**),

4. Notes

1. Biacore X-100 and Biacore S51 are a newer generation of SPR instruments reported to have higher sensitivities and are specially designed for small molecule drug screening with an automated DMSO calibration function and more advanced software package for kinetic analysis. The protocol detailed here can be readily applied to either instrument.
2. Ready-to-use HBS-EP buffer (sterile, filtered and degassed) can be purchased from Biacore.
3. Ready made EDC and NHS solutions of the required concentrations are readily available from Biacore.
4. Blocking reagent, ethanolamine, at a concentration of 1 M can be purchased from Biacore.
5. Flow cells 3 and 4 can be used to immobilise different PrP^Cs such as truncated $hPrP^C$ or mouse PrP^C by repeat manual injection, to ensure that the same immobilisation level as for $flhPrP^c$ is achieved, so that comparisons of a compound binding to different species of PrP^C can be easily made.
6. CM5 chip has been modified with carboxylated methyldextran. The carboxyl group is activated by EDC followed by reaction with NHS to form an active ester, which can then react with the amine groups on the PrP^C surface to yield stable amide bonds between the dextran surface and the protein. More details can be found in **Chapter 3**.
7. The immobilisation capacity varies from one protein to the other; optimisation of immobilisation conditions including protein concentrations is required. Here, 2 μg/mL is the optimal concentration to achieve the immobilisation level of around 4,000 RU for all prion proteins.
8. The required prion protein immobilisation level of 4,000 RU is calculated using the equation in **Note 12**. To account for the detection limits of the machine and baseline noise (5–10 RU), 40–100 RU for a small molecular weight compound is generally required at a given immobilisation level of the protein. For a compound like quinacrine (MW 400 Da), if a binding of 100 RU is required to be observed on the chip surface, the level of prion protein (MW 17,000 Da) required to be immobilised is around 4,000 RU, calculated by the manipulation of the RU_{max} equation in **Note 12**. A typical immobilisation sensorgram can be seen in **Fig. 9.1**.

9. Chemical principle of ethanolamine blocking can be found in **Chapter 3**.
10. Biacore 3000 does not have an auto solvent correction function; correction of solvent effect is carried out by two programmed DMSO calibration blocks each containing triple injections of five different DMSO concentrations. The data is exported to Excel to generate a calibration curve, and a correction factor can be extrapolated and used to adjust the RU obtained from any DMSO sample injections (Excel macro can be obtained from the author). Newer models of Biacore such as T100 and S51 can auto-correct DMSO solvent effects in both screening and kinetic analysis.
11. Detailed programmed procedures and macros can be obtained by contacting the author via e-mail: b.chen@sheffield.ac.uk.
12. $\%RU_{max}$ can be calculated in two steps. In Step 1, for a given immobilisation level of a protein (it can be extrapolated from immobilisation sensogram **Fig. 9.1**), the theoretical maximum binding resonance units (RU_{max}) for a ligand can be calculated using the following formula:

$$\text{Theoretical } RU_{max} = \left(\frac{\text{RU immobilised protein}}{\text{MW protein}}\right) \times \text{MW of the compound} \quad [1]$$

The above equation can be manipulated to calculate the immobilisation of a protein (RU-immobilised protein) if the theoretical RU_{max} is reset. As with quinacrine, a theoretical RU_{max} of 100 is deemed to be reasonable to take the baseline noise and its small molecular weight (MW = 400), the level of protein required to be immobilised (RU-immobilised protein) = 100 × 17,000 ÷ 400 = 4,250, hence the value of ~4,000 RU is proposed. When a specific immobilisation level is achieved, RU_{max} for the positive control, quinacrine, and every compound to be tested should be recalculated accordingly before $\%RU_{max}$ is calculated and any ranking of initial binding based on $\%RU_{max}$ takes place.

In Step 2, assuming 1:1 binding stoichiometry, $\%RU_{max}$ can be calculated by the following formula:

$$\%RU_{max} = \left(\frac{\text{RU of compound}}{\text{Theoretical } RU_{max} \text{ of the compound}}\right) \times 100 \quad [2]$$

13. For water-soluble compounds, rates of association and dissociation, k_a and k_d, as well as equilibrium kinetic constant K_D can be obtained by analysing using BIAevaluation software 4.1 equipped with Biacore 3000.

References

1. Collins, S. J., Lawson, V. A., and Masters, C. L. (2004) Transmissible spongiform encephalopathies. *Lancet* **363**, 51–61.
2. Perrier, V., Wallace, A. C., Kaneko, K., Safar, J., Prusiner, S. B., and Cohen, F. E. (2000) Mimicking dominant negative inhibition of prion replication through structure-based drug design. *Proc. Natl. Acad. Sci. USA* **97**, 6073–78.
3. Harris, D. A. (1999) Cellular biology of prion diseases. *Clin. Microbiol. Rev.* **12**, 429–44.
4. Martins, V. R., Linden, R., Prado, M. A. M., Walz, R., Sakamoto, A. C., Izquierdo, I., and Brentani, R. R. (2002) Cellular prion protein: on the road for functions. *FEBS Lett.* **512**, 25–28.
5. Griffoni, C., Toni, M., Spisni, E., Bianco, M. C., Santi, S., Riccio, M., and Tomasi, V. (2003) The cellular prion protein - Biochemistry, topology, and physiologic functions. *Cell Biochem. Biophys.* **38**, 287–304.
6. Ermonval, M., Mouillet-Richard, S., Codogno, P., Kellermann, O., and Botti, J. (2003) Evolving views in prion glycosylation: functional and pathological implications. *Biochimie.* **85**, 33–45.
7. Baron, G. S., and Caughey, B. (2003) Effect of glycosylphosphatidylinositol anchor-dependent and -independent prion protein association with model raft membranes on conversion to the protease-resistant isoform. *J. Biol. Chem.* **278**, 14883–92.
8. Ueda, Y., Yamagishi, K., Samata, H., Ikeya, N., Hirayama, H., Takashima, H., Nakaike, M., Tanaka, I., and Saiki, I. (2003) A novel low molecular weight antagonist of vascular endothelial growth factor receptor binding: VGA1155. *Mol. Cancer Therap.* **2**, 1105–11.
9. Kawatake, S., Nishimupa, Y., Sakaguchi, S., Iwaki, T., and Doh-ura, K. (2006) Surface plasmon resonance analysis for the screening of anti-prion compounds. *Biol. Pharm. Bull.* **29**, 927–32.
10. Touil, F., Pratt, S., Mutter, R., and Chen, B. (2006) Screening a library of potential prion therapeutics against cellular prion proteins and insights into their mode of biological activities by surface plasmon resonance. *J. Pharm. Biomed. Anal.* **40**, 822–32.
11. Hosokawa-Muto, J., Kamatari, Y. O., Nakamura, H. K., and Kuwata, K. (2009) Variety of antiprion compounds discovered through an in silico screen based on cellular-form prion protein structure: correlation between antiprion activity and binding affinity. *Antimicrob Agents Chemother* **53**(**2**), 765–71.
12. Zobeley, E., Flechsig, E., Cozzio, A., Enari, M., and Weissmann, C. (1999) Infectivity of scrapie prions bound to a stainless steel surface. *Mol. Med.* **5**, 240–43.
13. Flechsig, E., Hegyi, I., Enari, M., Schwarz, P., Collinge, J., and Weissmann, C. (2001) Transmission of scrapie by steel-surface-bound prions. *Mol. Med.* **7**, 679–84.
14. Brimacombe, D. B., Bennett, A. D., Wusteman, F. S., Gill, A. C., Dann, J. C., and Bostock, C. J. (1999) Characterization and polyanion-binding properties of purified recombinant recombinant protein. *Biochem. J.* **342**, 605–13.
15. Pan, T., Wong, B. S., Liu, T., Li, R. L., Petersen, R. B., and Sy, M. S. (2002) Cell-surface prion protein interacts with glycosaminoglycans. *Biochem. J.* **368**, 81–90.
16. Caughey, B., Brown, K., Raymond, G. J., Katzenstein, G. E., and Thresher, W. (1994) Heterologous PrP molecules interfere with accumulation of protease-resistant PrP in scrapie-infected murine neuroblastoma-cells. *J. Virol.* **68**, 2135–41.

Chapter 10

Carbohydrate–Lectin Interactions Assayed by SPR

Eric Duverger, Nathalie Lamerant-Fayel, Natacha Frison, and Michel Monsigny

Abstract

Surface plasmon resonance is a valuable tool to determine the affinity between glycoconjugates and sugar-binding proteins such as plant and animal lectins. The main interest of using such an approach is that neither the lectins – which are proteins – nor their ligands – natural compounds such as glycoproteins, oligosaccharides, polysaccharides, or synthetic glycoconjugates such as glycoclusters or neoglycoproteins – require any tag. Because lectins bear several binding sites, they behave like immunoglobulin eliciting avidity phenomena. This peculiarity may lead to erroneous results if special conditions are not applied. We obtained best and reproducible results when the lectin was immobilized and its ligands were used as soluble analytes. With heterogeneous glycoconjugates such as neoglycoproteins (which are heterogeneous in terms of nature, number, and position of sugar residues) or a mixture of oligosaccharides, the data may be more accurately gathered by using the Sips approach, which has been used to determine mean binding constants of polyclonal antibodies. With small analytes such as oligosaccharides, we found it convenient to determine binding constants by using an inhibitory approach: a neoglycoprotein ($M_r = \sim 80{,}000$) was allowed to bind to the immobilized lectin and small oligosaccharides were used as inhibitors. With larger glycoconjugates such as peptides substituted with glycoclusters, direct binding measurements gave accurate results. Because of the availability of low-cost simple sugars (mono- or disaccharides) it is very convenient to use large concentrations of such carbohydrates to clean the sensor chips instead of more drastic cleaning solutions such as acids or alkali, in such a way that the immobilized lectin is stable for many experiments.

Key words: Avidity, cluster effect, glycoclusters, glycoconjugates, lectins, multivalency, neoglycoproteins, Scatchard plot, Sips, sugar-binding proteins.

1. Introduction

Lectins are carbohydrate-binding proteins (or glycoproteins) of non-immune origin (1) which agglutinate cells and/or precipitate

N.J. de Mol, M.J.E. Fischer (eds.), *Surface Plasmon Resonance*, Methods in Molecular Biology 627,
DOI 10.1007/978-1-60761-670-2_10, © Springer Science+Business Media, LLC 2010

glycoconjugates (for a recent review, *see* (2)). They are widely distributed in plants, animals, and microorganisms. In animals, lectins have been identified in a great number of cells. They are either embedded in intracellular or cell surface membranes or soluble in the plasma; inside cells, they are also found in the cytosol and in the nucleus. Animal lectins play a crucial role in both physiological and pathological processes. Specific interactions between lectins and complex carbohydrates (glycoproteins, glycolipids, polysaccharides, or proteoglycans) are involved in numerous basic phenomena such as embryonic development, intracellular traffic, cell–cell and cell–matrix recognition, cell homing, endocytosis, phagocytosis, inflammation, and metastatic spreading of cancer cells.

Based on this, the sugar specificity of endogenous lectins and both the thermodynamics and the time course of interactions between lectins and their carbohydrate cognates are of a great importance for a better understanding of biological processes. With the development of apparatus based on surface plasmon resonance (SPR), it became easy to determine kinetic parameters k_{ass} and k_{diss} as well as thermodynamic parameters, including binding constant K_A of interacting partners. Neither partner (glycoconjugate or lectin) requires a tagging; therefore, it is easy and quite fast to acquire relevant data useful to decipher the biological specificity and functions of both glycoconjugates and lectins.

First, in a theoretical part, we will discuss two main points which have to be taken into account when studying lectin–carbohydrate interactions by SPR: the choice of the immobilized partner and the influence of avidity (also known as cluster effect). As shown by Shinohara et al. (3), the measured affinity is quite dependent on the partner immobilized in a solid-phase assay such as SPR. Binding constants measured with immobilized lectins were in good agreement with previous studies (mainly in homogeneous liquid phase); in contrast, when using glycoconjugates as the immobilized partner, the apparent binding constants could be 10,000 times higher. This discrepancy is related to multivalency including a phenomenon known as "avidity" or "cluster effect." Avidity is not troublesome when the immobilized partner is a lectin and the ligand used is a simple soluble oligosaccharide; conversely, avidity does interfere when the oligosaccharide is immobilized and the lectin is in solution.

In a second part, materials and methods currently used in our laboratory will be described. Finally, we will present two types of experiments: (i) an indirect binding experiment, where affinities of glycoclusters binding to MMR1-8 (human macrophage mannose receptor, domains 1–8) are deduced from their ability to inhibit the binding of a neoglycoprotein containing mannose (or fucose) to the immobilized lectin, and (ii) the direct measurement of the kinetic constants of the binding of glycocluster

peptide conjugates to immobilized DC-SIGN (dendritic cell-specific ICAM-3 grabbing non-integrin) lectin.

In the following section some basic considerations for experimental design are described.

1.1. Choice of the Immobilized Partner

Using two given partners, a lectin and a carbohydrate, the apparent affinity is greatly dependent on the nature of the immobilized partner; it is either a lectin-immobilized assay or a carbohydrate-immobilized assay (3). As an example, measurements were carried out by using WGA and *N*-acetyl-chito-oligosaccharides. K_A values obtained with the immobilized lectin were in the range of 10^3–10^4 L mol^{-1}, in good agreement with previous data obtained by classical methods. Conversely, using a carbohydrate-immobilized assay, K_A values were up to 10^8 L mol^{-1}. The K_A increase was mainly related to a change in the dissociation constant k_{diss}. Dissociation was relatively slow in the carbohydrate-immobilized assay but much faster in the lectin-immobilized assay. The k_{diss} was shown to depend on both the lectin valence and the immobilized oligosaccharide density, shedding light onto the cluster effect.

1.2. Avidity or Cluster Effect

"Avidity" is related to the apparent enhancement of functional affinities through multiple interactions between binding partners. While affinity describes the binding of a monovalent ligand to its receptor, avidity is used to take into account multivalent interactions. The recognition of a simple sugar by a lectin is usually in a very low affinity range (about 10^3 L mol^{-1}). Conversely, complex oligosaccharides, as well as saccharide clusters, bind lectins in a high-affinity range (up to 10^8 L mol^{-1}).

Avidity should not be assimilated to multivalency; indeed, a binding constant is defined as an interaction between soluble monovalent partners; in contrast, avidity is an apparent affinity, usually much larger than the true binding constant, because of kinetics, multivalency, or allosteric properties.

In 1965, Greenbury and coworkers (4) convincingly showed that rabbit anti-group A antibodies, which are bivalent (IgG type), were able to bind to group A red blood cells at much lower concentration than the monovalent Fab fragment. They clearly showed that the $(Fab')_2$ fragment behaves like the IgG itself with an association constant about 400 times higher than the monovalent Fab fragment. This avidity effect was interpreted on the basis of the density of the blood group substances (oligosaccharides of cell surface glycoconjugates) on the area where one of the two binding sites of the antibody or the $(Fab')_2$ binds. Similar results were also obtained with IgM antibodies which contain 10 binding sites and, as a consequence, bind their antigens with a quite high apparent affinity while their Fab fragments (which are monovalent) bind the red blood cells with a low affinity (5).

Lectins which usually have several binding sites (2, 3, 4, 6, or more; *see* **Table 10.1**) may behave in a similar way. Indeed, the binding of plant lectins to their cell surface ligands may be strong, even when the affinity constant of the corresponding soluble ligands is weak. For instance, wheat germ agglutinin mainly binds to the Neu5Ac residues on the cell surface with a high affinity ($>10^6$ L mol^{-1}) while the binding constant of soluble sialylated oligosaccharides is much lower: around 10^3 L mol^{-1} (6). Wheat germ agglutinin binds, with high affinity, glycoproteins bearing a cluster of oligosaccharides ending with Neu5Ac residues as in the case of the N-terminal moieties of glycophorin (7).

The avidity effect was clearly established by Lee and coworkers (8, 9), in the case of the Ashwell lectin, a lectin from liver parenchyma cells specific for terminal galactose (or *N*-acetylgalactosamine) residues at the non-reducing end of an oligosaccharide: the affinity of a single antenna ending with a β-galactopyranosyl residue was found to be close to 10^3 L mol^{-1}, while that of the bis-derivative was close to 10^6 L mol^{-1} and those of the tris and tetrakis derivatives were close to 10^9 L mol^{-1}. The avidity-related enhancement of the binding constant has been largely documented in the field of lectins from both plant and animal origins (for a review, *see* (10)).

1.3. Avidity in the Context of SPR Analysis

The effect of the oligomeric status of a plant lectin was studied (3) by comparing Ssa (the tetrameric *Sambucus sieboldiana* lectin) and its monomeric counterpart (mSsa). Lectins were injected over immobilized 6′-sialyl-Lac. Kinetics measurements showed that k_{ass} was quite close (around 2×10^4 L mol^{-1} s^{-1}) for both Ssa and mSsa, while k_{diss} was different: 2.4×10^{-3} s^{-1} for Ssa versus 53×10^{-3} s^{-1} for mSsa. The apparent affinity of the tetrameric lectin was about 10 times higher due to a slow dissociation process. Because of multivalency the rebinding is more efficient; when one binding site becomes free another one, because of its nearby position, will bind the same or a close-by ligand.

The influence of the carbohydrate surface density on affinity was also reported by Horan et al. (11). Using another plant lectin, Bpa (*Bauhinia purpurea*), these authors showed that the binding selectivity of the lectin switches from one carbohydrate ligand to another while the surface density increased. In addition, it was shown that the apparent k_{ass} and k_{diss} depend on the oligosaccharide-immobilized density.

Avidity effects were also evidenced in various SPR-based studies dealing with animal lectins such as DC-SIGN and MMR (12, 13) or MBL (mannan-binding lectin, a plasma lectin) (14, 15). The apparent affinity depends on the oligomeric status, the carbohydrate density (or presentation), and the lectin–carbohydrate binding properties. Teillet et al. (14) showed that the oligomeric state of MBL has a direct effect on its carbohydrate-binding

Table 10.1
Properties of some commonly used lectins, adapted from (10) and (26)

Name	Common name	Structure/cation dependence	CRD[a] by protein	Specificity	Regeneration conditions	References
ConA	*Canavalia ensiformis*	Tetrameric at pH 7.2 Dimeric at pH 4.5	4 2	Man > Glc	0.3 M α-methyl-mannoside	(12)
MaA	*Maackia amurensis*	Dimeric	2	Neu5Acα3Gal	50 mM H_3PO_4 50 mM HCl	(3) (27)
RCA_{120}	*Ricinus communis*	Tetrameric ($\alpha_2\beta_2$)	2	Gal and derivatives	0.3 M lactose 50 mM H_3PO_4	(12)
SnA	*Sambucus nigra*	Tetrameric ($\alpha_2\beta_2$)	2	Neu5Acα6Gal	50 mM HCl	(27)
WGA	*Triticum vulgare*	Dimeric at pH 7.2 Monomeric at pH 1.9	2 0	GlcNAc and NeuNAc Di-*N*-acetylchitobiose, etc. No binding	50 mM H_3PO_4	(3) (28)
DC-SIGN	Dendritic cell-specific ICAM-3 grabbing non-integrin	Hexameric Ca^{2+} dependent	6	Man oligosaccharides Fuc containing glycans Lewis-type oligosaccharide	0.3 M methyl α-mannopyranoside or 0.3 M methyl α-mannopyranoside+ 1 M NaCl + 1 mg mL^{-1} BSA	(13) (21)
MBL	Human mannan-binding lectin Rabbit mannan-binding lectin	Trimeric Ca^{2+} dependent	3	Man, GlcNAc, and Fuc	5 mM EDTA 20 mM EDTA	(14) (15)
MMR	Human macrophage mannose receptor	Ca^{2+} dependent	3	Man, GlcNAc, and Fuc-terminated glycoconjugates	0.3 M methyl α-mannopyranoside or 0.3 M methyl α-mannopyranoside+ 1 M NaCl + 1 mg mL^{-1} BSA	(13) (21)

[a]CRD, carbohydrate recognition domain.

properties; Terada et al. (15) clearly showed that the interactions between MBL and various neoglycoproteins depend (i) on the number of sugars bound on the protein (k_{ass} increases and k_{diss} decreases upon increasing the number of mannose residues bound on BSA) and (ii) on the protein backbone used to make the neoglycoproteins, the sugar density being constant.

Therefore, the analysis of interactions between carbohydrates and lectins can be greatly affected by an avidity effect. This is especially true when oligosaccharides are used as the immobilized partner and a multivalent lectin is used as the analyte. A lectin entrapped in the matrix will not freely leave the matrix because of the lectin plurivalency: the probability that, at any time, at least one binding site of the lectin is involved in an interaction with one immobilized sugar is high.

2. Materials

The protocol has been set up on a Biacore 2000 SPR biosensor (Uppsala, Sweden) with the Biacore control 3.1 and BiaEvaluation 3.1 softwares.

Two types of lectins are currently used, either soluble lectins such as WGA (wheat germ agglutinin), concanavalin A, and Rca (*Ricinus communis* lectin) or soluble carbohydrate recognition domains of membrane lectins (*see* **Table 10.1**). In our experiments, we used the following:

1. Soluble lectins:
   R. communis (Rca) lectin (a galactose-specific lectin) from Sigma-Aldrich (Saint Quentin Fallavier, France).
2. Soluble carbohydrate recognition domains of mammalian membrane lectins:
   a. *Soluble fragment (MMR1-8) of the macrophage mannose receptor* (a calcium-dependent mannose-specific lectin): A soluble fragment of the human mannose receptor consisting of the eight C-type carbohydrate recognition domains (MMR1-8) was produced in Chinese hamster ovary cells as described previously (13, 16). This receptor moiety contains all of the domains that bind Man/GlcNAc/Fuc-terminated glycoconjugates as the whole receptor does. MMR1-8 was isolated by affinity chromatography on mannose-substituted Sepharose (16).
   b. *Soluble form of the DC-SIGN lectin* (a fucose/mannose-specific lectin): A soluble fragment of the human DC-SIGN lectin consisting of the whole extracellular region

was produced by bacterial expression as described previously (17). The DC-SIGN fragment was purified by affinity chromatography and ion exchange chromatography (17).

We use different glyco-analytes:

1. Neoglycoproteins (Lac-BSA and Man-BSA) were synthesized as described previously (18–20) by random coupling of modified simple sugars on amine residues of bovine serum albumin which contains 60 lysines. Neoglycoproteins constitute heterogeneous ligands because they contain 25 ± 3 sugar moieties dispersed throughout the molecule.
2. Oligolysine-based oligosaccharide clusters (*see* **Fig. 10.1**) were prepared according to Frison et al. (12).
3. Glycocluster peptide conjugates were prepared according to Srinivas et al. (21).

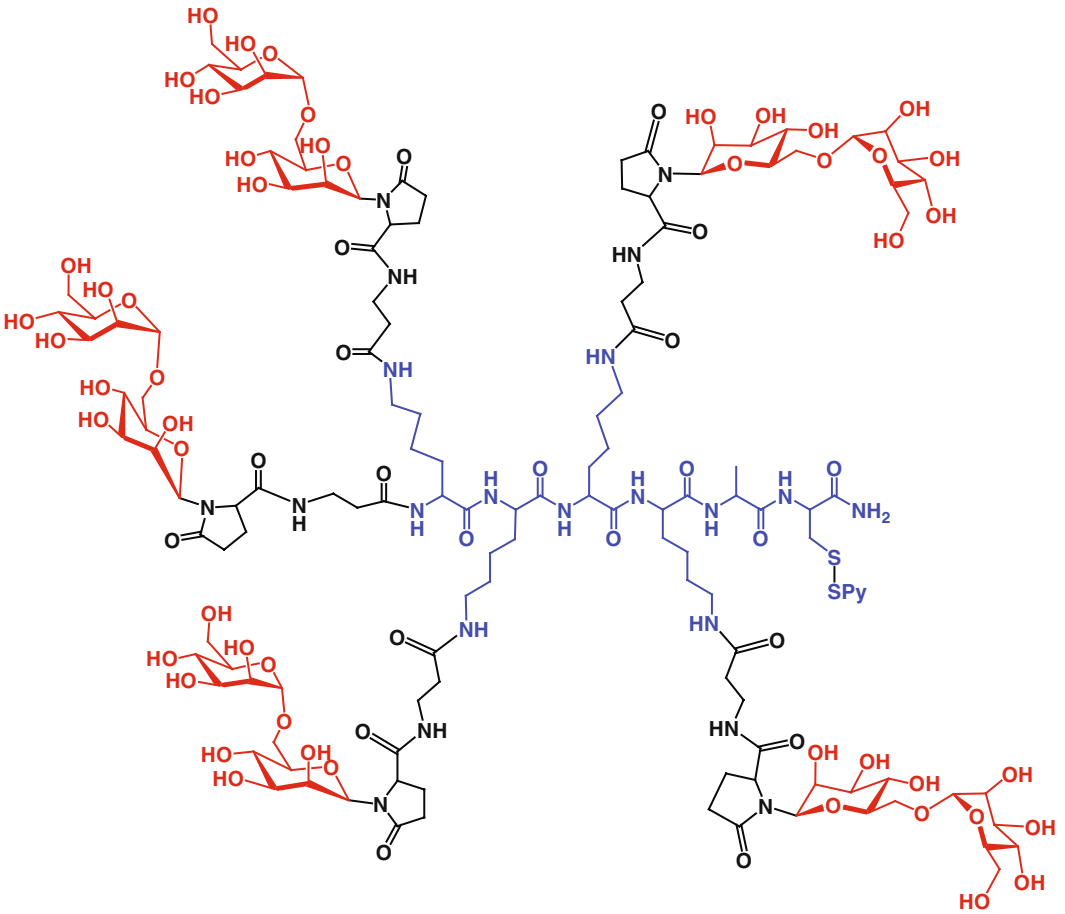

Fig. 10.1. Structure of a glycocluster. Manα-6Manβ-Glp-βAla-[Lys(Manα-6Man β-Glp-βAla)]$_4$-Ala-Cys(Spy)NH$_2$ or (Manα-6Man)$_5$Lys$_4$. With permission from (13).

2.1. Preparing the System

Materials for running SPR assays on the Biacore™ biosensors are commercially available:

1. *CM5 sensor chips*, research grade (pack of three chips): carboxymethylated dextran matrix on which molecules are coupled via amino groups. Chips on which lectins have been immobilized can be stored in a closed tube containing running buffer (see below).
2. Buffers and solution: all buffers and solution must be filtered (0.22 μm) and degassed by sonication for 15 min before use.

   Running buffer: 10 mM HEPES (*N*-2-hydroxyethylpiperazine-*N*′-2-ethanesulfonic acid), 150 mM NaCl, 0.005% P20 Biacore surfactant, 1 mM $CaCl_2$, 1 mM $MgCl_2$, and 17 mM NaN_3, pH 7.4 (*see* **Notes 1** and **2**).

   Pre-concentration buffers: 10 mM sodium acetate at various pHs (3.5–5.5).

   Solution for surface regeneration:

   a. Mannose regeneration solution: running buffer containing 1 M NaCl and 0.3 M methyl α-mannopyranoside.

   b. Lactose regeneration solution: running buffer containing 0.3 M lactose.
3. *BIAmaintenance kit* (for 6 months normal usage): Biatest solution (15% w/w sucrose in HBS-EP buffer) 65 mL, Bianormalizing solution (40% w/w glycerol for Biacore 2000 system), Biadesorb solution 1 (0.5% w/v sodium dodecyl sulfate) 90 mL, Biadesorb solution 2 (50 mM glycine-NaOH, pH 9.5) 90 mL, and Biadisinfectant solution (sodium hypochlorite, about 10% active chlorine) 90 mL. This last solution is stable up to 3 months at 4°C in the dark.

2.2. Pre-concentration Assays

As an example, the mannose-specific lectin (MMR1-8) was diluted at 10 μg mL^{-1} in a 10 mM sodium acetate buffer at various pHs (3.5–5.5).

In order to remove any remaining ligand, solution of 1 M ethanolamine hydrochloride, pH 8.5 (included in the amine coupling kit, see below), or of 50 mM NaOH should be available.

2.3. Lectin Immobilization

Amine coupling kit (for 50 immobilizations): 750 mg 1-ethyl-3-(3-dimethylaminopropyl) carbodiimide hydrochloride (EDC), 115 mg *N*-hydroxysuccinimide (NHS), and 10.5 mL 1 M ethanolamine hydrochloride, pH 8.5 (*see* **Note 3**).

Prepare, immediately before use, 0.4 M EDC and 0.1 M NHS, both in twice distilled and degassed water.

Lectin solution: Rca, MMR1-8, or DC-SIGN at 10 μg mL^{-1} in 10 mM sodium acetate, pH 4.6, optimal pH chosen on the basis of the pre-concentration assay.

2.4. Test for Mass Transfer Limitation

As an example, prepare Lac-BSA 10 μg mL^{-1} in running buffer. Lactose regeneration solution (*see* **Section 2.1**) should be available.

2.5. Direct Binding Experiment with Man-BSA

Prepare Man-BSA at concentration from 0.0125 M to 2.5 μM (1–200 μg mL^{-1}) in the running buffer.

2.6. Inhibition Experiment with Mannose Glycocluster

Prepare a solution of $(Man\alpha–2Man)_4Lys_3$ glycocluster (0.5–25 μM range) containing 0.125 μM Man-BSA in the running buffer.

2.7. Direct Binding Assay with DC-SIGN

Prepare solution of mannosylated peptide glycoclusters in running buffer containing 1 mg mL^{-1} BSA (*see* **Note 2**).

3. Methods

3.1. Preparing the System

System preparation and routine maintenance (*see* **Note 4**) will not be described in detail because they are available in the instrumentation manuals. During all the experiments, the temperature was kept at 25°C (*see* **Note 5**).

1. Replace the running buffer bottle by a fresh one, dock the new sensor chip, and prime the system.
2. Normalize the probe signal according to the manufacturer's instructions.

3.2. Pre-concentration Assays

At the ligand concentrations commonly used for immobilization (20–200 μg mL^{-1}), the expected levels of immobilized ligand would be low in the absence of a mechanism that retains the ligand molecules onto the sensor surface. The main mechanism for this accumulation process is an electrostatic attraction of the ligand onto the surface. This attraction is referred to as pre-concentration step and depends on three factors: the pH, the ionic strength, and the nature of the immobilization buffer. The carboxymethylated dextran matrix of a sensor chip carries a net negative charge when the pH is above 3.5. The pH of the immobilization buffer should, therefore, be between 3.5 and the lectin isoelectric point in order to achieve an efficient pre-concentration. For many proteins, a coupling at pH 4.5 with a low ionic strength buffer, such as 10 mM sodium acetate buffer, gives generally

satisfactory results; however, in some cases, pH 4.5 is not optimal. The ionic strength (I) of the immobilization buffer ($I = \frac{1}{2} \sum c_i z_i^2$, where c_i is the concentration of the i ion and z_i is the number of charges of the i ion) should be low, close to 10^{-2}, in order to favor an efficient electrostatic adsorption: higher salts concentrations impair protein–carboxymethylated matrix interactions. Obviously, the immobilization buffer must not contain reagent such as amines which will interfere in the coupling step. For these reasons, pre-concentration assays are performed in order to select an efficient immobilization buffer.

1. Select one out of the three independent CM5 sensor chip flow cells (flow cell 2, 3, or 4; *see* **Note 6**) and set the running buffer flow rate to 5 μL min^{-1}.
2. Inject sequentially 25 μL of each one of the MMR1-8 solutions with different pH (*see* **Section 2.2**), followed by a 5-min passage of running buffer (*see* **Fig. 10.2**).
3. Upon the last ligand injection cycle, a wash solution is injected to remove any remaining ligand molecules: a short pulse (1 min) of 1 M ethanolamine or 50 mM NaOH is commonly used for washing at this step.
4. Select the immobilization buffer pH leading to the highest ligand concentration on the sensor chip. In a typical example, using the MMR1-8 lectin as a ligand, the lectin optimally interacts with the sensor chip when the lectin was made soluble in sodium acetate buffer at pH 4.6 (*see* **Fig. 10.2**). Consequently, this buffer was selected to fix this lectin covalently on the chip.

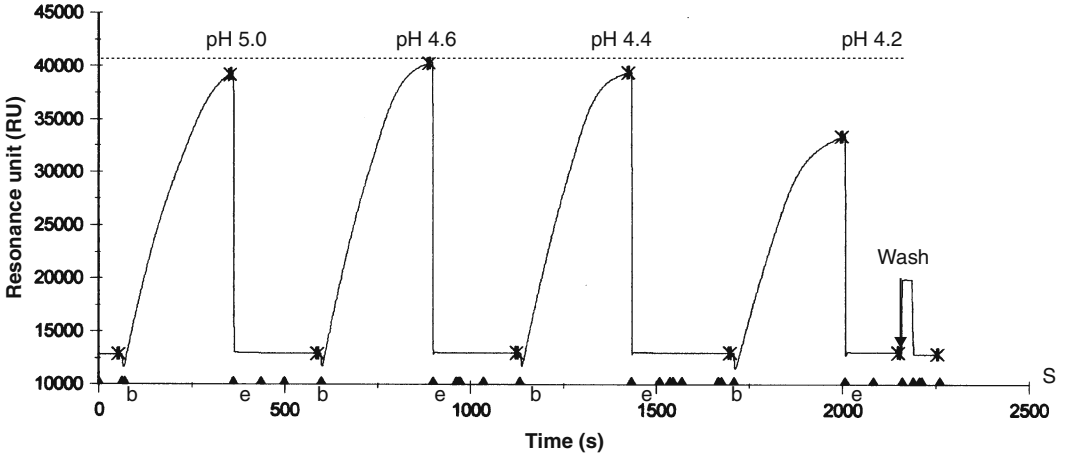

Fig. 10.2. Pre-concentration assay with the MMR1-8 lectin on a CM5 sensor chip using a 10 mM sodium acetate buffer at various pHs. The buffer at pH 4.6 gave the maximal pre-concentration. "*b*" indicates the beginning and "*e*" the end of the lectin injection step. The wash solution in this experiment was 50 mM NaOH, injected for 30 s. Blocking and cleaning requires a single step.

3.3. Lectin Immobilization

Once the optimal immobilization conditions are selected, the lectin is covalently bound to the sensor chip. The amine coupling procedure involves chemical activation of the CM5 surface carboxyl groups and subsequent covalent binding through the lectin primary amino groups. A typical sensorgram obtained after immobilization procedure is shown in **Fig. 10.3**.

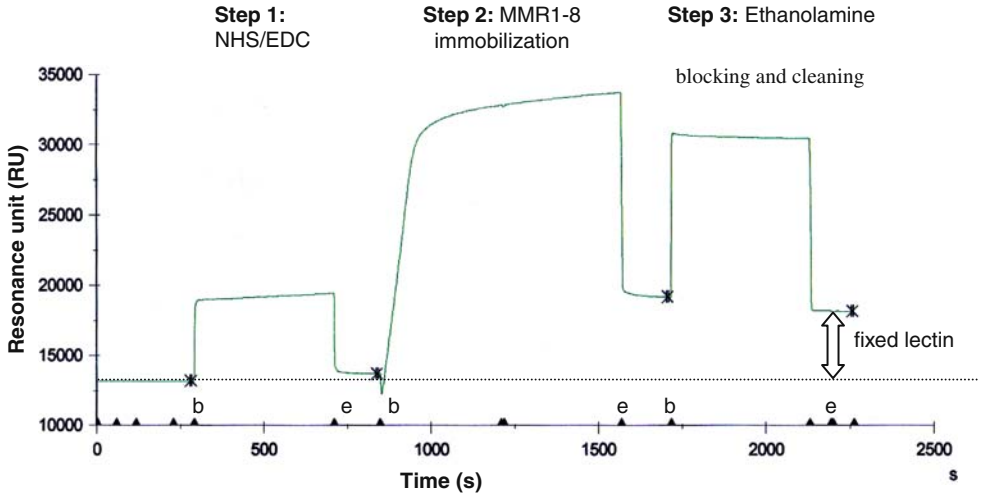

Fig. 10.3. Typical sensorgram of the MMR1-8 lectin immobilization on a CM5 sensor chip using a 10 mM sodium acetate buffer, pH 4.6. "*b*" indicates the beginning and "*e*" indicates the end of each injection step.

1. Prepare extemporaneously the activating mixture by adding 35 μL NHS to 35 μL EDC.
2. Select one flow cell and set the running buffer flow rate to 5 μL min^{-1}.
3. Inject 35 μL (7 min) of the activating mixture (a response will be observed due to a change in the refractive index: step 1, **Fig. 10.3**) (*see* **Note 7**).
4. Immobilize the protein by injecting 35 μL (7 min) of the lectin solution (MMR1-8 or DC-SIGN). Inspect carefully the slope of the response curve. As soon as the expected level is reached, stop the injection (step 2, **Fig. 10.3**). Alternatively, resume a new injection cycle at the end of the first one when the immobilization level has not been reached.
5. Block the residual surface NHS-activated carboxylic groups by injecting 35 μL (7 min) of 1 M ethanolamine hydrochloride, pH 8.5 (step 3, **Fig. 10.3**). It should be noticed that in addition to the neutralization of the activated groups this step allows the elimination of the majority of the noncovalently bound adsorbed material.
6. Measure the amount of immobilized ligand by subtracting the initial ("empty" flow cell) from the final baseline level

(1,000 resonance units (RU) roughly correspond to a 1 ng mm^{-2} ligand surface density). When performing time course analyses and as long as low molecular weight analytes such as small oligosaccharides (1,000–5,000) are used, it is recommended to reach a heavy lectin load, up to 5,000 RU, in order to obtain a signal high enough upon analyte binding. The control flow cell (flow cell 1, *see* **Note 6**) was also independently activated with EDC–NHS and blocked with ethanolamine. This procedure is strictly required in order to avoid the untreated flow cell acting as a cation-exchange matrix; upon such a treatment, the treated flow cell is neutral because the carboxylic groups have been substituted (*see* **Note 8**).

7. Search optimal regeneration conditions of the surface (*see* **Note 9**): this is done by repeated injection cycles of an analyte specific for the immobilized lectin such as a neoglycoprotein Man-BSA or Fuc-BSA (*see* **Note 10**), followed by a short (1–3 min) pulse of a regenerating solution. In the case of MMR1-8, the regeneration was carried out by using two consecutive pulses of 30 μL of mannose regeneration solution.

In binding experiments using lectins, the regeneration is usually carried out under very mild conditions by injecting a high concentration of either a monosaccharide, a mixture of monosaccharides, or a low-cost disaccharide: these "simple" saccharides compete with the analytes bound to the lectin-binding site. In this way, the analytes are washed away and then upon injection of a saccharide-free buffer, the simple saccharides are washed away because of their low affinity for the lectin.

3.4. Test for Mass Transport Limitation

Mass transport limitation (MTL) arises when there is a concentration gradient between the surface and the matrix inside. It can be tested by analyzing the effect of different buffer flow rates on analyte-binding rates. The interaction between the ligand and the analyte should not be dependent on the flow rate; if not, the calculation cannot be accurate.

As an example, to test MTL on the immobilized Rca lectin, we use one concentration of analytes (Lac-BSA), one time of injection (150 s) but several flow rates (in the 10 and 100 μL min^{-1} range).

The detailed procedure is as follows:

1. Replace the running buffer bottle by a new one, dock the sensor chip on which the Rca lectin is immobilized, and prime the system.
2. Inject 25 μL of Lac-BSA, using a flow rate of 10 μL min^{-1}.
3. Inject 30 μL of the lactose regeneration solution.

4. Inject 50 μL of Lac-BSA, using a flow rate of 20 μL min^{-1}.
5. Inject 30 μL of the lactose regeneration solution.
6. Inject 100 μL of Lac-BSA, using a flow rate of 40 μL min^{-1}.
7. Inject 30 μL of the lactose regeneration solution.
8. Inject 200 μL of Lac-BSA, using a flow rate of 80 μL min^{-1}.
9. Inject 30 μL of the lactose regeneration solution.

Compare the sensorgrams obtained for each injection (overlay them with the BiaEvaluation software) (**Fig. 10.4**).

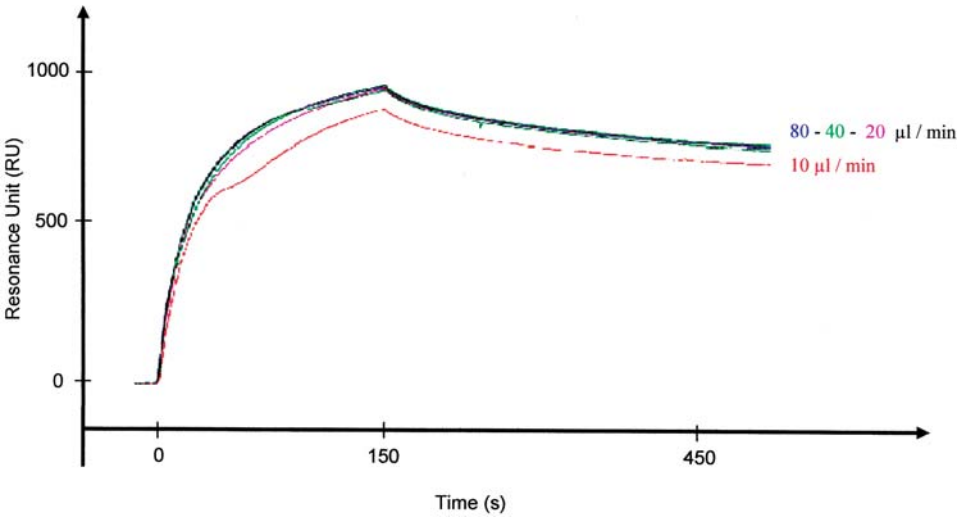

Fig. 10.4. Mass transport limitation analysis on the binding of the Lac-BSA neoglycoprotein (at 10 μg mL^{-1}) on the immobilized Rca lectin at various flow rates.

Accordingly, kinetic of the Lac-BSA neoglycoproteins association with the immobilized Rca lectin is slightly different when the neoglycoprotein is injected at 10 μL min^{-1}, compared to the other studied flow rates. It means that a limitation of mass transport occurred at 10 μL min^{-1}. For the following experiments, the selected flow rate was 20 μL min^{-1}.

3.5. Direct Binding Experiment with Man-BSA

Glycoclusters, which have a low molecular mass, give a low signal in a direct interaction with the MMR1-8 lectin. Also, we used a procedure based on the inhibition of the binding of a neoglycoprotein (Man-BSA or Fuc-BSA) on the immobilized MMR1-8 lectin by competition with glycoclusters. The affinities of mannose glycoclusters binding to MMR1-8 were deduced from their inhibitory effect on the Man-BSA binding to MMR1-8.

1. Soluble MMR1-8 protein was immobilized on a sensor chip CM5 in sodium acetate buffer at pH 4.6, as described previously (*see* **Section 3.3**). Efficient fixation was ascertained by a large increase in the refractive index: ΔRU = 5,000. The

control flow cell was also activated by EDC–NHS and then deactivated by using 1 M ethanolamine.

2. The neoglycoprotein (Man-BSA) was injected at various concentrations (*see* **Section 2.5**) on the immobilized MMR1-8 lectin (**Fig. 10.5**). The flow rate was set at 20 μL min^{-1} to avoid MTL. The duration of both the association and dissociation phases was set to 360 s in order to almost reach a plateau.
3. The regeneration of the sensor chip was achieved by adding mannose regeneration solution.
4. The number of resonance units (response, R) was obtained from the sensorgrams (response at the injection end). R_{max} and K_A were deduced from, respectively, the intercept and the slope of the linear transformation $(1/R)$ versus $(1/g)^{\alpha}$ (*see* **Note 11** for a complete description of the equations).

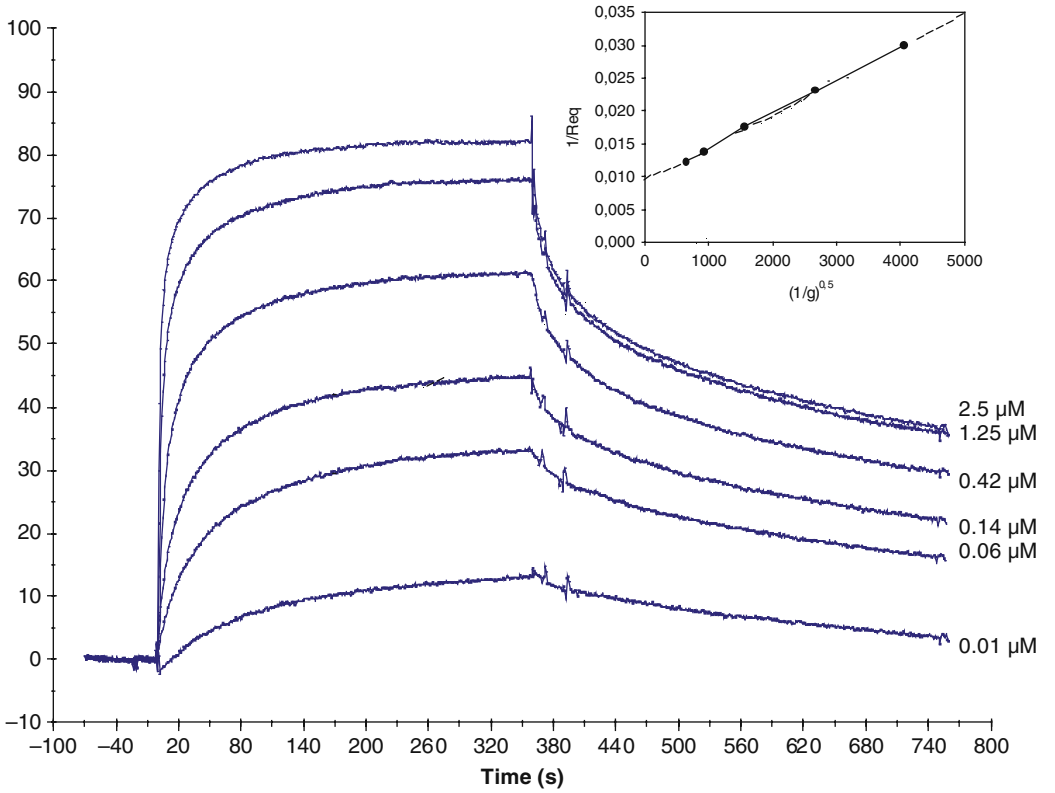

Fig. 10.5. Analysis of the concentration-dependent binding of Man-BSA with immobilized MMR1-8. Binding affinity was measured using a range of neoglycoprotein concentrations from 0.125 to 2.5 μM (1–200 μg mL^{-1}). The duration of both the association and dissociation phases was set to 360 s to reach a plateau value. Regeneration of the sensor chip was achieved by adding 0.3 M α-methyl-mannopyranoside in the running buffer. *Inset*: the $1/R_{eq} = f(g^{-1})^{\alpha}$ plot is linear with $\alpha = 0.5$. R_{eq} is determined from sensorgrams (response at the end of injection). Response obtained with 0.125 μM Man-BSA is in the range of the noise level and so was not taken into consideration.

The heterogeneity coefficient was $\alpha = 0.5$ for Man-BSA binding to immobilized MMR1-8. R_{max} was 124 and K_A was 4×10^6 L mol^{-1}. The concentration of neoglycoprotein (10 μg mL^{-1}, 0.125 μM) corresponding to $R_{max}/2$ was chosen to perform inhibition experiments with glycoclusters.

3.6. Inhibition Experiment with Mannose Glycocluster

In this assay the affinity data from the direct assay (*see* **Section 3.5**) are used.

1. A solution of glycocluster (*see* **Section 2.6**) was injected on the immobilized MMR1-8 lectin in the same conditions as described in **Section 3.5** (**Fig. 10.6**).
2. The regeneration of the sensor chip was achieved by adding mannose regeneration solution.
3. The number of resonance units (response, R) was obtained from the sensorgrams. K_I was deduced from the representation $(R_{max} \times R^{-1} - 1)^{1/\alpha} = f(i)$, where the apparent affinity K, given by the slope, is equal to $(1 + K_I \times g)K_A$ (*see* **Note 12**). In the present case, with $\alpha = 0.5$, $R_{max} = 124$, and $K_A = 4 \times 10^6$ L mol^{-1}, K_I was 8×10^5 L mol^{-1}.

3.7. Direct Binding Assay with DC-SIGN

1. DC-SIGN lectin was immobilized on a CM5 sensor chip, using a standard amine coupling procedure (*see* **Section 3.3**) with sodium acetate buffer at pH 4.5 (immobilization time of 8 min and a constant flow rate of 20 μL min^{-1}). An efficient fixation was indicated by a large increase in the refractive index (about 5,000 RU). The control flow cell was also activated by EDC–NHS and then deactivated by using 1 M ethanolamine.
2. The biosensor experiments were carried out in the running buffer. The temperature was kept at 25°C and the flow rate was 20 μL min^{-1} for both the association and dissociation steps for 5 and 10 min, respectively. The 20 μL min^{-1} flow rate was used based on preliminary experiments that ascertained that no MTL occurred (*see* **Section 3.4**).
3. Binding experiments with glycocluster peptide conjugates at concentrations from 0.1 to 5 μM (*see* **Section 2.7**) were carried out at 20 μL min^{-1}.
4. Regeneration was carried out using two consecutive pulses of 30 μL of the mannose regeneration solution containing 1 mg mL^{-1} BSA (*see* **Note 13**).
5. Kinetic constants were determined from the curve using the BiaEvaluation 3.1 software (*see* **Note 14**). In an SPR-binding study, the initial slope of the curve corresponding to the association phase depends on k_{bind}, the experimental kinetic constant with a value of

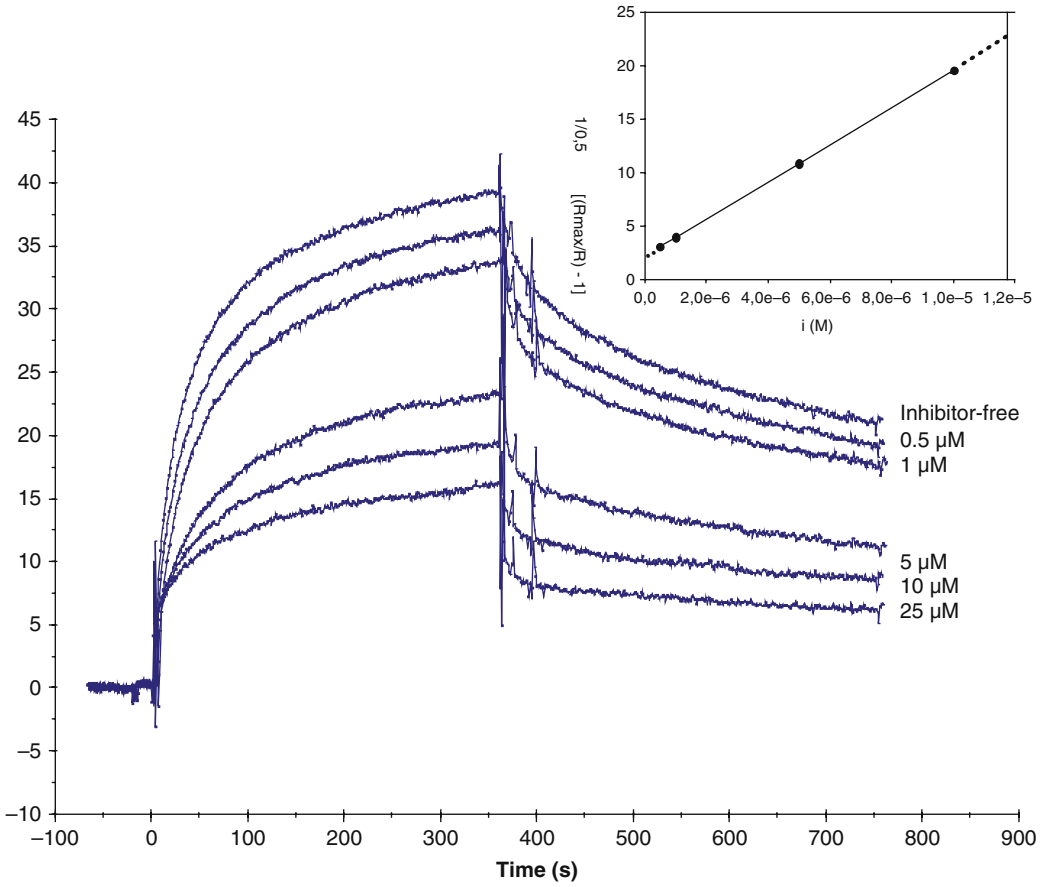

Fig. 10.6. Analysis of Man-BSA binding on immobilized MMR1-8 in the presence of various concentrations of a glycocluster inhibitor (Manα-2Man)$_4$Lys$_3$. Binding affinity of glycocluster was calculated from data obtained by injecting the Man-BSA neoglycoprotein (10 μg mL^{-1}, 0.125 μM) with the glycocluster acting as an inhibitor (0.5–25 μM concentration range). The duration of both the association and dissociation phases was set to 360 s. The regeneration of the sensor chip flow cell was achieved by adding 0.3 M α-methyl-mannopyranoside in the running buffer. *Inset*: the $(R_{max} \times R^{-1} - 1)^{-\alpha} = f(i)$ plot is linear with $\alpha = 0.5$. The response obtained with 25 μM inhibitor is in the range of noise level and so, it was not taken into consideration.

$$k_{bind} = k_{ass}\mathcal{g}_0 + k_{diss}$$

where k_{ass} stands for the kinetic association constant, k_{diss} for the kinetic dissociation constant, and $\mathcal{g}_0$ for the free ligand (i.e., the free glycopeptide) concentration. The calculated equilibrium association constant K_A ($K_A = k_{ass}/k_{diss}$) was 6.2×10^6 L mol^{-1} (with $k_{diss} = 8.8 \times 10^{-4}$ s^{-1}) for mannosylated peptide conjugate binding to DC-SIGN lectin.

4. Notes

1. The running buffer is supplemented with salts like $CaCl_2$, $MgCl_2$, or $MnCl_2$ when a lectin requires such ions for its activity.

   Buffers are available from Biacore as HBS-EP (0.01 M HEPES, 0.15 M NaCl, 3 mM EDTA, and 0.005% v/v P20 surfactant, pH 7.4), HBS-P (0.01 M HEPES, 0.15 M NaCl, and 0.005% v/v P20 surfactant, pH 7.4), or HBS-N (0.01 M HEPES and 0.15 M NaCl, pH 7.4).

   When lectin requires Ca^{2+}, Mg^{2+}, or Mn^{2+} ions for activity, HBS-EP should not be used as a running buffer because it contains EDTA. Sodium azide is used as preservative.
2. To prevent a non-specific binding on any flow cell upon analyte injection, it can be useful to add BSA (bovine serum albumin, 1–5 mg mL^{-1}, Sigma) into the running buffer or to increase the P20 surfactant concentration (up to 0.05%).
3. The NHS powder is kept at room temperature and the EDC powder is kept under nitrogen at 4°C.
4. The desorb procedure must be applied weekly and the sanitize procedure monthly. These cleaning procedures must be run anytime the apparatus is turned off.
5. The temperature of the system must be kept constant throughout all the experimental steps, which also means that the various solutions (buffer, analytes, etc.) must also be at the same temperature. This basic requirement is a sine qua non condition to get reproducible SPR RU values and to allow accurate calculation of the constants; indeed, the binding constants may be dramatically temperature dependent.
6. The flow cell 1 is used as reference (negative control). It is activated by the EDC–NHS solution and then blocked by using 1 M ethanolamine. The RU value obtained on this flow cell during the analyte injection is subtracted from that of the other flow cells on which the ligands were immobilized.
7. When the activation step is effective, the baseline level has increased, about 150 and 200 RU upon the activating mixture injection.
8. The chemical ends of the CM5 sensor ship are the following ones depending on the step:

Unactivated CM5: $R–CO_2^-$

Activated CM5: 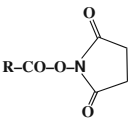

Neutralized CM5: $R–CO–NH–CH_2–CH_2OH$

9. A suitable regenerating agent provides full recovery of the baseline level at the end of each cycle while preserving ligand activity checked by the constancy of analyte binding level in repeated cycles.
   The most common regenerating agents are
   1. Acids (10–100 mM HCl or H_3PO_4).
   2. Alkali (10–100 mM NaOH).
   3. Salts (1 mM–1 M NaCl).
   4. Surfactant (0.5% SDS).
   5. Denaturing agents (8 M urea or 6 M guanidinium chloride).

When looking for the most appropriate regeneration conditions, it is important to test various conditions, such as a range of pH and ion concentrations. It is recommended to use mild conditions first and then increase the harshness of the treatment progressively until suitable conditions are established. In this way, the risk of damaging the compound immobilized on the sensor surface (especially when a protein is immobilized) is minimized.

Exploratory testing for regeneration conditions involves the injection of an analyte over the surface, followed by a regeneration solution. The extent to which the analyte is removed is indicated by the response level after the injection of a regeneration solution. A second injection of the analyte at the concentration previously used is requested to check the stability of the immobilized compound.

10. According to the structural similarity between L-fucose and D-mannose (22), various lectins which recognize mannosyl residues do also accommodate fucosyl residues as well; this is also the case for MMR.
11. Theoretical approach for assays conducted with heterogeneous ligands such as neoglycoproteins which contain in average 25 sugar residues (heterogeneity comes from the number and the position of sugar residues in the neoglycoproteins): in the case of a typical 1:1 interaction, such

as between an immobilized lectin (L) and a glycoconjugate (g) used as analyte, at equilibrium, Scatchard equation (23) can be written as follows:

$$K_A g = L_{bound}/(L_{total} - L_{bound})$$

or

$$K_A g = L_{bound}(L_{total} - L_{bound})^{-1}$$

where K_A is the binding constant expressed in L mol^{-1}, L_{total} is the total number of sites on the sensor chip flow cell, L_{bound} is the number of sites occupied by the glycoconjugate (here the neoglycoprotein), and g is its concentration, expressed in M, in the injected analyte solution.

In an SPR experiment, L_{bound} is proportional to the response R, value read on the SPR machine, and L_{total} to R_{max} (response at saturation). The equation becomes

$$K_A g = R(R_{max} - R)^{-1}$$

or

$$R^{-1} = (R_{max} K_A g)^{-1} + (R_{max})^{-1}$$

K_A and R_{max} can be deduced from the Langmuir plot:

$$R^{-1} = f(g)^{-1}$$

where $1/R_{max}$ is the intercept with y axis and $(R_{max} \times K_A)^{-1}$, the slope.

More often, this representation exhibits a curvature related to binding site heterogeneity. To take into account the heterogeneity of polyclonal antibodies, it was found (24) to be more convenient to use the Sips distribution (25) allowing the data to be fitted to a straight line. Using Sips approach, Scatchard equation becomes

$$(K_A g)^{\alpha} = R(R_{max} - R)^{-1}$$

For a homogeneous group of sites, the Sips coefficient α is equal to +1; decreasing values of α correspond to increasing degrees of heterogeneity either related to the ligands or to the receptors. In our case, the heterogeneity comes from the neoglycoprotein which contains in average 25 sugars and from a non-homogeneous density of immobilized lectin molecules on the sensor chip.

Corrected by the Sips coefficient (established by successive iterations, this can be done manually), Scatchard equation gives access to $(R_{max})^{-1}$ as the intercept of the y axis and K_A (an average value) determined from the $(R_{max} \times K_A{}^{\alpha})^{-1}$ slope of the $R^{-1} = f(g)^{-\alpha}$ plot.

12. Theoretical approach for assays in the presence of an inhibitor: the association constant of the inhibitor K_I was calculated from the apparent affinity K of a neoglycoprotein relevant for the immobilized lectin, measured in the presence of a glycocluster used as an inhibitor. In the presence of an inhibitor I with a binding constant K_I, at equilibrium two equations may be written:

$$K_A g = L_{bound}(L_{total} - L_{bound} - L_I)^{-1}$$

$$K_I i = L_I(L_{total} - L_{bound} - L_I)^{-1}$$

where L_I is the number of sites occupied by the inhibitor (here the glycocluster) and i its concentration, expressed in M. From the two previous equations, it can be derived that

$$L_I = L_{bound} K_I i (K_A g)^{-1}$$

As a consequence, in the presence of an inhibitor, the Scatchard equation becomes

$$K_A g = L_{bound}\,[L_{total} - L_{bound} - L_{bound} K_I i (K_A g)^{-1}]^{-1}$$

or

$$K_A[L_{total} - L_{bound} - L_{bound} K_I i (K_A g)^{-1}] = L_{bound} g^{-1}$$

Therefore

$$(L_{total} - L_{bound})\, L_{bound}^{-1} = (K_A g)^{-1} + K_I i (K_A g)^{-1}$$

or

$$R_{max} R^{-1} - 1 = (1 + K_I i)(K_A g)^{-1}$$

When the binding is heterogeneous, this last equation becomes

$$(R_{max} R^{-1} - 1)^{-\alpha} = (1 + K_I i)\,(K_A g)^{-1}$$

According to this equation, K_I can be deduced from the plot

$$(R_{max} R^{-1} - 1)^{-\alpha} = f(i)$$

13. The presence of BSA in the regeneration buffer was found to be required when hydrophobic or amphiphilic glycocon-

jugates (such as glycopeptides) were tested. Following this finding, we now systematically add BSA in the regeneration buffer.

14. This procedure (global fit, simultaneous k_{ass} and k_{diss} determination) only works well if (i) there is no MTL and (ii) a pure 1:1 binding model and kinetics apply.

Acknowledgments

We thank Dr. Annie-Claude Roche, on leave from the Glycobiology Department, at the *Centre de Biophysique Moléculaire, C.N.R.S.,* Orléans, for her constant support and for her very valuable help over the years in developing protein–sugar interaction research at both molecular and cellular levels. The Biacore apparatus was purchased thanks to grants from ARC (*Association de Recherche contre le Cancer*), from the University of Orléans, and from the *Région Centre* council.

References

1. Goldstein, I., Hughes, C., Monsigny, M., Osawa, T., and Sharon, N. (1980) What should be called a lectin? *Nature* **285**, 66.
2. Sharon, N. (2007) Lectins: carbohydrate-specific reagents and biological recognition molecules. *J. Biol. Chem.* **282**, 2753–64.
3. Shinohara, Y., Hasegawa, Y., Kaku, H., and Shibuya, N. (1997) Elucidation of the mechanism enhancing the avidity of lectin with oligosaccharides on the solid phase surface. *Glycobiology* **7**, 1201–08.
4. Greenbury, C. L., Moore, D. H., and Nunn, L. A. (1965) The Reaction with red cells of 7 s rabbit antibody, its sub-units and their recombinants. *Immunology* **35**, 420–31.
5. Crothers, D. M., and Metzger, H. (1972) The influence of polyvalency on the binding properties of antibodies. *Immunochemistry* **9**, 341–57.
6. Monsigny, M., Roche, A. C., Sené, C., Maget-Dana, R., and Delmotte, F. (1980) Sugar-lectin interactions. how does wheat-germ agglutinin bind sialoglycoconjugates? *Eur. J. Biochem.* **104**, 147–53.
7. Bhavanandan, V. P., and Katlic, A. W. (1979) The interaction of wheat germ agglutinin with sialoglycoproteins. The role of sialic acid. *J. Biol. Chem.* **254**, 4000–08.
8. Lee, R. T., Lin, P., and Lee, Y. C. (1984) New synthetic cluster ligands for galactose/N-acetylgalactosamine-specific lectin of mammalian liver. *Biochemistry* **23**, 4255–61.
9. Lee, Y. C., Townsend, R. R., Hardy, M. R., et al. (1983) Binding of synthetic oligosaccharides to the hepatic Gal/GalNAc lectin. Dependence on fine structural features. *J. Biol. Chem.* **258**, 199–202.
10. Monsigny, M., Mayer, R., and Roche, A. C. (2000) Sugar-lectin interactions: sugar clusters, lectin multivalency and avidity. *Carbohydr. Lett.* **4**, 35–52.
11. Horan, N., Yan, L., Isobe, H., Whitesides, G. M., and Kahne, D. (1999) Nonstatistical binding of a protein to clustered carbohydrates. *Proc. Natl. Acad. Sci. USA* **96**, 11782–86.
12. Frison, N., Marceau, P., Roche, A. C., Monsigny, M., and Mayer, R. (2002) Oligolysine-based saccharide clusters: synthesis and specificity. *Biochem. J.* **368**, 111–19.
13. Frison, N., Taylor, M. E., Soilleux, E., et al. (2003) Oligolysine-based oligosaccharide clusters: selective recognition and endocytosis by the mannose receptor and dendritic cell-specific intercellular adhesion

molecule 3 (ICAM-3)-grabbing nonintegrin. *J. Biol. Chem.* **278**, 23922–29.
14. Teillet, F., Dublet, B., Andrieu, J. P., Gaboriaud, C., Arlaud, G. J., and Thielens, N. M. (2005) The two major oligomeric forms of human mannan-binding lectin: chemical characterization, carbohydrate-binding properties, and interaction with MBL-associated serine proteases. *J. Immunol.* **174**, 2870–77.
15. Terada, T., Nishikawa, M., Yamashita, F., and Hashida, M. (2006) Analysis of the molecular interaction between mannosylated proteins and serum mannan-binding lectins. *Int. J. Pharm.* **316**, 117–23.
16. Simpson, D. Z., Hitchen, P. G., Elmhirst, E. L., and Taylor, M. E. (1999) Multiple interactions between pituitary hormones and the mannose receptor. *Biochem. J.* **343**(**Pt 2**), 403–11.
17. Mitchell, D. A., Fadden, A. J., and Drickamer, K. (2001) A novel mechanism of carbohydrate recognition by the C-type lectins DC-SIGN and DC-SIGNR. Subunit organization and binding to multivalent ligands. *J. Biol. Chem.* **276**, 28939–45.
18. Roche, A. C., Barzilay, M., Midoux, P., Junqua, S., Sharon, N., and Monsigny, M. (1983) Sugar-specific endocytosis of glycoproteins by Lewis lung carcinoma cells. *J. Cell. Biochem.* **22**, 131–40.
19. Monsigny, M., Roche, A. C., and Midoux, P. (1984) Uptake of neoglycoproteins via membrane lectin(s) of L1210 cells evidenced by quantitative flow cytofluorometry and drug targeting. *Biol. Cell.* **51**, 187–96.
20. Quétard, C., Bourgerie, S., Normand-Sdiqui, N., et al. (1998) Novel glycosynthons for glycoconjugate preparation: oligosaccharylpyroglutamylanilide derivatives. *Bioconjug. Chem.* **9**, 268–76.
21. Srinivas, O., Larrieu, P., Duverger, E., et al. (2007) Synthesis of glycocluster-tumor antigenic peptide conjugates for dendritic cell targeting. *Bioconjug. Chem.* **18**, 1547–54.
22. Monsigny, M., Kieda, C., and Roche, A. C. (1983) Membrane glycoproteins and membrane lectins as recognition signals in normal and malignant cells. *Biol. Cell.* **47**, 95–110.
23. Scatchard, G. (1949) The attraction of proteins for small molecules and ions. *Am. Ny Acad. Sci.* **51**, 660–72.
24. Nisonoff, A., and Pressman, D. (1958) Heterogeneity and average combining constants of antibodies from individual rabbits. *J. Immunol.* **80**, 417–28.
25. Sips, R. (1948) Structure of catalyst surface. *J. Chem. Phys.* **16**, 490–95.
26. Rudiger, H., and Gabius, H. J. (2001) Plant lectins: occurrence, biochemistry, functions and applications. *Glycoconj. J.* **18**, 589–613.
27. Duverger, E., Coppin, A., Strecker, G., and Monsigny, M. (1999) Interaction between lectins and neoglycoproteins containing new sialylated glycosynthons. *Glycoconj. J.* **16**, 793–800.
28. Bouchard, P., Moroux, Y., Tixier, R., Privat, J. P., and Monsigny, M. (1976) An improved method for purification of wheat germ agglutinin (lectin) by affinity chromatography. *Biochimie* **58**, 1247–53.

Chapter 11

DNA Sensors Based on Mixed Self-Assembled DNA/Alkanethiol Films

Sara Peeters and Tim Stakenborg

Abstract

When designing DNA biosensors, the immobilization of specific DNA probes is one of the most essential parts. Unfortunately, many of the existing strategies (e.g., adsorption, complexation, and entrapment) can only be used on standard microscope slides, while for more tailored surfaces alternative strategies are still required. In the case of gold surfaces, the self-assembly of mixed DNA/alkanethiol films is a very common approach to directly couple single-stranded DNA probes. The quality of these mixed films greatly depends on different parameters including the sensitivity and the detection limit. We have shown a positive relation between the length of the used carbon spacer and the general performance of the DNA biosensor. In this chapter an extended protocol for the controlled immobilization and subsequent hybridization of DNA is described.

Key words: DNA biosensor, surface chemistry, alkanethiol, SPR, DNA immobilization, DNA hybridization.

1. Introduction

For most biosensor applications the efficient and reproducible coupling of DNA is one of the most essential parts. However, the coupling depends to a great extent on the surface type. The leading methods for glass slides to synthesize DNA probes on site are still not fully adapted to other surfaces and often alternative DNA-coupling strategies are required (1, 2). In this chapter we will focus on the immobilization of single-stranded DNA

N.J. de Mol, M.J.E. Fischer (eds.), *Surface Plasmon Resonance*, Methods in Molecular Biology 627,
DOI 10.1007/978-1-60761-670-2_11,

fragments on gold surfaces for which thiolated DNA probes in combination with alkanethiols remain the method of choice. The method is usually performed in two steps. In a first step, thiolated DNA molecules will directly couple to the surface by means of self-assembly (3), while in the second step alkanethiol backfilling will improve the final order and the stability of the formed DNA-layers. This combination has proven to positively affect subsequent hybridization steps (4, 5). The length of the carbon spacer of both DNA probes and backfilling molecules plays an important role herein. By the use of an 11-carbon long spacer (i.e., mercapto-undecyl or C_{11}), instead of the generally used 6-carbon long spacer (i.e., mercaptohexyl or C_6), we have confirmed the positive relation between the spacer length and the general biosensor performance (6). To validate this relation, parameters such as the sensitivity and the detection limit need to be determined. These parameters can easily be calculated based on the immobilization and hybridization steps, monitored in real-time with SPR (7). Since commercial SPR devices make use of an integrated flow system (i.e., IFC microfluidic chip), they allow the comparison of a flow-mediated immobilization approach to a diffusion-controlled approach. Hence, the impact of the immobilization approach on the biosensor performance can be estimated (*see* **Section 3.4**). In this chapter, a general protocol for the reproducible immobilization of mixed DNA/alkanethiol films and the following hybridization steps is described. An alternative protocol for the diffusion-controlled immobilization is included as well.

2. Materials

2.1. Buffers and Solutions

1. A 5′-thiolated DNA probe (25 nt) with C_6 (Eurogentec, Belgium) or C_{11} spacer (*see* **Note 1**). The probes with C_{11} spacer were synthesized by Dr. Van Aerschot (Rega Institute, Belgium) (8). The spacers (*see* **Fig. 11.1**) are inserted to link the thiol moiety to the 5′-end of the probe.
2. A complementary (25 cp) and non-complementary (25 np) probe (*see* **Note 1**).
3. Backfilling molecules: 6-Mercapto-1-hexanol (MCH, Sigma, USA) and 11-mercapto-1-undecanol (MCU, Sigma, USA).
4. Immobilization buffer: 1 M KH_2PO_4, pH 3.8 (*see* **Note 2**).
5. Hybridization buffer or running buffer: 1 M NaCl, 10 mM Tris–HCl, 2 mM EDTA, pH 7.0.
6. Regeneration solution: 2.5 mM HCl or 20 mM NaOH.

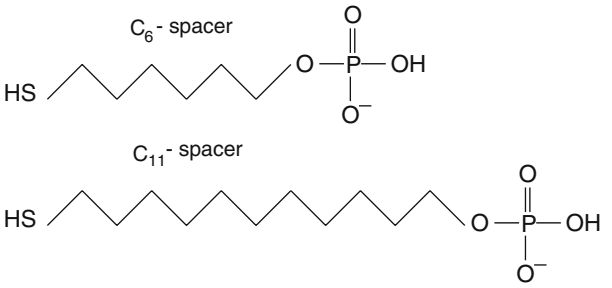

Fig. 11.1. Chemical structure of the short traditional C_6 and the longer C_{11} spacer. These two spacers are coupled to the 5′thiol moiety to separate the 25nt probe from the surface (See 2.1 buffers and solutions).

2.2. Devices

1. Unmounted gold-coated surfaces and separate chip supports (SIA Kit Gold, GE Healthcare, UK) (*see* **Note 3**).
2. A homemade UV/O_3 device (*see* **Fig. 11.2**) containing a mercury grid lamp to clean the SPR samples (*see* **Note 4**).
3. 24-Well microplate containers for the diffusion-controlled immobilization (BD Falcon™, BD Biosciences, USA).
4. Microplate shaker (Thermomixer, Eppendorf, Germany) for homogenous immobilization.
5. SPR system (Biacore™ 2000, GE Healthcare, UK) for real-time monitoring.

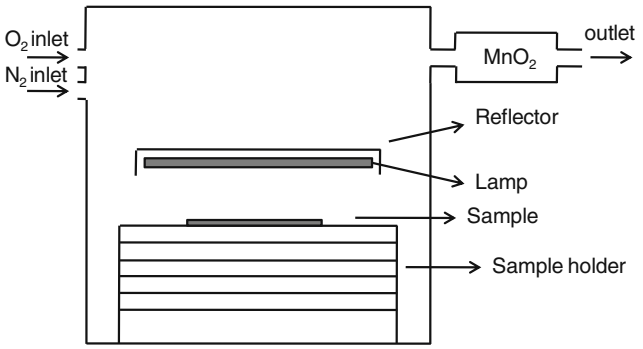

Fig. 11.2. Schematic illustration of the IMEC homemade UV/O_3 cleaning device.

3. Methods

3.1. Sample Preparation

For reproducible immobilizations, the quality and the cleanliness of the gold-coated surfaces are essential (9). The surface cleaning, handling (i.e., mounting of the gold surface on the chip support

and insertion of the chip in the SPR device) as well as the device settings used are described.

1. Clean the gold surfaces by UV/O_3 for 15 min.
2. In the case of a flow-assisted immobilization, mount the gold surface on a chip support and insert the chip in the SPR system according to the instructions of the manufacturer. For the diffusion-controlled approach (*See* **Section 3.4**), functionalize the gold surface with the thiolated DNA before mounting it on the chip support.
3. Set the temperature (25°C) and the flow rate (5 μL/min) constant during the entire SPR run. Before immobilization of thiolated 25 nt DNA probes, inject running buffer to set a baseline (*See* **Note 5**) (See **Fig. 11.3**) .

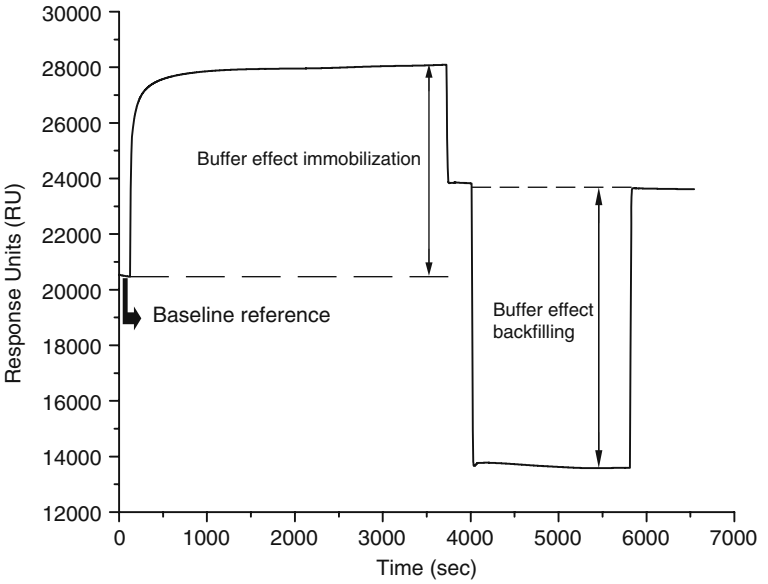

Fig. 11.3. By using buffers with different refractive indices, with respect to the running buffer, buffer effects appear. In case of the immobilization this is shown as an increase in signal whereas for the backfilling a decrease in signal is observed.

3.2. Determination and Optimization of the Probe Concentration

The amount of immobilized probes is a crucial element for further hybridization steps. By testing and comparing different concentrations of thiolated DNA during immobilization, an optimal probe concentration can be found. Based on these results a standard probe concentration can be determined for use in future tests.

1. Prepare a 1:10 dilution series in immobilization buffer, ranging from 1 fM to 10 μM, of thiolated DNA probes with C_6 spacer and test all these concentrations individually.
2. Inject the thiolated probe solution for 1 h.

3. Rinse the surface with running buffer (i.e., ExtraClean step in the Biacore software) to wash away all unbound probe and to set a new baseline.
4. Dissolve 1 mM MCH backfilling in water, sonicate for 15 min, and inject this solution over the sample for 30 min. After the backfilling insert again an ExtraClean step.
5. Determine the changes in resonance units (RU) after both the injection of the thiolated probe and the MCH backfilling step as shown in **Fig. 11.4a**.
6. Prepare different concentrations of 25 cp, ranging between 10 and 320 nM, in hybridization buffer and inject each concentration randomly in the system for 10 min.
7. After each hybridization step inject 2.5 mM of HCl for 2 min to regenerate the surface. Alternatively, 20 mM NaOH can be used (*see* **Note 6**).
8. Determine the RU changes after each hybridization step. The relation between the used probe concentration and the hybridization is presented in **Fig. 11.4b** (*see* **Note 7**).

3.3. Immobilization and Hybridization of DNA on Gold: General Protocol

Based on the probe optimization as described above, a general immobilization protocol has been designed. This protocol can function as a starting point during experiments for which a controlled immobilization of thiolated DNA is required. By following this protocol various parameters, affecting the biosensor performance, can be calculated. As such, the relation between the spacer length and the biosensor behavior was determined. In addition to the immobilization, the protocol describes the subsequent hybridization steps on the mixed DNA/alkanethiol films.

1. Prepare 1 μM of thiolated probe, either with C_6 or with C_{11} spacer, in immobilization buffer and inject this solution for 1 h in the system.
2. Rinse the surface following the ExtraClean procedure.
3. Dissolve 1 mM MCH in water or 1 mM MCU in a mixture of 90:5 water/ethanol and sonicate (*see* **Note 8**). Use MCH for surfaces prepared with the C_6 spacer and MCU for surfaces prepared with the C_{11} spacer. Inject the backfilling solution for 30 min.
4. Rinse the surface following the ExtraClean procedure.
5. Determine the RU changes after deposition of the mixed DNA/alkanethiol film and calculate the immobilization degree using following conversion factor: 1,000 RU $\approx$ 100 ng/cm^2 (10) (*see* **Table 11.1**).
6. Prepare different concentrations of 25 cp in hybridization buffer. For the short C_6 spacer concentrations between 10 and 320 nM are used (*see* **Section 3.2**; step 6), whereas for

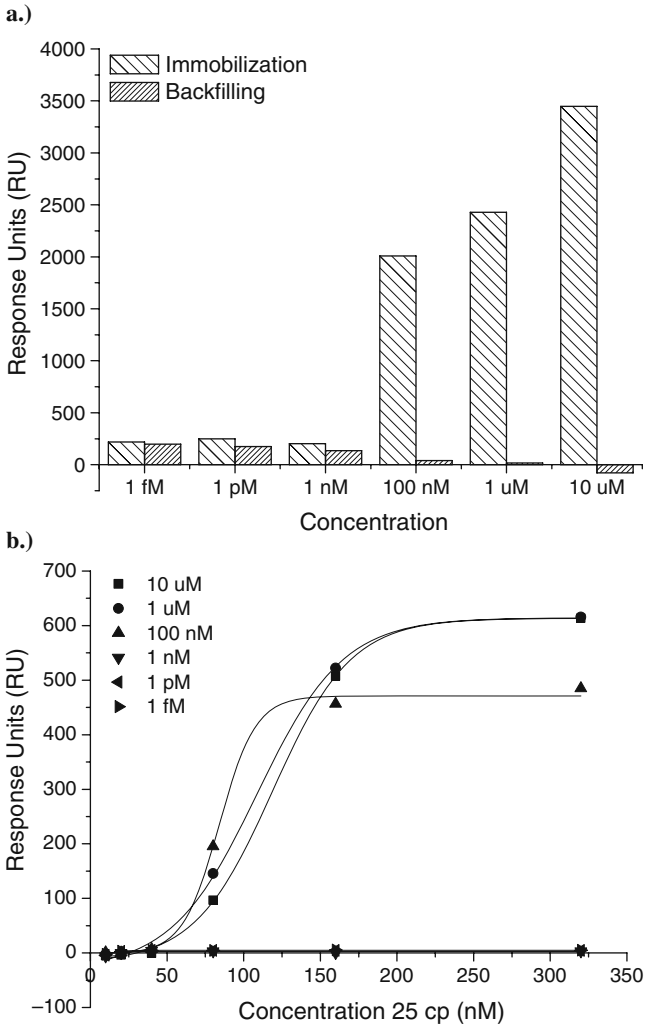

Fig. 11.4. (**a**) Comparison of the RU changes obtained after 1 h of immobilization for different concentrations of thiolated 25 nt probe (i.e., 1 fM–10 μM) and after post-treatment of the surface with 1 mM MCH backfilling. Based on their molar mass, only a limited exchange between the probes and the backfilling takes place for concentrations >1 nM of DNA (i.e., 100 nM, 1 μM, and 10 μM). When the lower probe concentrations are used a clear RU increase (i.e., increase in mass) is seen after backfilling. This clearly indicates that the immobilized DNA layer is less dense. (**b**) Hybridization of 25 cp on the different DNA layers with positive signals for the three highest concentrations, i.e., 100 nM, 1 μM, and 10 μM.

the C_{11} spacer concentrations between 0.625 and 320 nM are used. For the 25 np only prepare a concentration of 320 nM.

7. Inject each concentration of 25 cp randomly on the mixed DNA/alkanethiol layer for 10 min and regenerate the surface after each hybridization step using 2.5 mM HCl

Table 11.1
Calculated immobilization and hybridization degrees at saturation for the short C_6 and long C_{11} spacer. The hybridization of the 25 np is negligible and therefore not included

Spacer	Immobilization ($\times 10^{13}$ molecules/cm^2)	Hybridization ($\times 10^{12}$ molecules/cm^2)
C_6	2.0 ± 0.2	4.7 ± 0.19
C_{11}	2.3 ± 0.02	5.8 ± 0.02

(*see* **Section 3.2**; step 7). Test the non-complementary 25 np fragment in a separate step.

8. Determine the RU changes after hybridization of both the 25 cp and 25 np and calculate the hybridization degree at saturation (*see* **Note 9**) as explained for the immobilization. *See* **Table 11.1** for the obtained values.
9. Linearly fit the dose–response hybridization curves using the Origin Data Analysis software (Linear Fit, Origin v 6.0, OriginLab, USA) and determine the sensitivity, the detection limit, and the dynamic range (*see* **Note 10**). **Figure 11.5** gives an example of such a hybridization curve whereas **Table 11.2** contains the calculated values.

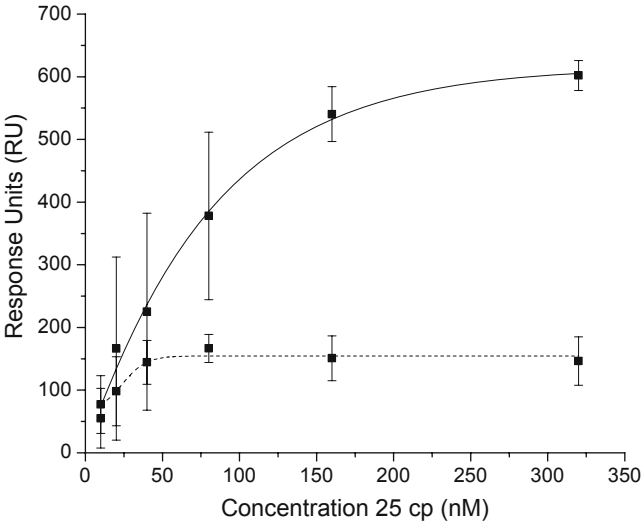

Fig. 11.5. Example of fitted dose–response hybridization curves using thiolated probes with C_6 spacer for the flow-assisted (*solid line*) and the diffusion-controlled immobilization approaches (*dashed line*). This figure clearly shows the impact of the immobilization approach.

Table 11.2
Summary of the sensitivity, the detection limit, and the dynamic range, calculated for both the flow-assisted and diffusion-controlled (indicated by no flow) immobilization of thiolated 25 nt probes.

Spacer	Sensitivity[a] (RU/nM)	Detection limit[a] (nM)	Dynamic range (nM)
C_6	3.6 ± 2.1	21.6 ± 1.9	21.6–160
C_{11}	99.2 ± 13.7	0.3 ± 0.2	0.3–20
C_6, no flow	2.3 ± 0.9	12.9 ± 31.0	12.9–40
C_{11}, no flow	4.7 ± 0.2	8.4 ± 0.71	8.4–40

[a]The standard deviations were determined based on the average of the individual experiments.

3.4. Diffusion-Controlled Immobilization

Besides the length of the carbon spacer, the immobilization approach itself can have a great impact on the biosensor performance. Since this aspect can easily be tested using the SPR device a protocol for the diffusion-controlled immobilization is given below. By comparing hybridization on the surfaces, prepared according to the two described protocols (i.e., flow-assisted and diffusion-controlled), the effect of the immobilization approach can be estimated as is done here for again both spacers.

1. Prepare 1 μM thiolated probe, with either a C_6 or a C_{11} spacer, in immobilization buffer.
2. Incubate the gold-coated surfaces overnight at 25°C in 500 μL of the DNA solution while continuously shaking.
3. Rinse the DNA-functionalized surfaces thoroughly with water, dry them under a flow of nitrogen, and finally mount them on the chip support.
4. From this point on, follow steps 3 to 9 as described in **Section 3.3**.

4. Notes

1. As an example we have studied a 25-nucleotide (nt) long fragment of an *Escherichia coli stx2* gene (AF461171). However, the protocol is also valid when using other sequences with different lengths. The exact sequences used in this chapter are:
   25 nt (5′-TTCACAGGTACTGGATTTGATTGTG),
   25 cp (5′-CACAATCAAATCCAGTACCTGTGAA),
   25 np (5′-GTGCTCAGTTGACAGGAATGACTGT).

2. All buffer solutions (i.e., immobilization, hybridization, and running buffer) were stored at 4°C and were degassed and filtered before use.
3. The combination of unmounted gold surfaces and separate chip supports allows the easy assembly of the SPR sensor chips after cleaning and/or coating of the surface.
4. **Figure 11.2** includes a schematic illustration of our homemade UV/O_3 device. The device has an O_2 inlet to elevate the amount of O_2 in the chamber as well as a N_2 inlet to flush away the O_3 (after cleaning). In addition manganese(IV)dioxide (MnO_2) is used to reduce the toxic O_3 to O_2 before releasing it into the atmosphere. The used mercury grid lamp (BHK Inc., USA) emits both the wavelengths 185.0 and 253.7 nm which allow the following reactions, responsible for the sample cleaning, to occur:

$$O_2 + O^* \xrightarrow{185\text{nm}} O_3$$
$$O_3 \xrightarrow{253.7\text{nm}} O_2 + O^*$$

   During this photosensitized cleaning mechanism, the contaminant molecules are excited and/or dissociated by absorption of short-wavelength UV light. Simultaneously, atomic oxygen is generated when O_2 is dissociated by the absorption of UV with a wavelength of 185 nm and when O_3 is dissociated by the absorption of the 253.7 nm and longer wavelengths of radiation. The products of the excitation of contaminant molecules react with atomic oxygen to form simpler volatile molecules such as CO_2, H_2O, N_2. This combination of short-wavelength UV light and O_3, as used in our homemade device, has shown to produce clean surfaces about 200–2,000 times faster than UV light or O_3 alone (11).
5. SPR is sensitive to changes in refractive index causing the SPR angle to change, for instance as a result of using different buffers. To limit these buffer effects, when hybridizing different concentrations of 25 cp on the same chip and to calculate RU changes the hybridization buffer is chosen as running buffer. The buffer effects thus only appear during all other SPR steps (i.e., immobilization, backfilling, and regeneration). **Figure 11.3** clearly demonstrates the buffer effects seen during immobilization and backfilling.
6. The regeneration of the DNA surfaces is studied by hybridization of the 25 cp followed by a regeneration step with either 2.5 mM HCl or 20 mM NaOH. Based on earlier results (not shown), only a negligible decrease (i.e., on

average 2% for each cycle) in hybridization efficiency was observed for both regeneration solutions. As a result different hybridization experiments can be performed on the same sample.

7. A probe concentration of 1 μM was chosen as optimal probe concentration since maximum hybridization signals were observed using this concentration. In addition, hybridization performed on these DNA layers was more reproducible than using lower concentrations.
8. Because the use of >70% ethanol is not compatible with the integrated fluidic system (IFC) of the Biacore™ 2000 device, the MCU backfilling solution is first dissolved in a minimal amount of ethanol. The final solution is a water/ethanol mixture.
9. As saturation appears for hybridization at 320 nM of 25 cp, the amount of hybridized probes is only calculated for this concentration.
10. For each concentration of 25 cp and 25 np the corresponding RU changes are plotted in a dose–response curve. The slope of these hybridization curves is taken as the sensitivity (S), whereas the detection limit (DL) can be calculated using following formula:

$$\mathrm{DL} = \frac{\left|(3\,N) - I\right|}{S}$$

with N the noise and I the intercept in RU.

Acknowledgments

The authors would like to thank Dr. Van Aerschot for providing 5′-end thiol-modified DNA probes with C_{11} spacer. The authors are also grateful to the Institute for the Promotion and Innovation Through Science and Technology (IWT-Flanders) and the Fund for Scientific Research – Flanders (FWO G. 0298.06) for their funding.

References

1. Nakaya, H. I., Reis, E. M., and ANDVerjovski-Almeida, S. (2007) *Nucleic Acids Hybridization Modern Applications.* Springer, Netherlands, pp. 265–307.
2. Lobert, P. E., Bourgeois, D., Pampin, R., Akheyar, A., Hagelsieb, L. M., Flandre, D., and Remacle, J. (2003) Immobilization of DNA on CMOS compatible materials. *Sensor. Actuator. B* **92**, 90–97.
3. Herne, T. M., and Tarlov, M. J. (1997) Characterization of DNA probes immobilized on gold surfaces. *J. Am. Chem. Soc.* **119**, 8916–20.
4. Levicky, R., Herne, T. M., Tarlov, M. J., and Satija, S. K. (1998) Using self-assembly to control the structure of DNA monolayers on gold: a neutron reflectivity study. *J. Am. Chem. Soc.* **120**, 9787–92.
5. Gong, P., Lee, C. H., Gamble, J. L., Castner, D. G., and Grainger, D. W. (2006) Hybridization behavior of mixed DNA/alkanethiol monolayers on gold: characterization by surface plasmon resonance and 32P radiometric assay. *Anal. Chem.* **78**, 3326–34.
6. Peeters, S., Stakenborg, T., Reekmans, G., Laureyn, W., Lagae, L., Van Aerschot, A., and Van Ranst, M. (2008) Impact of spacers on the hybridization efficiency of mixed self-assembled DNA/alkanethiol films. *Biosens. Bioelectron.* **24**, 72–77.
7. Wang, R., Tombelli, S., Minunni, M., Spiriti, M. M., and Mascini, M. (2004) Immobilization of DNA probes for the development of SPR-based sensing. *Biosensor. Bioelectron.* **20**, 967–74.
8. Van Aerschot, A., and Rozenski, J. (2006) Characterization and sequence verification of thiolated deoxyoligonucleotides used for microarray construction. *J. Am. Chem. Soc. Mass Spec.* **17**, 1396–400.
9. King, D. E. (1995) Oxidation of gold by ultraviolet light and ozone at 25°C. *J. Vac. Sci. Technol. A* **13**, 1247–53.
10. Bunimovich, Y. L., Shin, Y. S., Yeo, W. -S., Amori, M., Kwong, G., and Heath, J. R. (2006) Quantitative real-time measurements of DNA hybridization with alkylated nonoxidized silicon nanowires in electrolyte solution. *J. Am. Chem. Soc.* **128**, 16323–31.
11. Vig, R. J. (1985) UV/ozone cleaning of surfaces. *J. Vac. Sci. Technol. A* **3**, 1027–34.

Chapter 12

Preparation of Lipid Membrane Surfaces for Molecular Interaction Studies by Surface Plasmon Resonance Biosensors

Mojca Podlesnik Beseničar and Gregor Anderluh

Abstract

Surface plasmon resonance has become one of the most important techniques for studying bimolecular interactions. Most of the researchers are using it to study protein–protein interactions, but in recent years membrane model systems have also become available and this makes it possible to study protein–membrane interactions as well. In this review chapter we describe possible ways to prepare lipid membrane surfaces on various sensor chips and some of the experimental considerations one has to take into account when performing such experiments.

Key words: Protein–membrane interactions, lipid membrane, sensor chip L1, sensor chip SA, sensor chip HPA, Biacore.

1. Introduction

Use of optical sensors based on surface plasmon resonance (SPR) has become the most important tool in molecular interaction analysis. More than 1,000 scientific papers were published in 2007 using biosensor platforms from 25 different manufacturers (1). SPR biosensors are used in either qualitative or quantitative mode to determine the binding partners or kinetics and affinity parameters of the interaction, respectively. The use of SPR biosensors is not confined only to basic research laboratories, but is also extensively used in medical diagnostics, monitoring of environmental samples, food analysis, etc. Traditionally, most of the references describe interactions, where both binding partners are proteins, e.g. protein–protein, antigen–antibody,

N.J. de Mol, M.J.E. Fischer (eds.), *Surface Plasmon Resonance*, Methods in Molecular Biology 627,
DOI 10.1007/978-1-60761-670-2_12,

peptide–receptor. Even though lipid membranes are important cell constituents with many associated peripheral and transmembrane proteins, only a small fraction of the rich SPR literature describes interactions of proteins with lipid membranes (1, 2). This is mainly due to difficulties associated with preparations of pure and homogeneous membrane protein samples used for SPR studies. Furthermore, suitable membrane model systems that could be used on optical biosensors became available only recently. In this chapter we provide some examples on the kind of information one can obtain from experiments with SPR biosensors, we give an overview of lipid membrane-mimetic systems that can be prepared and used on Biacore platforms, and we discuss briefly some experimental considerations that are particular for protein–membrane interaction studies. The interested reader will find more information on protein–membrane interaction studies in the following chapters that describe the use of optical biosensors based on SPR in protein–membrane interactions (2), in studies of peripheral membrane proteins that associate with lipid membranes (3–5), membrane-interacting peptides (6, 7), or pore-forming toxins (8).

2. Use of SPR Biosensors in Protein–Membrane Interaction Studies

The SPR literature on interactions of proteins with membranes mainly describes the qualitative and quantitative aspects of peripheral membrane protein interactions with lipid membranes. Typically, one can explore lipid specificity of a peripheral membrane protein by changing the lipid composition of the membrane. Determination of the rate and affinity constants from sensorgrams gives additional information about the interaction of proteins with membranes, especially when the differences between different types of membranes or different variants of proteins are subtle. Often researchers wish to examine effects of particular amino acids on the binding to the membranes (9). Such experiments are relatively easy to perform when the protein attaches reversibly to the membranes. However, most of the membrane proteins are very hydrophobic and may attach non-specifically to the surface of the chip (see below). Sometimes they further aggregate on the surface of the membrane and that often leads to irreversible association with the membranes. A group of peripheral proteins, protein toxins that generate pores in lipid membranes, actually assemble on the surface of the membrane in a multi-step mechanism that involves attachment to the lipid membrane, oligomerization in the plane of the membrane, and irreversible insertion into the membrane (8). It is difficult to interpret the results in such cases and complex binding models should be applied. These

models, however, should be used with caution and it is desirable that some other independent experimental verification of a multi-step mechanism is provided.

Other studies on membrane structure and function have been performed by employing SPR-based biosensors and membrane-mimetic systems. They were, for example, used to study drug–membrane interactions in preclinical drug discovery (10–14), to reconstitute transmembrane proteins on the surface of sensor chips (15, 16), to study the kinetics of removal of particular lipid components from the membrane by either proteins or other molecules (17–19), to characterize intact synaptic vesicles (20), to functionally characterize transmembrane receptors (21, 22). The described studies indicate that SPR-based biosensors can be used in versatile experimental set-ups. For example, varying the membrane model (liposomes vs. bilayer, see below) and composition is one of the basic and yet very informative ways of characterizing the membrane-binding requirements of the protein of interest.

3. Lipid Membrane Model Systems Used in SPR Biosensors

In a typical protein–membrane interaction study the membrane is prepared on the surface of the sensor chip and the protein of interest is injected across such a surface. Although many different approaches on how to prepare a membrane-mimetic surface have been reported, there are only few general methods (*see* **Table 12.1** and **Fig. 12.1**). It is possible to prepare either planar

Table 12.1
Biacore sensor chips that may be used for the preparation of membrane-mimetic surfaces with key references that describe their use

Sensor chip	Description	References
HPA	Formation of stable hybrid bilayer membrane. Only one monolayer is formed on the surface of the chip	(23)
L1	Capture of intact liposomes or other cellular membrane preparations	(37–39)
SA	Capture of liposomes that possess minor amounts of biotin	(42)
CM5	Capture of liposomes by antibodies	(33)
Gold	Capture of liposomes by DNA-derivatized liposomes	(34)

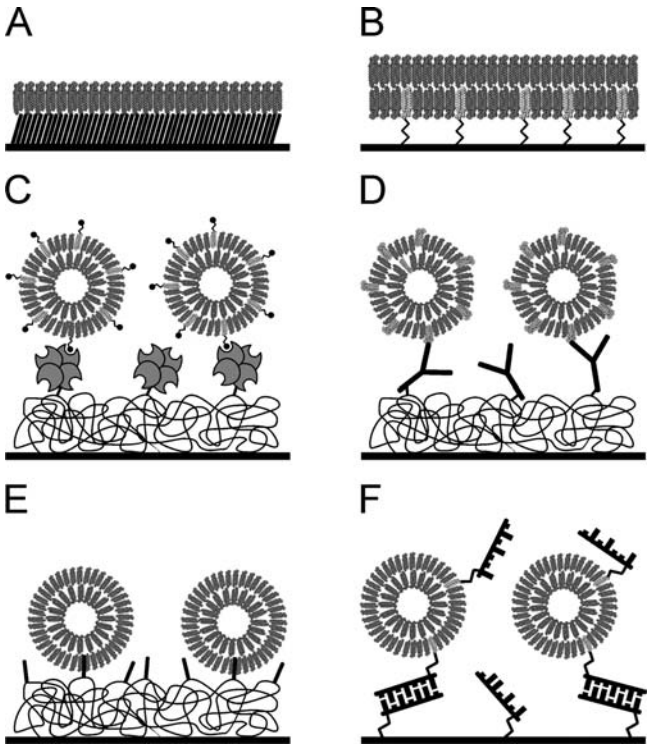

Fig. 12.1. Lipid membrane model systems used in SPR biosensors. (**a**) Hybrid membrane bilayers formed on the surface of hydrophobic layer of alkanes. These can be prepared by using a Biacore HPA sensor chip. (**b**) Tethered membrane bilayers formed on the surface of a gold chip by the use of thiolipids (*light grey*). (**c–f**) Capture of intact liposomes on the surface of sensor chips. (**c**) Capturing may be achieved by the biotin–avidin system, employing low percentage of biotinylated lipids (*light grey*). (**d**) Capture by binding of liposomes to an antibody directed to a lipid component of a membrane bilayer. (**e**) Capture by long lipophilic molecules attached to the dextran matrix (Biacore sensor chip L1). (**f**) Capture by DNA tethers, which allows formation of a 3D liposomal matrix. Reprinted from Beseničar M. et al. (2) with permission from Elsevier.

lipid bilayers or intact liposomes that are captured on the surface of the sensor chips.

3.1. Preparation of Membrane Bilayers

Hybrid bilayer membranes are usually prepared on the surface of alkanethiol self-assembled monolayers, such as Biacore HPA sensor chips (*see* **Fig. 12.1a**). When a solution of small unilamellar liposomes is injected across such a hydrophobic surface, a stable lipid monolayer is formed. Cooper et al. described the general methodology for formation of supported lipid monolayers by using an HPA sensor chip and this study should be taken as a starting point, if one has no experience (23). They compared the monolayer formation when different methods for vesicle preparation, e.g. extrusion or sonication, different lipids, or different buffers were used. Bovine serum albumin was used to check

the quality of the prepared surface. They have also determined the amount of deposited lipids by using ^{3}H-labelled dipalmitoylphosphatidylcholine and found that the correlation of mass of deposited material with the response observed (RU) is the same as for proteins (24). So when a monolayer is formed, fully covering the HPA chip, a response of around 2,200 RU should be expected, corresponding to a mass of 2.0 ng/mm^2 (23). Hybrid bilayer surfaces may be used to study many aspects of protein interactions with membranes, as highlighted by three examples by Cooper et al. (23), but it has some disadvantages that preclude its widespread use. They are hard to work with, as they are very hydrophobic and, more importantly, hybrid bilayers represent only one monolayer of the lipid membrane and, hence, it is not possible to use them to study transmembrane proteins in active form.

There is another model bilayer system encompassing the disadvantages of the hybrid bilayers. A stable membrane bilayer can be tethered on the surface of the gold chip by thiolipids (25–27). The headgroup of these lipids is linked to a thiol group by a long flexible linker. This approach first requires the deposition of thiolipids to form a sparse monolayer. Lipid vesicles are subsequently injected and a continuous bilayer is formed encompassing thiolipids as part of the lipid membrane (*see* **Fig. 12.1b**). In this system both layers of the membrane are fluid and there is an additional aqueous layer between the membrane and the sensor chip. It is possible to include transmembrane proteins in such a membrane (26, 28, 29).

3.2. Capture of Intact Liposomes

Capture of intact liposomes is perhaps the most appealing possibility and a few different approaches were described in the literature. Initial studies involved biotin–avidin interactions, where minor amounts of biotinylated lipid are included in the liposome (30, 31) (*see* **Fig. 12.1c**).

Liposomes can also be retained on the chip by binding to an antibody directed against a specific membrane component, such as lipopolysaccharide (LPS) (32, 33). The paper by MacKenzie and Hirama gives a detailed description of the quantitative analysis of the binding affinity for glycolipid receptors. The authors describe the preparation of liposomes, which include LPS at 1% (w/w) of the total lipid, the deposition of the liposomes on an IgG surface, and the binding of an analyte, a bivalent single-chain Fv (33).

Liposomes may also be captured via DNA tethers; the method requires the use of a membrane lipid attached to a DNA molecule (*see* **Fig. 12.1f**) (34, 35). This approach allows a construction of a 3D surface of liposomes on the surface of the dextran layer. It may find its use in the functional characterization of membrane

proteins embedded in liposomes, as shown recently by Graneli et al. (36). This is particularly appealing, as the transmembrane protein is located away from the sensor chip and at the same time the amount of the protein under study is also increased. Such method is described in **Chapter 16**.

3.3. Capture of Intact Liposomes by the Biacore Sensor Chip L1

By far most of the references in the literature employ sensor chip L1 for studying protein–membrane interactions. This sensor chip possesses lipophilic groups on the surface of the dextran matrix (*see* **Fig. 12.1e**), which efficiently capture intact liposomes. This chip offers some advantages over other described approaches, the most appealing being the easy capturing of liposomes and regeneration of the captured material from the chip, so it may be reused many times. The novice users are directed to papers that describe the deposition of the liposomes on L1 sensor chip and characterization of the so-formed surface (37–39). The advantage of this chip over others is that not only liposomes but also membrane preparations from cell lysates can be used for immobilization. They will be retained by lipophilic anchors and, hence, allow studying membrane binding with biologically more relevant membranes, e.g. binding of pore-forming toxins was studied by using erythrocyte ghosts (40, 41), binding of various drugs to vesicles prepared from intestinal brush-border membranes (13), binding of nanosomes prepared from yeast expressing a mammalian odorant receptor (21).

4. Some Experimental Considerations

Below are some experimental considerations that we found particularly important for experiments on SPR biosensors where membrane systems are used.

4.1. Baseline

There are several reasons for the formation of the drift of the baseline in SPR biosensors, which are extensively covered in instrument manuals. However, when working with hydrophobic surfaces, such as hydrophobic chips (HPA sensor chips) or membranes and liposomes, one should take extra care to minimize all causes that could contribute to the drift formation. One such reason may be the remnants of detergents on the glassware, if common washing services are used. From our own experience, we recommend that all glassware is thoroughly cleaned with copious amounts of distilled water to remove traces of detergents.

Frostell-Karlsson et al. have observed a slight upward drift in the liposome baseline (14). They have systematically checked for the causes of the drift (e.g. buffer composition, lipid membrane

composition, flow rate, liposome injection time, stabilization time after injection, type of regeneration solution used) and found out that the most important parameters for minimizing the baseline drift were a long liposome injection time and additional time used for stabilization of the surface after the liposome injection.

4.2. Referencing

A reference cell is used to subtract the contributions of the buffer to the refractive index and possible unspecific interactions of proteins with the sensor chip. However, hydrophobic molecules may attach to lipophilic anchors on an L1 sensor chip. This is particularly valid for membrane proteins, as they possess extensive hydrophobic surfaces. If it is possible to fully cover the sensor chip, i.e. the sample cell as well as the reference cell, with the lipids, so that no anchors are exposed, and if protein of interest may be prepared in running buffer, so that refractive indexes match, then it is still possible to perform experiments and correct the sensorgrams with the injections of the buffer. However, if the chip surface is only partially covered with lipids, then binding to the lipophilic anchors will be extensive and therefore the flow cell without lipids cannot be used for referencing, as the binding may be even better for the latter. Some other systems that possess a more polar surface should be considered, i.e. a streptavidin sensor chip (SA sensor chip) or an avidin-covered chip, as was used for the characterization of mitochondrial kinases (42, 43).

Another way for referencing is to use a lipid membrane for which the protein of interest has a low affinity. In this way one can account also for non-specific binding of protein to the lipid membrane. Membranes without or with a small percentage of lipid that is recognized by the protein are immobilized on the reference and test flow cell, respectively. Such referencing was used for the protein domains that specifically bind to phosphorylated variants of glycerophosphatidylinositol (5).

4.3. Regeneration

Liposomes captured on the surface of sensor chips are stable for hours. If proteins bind weakly and it is possible to remove them from the liposome surface by buffers with high salt or a change in pH, one can use such surface for many injections with different concentrations of proteins. However, some proteins bind irreversibly and it is impossible to remove them from the membranes. This is particularly true for proteins that insert stably into the membranes. In such cases one should regenerate sensor chips by injections with buffer that contains either detergents or organic solvents to remove all of the lipids from the surface of the sensor chip. Most commonly employed and efficient are solutions of 40 mM *N*-octyl-β-D-glucopyranoside and 100 mM NaOH:isopropanol (2:3; v/v).

5. Conclusions

Optical biosensors are perhaps not so commonly used in membrane biology studies as in some other fields. We believe, however, that a lot of useful qualitative and quantitative information about the interactions of proteins or other molecules with membranes may be obtained. Researchers that study various aspects of membrane biology may benefit tremendously, as highlighted by the cited examples in this chapter. For example, one can look into the membrane-binding properties of the protein of interest without consuming large quantities of the material. Questions can be answered as, does the protein insert into the membrane, or does it bind only superficially? Does a rigid membrane monolayer suffice for binding or does the protein require membrane curvature of the liposomes or at least a more fluid membrane bilayer? What are the pH and salt requirements for the stable binding? How can one prevent binding and the membranolytic activity (if there is one)? All these and many more questions can be answered in quite a short time and with low amounts of protein.

Acknowledgments

We would like to thank the Slovenian Research Agency for support and Vesna Hodnik for critically reading the manuscript.

References

1. Rich, R. L., and Myszka, D. G. (2008) Survey of the year 2007 commercial optical biosensor literature. *J. Mol. Recognit.* **21**, 355–400.
2. Beseničar, M., Maček, P., Lakey, J. H., and Anderluh, G. (2006) Surface plasmon resonance in protein-membrane interactions. *Chem. Phys. Lipids* **141**, 169–78.
3. Cho, W., Bittova, L., and Stahelin, R. V. (2001) Membrane binding assays for peripheral proteins. *Anal. Biochem.* **296**, 153–61.
4. Cooper, M. A. (2004) Advances in membrane receptor screening and analysis. *J. Mol. Recognit.* **17**, 286–315.
5. Narayan, K., and Lemmon, M. A. (2006) Determining selectivity of phosphoinositide-binding domains. *Methods* **39**, 122–33.
6. Mozsolits, H., and Aguilar, M. I. (2002) Surface plasmon resonance spectroscopy: an emerging tool for the study of peptide-membrane interactions. *Biopolymers* **66**, 3–18.
7. Mozsolits, H., Thomas, W. G., and Aguilar, M. I. (2003) Surface plasmon resonance spectroscopy in the study of membrane-mediated cell signalling. *J. Pept. Sci.* **9**, 77–89.
8. Anderluh, G., Maček, P., and Lakey, J. H. (2003) Peeking into a secret world of pore-forming toxins: membrane binding processes studied by surface plasmon resonance. *Toxicon* **42**, 225–28.
9. Stahelin, R. V., and Cho, W. (2001) Differential roles of ionic, aliphatic, and aromatic residues in membrane-protein interactions: a

surface plasmon resonance study on phospholipases A_2. *Biochemistry* **40**, 4672–78.
10. Danelian, E., Karlen, A., Karlsson, R., Winiwarter, S., Hansson, A., Lofas, S., Lennernas, H., and Hamalainen, M. D. (2000) SPR biosensor studies of the direct interaction between 27 drugs and a liposome surface: correlation with fraction absorbed in humans. *J. Med. Chem.* **43**, 2083–86.
11. Baird, C. L., Courtenay, E. S., and Myszka, D. G. (2002) Surface plasmon resonance characterization of drug/liposome interactions. *Anal. Biochem.* **310**, 93–99.
12. Abdiche, Y. N., and Myszka, D. G. (2004) Probing the mechanism of drug/lipid membrane interactions using Biacore. *Anal. Biochem.* **328**, 233–43.
13. Kim, K., Cho, S., Park, J. H., Byun, Y., Chung, H., Kwon, I. C., and Jeong, S. Y. (2004) Surface plasmon resonance studies of the direct interaction between a drug/intestinal brush border membrane. *Pharm. Res.* **21**, 1233–39.
14. Frostell-Karlsson, A., Widegren, H., Green, C. E., Hamalainen, M. D., Westerlund, L., Karlsson, R., Fenner, K., and van de Waterbeemd, H. (2005) Biosensor analysis of the interaction between drug compounds and liposomes of different properties; a two-dimensional characterization tool for estimation of membrane absorption. *J. Pharm. Sci.* **94**, 25–37.
15. Karlsson, O. P., and Lofas, S. (2002) Flow-mediated on-surface reconstitution of G-protein coupled receptors for applications in surface plasmon resonance biosensors. *Anal. Biochem.* **300**, 132–38.
16. Stenlund, P., Babcock, G. J., Sodroski, J., and Myszka, D. G. (2003) Capture and reconstitution of G protein-coupled receptors on a biosensor surface. *Anal. Biochem.* **316**, 243–50.
17. Locatelli-Hoops, S., Remmel, N., Klingenstein, R., Breiden, B., Rossocha, M., Schoeniger, M., Koenigs, C., Saenger, W., and Sandhoff, K. (2006) Saposin A mobilizes lipids from low cholesterol and high bis(monoacylglycerol)phosphate-containing membranes: patient variant Saposin A lacks lipid extraction capacity. *J. Biol. Chem.* **281**, 32451–60.
18. Remmel, N., Locatelli-Hoops, S., Breiden, B., Schwarzmann, G., and Sandhoff, K. (2007) Saposin B mobilizes lipids from cholesterol-poor and bis(monoacylglycero)phosphate-rich membranes at acidic pH. Unglycosylated patient variant saposin B lacks lipid-extraction capacity. *FEBS J.* **274**, 3405–20.
19. Beseničar Podlesnik, M., Bavdek, A., Kladnik, A., Maček, P., and Anderluh, G. (2008) Kinetics of cholesterol extraction from lipid membranes by methyl-[beta]-cyclodextrin – A surface plasmon resonance approach. *Biochim. Biophys. Acta* **1778**, 175–84.
20. Ferracci, G., Seagar, M., Joël, C., Miquelis, R., and Léveque, C. (2004) Real time analysis of intact organelles using surface plasmon resonance. *Anal. Biochem.* **334**, 367–75.
21. Vidic, J. M., Grosclaude, J., Persuy, M. A., Aioun, J., Salesse, R., and Pajot-Augy, E. (2006) Quantitative assessment of olfactory receptors activity in immobilized nanosomes: a novel concept for bioelectronic nose. *Lab Chip.* **6**, 1026–32.
22. Vidic, J., Grosclaude, J., Monnerie, R., Persuy, M. A., Badonnel, K., Baly, C., Caillol, M., Briand, L., Salesse, R., and Pajot-Augy, E. (2008) On a chip demonstration of a functional role for Odorant Binding Protein in the preservation of olfactory receptor activity at high odorant concentration. *Lab Chip.* **8**, 678–88.
23. Cooper, M. A., Try, A. C., Carroll, J., Ellar, D. J., and Williams, D. H. (1998) Surface plasmon resonance analysis at a supported lipid monolayer. *Biochim. Biophys. Acta* **1373**, 101–11.
24. Stenberg, E., Persson, B., Roos, H., and Urbaniczky, C. (1990) Quantitative determination of surface concentration of protein with surface plasmon resonance using radiolabeled proteins. *J. Colloid Interf. Sci.* **143**, 513–26.
25. Lang, H., Duschl, C., and Vogel, H. (1994) A new class of thiolipids for the attachment of lipid bilayers on gold surfaces. *Langmuir* **10**, 197–210.
26. Stora, T., Lakey, J. H., and Vogel, H. (1999) Ion-channel gating in transmembrane receptor proteins: functional activity in tethered lipid membranes. *Angew. Chem. Int. Ed.* **38**, 389–91.
27. Hong, Q., Gutiérrez-Aguirre, I., Barlič, A., Malovrh, P., Kristan, K., Podlesek, Z., Maček, P., Turk, D., González-Mañas, J. M., Lakey, J. H., and Anderluh, G. (2002) Two-step membrane binding by Equinatoxin II, a pore-forming toxin from the sea anemone, involves an exposed aromatic cluster and a flexible helix. *J. Biol. Chem.* **277**, 41916–24.
28. Heyse, S., Ernst, O. P., Dienes, Z., Hofmann, K. P., and Vogel, H. (1998) Incorporation of rhodopsin in laterally structured supported membranes: observation of transducin activation with spatially and time-resolved

surface plasmon resonance. *Biochemistry* **37**, 507–22.
29. Schmidt, E. K., Liebermann, T., Kreiter, M., Jonczyk, A., Naumann, R., Offenhausser, A., Neumann, E., Kukol, A., Maelicke, A., and Knoll, W. (1998) Incorporation of the acetylcholine receptor dimer from Torpedo californica in a peptide supported lipid membrane investigated by surface plasmon and fluorescence spectroscopy. *Biosens. Bioelectron.* **13**, 585–91.
30. Masson, L., Mazza, A., and Brousseau, R. (1994) Stable immobilization of lipid vesicles for kinetic studies using surface plasmon resonance. *Anal. Biochem.* **218**, 405–12.
31. Stachowiak, O., Dolder, M., and Wallimann, T. (1996) Membrane-binding and lipid vesicle cross-linking kinetics of the mitochondrial creatine kinase octamer. *Biochemistry* **35**, 15522–28.
32. MacKenzie, C. R., Hirama, T., Lee, K. K., Altman, E., and Young, N. M. (1997) Quantitative analysis of bacterial toxin affinity and specificity for glycolipid receptors by surface plasmon resonance. *J. Biol. Chem.* **272**, 5533–38.
33. MacKenzie, C. R., and Hirama, T. (2000) Quantitative analyses of binding affinity and specificity for glycolipid receptors by surface plasmon resonance. *Methods Enzymol.* **312**, 205–16.
34. Graneli, A., Edvardsson, M., and Hook, F. (2005) DNA-Based Formation of a supported, three-dimensional lipid vesicle matrix probed by QCM-D and SPR. *ChemPhysChem.* **5**, 729–33.
35. Wikstrom, A., and Deinum, J. (2007) Probing the interaction of coagulation factors with phospholipid vesicle surfaces by surface plasma resonance. *Anal. Biochem.* **362**, 98–107.
36. Graneli, A., Benkoski, J. J., and Hook, F. (2007) Characterization of a proton pumping transmembrane protein incorporated into a supported three-dimensional matrix of proteoliposomes. *Anal. Biochem.* **367**, 87–94.
37. Cooper, M. A., Hansson, A., Lofas, S., and Williams, D. H. (2000) A vesicle capture sensor chip for kinetic analysis of interactions with membrane-bound receptors. *Anal. Biochem.* **277**, 196–205.
38. Erb, E. M., Chen, X., Allen, S., Roberts, C. J., Tendler, S. J., Davies, M. C., and Forsen, S. (2000) Characterization of the surfaces generated by liposome binding to the modified dextran matrix of a surface plasmon resonance sensor chip. *Anal. Biochem.* **280**, 29–35.
39. Anderluh, G., Beseničar, M., Kladnik, A., Lakey, J. H., and Maček, P. (2005) Properties of nonfused liposomes immobilized on an L1 Biacore chip and their permeabilization by a eukaryotic pore-forming toxin. *Anal. Biochem.* **344**, 43–52.
40. Bavdek, A., Gekara, N. O., Priselac, D., Gutiérrez-Aguirre, I., Darji, A., Chakraborty, T., Maček, P., Lakey, J. H., Weiss, S., and Anderluh, G. (2007) Sterol and pH interdependence in the binding, oligomerization, and pore formation of Listeriolysin O. *Biochemistry* **46**, 4425–37.
41. Bakrač, B., Gutiérrez-Aguirre, I., Podlesek, Z., Sonnen, A. F., Gilbert, R. J., Maček, P., Lakey, J. H., and Anderluh, G. (2008) Molecular determinants of sphingomyelin specificity of a eukaryotic pore-forming toxin. *J. Biol. Chem.* **283**, 18665–77.
42. Schlattner, U., and Wallimann, T. (2000) A quantitative approach to membrane binding of human ubiquitous mitochondrial creatine kinase using surface plasmon resonance. *J. Bioenerg. Biomembr.* **32**, 123–31.
43. Schlattner, U., and Wallimann, T. (2000) Octamers of mitochondrial creatine kinase isoenzymes differ in stability and membrane binding. *J. Biol. Chem.* **275**, 17314–20.

Chapter 13

Capture of Intact Liposomes on Biacore Sensor Chips for Protein–Membrane Interaction Studies

Vesna Hodnik and Gregor Anderluh

Abstract

Qualitative and quantitative aspects of protein interactions with membranes may be studied by optical sensors. Biacore offers two dedicated chips for working with lipids and membranes: the L1 and HPA sensor chips. The L1 chip is the most frequently used in protein–membrane interaction studies and it allows the capture of intact liposomes. This chapter describes the protocol for immobilization of liposomes on L1 sensor chips and discusses some of the experimental considerations. An alternative approach that utilizes a streptavidin-coated sensor chip (SA sensor chip) is described for cases when it is not possible to use an L1 chip.

Key words: Liposome, sensor chip L1, sensor chip SA, Biacore, protein–membrane interactions.

1. Introduction

Various aspects of protein–membrane interactions may be conveniently studied by optical sensors based on surface plasmon resonance (SPR) (1–4). The number of publications that describe protein–membrane interactions by SPR is steadily increasing since the introduction of commercial machines and dedicated sensor chips that exploit the phenomenon of SPR for detection of bimolecular interactions. Biacore GE has introduced HPA and L1 sensor chips for work with lipids and membranes. The HPA sensor chip is used mainly for the preparation of hybrid lipid bilayers (5). Many researchers use L1 sensor chips for capture of liposomes in order to study protein–membrane interactions (4). Reported applications of this chip include the qualitative description of

N.J. de Mol, M.J.E. Fischer (eds.), *Surface Plasmon Resonance*, Methods in Molecular Biology 627,
DOI 10.1007/978-1-60761-670-2_13,

protein binding to membranes, determination of kinetic constants of protein binding to the membrane, drug–membrane interactions, the kinetics of lipid extraction from liposomes, reconstitution of membrane receptors and functional studies of membrane receptors (4). However, the L1 sensor chip is mostly used to study the kinetics of binding of peripheral membrane proteins (6). Other ways to prepare artificial membrane surfaces on the surface of sensor chips include the preparation of a tethered membrane bilayer on the surface of gold chips, capture of liposomes by the biotin–avidin system, by antibodies and via complementary oligonucleotides (4). Here we describe the procedures for capturing of liposomes on Biacore L1 and streptavidin (SA) chips, as these are the most frequently used.

The properties of the surface generated by the injection of liposomes over a L1 sensor chip were characterized by several researchers (7–10). Some of the reports have indicated that a continuous bilayer is formed on the surface of the chip upon injection of liposomes (8). However, the evidence gathered in the last years indicate that intact liposomes are captured, at least when some of the most common lipids are used for liposome preparation, e.g. DOPC, POPC, SM, DOPG (9, 10). It was, however, noticed that the fusion of liposomes on the surface of L1 chips may be lipid dependent (11). Therefore, we propose to check for the status of liposomes on the surface of L1 sensor chips, if lipids are used of which it is not known which surface they form.

The use of sensor chip L1 offers a number of advantages over other methods of capture, e.g. the capture is easy to perform, the chips are easily regenerated to remove the captured material, the chips may be reused many times. However, lipophilic anchors of L1 sensor chip may interact with some of the substances present in the samples, which can compete with liposomes for binding (12). Consequently, desorption of vesicles from the chip may be observed. Problems may also arise in preparing a proper reference surface, if the protein of interest has a great affinity for lipophilic anchors and complete coverage of the chip is hard to achieve. These and some other considerations are extensively explained in Section 4. If it is not possible to account for these problems, then it is advisable to use other ways to capture the liposomes. As an alternative method the capture of biotin-tagged liposomes on SA chips is described.

2. Materials

2.1. Liposome Preparation

1. Lipid 1,2-dioleoyl-*sn*-glycero-3-phosphocholine (DOPC) as powder. It should be stored under nitrogen atmosphere at –80°C.

2. Glass vials with screw caps and Teflon cap-liners (Reacti-Vials, Pierce, USA).
3. Parafilm "M" (Pechiney Plastic Packaging, Menasha, USA).
4. Chloroform (Merck KGaA, Germany).
5. Round-bottom glass flasks.
6. Rotary evaporator.
7. Distilled water of high quality, e.g. MilliQ water.
8. Vesicles buffer: 20 mM Tris–HCl, 140 mM NaCl, pH 7.4. Pass through filters with 0.22 μm pores (Millipore) and store at room temperature.
9. Acid washed glass beads (Sigma-Aldrich, USA).
10. Vortex mixer.
11. Cryogen vials (Pierce).
12. Liquid nitrogen.
13. Lipid extruder (LiposoFast-Basic) and polycarbonate membranes with a pore size of 100 nm (Avestin, Mannheim, Germany).
14. Enzymatic colorimetric test for determination of lipids containing choline headgroups (Wako LabAssay™ Phospholipid; Wako Pure Chemical Industries, Ltd.).

2.2. Liposome Capture on the L1 Sensor Chip

1. Instruments Biacore X or Biacore T100 (Biacore, GE Healthcare).
2. L1 sensor chip (Biacore, GE Healthcare).
3. 50 mL self-standing centrifuge tubes (Corning Life Sciences, the Netherlands).
4. Compressed air spray (Dust Off; Teslanol AG, Germany).
5. 100 mM NaOH. Pass through 0.22 μm pores filter and store at room temperature.
6. Bovine serum albumin (BSA) (Sigma-Aldrich). Prepare 5 mg/mL solution in water, store at –20°C before use. Prepare 0.1 mg/mL solution in vesicles buffer just prior to the injection.

2.3. Liposome Capture on the SA Sensor Chip

1. SA sensor chip (Biacore, GE Healthcare).
2. 1,2-Dioleoyl-*sn*-glycero-3-phosphoethanolamine-*N*-(Cap Biotinyl) (biotin-DOPE) (Avanti Polar Lipids) as powder. It should be stored under nitrogen atmosphere at –80°C.
3. 1 M NaCl in 50 mM NaOH.
4. 0.5% SDS (m:v) (Merck KGaA, Germany). Pass through filter with 0.22 μm pores and store at room temperature.

2.4. Regeneration of Sensor Chips

1. Regeneration solution: 50 mM NaOH:isopropanol (Kemika, Zagreb) 2:3 (v:v). Pass through filter with 0.22 μm pores and store at room temperature.
2. 20 mM CHAPS (Sigma-Aldrich, USA).
3. 40 mM *N*-octyl-β-D-glucopyranoside (Sigma-Aldrich, USA).

3. Methods

The capture approaches described below are used with Biacore sensor chips and equipment. All the mentioned procedures, e.g. *Dock*, *Prime*, *Continue*, *Desorb*, are not explained in detail here; the user should refer to application manuals for a particular Biacore instrument (Biacore X or Biacore T100). **Figure 13.1**

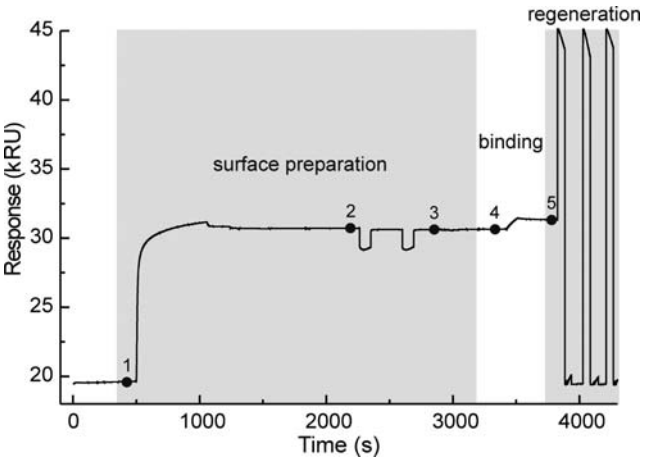

Fig. 13.1. A typical cycle in a protein–membrane interaction experiment. The three parts of the cycle are surface preparation, actual binding experiment and regeneration. Surface preparation (*1–3*) includes deposition of liposomes at a low flow rate of 1–2 μL/min (*1*), conditioning of the surface by two consecutive 1 min injections of 100 mM NaOH at a flow rate of 10 μL/min (*2*) and checking of the surface by binding of 0.1 mg/mL BSA for 1 min at 10 μL/min (*3*). BSA is used to assess the degree of exposure of lipophilic groups on the sensor chip. In this case no BSA is bound, indicating saturation of the surface with liposomes. The protein of interest is injected over the so-prepared surface (*4*). An example of binding of equinatoxin, a pore-forming toxin from sea anemones, is presented. Regeneration (*5*): sometimes the protein binds stably to the lipid membrane and cannot be removed after the binding experiment from the chip by regeneration with some of the commonly used solutions, such as buffers with high salt concentration, low pH or high pH. In that case the liposomes surface cannot be used anymore and should be regenerated by one of the regeneration solutions containing detergents or organic solvents. Usually, three consecutive 1 min injections of 50 mM NaOH:isopropanol 2:3 at a flow rate of 10 μL/min should suffice (*5*).

presents an overview of a typical experiment performed to study protein–membrane interactions. It is composed of three parts: preparation of the surface, binding experiment and regeneration of the surface. The protocols below cover the first and last steps, which have a general character. How an actual binding experiment is performed depends on the protein of interest.

3.1. Liposome Preparation

1. Equilibrate lipids, e.g. DOPC, at room temperature (approximately 22°C). Weigh a few milligrams into the small glass vials with screw cap and Teflon cap-liner. Add chloroform to reach a final 100 mg/mL concentration. Screw tightly and additionally wrap the cap with parafilm. Store at –20°C before use.
2. Pipette approximately 5 mg of DOPC dissolved in chloroform to a round-bottom glass flask. Prepare a thin lipid film by a rotary evaporator. Dry under vacuum for at least 3 h to remove all traces of chloroform. Add 1 mL of vesicles buffer to the lipid film, together with small amount of glass beads. Vortex vigorously for 1 min or until the entire lipid is removed from the walls. Remove the lipid suspension from the glass flask, put in a cryogen vial and freeze–thaw six times in liquid nitrogen. The resulting multi-lamellar vesicles are converted to large unilamellar vesicles (LUVs) by extrusion through 100 nm polycarbonate membranes (*see* **Note 1**) (13). Usually, 30 passages through the membrane should suffice. Generated LUVs have a well-defined and narrow distribution of size with average of approximately 100 nm.
3. Determine the concentration of lipids by an enzymatic colorimetric test according to the instructions of the producer (*see* **Note 2**). Store vesicles at 4°C immediately after preparation and use within 2 days.

3.2. Liposome Capture on the L1 Sensor Chip

1. Equilibrate an L1 sensor chip at room temperature (approximately 22°C) for 30 min. If you are using a new chip, open the protective pouch by scissors. If you are using a previously used chip, take the polystyrene support with the mounted chip out from the 50 mL centrifuge tube in which it was stored. If the chip was fully immersed in the buffer, gently wipe it with paper tissue. Do not touch the glass from either side. Blow away the remaining buffer with compressed air (*see* **Note 3**). Put the chip in protective sheath.
2. Degas the vesicles buffer, if you work with Biacore X apparatus. Stop the *Continue* mode of the instrument. Set the temperature of the instrument to 25°C. Insert the sensor chip with the *Dock* procedure. Perform the *Prime* procedure with vesicles buffer for at least two times. Start new sensorgram. Set the flow rate to 10 μL/min over all flow cells.

3. Clean the sensor chip with three 1 min injections of regeneration solution at the same flow rate (*see* **Section 3.4** below). Wait till the baseline stabilizes (*see* **Note 4**).
4. Change the flow rate to 1 or 2 μL/min. Inject the liposome solution at a final 1 mM lipid concentration for 10 min over all flow cells (*see* **Notes 5** and **6**). Repeat injection, if the level of the immobilized lipids is not enough (*see* **Note 7**).
5. Change the flow rate to 150 μL/min for at least 2 min. Change the flow rate to 10 μL/min. Inject twice 100 mM NaOH for 1 min. Wait till the baseline stabilizes. Inject 0.1 mg/mL BSA for 1 min (*see* **Note 8**).
6. Perform your binding experiment (*see* **Note 9**).

3.3. Liposome Capture on the SA Sensor Chip

1. The liposome preparation is in principle the same as described in **Section 3.1**, only a small amount of the biotinylated lipid should be included in order to allow capture by the SA sensor chip. Add 0.1% of biotin-DOPE (by mole) to DOPC dissolved in chloroform. The rest of the liposome preparation is the same as described in **Section 3.1**.
2. Equilibrate the sensor chip at room temperature and prepare the instrument as described in **Section 3.2**. Set the flow rate to 10 μL/min over both flow cells.
3. Condition the chip with three consecutive 1 min injections of 1 M NaCl in 50 mM NaOH.
4. Change the flow rate to 1 or 2 μL/min. Inject diluted liposome solution at a final 1 mM lipid concentration for 10 min over both flow cells. Repeat injection, if the level of the immobilized lipids is not enough.
5. Change the flow rate to 150 μL/min for 2–5 min. Change the flow rate to 10 μL/min.
6. Perform your binding experiment.
7. Set flow rate to 10 μL/min. Regenerate with consecutive 1 min injections of 0.5% SDS until the response level drops to the value at the beginning of the experiment (*see* **Note 10**).
8. Finish the experiment as explained in point 2 of **Section 3.4**.

3.4. Regeneration of Sensor Chips

1. This procedure cleans the surface of L1 sensor chip. One should use it prior to injection of liposomes, when chip is docked in the instrument to start with the new experiment or after the binding experiment for the preparation of fresh liposome-covered surface. Set flow rate to 10 μL/min. Regenerate with three 1 min injections of regeneration solution at the same flow rate (*see* **Notes 11** and **12**).

2. Stop the sensorgram and remove the chip from the machine with the *Undock* procedure. Take the chip from the protective sheath and store it in the 50 mL centrifuge tube at 4°C (*see* **Note 13)**. Insert the Biacore Maintenance chip, perform the *Prime* procedure two times with water and perform the *Desorb* procedure according to the instructions (*see* **Note 14**). Leave the instrument in the *Continue* mode.

4. Notes

1. Liposomes of composition or size different from the one specified here may be used with the L1 sensor chip. Small unilamellar vesicles may be prepared by sonication of multilamellar vesicles (14). It is also possible to use L1 sensor chips to deposit cell membrane preparations, e.g. red blood cell ghosts, plasma membrane remnants, synaptosomes (15).
2. The concentration of the phospholipids can be measured also by other methods, e.g. according to Bartlett (16).
3. Prevent contaminating either sides of the glass slide of the chip by dust particles. Keep the sensor chip support fully inserted into the sheath at all times.
4. It is very important to use solutions and equipment as clean as possible. Liposomes represent very hydrophobic surfaces into which hydrophobic impurities from the buffer will partition. Use only water of high purity, i.e. MilliQ water, and thoroughly cleaned and washed glassware. Extra care should be taken that no traces of detergents, used for example in washing procedures, are present. As a guide, a baseline drift of 0.3 response units (RU) per min is acceptable (17).
5. Approximately 10,000 RU should be deposited under these conditions. The amount of captured liposomes depends on the concentration of lipids injected over the sensor chip (9).
6. The amount of the liposomes deposited on the sensor chip depends on the assay developed by the user. It is advisable to perform a test for the binding of protein to lipophilic groups on the sensor chip, i.e. in the absence of liposomes. If binding of the studied protein is negligible, then an

empty flow cell, i.e. flow cell 1, can be used as a reference to account for changes in the refractive index due to bulk effects. But if binding of protein to lipophilic groups of the sensor chip is significant, then other ways of referencing should be used. In such cases the user should aim to cover completely the sensor chip with liposomes.

7. Liposomes that contain negatively charged lipids, such as phosphatidylglycerol or phosphatidylserine, contain a net excess of negative charge. It will, therefore, not be possible to fully cover the sensor chip due to electrostatic repulsion between the vesicles (9). The binding may be improved by including a higher concentration of NaCl in the running buffer. Avoid using buffers with a low salt content.
8. BSA is used as an indicator that gives information about the extent of coverage of the chip with liposomes. At full coverage of the sensor chip with liposomes no binding of BSA should be observed (7, 9). If the surface is not fully covered by liposomes, BSA will bind to exposed lipophilic groups on the sensor chip, since it has great affinity for alkyl chains. In this way BSA will prevent non-specific binding of the protein to the lipophilic groups on the chip. However, for detailed kinetic analysis this may not be the most optimal approach, as BSA dissociates slowly from the lipophilic groups and one needs to account for that in the kinetic models used for the description of the binding.
9. It is not explained here how to perform the actual binding experiment, as this largely depends on the nature of the protein and the information you wish to obtain. Many binding cycles may be performed on surfaces prepared in this way, if the protein binds to lipid membranes reversibly or if it is possible to remove the protein from the surface of the liposomes with regeneration solutions that do not contain detergents or organic solvents, which may damage or disintegrate the liposomes. The removal of the protein may be accomplished with high-concentration salt solution (2 M NaCl), low pH (glycine pH 2–3) or high pH (100 mM NaOH). Sometimes proteins will bind very strongly and it will be impossible to remove them from the surface of liposomes by these solutions. In this case, the sensor chip surface should be regenerated by a solution containing detergents or organic solvents and a new liposome-covered surface should be prepared for each cycle (*see* **Fig. 13.1**).

10. The treatment with SDS will remove lipids with bound protein, but not biotinylated lipid. As a consequence less and less liposomes can be immobilized and finally the chip cannot be used any more.
11. Regeneration of the sensor chip L1 can be performed by detergents or organic solvents. This will remove any liposomes or other hydrophobic substances attached to lipophilic groups of the sensor chip. We have found that the most efficient regeneration is achieved by the regeneration solution specified in this protocol (50 mM NaOH:isopropanol 2:3); however, if used extensively it may damage the microfluidic cell of the instrument. We found equally effective solutions of 50 mM HCl:isopropanol 2:3 or 40 mM *N*-octyl-β-D-glucopyranoside in water. Some researchers also use 0.5% SDS or 20 mM CHAPS (3-[(3-cholamidopropyl)dimethylammonio]-1-propanesulfonate) in water for regeneration, but we found them less effective (*see* **Fig. 13.2**).

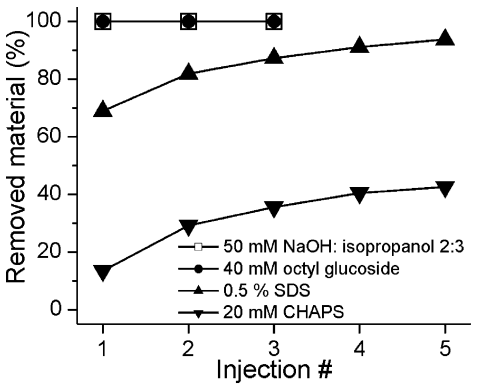

Fig. 13.2. Efficiency of some of the most commonly used regeneration solutions in removing DOPC liposomes from an L1 sensor chip. DOPC liposomes were immobilized to approximately 10,000 RU to the surface of an L1 sensor chip. Various regeneration solutions, as specified in the figure, were then injected for 1 min to desorb liposomes from the surface of the chip. The signal of remaining material on the surface of the sensor chip was determined after each injection and percentage of removed material calculated.

12. Regeneration solutions described in **Note 11** will remove mostly the lipid material from the surface of the sensor chip. If the response level after regeneration does not drop to the initial value this implies that the proteins are irreversibly attached to the lipophilic groups on the chip. Additional treatment with Pronase may further remove the

bound material. Take the sensor chip support from the protective sheath and place it in the 50 mL centrifuge tube filled with 1 mg/mL Pronase (Protease, type XIV from *Streptomyces griseus*; P5147, Sigma) in 20 mM NaH_2PO_4, 150 mM NaCl, pH 7.2 (18). Leave for 1 h at room temperature. Take the support from the tube, rinse it well with distilled water and remove excess water as explained in **Section 3.2**. Put the support with the sensor chip in the protective sheath, place it in the instrument and check the response level.

13. L1 and SA sensor chips may be stored in 50 mL centrifuge tubes for longer periods. The sensor chip support is removed from the protective sheath and placed in a 50 mL centrifuge tube filled with running buffer. This method of storage is equally effective if only 5 mL of the running buffer is put at the bottom of the tube (*see* **Fig. 13.3**).
14. It is important to perform the *Desorb* procedure regularly, when working with hydrophobic lipids and proteins. We perform it at the end of each day of experimentation.

Fig. 13.3. Long-term storage of Biacore sensor chips. Chips may be stored for longer periods of time (months) at 4°C in 50 mL centrifuge tubes as shown. Tubes may be filled to the top with the preferred buffer (*right*). However, it is also possible to store chips in tubes filled with only a few millilitres of the buffer (*left*), which will provide a moist atmosphere.

Acknowledgments

We would like to thank Slovenian Research Agency for support and Mojca Podlesnik Beseničar for critically reading the manuscript.

References

1. Mozsolits, H., and Aguilar, M. I. (2002) Surface plasmon resonance spectroscopy: an emerging tool for the study of peptide-membrane interactions. *Biopolymers* **66**, 3–18.
2. Anderluh, G., Maček, P., and Lakey, J. H. (2003) Peeking into a secret world of pore-forming toxins: membrane binding processes studied by surface plasmon resonance. *Toxicon* **42**, 225–28.
3. Mozsolits, H., Thomas, W. G., and Aguilar, M. I. (2003) Surface plasmon resonance spectroscopy in the study of membrane-mediated cell signalling. *J. Pept. Sci.* **9**, 77–89.
4. Beseničar, M., Maček, P., Lakey, J. H., and Anderluh, G. (2006) Surface plasmon resonance in protein-membrane interactions. *Chem. Phys. Lipids* **141**, 169–78.
5. Cooper, M. A., Try, A. C., Carroll, J., Ellar, D. J., and Williams, D. H. (1998) Surface plasmon resonance analysis at a supported lipid monolayer. *Biochim. Biophys. Acta* **1373**, 101–11.
6. Cho, W., Bittova, L., and Stahelin, R. V. (2001) Membrane binding assays for peripheral proteins. *Anal. Biochem.* **296**, 153–61.
7. Cooper, M. A., Hansson, A., Lofas, S., and Williams, D. H. (2000) A vesicle capture sensor chip for kinetic analysis of interactions with membrane-bound receptors. *Anal. Biochem.* **277**, 196–205.
8. Erb, E. M., Chen, X., Allen, S., Roberts, C. J., Tendler, S. J., Davies, M. C., and Forsen, S. (2000) Characterization of the surfaces generated by liposome binding to the modified dextran matrix of a surface plasmon resonance sensor chip. *Anal. Biochem.* **280**, 29–35.
9. Anderluh, G., Beseničar, M., Kladnik, A., Lakey, J. H., and Maček, P. (2005) Properties of nonfused liposomes immobilized on an L1 Biacore chip and their permeabilization by a eukaryotic pore-forming toxin. *Anal. Biochem.* **344**, 43–52.
10. Honing, S., Ricotta, D., Krauss, M., Spate, K., Spolaore, B., Motley, A., Robinson, M., Robinson, C., Haucke, V., and Owen, D. J. (2005) Phosphatidylinositol-(4,5)-bisphosphate regulates sorting signal recognition by the clathrin-associated adaptor complex AP2. *Mol. Cell* **18**, 519–31.
11. Cooper, M. A. (2004) Advances in membrane receptor screening and analysis. *J. Mol. Recognit.* **17**, 286–315.
12. Podlesnik Beseničar, M., Bavdek, A., Kladnik, A., Maček, P., and Anderluh, G. (2008) Kinetics of cholesterol extraction from lipid membranes by methyl-β-cyclodextrin – A surface plasmon resonance approach. *Biochim. Biophys. Acta* **1778**, 175–84.
13. MacDonald, R. C., MacDonald, R. I., Menco, B. P., Takeshita, K., Subbarao, N. K., and Hu, L. R. (1991) Small-volume extrusion apparatus for preparation of large, unilamellar vesicles. *Biochim. Biophys. Acta* **1061**, 297–303.
14. Torchilin, V. and Weissig, V. (Eds.) (2003) *Liposomes A Practical Approach.* Oxford University Press, Oxford, UK.
15. Bakrač, B., Gutiérrez-Aguirre, I., Podlesek, Z., Sonnen, A. F., Gilbert, R. J., Maček, P., Lakey, J. H., and Anderluh, G. (2008) Molecular determinants of sphingomyelin specificity of a eukaryotic pore-forming toxin. *J. Biol. Chem.* **283**, 18665–77.
16. Bartlett, G. R. (1959) Phosphorus assay in column chromatography. *J. Biol. Chem.* **234**, 466–68.
17. Stahelin, R. V., and Cho, W. (2001) Differential roles of ionic, aliphatic, and aromatic residues in membrane-protein interactions: a surface plasmon resonance study on phospholipases A2. *Biochemistry* **40**, 4672–78.
18. Chatelier, R. C., Gengenbach, T. R., Griesser, H. J., Brigham-Burke, M., and O'Shannessy, D. J. (1995) A general method to recondition and reuse BIAcore sensor chips fouled with covalently immobilized protein/peptide. *Anal. Biochem.* **229**, 112–18.

Chapter 14

Surface Plasmon Resonance Spectroscopy for Studying the Membrane Binding of Antimicrobial Peptides

Kristopher Hall and Marie-Isabel Aguilar

Abstract

Surface plasmon resonance (SPR) employs the optical principle of SPR to measure changes in mass on a sensor chip surface in real time. Surface chemistry has been developed which enables the immobilization of lipid bilayers and determination of protein–membrane interactions in real time. Antimicrobial peptides are being increasingly recognized as potential candidate antibacterial drugs in the face of the rapidly emerging bacterial resistance to conventional antibiotics in recent years. However, a precise understanding of the relationship between antimicrobial peptide structure and their cytolytic function in a range of organisms is still lacking. This is a result of the complex nature of the interactions of antimicrobial peptides with the cell membrane, the mechanism of which can vary considerably between different classes of antimicrobial peptides. SPR has recently been applied to the study of biomembrane-based systems which has allowed a real-time analysis of binding affinity and kinetics. This chapter describes an SPR method to study the membrane interactions of melittin, a well-known antimicrobial peptide.

Key words: Antimicrobial peptides, surface plasmon resonance (SPR), biosensor, plasma membrane, lipid vesicle, binding.

1. Introduction

Antimicrobial peptides are ancient weapons that have survived the slow process of evolution. With more than 1,000 characterized to date (an online catalogue can be found at http://aps.unmc.edu/AP/main.php), these peptides show a marked degree of variability, evolving to act against microbial targets, with even a single mutation having a dramatic affect on biological activity. There are many different antimicrobial peptides found in nature providing evidence for their successful role throughout evolution. With society facing a therapeutic crisis in the increasing bacterial resistance to conventional antibiotics,

N.J. de Mol, M.J.E. Fischer (eds.), *Surface Plasmon Resonance*, Methods in Molecular Biology 627,
DOI 10.1007/978-1-60761-670-2_14, © Springer Science+Business Media, LLC 2010

these antimicrobial peptides hold promise as a new generation of antibiotic compounds.

A wide range of antimicrobial peptides act via binding to and subsequent disruption of cell membranes (1). Antimicrobial peptides target the membrane with their cationic amphipathic structure, a mix of positively charged and hydrophobic residues (2–4). It is this net positive charge that facilitates the interaction via electrostatic attraction to the negative charge on the head groups in the microbial membrane surface having predominantly anionic lipids. There are six main structural and physicochemical parameters that modulate antimicrobial peptide activity and specificity: charge, amphipathicity, sequence, size, secondary structure and hydrophobicity. All of these parameters are closely interrelated; an alteration of one of these parameters can result in significant changes to one or more of the others. These characteristics must be further understood if novel peptides with potent directed activity are to be designed.

A number of different mechanisms have been proposed to describe the mode of action of these peptides (4, 5). These models vary from general bilayer disruption following the binding of a critical concentration of peptide, the formation of pores or through the binding with specific lipophilic components of the membrane such as lipopolysaccharides. While the lipid bilayer forms the basis of membranes in all organisms, there are considerable variations in the structure and complexity between eukaryotic and prokaryotic cells. The phospholipid composition varies between strains and growth conditions, and the structure and organization of the cell envelope differ in Gram-positive and Gram-negative bacteria (6–8). Cholesterol is also uniquely present in mammalian cells and functions to help maintain membrane integrity; this also hampers antimicrobial peptides making permeabilization more difficult. These factors may prove useful in drug targeting to facilitate the design of novel antimicrobial peptides that target bacteria, but are not toxic to the host cell.

Irrespective of the molecular details of the lysis mechanism, it is clear that the relative affinity of the peptides for a particular membrane is an important parameter in fully characterizing their membrane-binding properties. Since these models all involve the binding of peptides to the membrane, the determination of the relative affinity of the peptides for a particular target membrane is central to the delineation of the mechanism of action of these peptides. Surface plasmon resonance (SPR)-based biosensors have been developed to allow quantitative analysis of biomolecular-membrane interactions and therefore have a very important role in furthering our understanding of the molecular basis of action of this class of peptides (9–11).

SPR spectroscopy relies on the surface plasmon resonance phenomenon, which allows the real-time measurement of biomolecules binding to biomimetic surfaces without the

application of a specific label as the SPR method is dependent on the change in adsorbed mass at the sensor surface. It is a surface-sensitive technique where the ligand is immobilized onto a solid support and the solute is in solution and the binding event can be readily detected and analysed.

A typical SPR system consists of an SPR detector, light source, flow channel and sensor surface, comprising a conducting surface such as gold or silver. P-polarized light is emitted by the light source and reflected on the gold-coated sensor surface and detected by the diode array detector. The SPR phenomenon causes a change in the intensity of reflected light at a specific angle and the SPR detector detects these changes in optical properties at the sensor surface following adsorption and desorption of a solute bound to the sensor surface. The change in optical properties depends on a number of factors including the thickness of the gold surface, the wavelength of the light and most importantly on the adsorbed mass on the sensor surface.

The technique can also be fully automated using the commercially available SPR instruments such as the Biacore instruments and large numbers of samples can be rapidly and conveniently analysed (12, 13). Typically, in the Biacore system ligands are immobilized on the surface of a sensor chip, which is covered by a thin gold layer. When the analyte is injected over the surface in a continuous flow, it adsorbs onto the immobilized ligand and so changes the incidence angle by modifying the refractive index at the surface of the sensor chip. The resulting sensorgram is a plot of the change in SPR incidence angle against time, which allows the binding event between the analyte and the ligand to be visualized as shown in **Fig. 14.1** and can be used to gain information

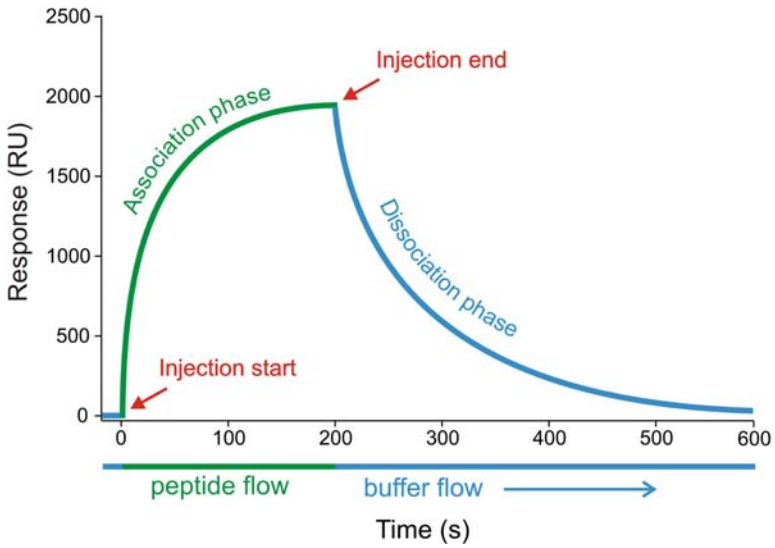

Fig. 14.1. Diagram showing the changes in the SPR response (RU) as a function of time upon immobilizing liposomes on the surface of the sensor chip and binding of proteins on the mimetic membrane, including both the association and dissociation phases.

on the binding kinetics of the interaction. This chapter outlines an SPR method for analysing the membrane interaction of the antimicrobial peptide melittin which has been widely studied by many biophysical methods (2, 14, 15).

2. Materials

2.1. Preparation of Lipid Vesicles

1. Stock solutions of synthetic lipids: dimyristoyl-L-*R*-phosphatidylcholine (DMPC) and dimyristoyl-L-*R*-phosphatidylglycerol (DMPG) (Avanti Polar Lipids, Alabaster, AL) in a chloroform/methanol mixture (1:1, v/v) at 2 mM (*see* **Note 1**).
2. Store all lipid solutions at –20°C.
3. Resuspension buffer: 20 mM sodium phosphate (pH 7.4) containing 150 mM NaCl.
4. Polycarbonate filter membranes with a pore size of 100 nm (Avestin, Ottawa, ON).

2.2. SPR Spectroscopy

1. BIACORE 3000 analytical system (Biacore-GE Healthcare, Uppsala, Sweden).
2. An L1 sensor chip (Biacore-GE Healthcare, Uppsala, Sweden). The L1 sensor chip is composed of dextran modified with lipophilic compounds covalently linked to the thin gold surface (*see* **Fig. 14.2** and **Note 2**).
3. Running buffer: 20 mM sodium phosphate (pH 7.4) containing 150 mM NaCl.
4. Cleaning buffer: 40 mM CHAPS; 2-propanol/50 mM NaOH (4:6, v/v).
5. Regeneration buffer: 10 mM NaOH.
6. Melittin (NH_2-GIGAVLKVLTTGLPALISWIKRKRQQ-NH_2) (Sigma, USA).

3. Methods

3.1. Preparation of Synthetic Lipids

1. Mix stock solutions (2 mM) of synthetic DMPC and DMPG at a ratio of 4:1 to mimic the lipid composition of mammalian membranes (*see* **Note 3**).
2. Dry aliquots (408 μL) of the lipid mixture under a stream of N_2 gas and then further dehydrate in vacuo overnight (*see* **Note 4**).
3. Store the dehydrated lipid samples at –20°C.

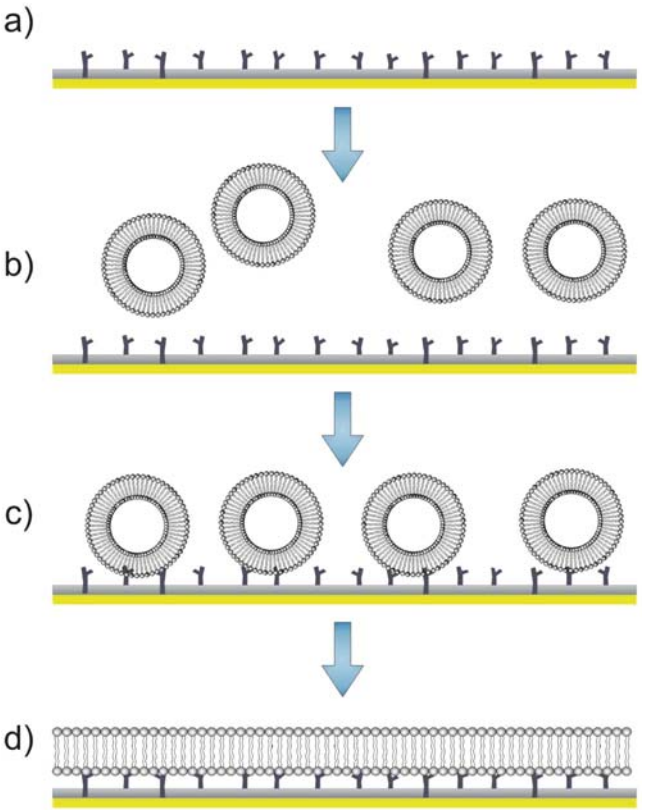

Fig. 14.2. Schematic showing the formation of a phospholipid bilayer on an L1 chip. (**a**) The L1 sensor chip surface before (**b**) liposomes are injected, then (**c**) they are captured on the surface before forming (**d**) a model bilayer (*see* **Note 7**).

3.2. Preparation of Lipid Vesicles

1. Add 600 μL of 20 mM sodium phosphate (pH 7.4) containing 150 mM NaCl to the dried lipids.
2. Sonicate the lipid suspension in a water bath sonicator until the solution becomes clear (*see* **Note 5**).
3. Prepare unilamellar lipid vesicles by extrusion through an Avestin polycarbonate filter membrane with a 100 nm pore size using a LiposoFast extruder (Avestin, Ottawa, ON) 17 times (*see* **Note 6**).

3.3. Determination of Melittin–Membrane Interactions by SPR Spectroscopy

1. Set the operating temperature at 25°C.
2. Freshly prepare, degass and filter all solutions through a 0.22 μm filter.
3. After docking an L1 sensor chip into a Biacore 3000 biosensor according to manufacturer's instructions (Biacore AB, Uppsala, Sweden), condition the chip at room temperature by passing 10 μL of cleaning buffer at 50 μL/min to clean

the surface. Perform the prime procedure (which flushes the instrument fluidic system and chip surface) twice.

4. Immobilize lipid vesicles (100 μL) in running buffer onto the sensor chip surface by passing over the surface at a flow rate of 2 μL/min at room temperature (*see* **Note 7**).
5. Pass the running buffer over the surface for 10 min after the end of injection to allow for equilibration.
6. Apply NaOH (10 μL of 10 mM solution) at a rate of 50 μL/min to remove multilamellar lipids on the sensor chip surface. Successful coating of the chip surface is demonstrated by an increase in the instrument response unit (RU) to approximately 5,000 RU (*see* **Note 8**).
7. Inject a solution of melittin (0.1 μM, 100 μL) in running buffer to the immobilized membrane at 30 μL/min over a period of 200 s (*see* **Note 9**).
8. Replace melittin with the running buffer at the end of injection for a further 10 min and monitor the dissociation of melittin.
9. To remove surface-bound melittin from the membrane surface after dissociation for 10 min, inject NaOH (10 μL of a 10 mM solution) at 50 μL/min (*see* **Note 10**).
10. At the end of the assay, inject 10 μL of cleaning buffer at 50 μL/min to strip the membrane bilayer off the sensor chip (*see* **Note 11**).
11. Repeat steps 1–8 for a series of melittin solutions ranging from 0.1 to 20 μM (*see* sample sensorgrams in **Fig. 14.3**).

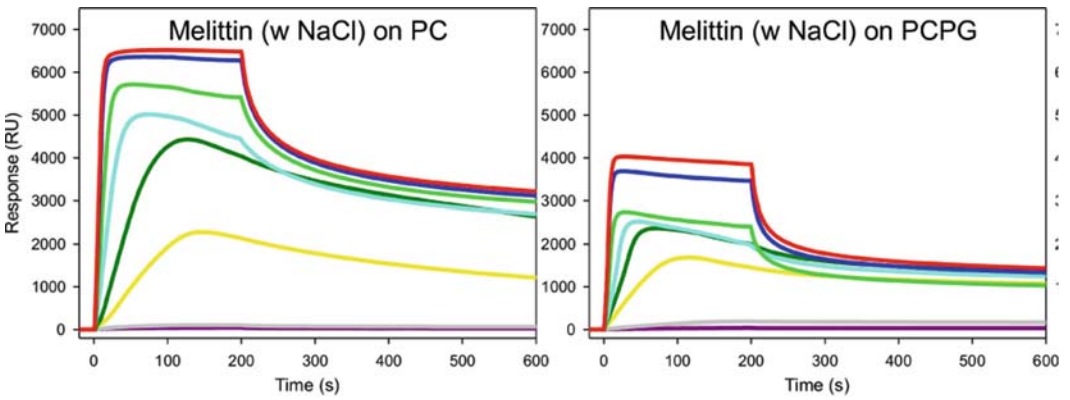

Fig. 14.3. (**a**) Sensorgram showing the binding of melittin to DMPC and DMPC/DMPG (4:0) at concentrations of 0.120 μM. The amount of binding is measured from the change in RU in the sensorgrams. Binding kinetics is determined by fitting the sensorgrams with various numerical models using the BIAevaluation software. The kinetic parameters calculated from the two-state reaction model are listed in **Table 14.1** (*see* **Notes 11, 12, 13** and **14**).

3.4. Data Analysis

1. Determine the binding kinetics by fitting the binding curves to different predefined numerical models according to manufacturer's instructions (10, 16) (*see* **Note 12**).
2. Fit R_{max} locally and the other variables globally by simultaneously fitting the different peptide sensorgrams obtained with four to six different concentrations.
3. Use the simple 1:1 Langmuir binding model first (*see* **Note 13**), followed by the parallel (*see* **Note 14**) and the two-state binding models (*see* **Note 15**), both of which describe more complex binding interactions than the simple 1:1 Langmuir. *See* **Table 14.1** for parameters obtained with the two-state model.

Table 14.1
Results of the curve fitting with melittin fitting the data with a two-state binding model

	Two-state reaction					
	k_{a1} (1/ms)	k_{d1} (1/s)	k_{a2} (1/s)	k_{d2} (1/s)	K (1/M)	χ^2
PC	1.23E+04	7.56E-03	3.06E-03	5.02E-06	9.90E+08	2.91E+04
PC/PG	2.09E+04	1.20E-02	3.07E-03	8.75E-05	6.27E+07	8.25E+03

4. Notes

1. Any mixture of lipids can be prepared with different phospholipids and other components such as sphingomyelin, gangliosides and cholesterol.
2. There are two different chips commercially available from Biacore which allow the study of immobilized membrane systems, namely the HPA and the L1 chips. The HPA chip consists of self-assembled alkanethiol molecules covalently attached to the gold surface of the chip and can be used to prepare hybrid bilayer lipid membranes by the fusion of liposomes onto the hydrophobic surface (10, 17). One consequence of the covalent attachment of the supported hybrid bilayer membrane (HBM) with the HPA chip is the restricted insertion of integral peptides and proteins into the HBM. Thus in order to provide a more appropriate experimental model for the characterization of

these interactions, the vesicle capture (L1) sensor chip was introduced to more closely mimic the fluid bilayer structure of the cell membrane and further improve the ease of preparation of model membrane systems for analysis by SPR (10, 17). The L1 sensor chip is composed of a thin dextran matrix modified by lipophilic compounds on a gold surface where the lipid bilayer system can be prepared by the capture of liposomes as shown in **Fig. 14.2**. The immobilization of the biomimetic lipid surface onto the sensor chip is generally a fast and reproducible process and there are a rapidly increasing number of examples of the use of this membrane surface in a wide range of biological applications. Both the HPA and L1 sensor chips can be conveniently applied to the study of membrane-based biomolecular interactions and to measure the binding affinity related to these interactions.

3. Microbial membranes can be mimicked by the use of dimyristoyl-L-*R*-phosphatidylethanolamine in place of dimyristoyl-L-*R*-phosphatidylcholine.
4. By drying the lipids, a uniform lipid film adhering to the glass is created that can form lipid vesicles upon hydration.
5. To facilitate hydration of the lipids, it is necessary to let the water bath sonicator heat up gradually to beyond the transition temperature of the lipids (usually 40–50°C produces good hydration).
6. Multilamellar lipid micelles can be disrupted by the extrusion procedure. Empirically 17 times of extrusion produces a satisfactory uniformity of the resulting lipid vesicles. It is necessary to extrude lipids at a temperature higher than the transition temperature. Therefore, if the resistance is too high, extrude in a water bath at 40–50°C.
7. After the chip has been coated with lipids, an increase of 5,000–7,000 RU is expected, indicating complete coverage of the chip by the lipid bilayer. In case the coverage is not satisfactory, a second injection of lipid vesicles is needed. It is not known whether the captured lipid vesicles fuse and form a homogeneous lipid bilayer on the chip surface, or intact liposomes are stably retained after injection and stay as separate liposomes on the chip surface.
8. The NaCl treats the membrane bilayer for further binding studies without damaging the immobilized membrane bilayer.
9. Selection of the most appropriate flow rate is a balance between minimizing sample use (requiring lower flow rates) and minimizing mass transfer (requiring higher flow rates). The binding of an analyte to a target ligand on a

sensor chip surface is a two-step process of mass transfer from the bulk solution, which is dependent on convection and diffusion, followed by the specific, high-affinity interaction between the binding partners. It is important that the rate of mass transfer from the bulk solution to the surface and vice versa be the same to avoid mass transfer influencing the specific interaction that is being studied. To determine whether there is a limitation of mass transfer to or from the surface in peptide–membrane interactions, peptides at the same concentration are injected over the lipid surfaces at five different flow rates. For example, after the preparation of the model lipid membranes, the flow rate is adjusted to 2, 5, 15, 30 and 50 μL/min, the same concentration of peptide is injected over the lipid surface for 100 s and the peptide–lipid complex is then allowed to dissociate for 700 s (as shown in **Fig. 14.4** for melittin). Because the interaction between a peptide and membrane depends only on the rates of the interaction and because mass transfer events are influenced by the flow rate, if the initial binding rate (k_a) does not vary notably with the variation of the flow rate, then the peptide–membrane interactions are not mass transfer limited (as shown in **Fig. 14.4**) (13).

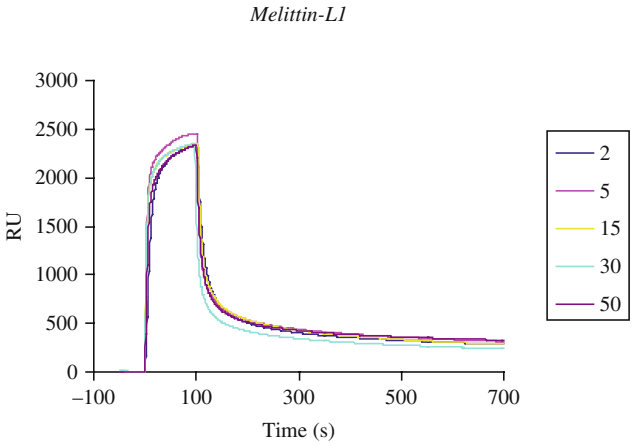

Fig. 14.4. Variation of flow rate to determine whether melittin binding to the membrane is mass transfer limited. Melittin (10 μM) was injected over the DMPC bilayer at five different flow rates ranging from 2 to 50 μL/min.

10. This treatment will remove peptide that is bound electrostatically to the surface of the bilayer and is a useful test to determine the relative contribution of this interaction to the overall binding mechanism. However, for most cytolytic peptides, very little peptide is removed at this step.
11. After the cleaning procedure, the baseline is expected to return to the RU level observed before the binding assay.

Other cleaning reagents can be used in combination with those mentioned in Section **3**), such as 6 M guanidine–HCl, 0.1 M acetic acid and 0.2% SDS.

12. Both the association and dissociation phases of the binding curves of melittin at different concentrations can be fitted to a number of predefined numerical models, such as 1:1 Langmuir binding, parallel reactions and a two-state reaction model, using the BIAevaluation software. Detailed interpretation of these numerical binding models can be found elsewhere (10, 16). Binding kinetics are calculated from the model providing the best fit (lowest chi^2 (χ^2)).
13. The 1:1 Langmuir model implies that the peptide (P) simply binds to the lipid layer (L) and/or inserts into the lipid surface, with no other interactions involved. During the binding process, the association (k_a) and the dissociation (k_d) rate constants determine the formation and breakdown of the complex (PL) at the sensor surface as shown in **Eq. [1]**:

$$\mathrm{P} + \mathrm{L} \underset{k_d}{\overset{k_a}{\rightleftharpoons}} \mathrm{PL} \qquad [1]$$

14. The parallel reaction model suggests that two simple bimolecular interactions occur in parallel with different rate constants, giving a complex bimolecular interaction. One step corresponds to the initial binding of the peptide onto the membrane surface. In the second step (which follows the first step) an incoming peptide has two different regions of the membrane surface to interact with: either (1) the continuous membrane or (2) a region altered by low concentrations of the previously bound peptide, thus
    (1) Peptide P binds to lipid layer (L_1):

$$\mathrm{P} + \mathrm{L}_1 \underset{k_{d1}}{\overset{k_{a1}}{\rightleftharpoons}} \mathrm{PL}_1 \qquad [2]$$

    (2) The bound peptide–membrane complex (PL_1) then acts as a new surface (L_2) for the binding of additional peptide molecules:

$$\mathrm{P} + \mathrm{L}_2 \underset{k_{d2}}{\overset{k_{a2}}{\rightleftharpoons}} \mathrm{PL}_2 \qquad [3]$$

15. Two-state binding model describes two reaction steps, which in terms of peptide–lipid interaction may correspond to the peptide (P) binding to the lipid (L) to form a complex (PL); the complex then undergoes a conformational

change (PL*) or insertion into the membrane surface as follows:

$$P + L \underset{k_{d1}}{\overset{k_{a1}}{\rightleftharpoons}} PL \underset{k_{d2}}{\overset{k_{a2}}{\rightleftharpoons}} PL^* \quad [4]$$

References

1. Bessalle, R., Kapitkovsky, A., Gorea, A., Shalit, I., and Fridkin, M. (1990) All-D-magainin: chirality, antimicrobial activity and proteolytic resistance. *FEBS Lett.* **274**, 151–55.
2. Dempsey, C. E. (1990) The actions of melittin on membranes. *Biochim. Biophys. Acta* **1031**, 143–61.
3. Matsuzaki, K. (1998) Magainins as paradigm for the mode of action of pore forming polypeptides. *Biochim. Biophys. Acta* **1376**, 391–400.
4. Shai, Y. (1999) Mechanism of the binding, insertion and destabilization of phospholipid bilayer membranes by alpha-helical antimicrobial and cell non-selective membrane-lytic peptides. *Biochim. Biophys. Acta* **1462**, 55–70.
5. Zasloff, M. (2002) Antimicrobial peptides of multicellular organisms. *Nature* **415**, 389–95.
6. Blondelle, S. E., Lohner, K., and Aguilar, M. (1999) Lipid-induced conformation and lipid-binding properties of cytolytic and antimicrobial peptides: determination and biological specificity. *Biochim. Biophys. Acta* **1462**, 89–108.
7. Matsuzaki, K., Sugishita, K., Fujii, N., and Miyajima, K. (1995) Molecular basis for membrane selectivity of an antimicrobial peptide, magainin 2. *Biochemistry* **34**, 3423–29.
8. Vaara, M. (1992) Agents that increase the permeability of the outer membrane. *Microbiol Rev.* **56**, 395–411.
9. Mozsolits, H., and Aguilar, M. I. (2002) Surface plasmon resonance spectroscopy: an emerging tool for the study of peptide-membrane interactions. *Biopolymers* **66**, 3–18.
10. Mozsolits, H., Wirth, H. J., Werkmeister, J., and Aguilar, M. I. (2001) Analysis of antimicrobial peptide interactions with hybrid bilayer membrane systems using surface plasmon resonance. *Biochim. Biophys. Acta* **1512**, 64–76.
11. Papo, N., and Shai, Y. (2003) Exploring peptide membrane interaction using surface plasmon resonance: differentiation between pore formation versus membrane disruption by lytic peptides. *Biochemistry* **42**, 458–66.
12. Cooper, M. A. (2002) Optical biosensors in drug discovery. *Nat. Rev. Drug Discov.* **1**, 515–28.
13. Karlsson, R., and Falt, A. (1997) Experimental design for kinetic analysis of protein–protein interactions with surface plasmon resonance biosensors. *J. Immunol. Methods* **200**, 121–33.
14. Bechinger, B. (1999) The structure, dynamics and orientation of antimicrobial peptides in membranes by multidimensional solid-state NMR spectroscopy. *Biochim. Biophys. Acta* **1462**, 157–83.
15. Raghuraman, H., and Chattopadhyay, A. (2007) Melittin: a membrane-active peptide with diverse functions. *Biosci. Rep.* **27**, 189–223.
16. BIAtechnology_handbook3-2.
17. Cooper, M. A., Hansson, A., Lofas, S., and Williams, D. H. (2000) A vesicle capture sensor chip for kinetic analysis of interactions with membrane-bound receptors. *Anal. Biochem.* **277**, 196–205.

Chapter 15

Surface Plasmon Resonance Spectroscopy in Determination of the Interactions Between Amyloid β Proteins (Aβ) and Lipid Membranes

Xu Hou, David H. Small, and Marie-Isabel Aguilar

Abstract

Surface plasmon resonance (SPR) spectroscopy is emerging as a useful tool for determination of molecular interactions in real time. Studies on the molecular pathogenesis of amyloidoses have shown that the plasma membrane plays an important role in amyloidogenesis and cytotoxicity induced by amyloidogenic proteins. By immobilizing lipid bilayers on a sensor chip surface, SPR spectroscopy has been employed to examine the binding of amyloidogenic proteins, such as amyloid β protein (Aβ), to a variety of lipid membranes, and it provided new insights into the molecular interactions between these amyloidogenic proteins and membranes. In this chapter, we describe the application of SPR spectroscopy to the determination of the binding of Aβ to lipid membranes.

Key words: Surface plasmon resonance (SPR), amyloid, transthyretin (TTR), amyloid β protein (Aβ), lipid, membrane.

1. Introduction

In the last decade, many studies have shown that binding to the lipids of the plasma membrane may play an important role in the amyloidogenesis of amyloidogenic proteins (1–6) and the induction of cytotoxicity by these proteins (7–10). Membrane lipids may provide a favourable local environment which facilitates misfolding and aggregation of amyloidogenic proteins (1, 5, 11–13). Membrane binding of amyloidogenic proteins can compromise cellular viability by triggering dysregulation of intracellular Ca^{2+} concentration (14, 15). Amyloidogenesis and cytotoxicity of amyloidogenic proteins can be modulated by the composition of the lipid membrane to which they bind (1, 7, 10, 16, 17).

N.J. de Mol, M.J.E. Fischer (eds.), *Surface Plasmon Resonance*, Methods in Molecular Biology 627,
DOI 10.1007/978-1-60761-670-2_15, © Springer Science+Business Media, LLC 2010

Therefore, characterization of membrane binding of amyloidogenic proteins bears enormous significance in the elucidation of the molecular pathogenesis of amyloidoses and identification of therapeutic reagents that inhibit amyloidoses-associated cytotoxicity via modulating membrane binding of amyloidogenic proteins. Surface plasmon resonance (SPR) spectroscopy has emerged as a useful tool for determination of the interactions between amyloidogenic proteins and lipid membranes (18).

Surface plasmon resonance (SPR) spectroscopy measures biomolecular interactions on biomimetic surfaces in real time by the principle of SPR (19). Under the condition of total internal reflection, when a polarized laser light is directed through a medium with high refractive index (often a prism) to a thin layer of certain metals (e.g. gold) that lies on the border with a medium of low refractive index, a fraction of the light energy can penetrate the metal layer and excite electromagnetic waves (surface plasmons) that propagate within the metal surface at the interface with the sample solution. When the incident light enters at a critical angle, i.e. the SPR angle, SPR occurs in which energy of the incident light can be transferred to plasmons, resulting in a reduction in the intensity of reflected light (20). The SPR angle is dependent on the refractive index within a few hundred nanometres of the surface (19). Using the SPR principle, SPR spectroscopy can examine molecular interactions in real time on a sensor surface by measuring changes in the refractive index of the solution close to the sensor surface, which are induced by binding of molecules onto the surface (21). The invention of SPR spectroscopy makes studying molecular interactions possible without the need for labelling.

In an SPR spectroscopy system (e.g. a Biacore biosensor), polarized light emitted from a light source is reflected on the gold-coated surface of a sensor chip and then detected by a diode array detector (**Fig. 15.1a**). After immobilizing one of the interacting partners (the ligand) onto the surface of a sensor chip, the other partner (the analyte) is injected over the chip surface at a constant flow rate through a microfluidic channel system (22) (**Fig. 15.1a**). Association and dissociation between the ligand molecules and the analyte molecules lead to fluctuations in the intensity of reflected light, thereby changes in mass concentration at the chip surface can be measured in SPR response unit (RU) (**Fig. 15.1b**). There is a linear relationship between the mass concentration at the chip surface and the SPR response such that 1 RU = 1 pg/mm^2 (23). The size of change in SPR response can thus be interpreted in terms of the stoichiometry of the ligand–analyte interaction. The rate of change in SPR response can be used to determine the apparent rate constants for the association and dissociation phases of the interaction, which can be used to calculate the apparent equilibrium constant, a parameter of affinity.

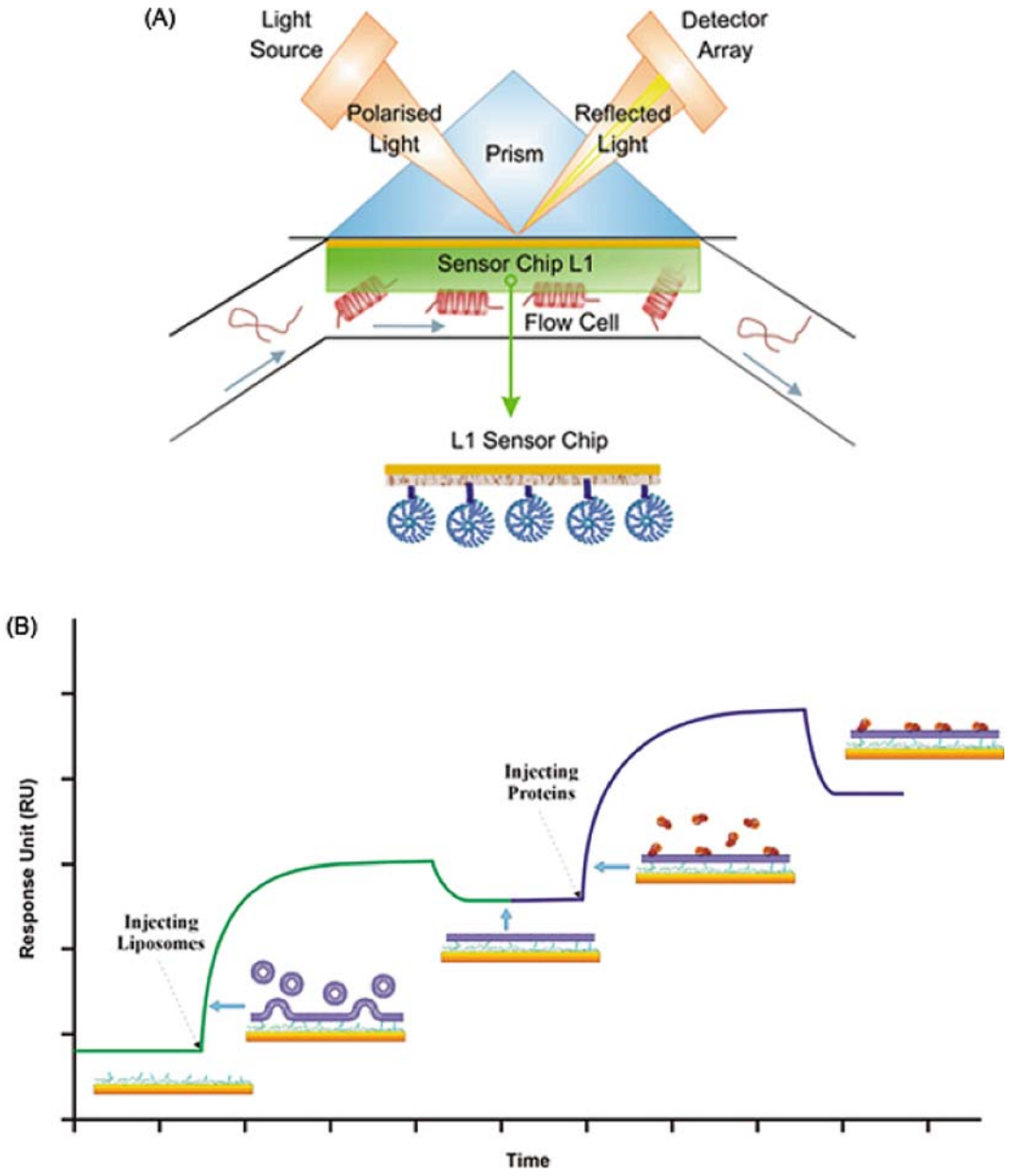

Fig. 15.1. (**a**) Schematic representation of SPR spectroscopy for protein–membrane interactions. The angle of incident light at which SPR occurs is dependent on the refractive index of the solution close to the surface of the sensor chip. Liposomes are immobilized onto an L1 sensor chip by lipophilic anchors attached to a dextran matrix on the chip surface. Protein samples are then injected over the sensor chip surface at a constant flow rate. Variations in mass concentration at the chip surface caused by protein binding are measured in real time by changes in the refractive index of the solution. (**b**) Diagram showing the changes of SPR response (RU) as a function of time upon immobilizing liposomes on the surface of the sensor chip and binding of proteins on the mimetic membrane, including both the association and dissociation phases.

Since the invention of the L1 sensor chip which contains a carboxymethyldextran hydrogel derivatized with lipophilic alkyl chain anchors to capture lipid vesicles (**Fig. 15.1a**) (24), there has been a steady increase in the application of Biacore biosensors in studies on protein-membrane interactions (25–30, *see* also **Chapter 12**, **13**, **14 and 16**), including the interactions between amyloidogenic proteins, such as amyloid β protein (Aβ), prion protein (PrP) and transthyretin (TTR), and membranes (including the plasma membrane and artificial lipid membranes) (1, 3, 9, 10, 18, 31–33). SPR spectroscopy has thus significantly expanded our understanding of the pathogenesis of amyloidosis. In this chapter, we describe the application of SPR spectroscopy for studying the binding of Aβ to the plasma membrane from vascular smooth muscle cells (SMCs) and lipid membranes made from synthetic lipids. Technical considerations related to the assay are also discussed.

2. Materials

2.1. Cell Culture

1. Dulbecco's modified Eagle's medium (DMEM) cell culture medium (Gibco, Mt Waverly, VIC, Australia) supplemented with 10% (v/v) fetal calf serum (Commonwealth Serum Laboratories, Melbourne, VIC, Australia).
2. Penicillin and streptomycin (Sigma-Aldrich, Castle Hill, NSW, Australia) for addition to the cell culture medium at 50 U/mL and 50 μg/mL, respectively.

2.2. Preparation of Plasma Membrane

1. STM buffer: 0.25 M sucrose, 5 mM Tris–HCl (pH at 7.4) and 1 mM $MgCl_2$, made fresh and kept on ice before use.
2. Resuspension buffer: 20 mM sodium phosphate (pH at 7.4), stored at room temperature and kept on ice before use.

2.3. Preparation of Synthetic Lipid Vesicles

1. Stock solutions of synthetic lipids: dimyristoyl-L-*R*- phosphatidylcholine (DMPC), dimyristoyl-L-*R*-phosphatidylglycerol (DMPG), dimyristoyl-L-*R*-phosphatidylserine (DMPS), dimyristoyl-L-*R*-phosphatidylethanolamine (DMPE) and sphingomyelin (SM) (Avanti Polar Lipids, Alabaster, AL, USA) dissolved in a chloroform/methanol mixture (1:1, v/v) at 2 mM. Cholesterol (CL) dissolved in chloroform/methanol (3:1, v/v) at 2 mM. All lipid solutions are stored at –20°C.
2. Resuspension buffer: 20 mM sodium phosphate (pH 6.8).
3. Polycarbonate filter membranes with a pore size of 100 nm (Avestin, Ottawa, ON, Canada).

2.4. SPR Spectroscopy

1. $A\beta_{1-42}$ and $A\beta_{1-40}$ [recombinant (98% purity) RPeptides Inc., Athens, GA, USA].
2. Running buffer: 20 mM sodium phosphate (pH 6.8).
3. Regeneration buffer: 10 mM NaOH.
4. Cleaning buffer: 40 mM CHAPS; 2-propanol/50 mM NaOH (4:6, v/v).

3. Methods

3.1. Preparation of Aβ

1. Dissolve $A\beta_{1-42}$ and $A\beta_{1-40}$ in dimethyl sulphoxide (DMSO) at 2 mM. Sonicate the peptide solutions at 42 kHz for 5 min to facilitate dissolution and then centrifuge at 6,000*g* at room temperature for 1 min to remove insoluble materials. Store the supernatant fractions at –80°C.
2. To prepare monomeric Aβ, thaw Aβ solutions in DMSO on ice and then dissolve in 20 mM sodium phosphate (pH 6.8) to a concentration of 10 μM immediately prior to use. To prepare aggregated Aβ, incubate Aβ solutions (10 μM in 20 mM sodium phosphate, pH 6.8) in a humidified atmosphere containing 5% CO_2 at 37°C for 7 days, a process known as aging (*see* **Note 1**).

3.2. Preparation of Plasma Membrane

A crude plasma membrane fraction is prepared from cultured vascular SMCs derived from Sprague–Dawley rats by means of differential centrifugation (34).

1. Harvest vascular SMCs by centrifugation at 1,600*g* at 4°C for 3 min. Wash the cell pellet in phosphate-buffered saline and then resuspend 10 mL of STM buffer.
2. Disrupt the cells with a Dounce glass–glass homogenizer (Kontes, Vineland, NJ, USA) for approximately 30 strokes on ice (*see* **Note 2**).
3. Centrifuge the cell lysate at 220*g* at 4°C for 5 min to remove unbroken cells and nuclei. Homogenize the pellet a second time in 5 mL of STM buffer, and centrifuge the suspension again. Combine the supernatant fractions.
4. Further centrifuge the supernatant at 100,000*g* at 4°C for 2 h.
5. Resuspend the resulting crude plasma membrane fraction in the pellet in 20 mM sodium phosphate (pH 7.4). Store the plasma membrane preparation at –80°C.

3.3. Preparation of Lipid Vesicles

1. Stock solutions (2 mM) of synthetic DMPC, DMPE, DMPS, SM and CL are mixed at various ratios. Dry aliquots

(408 μL) of the lipid mixtures under a stream of N_2 gas and then further dehydrate in vacuo overnight. Store the dehydrated lipid samples at –20°C.

2. Add an aqueous solution, 600 μL of 20 mM sodium phosphate (pH 6.8), to the dried lipids. Sonicate the lipid suspension in a water bath sonicator until the solution becomes clear (*see* **Note 3**).
3. Prepare unilamellar lipid vesicles by extrusion through an Avestin polycarbonate filter membrane with a 100 nm pore size using a LiposoFast extruder (Avestin, Ottawa, ON) for 17 times (*see* **Note 4**).

3.4. Determination of Aβ–Membrane Interactions by SPR Spectroscopy

1. Dock an L1 sensor chip into a Biacore 3000 biosensor (GE Healthcare-Biacore AB, Uppsala, Sweden). Condition the chip at room temperature by injecting 10 μL of cleaning buffer at 50 μL/min to clean the surface. Perform the prime procedure, which flushes the instrument fluidic system and chip surface, twice.
2. Immobilize lipid vesicles made from synthetic lipids (100 μL) onto the sensor chip surface by passing over the surface at a flow rate of 2 μL/min at room temperature. Alternatively, immobilize the plasma membrane preparation (100 μL) onto the sensor chip surface in a similar manner (*see* **Note 5**).
3. Pass the running buffer over the surface for 10 min at 2 μL after the end of injection to allow for equilibration.
4. Apply NaOH (10 μL of 10 mM solution) at a rate of 50 μL/min to remove multilamellar lipids on the sensor chip surface. Successful coating of the chip surface is demonstrated by an increase in SPR response (RU) (**Fig. 15.2a**) (*see* **Note 6**).
5. Apply Aβ solution (100 μL, either freshly made or aged) in 20 mM sodium phosphate (pH 6.8) to the immobilized membrane at 30 μL/min over a period of 200 s (*see* **Note 7**). Replace Aβ by the running buffer at the end of injection for a further 10 min to monitor the dissociation of Aβ.
6. To remove residual Aβ from the membrane surface after dissociation for 10 min, inject NaOH (10 μL of a 10 mM solution) at 50 μL/min (*see* **Note 8**).
7. Repeat steps 5 and 6 with a series of Aβ solutions ranging from 0.5 to 10 μM. The amount of Aβ binding is measured by the difference in RU between before Aβ injection and 20 s after removal of Aβ (**Fig. 15.2b**) (*see* **Note 9**).

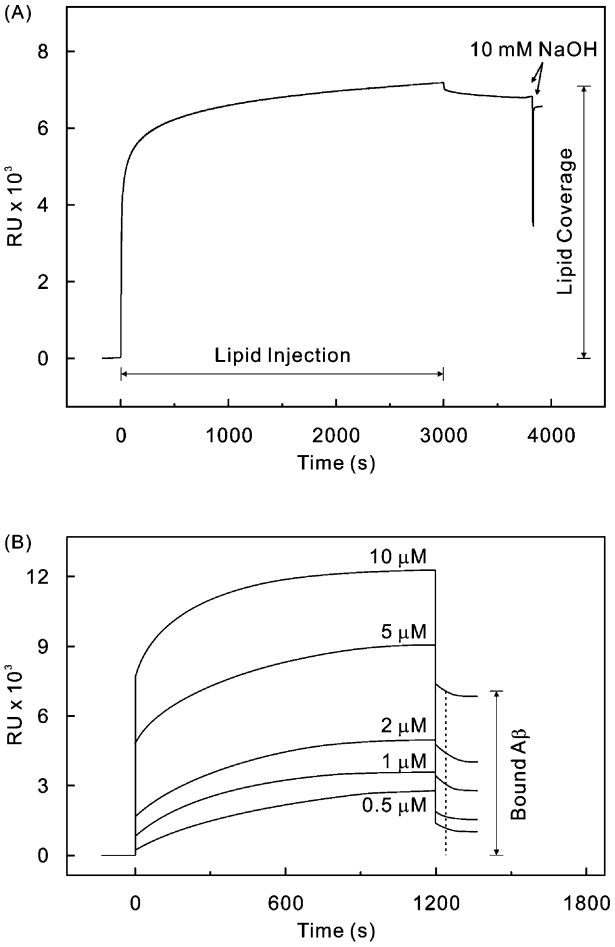

Fig. 15.2. (**a**) Sensogram showing the immobilization of DMPC onto the surface of an L1 sensor chip. (**b**) Sensogram showing the binding of freshly made $A\beta_{1-42}$ solutions (0.5–10 μM) to an immobilized lipid membrane made of synthetic lipids (DMPC:DMPE:DMPS:DMPG:CL at 30:8:1:1:60). The difference between the RU value before Aβ injection and 20 s after removal of Aβ is taken as the amount of Aβ bound to the membrane.

8. At the end of the assay, inject 10 μL of 40 mM CHAPS and 2-propanol/50 mM NaOH (4:6, v/v) at 50 μL/min to strip the membrane bilayer off the sensor chip (*see* **Note 10**).

4. Notes

1. Aging of Aβ has been demonstrated to increase the proportion of aggregated forms of Aβ, such as oligomers and fibrillar structures (35). The presence of irregular and fibrillar

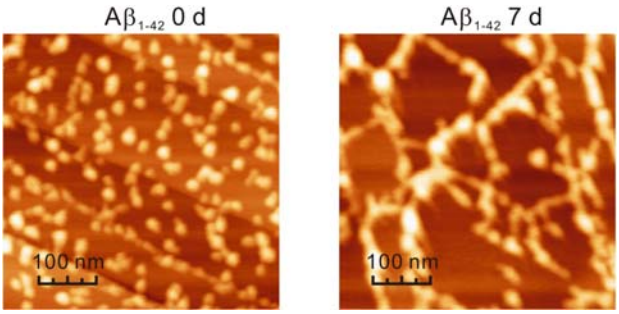

Fig. 15.3. Aggregation of $A\beta_{1-42}$ determined by AFM. $A\beta_{1-42}$ solution is examined on a surface of highly oriented pyrolytic graphite before and after aging for 7 days. Aβ is present predominantly in the form of monomers before aging whereas irregular and fibrillar aggregates are the predominant species after aging for 7 days.

Aβ aggregates after aging can be detected by atomic force microscopy (AFM) (**Fig. 15.3**).

2. Cell lysis can be examined by staining with 0.4% trypan blue. It is critical to keep the cell lysate on ice all the time.
3. To facilitate hydration of the lipids, it is necessary to let the water bath sonicator heat up gradually to beyond the transition temperature of the lipids (usually 40–50°C produces good hydration).
4. Multilamellar lipid micelles can be disrupted by the extrusion procedure. Empirically 17 times of extrusion produces a satisfactory uniformity of the resulting lipid vesicles. It is necessary to extrude lipids at a temperature higher than the transition temperature. Therefore, if the resistance is too high, extrude in a water bath at 40–50°C.
5. The plasma membrane should not be sonicated as sonication may disrupt the structure and integrity of the plasma membrane.
6. After the chip has been coated with lipids, an increase of 5,000–7,000 RU is expected, indicating complete coverage of the chip by the lipid bilayer (24, 36). In case the coverage is not satisfactory, a second injection of lipid vesicles is needed. It is not known whether the captured lipid vesicles fuse and form a homogeneous lipid bilayer on the chip surface (36), or intact liposomes are stably retained after injection and stay as separate liposomes on the chip surface (24, 37).
7. As insoluble materials can clog the fluidic system of the Biacore biosensor, all Aβ solutions are centrifuged at 18,000*g* for 1 min prior to their application on the biosensor

to remove insoluble mature amyloid fibrils. Therefore, although the aged Aβ solutions contain a wide range of aggregates from oligomers to mature amyloid fibrils, SPR spectroscopy actually measures the membrane binding of the soluble forms of Aβ, i.e. monomers and soluble oligomers.

8. This treatment regenerates the membrane bilayer for further binding studies without damaging the immobilized membrane bilayer.
9. Since a significant bulk effect (a rapid increase of signal at the start of Aβ injection and a rapid drop of signal at the end of injection) is observed in the sensorgram, the difference between the RU value before Aβ injection and 20 s after removal of Aβ is taken as the amount of Aβ bound to the membrane. A few alternative ways can be used for analysing the membrane binding of amyloidogenic proteins. R_{eq}, the theoretical amount of binding at equilibrium which can be calculated using the BIAevaluation software (Biacore AB), has been used to determine the amount of binding between amyloidogenic TTR and lipid membranes (9). Scatchard plots of equilibrium binding using R_{eq} have been employed to determine the binding kinetics at equilibrium (1, 9). The rate of association at the steady state of binding (close to the completion of injection in the sensogram) has also been selected to deduce the affinity of PrP binding to lipid membranes (3). Alternatively, when the binding curves have been obtained at a series of protein concentrations under similar conditions, the association and dissociation phases of the binding curves can be fitted to a number of predefined numerical models, such as 1:1 Langmuir binding, bivalent analyte and two-state reaction, using the BIAevaluation software. Detailed interpretation of these numerical binding models can be found elsewhere (28, 38, 39). Binding kinetics are calculated from the best fitted model.
10. After the cleansing procedure, the baseline is expected to return to the level before the binding assay. Other cleansing reagents can be used in combination with those mentioned in Section **3**, such as 6 M guanidine–HCl, 0.1 M acetic acid and 0.2% SDS.

References

1 Hou, X., Mechler, A., Martin, L. L., Aguilar, M. I., and Small, D. H. (2008) Cholesterol and anionic phospholipids increase the binding of amyloidogenic transthyretin to lipid membranes. *Biochim. Biophys. Acta.* **1778**, 198–205.

2 Kakio, A., Nishimoto, S., Kozutsumi, Y., and Matsuzaki, K. (2003) Formation of

a membrane-active form of amyloid beta-protein in raft-like model membranes. *Biochem Biophys. Res. Commun.* **303**, 514–18.
3 Critchley, P., Kazlauskaite, J., Eason, R., and Pinheiro, T. J. (2004) Binding of prion proteins to lipid membranes. *Biochem. Biophys. Res. Commun.* **313**, 559–67.
4 Elfrink, K., Nagel-Steger, L., and Riesner, D. (2007) Interaction of the cellular prion protein with raft-like lipid membranes. *Biol. Chem.* **388**, 79–89.
5 Yip, C. M., Darabie, A. A., and McLaurin, J. (2002) Abeta 42-peptide assembly on lipid bilayers. *J. Mol. Biol.* **318**, 97–107.
6 Zhao, H., Tuominen, E. K., and Kinnunen, P. K. (2004) Formation of amyloid fibers triggered by phosphatidylserine-containing membranes. *Biochemistry* **43**, 10302–07.
7 Yip, C. M., Elton, E. A., Darabie, A. A., Morrison, M. R., and McLaurin, J. (2001) Cholesterol, a modulator of membrane-associated Abeta-fibrillogenesis and neurotoxicity. *J. Mol. Biol.* **311**, 723–34.
8 Rymer, D. L., and Good, T. A. (2000) The role of prion peptide structure and aggregation in toxicity and membrane binding. *J. Neurochem.* **75**, 2536–45.
9 Hou, X., Richardson, S. J., Aguilar, M. I., and Small, D. H. (2005) Binding of amyloidogenic transthyretin to the plasma membrane alters membrane fluidity and induces neurotoxicity. *Biochemistry* **44**, 11618–27.
10 Subasinghe, S., Unabia, S., Barrow, C. J., Mok, S. S., Aguilar, M. I., and Small, D. H. (2003) Cholesterol is necessary both for the toxic effect of Abeta peptides on vascular smooth muscle cells and for Abeta binding to vascular smooth muscle cell membranes. *J. Neurochem.* **84**, 471–79.
11 Gorbenko, G. P., and Kinnunen, P. K. (2006) The role of lipid-protein interactions in amyloid-type protein fibril formation. *Chem. Phys. Lipids* **141**, 72–82.
12 Chauhan, A., Ray, I., and Chauhan, V. P. (2000) Interaction of amyloid beta-protein with anionic phospholipids: possible involvement of Lys28 and C-terminus aliphatic amino acids. *Neurochem. Res.* **25**, 423–29.
13 Morillas, M., Swietnicki, W., Gambetti, P., and Surewicz, W. K. (1999) Membrane environment alters the conformational structure of the recombinant human prion protein. *J. Biol. Chem.* **274**, 36859–65.
14 Hou, X., Aguilar, M. I., and Small, D. H. (2007) Transthyretin and familial amyloidotic polyneuropathy: clues to the molecular mechanism of neurodegeneration in amyloidosis. *FEBS J.* **274**, 1637–50.
15 Demuro, A., Mina, E., Kayed, R., Milton, S. C., Parker, I., and Glabe, C. G. (2005) Calcium dysregulation and membrane disruption as a ubiquitous neurotoxic mechanism of soluble amyloid oligomers. *J. Biol. Chem.* **280**, 17294–300.
16 Kakio, A., Nishimoto, S., Yanagisawa, K., Kozutsumi, Y., and Matsuzaki, K. (2002) Interactions of amyloid beta-protein with various gangliosides in raft-like membranes: importance of GM1 ganglioside-bound form as an endogenous seed for Alzheimer amyloid. *Biochemistry* **41**, 7385–90.
17 Wang, S. S., Rymer, D. L., and Good, T. A. (2001) Reduction in cholesterol and sialic acid content protects cells from the toxic effects of beta-amyloid peptides. *J. Biol. Chem.* **276**, 42027–34.
18 Aguilar, M. I., and Small, D. H. (2005) Surface plasmon resonance for the analysis of beta-amyloid interactions and fibril formation in Alzheimer's disease research. *Neurotox. Res.* **7**, 17–27.
19 Markey, F. (2000) *Principles of Surface Plasmon Resonance* (Nagata, K., and Handa, H. (Eds.)). pp. 13–22, Springer-Verlag, Tokyo.
20 Kretschmann, E. (1971) Die Bestimmung optischer Konstanten von metallen durch Anregung von Oberflachenplasmaschwingungen. *Z. Phys.* **241**, 313–24.
21 Jonsson, U., Fagerstam, L., Ivarsson, B., Johnsson, B., Karlsson, R., Lundh, K., Lofas, S., Persson, B., Roos, H., Ronnberg, I., et al. (1991) Real-time biospecific interaction analysis using surface plasmon resonance and a sensor chip technology. *Biotechniques* **11**, 620–27.
22 Hashimoto, S. (2000) *Principles of BIACORE* (Nagata, K., and Handa, H. (Eds.)). pp. 23–32, Springer-Verlag, Tokyo.
23 Stenberg, E., Persson, B., Roos, H., and Urbaniczky, C. (1990) Quantitative determination of surface concentration of protein with surface plasmon resonance by using radiolabeled proteins. *J. Colloid Interface Sci.* **143**, 513–26.
24 Cooper, M. A., Hansson, A., Lofas, S., and Williams, D. H. (2000) A vesicle capture sensor chip for kinetic analysis of interactions with membrane-bound receptors. *Anal. Biochem.* **277**, 196–205.
25 Plant, A. L., Brigham-Burke, M., Petrella, E. C., and O'Shannessy, D. J. (1995) Phospholipid/alkanethiol bilayers for cell-surface receptor studies by surface plasmon resonance. *Anal. Biochem.* **226**, 342–48.
26 Besenicar, M., Macek, P., Lakey, J. H., and Anderluh, G. (2006) Surface plasmon

resonance in protein-membrane interactions. *Chem. Phys. Lipids* **141**, 169–78.
27 McDonnell, J. M. (2001) Surface plasmon resonance: towards an understanding of the mechanisms of biological molecular recognition. *Curr. Opin. Chem. Biol.* **5**, 572–77.
28 Mozsolits, H., and Aguilar, M. I. (2002) Surface plasmon resonance spectroscopy: an emerging tool for the study of peptide-membrane interactions. *Biopolymers* **66**, 3–18.
29 Cooper, M. A. (2004) Advances in membrane receptor screening and analysis. *J. Mol. Recognit.* **17**, 286–315.
30 Mozsolits, H., Thomas, W. G., and Aguilar, M. I. (2003) Surface plasmon resonance spectroscopy in the study of membrane-mediated cell signalling. *J. Pept. Sci.* **9**, 77–89.
31 Ariga, T., Kobayashi, K., Hasegawa, A., Kiso, M., Ishida, H., and Miyatake, T. (2001) Characterization of high-affinity binding between gangliosides and amyloid beta-protein. *Arch. Biochem. Biophys.* **388**, 225–30.
32 Inaba, S., Okada, T., Konakahara, T., and Kodaka, M. (2005) Specific binding of amyloid-b-protein to IMR-32 neuroblastoma cell. *J. Pept. Res.* **65**, 485–90.
33 Kremer, J. J., and Murphy, R. M. (2003) Kinetics of adsorption of beta-amyloid peptide Abeta(1–40) to lipid bilayers. *J. Biochem. Biophys. Methods* **57**, 159–69.
34 Hubbard, A. L., Wall, D. A., and Ma, A. (1983) Isolation of rat hepatocyte plasma membranes. I. Presence of three major domains. *J. Biol. Chem.* **96**, 217–29.
35 Jarrett, J. T., and Lansbury, P. T. Jr. (1993) Seeding "one-dimensional crystallization" of amyloid. A pathogenic mechanism in Alzheimer's disease and scrapie? *Cell* **73**, 1055–58.
36 Erb, E. M., Chen, X., Allen, S., Roberts, C. J., Tendler, S. J., Davies, M. C., and Forsen, S. (2000) Characterization of the surfaces generated by liposome binding to the modified dextran matrix of a surface plasmon resonance sensor chip. *Anal. Biochem.* **280**, 29–35.
37 Anderluh, G., Besenicar, M., Kladnik, A., Lakey, J. H., and Macek, P. (2005) Properties of nonfused liposomes immobilized on an L1 Biacore chip and their permeabilization by a eukaryotic pore-forming toxin. *Anal. Biochem.* **344**, 43–52.
38 Henriques, S. T., Pattenden, L. K., Aguilar, M. I., and Castanho, M. A. (2008) PrP(106-126) does not interact with membranes under physiological conditions. *Biophys. J.* Epub, doi:10.1529/biophysj.1108.131458.
39 Mozsolits, H., Wirth, H. J., Werkmeister, J., and Aguilar, M. I. (2001) Analysis of antimicrobial peptide interactions with hybrid bilayer membrane systems using surface plasmon resonance. *Biochim. Biophys. Acta* **1512**, 64–76.

Chapter 16

Incorporation of a Transmembrane Protein into a Supported 3D-Matrix of Liposomes for SPR Studies

Annette Granéli

Abstract

Surface analytical tools as surface plasmon resonance (SPR) have become increasingly important in biomedical research since they offer high detection sensitivity compared to traditional biomedical methods. For the use of SPR as a biomedical research tool there is a need to immobilize the reactants to a solid sensor surface. It is nowadays fairly straightforward to immobilize various reactants and hydrophilic proteins to a solid sensor surface and SPR has successfully been used in several applications using such proteins when studying various protein interactions. When using SPR for the analysis of transmembrane proteins the immobilization onto the solid surface becomes more difficult. Transmembrane proteins are more sensitive to the surroundings and need to be incorporated into a structure where it can reside in a natural environment. Supported liposomes offer such environment. In this chapter a new method is presented where multilayers of such supported liposomes are used to immobilize transmembrane proteins onto a solid sensor surface which is suitable for use in SPR detection.

Key words: Transmembrane proteins, SPR, proteoliposomes, DNA, cholesterol.

1. Introduction

SPR analysis is used in several applications in biomedical research such as protein–protein interactions, DNA–protein interactions, protein–drug interactions and lipid–drug interactions (1–4). Most of the protein interaction studies performed by SPR are using water-soluble proteins. When using SPR equipment for protein analysis the proteins can be immobilized on the flat solid sensor surface using a variety of linker molecules such as various types of PEGs (polyethylene glycol) or other polymeric material, lipids and proteins (5–7). Such immobilization strategy is fairly

N.J. de Mol, M.J.E. Fischer (eds.), *Surface Plasmon Resonance*, Methods in Molecular Biology 627,
DOI 10.1007/978-1-60761-670-2_16,

straightforward to use for the immobilization of water-soluble proteins. When using transmembrane proteins in SPR analysis the immobilization strategy becomes more difficult. Small transmembrane proteins, transmembrane proteins with mainly hydrophobic parts and various other transmembrane proteins have been successfully immobilized within a supported lipid bilayer on a solid surface (8–12). This strategy has limitations and cannot be used for a whole range of proteins and there is a need for alternative methods to immobilize transmembrane proteins on a solid surface. When using SPR as an analysing tool it is also important to reach a high enough concentration of the protein so that binding or dissociation events can be detected. Thus, to be able to study transmembrane proteins using SPR, the proteins need to be immobilized on a solid surface in a structure where they can reside in a natural environment and where they can reach a detectable concentration. The method that is described in this chapter fulfils these criteria. Since the transmembrane protein must reside in a natural environment the protein is reconstituted into preformed liposomes and in order to reach detectable concentrations a multilayer of the proteoliposomes is built on a solid surface (*see* **Note 1**) (13, 14). DNA is used as linker molecules between the surface and the liposomes in the first layer and between the liposomes in the following layers. The DNA strands that are used are short oligos of 20 bp and attached in the 3′ end with either biotin or cholesterol (biotin for the first layer of liposomes and cholesterol for the following layers). **Figure 16.1** shows a schematic picture of the multilayer structure. The transmembrane protein that is used to confirm this method is proton-translocating nicotinamide nucleotide transhydrogenase (TH) from *Escherichia coli*. TH is a 105 kDa protein with three subunits, one hydrophobic part that consist of 13 α-helices and two hydrophilic parts where one of the hydrophilic parts can be cleaved off using the digestion enzyme trypsin. Trypsin is used to verify that the protein is reconstituted into the multilayer structure and to confirm that the concentration of TH is increased in the multilayer structure.

2. Materials

2.1. Protein Preparation

1. TH from *E. coli*. The preparation of TH has been described elsewhere (15).

2.2. Liposome Preparations

1. Buffer A used in the preparation of liposomes is 10 mM Tris–HCl and 100 mM NaCl at pH 7.2 (*see* **Note 2**).

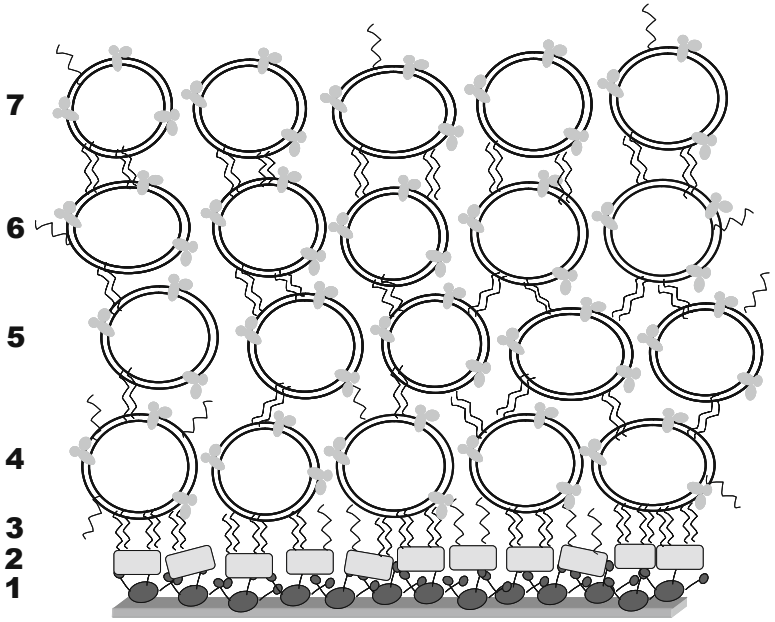

Fig. 16.1. The schematic build-up of the multilayer structure using a transmembrane protein reconstituted into uni-lamellar liposomes. The different layers are as follows: 1. biotinylated BSA adsorbed onto a SPR sensor chip with a gold surface. 2. Neutravidin. 3. Biotinylated 20 bp long DNA strand. 4. Proteoliposomes containing transmembrane protein and cholesterol-tagged DNA complementary to the DNA in the previous layer. 5–7. Proteoliposomes with altering type of DNA (1 or 2) complementary to the DNA in the previous layer.

2. The lipids used are phosphatidyl-serine (PS), phosphatidyl-ethanolamine (PE) and phosphatidyl-choline (PC). The total lipid concentration in buffer A is 10 mg/mL (*see* **Notes 3,5** and **8**).
3. DNA strands that are 20 bp in length and tagged with cholesterol in the 3′ end are used in the liposome preparations (Medprobe, Norway). The sequences of the DNA strands are 5′-TAT-TTC-TGA-TGT-CCA-CCC-CC-3′ (DNA1) and the complementary strand 5′-TGG-ACA-TCA-GAA-ATA-CCC-CC-3′ (DNA2).
4. Buffer B used for the storage of DNA strands is 10 mM Tris–HCl and 1 mM EDTA at pH 8.0.
5. The DNA is dissolved in buffer B in a concentration of 20 μM and stored at –20°C.
6. An extruder is needed to extrude the lipid solution. The extruder used in the development of this method is a mini-extruder from Avanti Polar Lipids Inc, Alabaster, Alabama, USA. The size of the liposomes in this method is 100 nm in diameter and a filter with that pore size is used in the extruding process (*see* **Note 4**).

2.3. Reconstitution of the Transmembrane Protein

1. Transmembrane protein TH.
2. Preformed liposomes tagged with cholesterol-DNA (both DNA1 and DNA2) dissolved in buffer A.
3. Detergent Triton X-100.
4. Bio-Beads SM2 from Bio-Rad, USA.
5. Methanol and water for pre-washing of the Bio-Beads.
6. Rolling table.
7. Cold room needed when working with a heat-sensitive protein such as TH.

2.4. Surface Functionalization and SPR Analysis

1. Biotinylated bovine serum albumin (biotin-amido-caproyl-labeled BSA, biotin-BSA) (Sigma). The biotin-BSA is dissolved in buffer A in a concentration of 1 mg/mL and stored at –20°C.
2. Neutravidin (Pierce). Neutravidin is dissolved in buffer A in a concentration of 1 mg/mL and stored at –20°C (*see* **Note 12**).
3. Biotin-DNA. The DNA is dissolved in buffer B in a concentration of 20 μM and stored at –20°C. The sequence of the DNA strand is 5′-TAT-TTC-TGA-TGT-CCA-CCC-CC-3′ (DNA1). The DNA strand is tagged with a biotin in the 3′ end.
4. SPR sensor chips and equipment. A Biacore 2000 is used. The sensor chips used are SIA Kit Au (Biacore). The sensor surface used is an untreated gold surface.
5. Trypsin. Trypsin is dissolved in buffer A at a concentration of 10 μg/mL.
6. Sodium dodecyl sulphate (SDS) is used for cleaning of the sensor chips. The concentration used is 10 mM in H_2O.
7. NH_3 solution (25%) and H_2O_2 solution (30%) for cleaning of the sensor chips.
8. UV-ozone chamber (*see* **Note 16**).

3. Methods

3.1. Preparation of Lipids

1. Prior to the liposome preparation they are mixed in a small round flask. The lipid mixture is composed of 5% PS, 45% PE and 50% PC (*see* **Note 8**).
2. The chloroform is evaporated from the lipid mixture using a stream of nitrogen. When evaporating the chloroform the

round flask should be rotated so that an even film of lipids is formed on the glass walls of the round flask. When the majority of the chloroform has been evaporated the nitrogen stream should flow over the lipid film for 2 h in order to make sure that all the chloroform has evaporated, which can be done without rotating the flask. This can be done using a membrane where two syringe needles can be used as both inlet and outlet of the nitrogen stream or using a vacuum rotator.

3. Resolve the lipid film in buffer A. Vortex well so that all the lipids are resolved in the buffer. The concentration of the lipids in buffer A is 10 mg/mL (*see* **Note 3**).
4. Add cholesterol-DNA1 to one part of the liposome solution and cholesterol-DNA2 to the other part. The cholesterol-DNA is added to the lipid solution with a final concentration of 8 μM, which gives three cholesterol-DNA molecules per liposome/proteoliposome.

3.2. Preparation of Liposomes

The liposomes are prepared using extrusion of the lipid mixture. To be able to extrude the lipid mixture an extruder must be needed. The extruder is worked manually. Extrusion is a technique where the lipid mixture is passed through a polycarbonate filter with holes that match the desired size of the liposomes. The lipid solution is passed through the filter using pressure on two syringes, one from each side. Liposomes of various sizes can be prepared using extrusion, from 30 nm in diameter to 1 μm in diameter. The liposomes used for this multilayer structure are 100 nm in diameter.

1. The extruder is assembled according to the manufacturer's description. Make sure that the syringes are sealed tight.
2. The lipid mixture containing cholesterol-DNA is placed in one of the two syringes.
3. The lipid mixture is passed from one syringe to the other through the filter 11 times. Make sure that the lipid mixture gets clearer during the extrusion otherwise there might be a problem with the filter so that the extrusion does not work. After the solution has been passed through the filter 11 times it is homogeneous and ready to use (*see* **Note 4**).

3.3. Preparation of Proteoliposomes/ Reconstitution

The protein that has been used in this study is proton-translocating nicotinamide nucleotide transhydrogenase (TH). The protein consists of three domains, two hydrophilic domains and one hydrophobic domain. The hydrophobic domain consists of 13 membrane-spanning α-helices. TH has a trypsin cleaving site which cleaves off one of the hydrophilic parts. The entire protein is 105 kDa and the part that is cleaved off using trypsin is 43 kDa (16) (*see* **Note 6**).

1. TH and the preformed liposomes with cholesterol-DNA are mixed with the detergent Triton X-100. The concentration of lipids is 6.6 mg/mL, Triton X-100 5 mg/mL and TH 5.6 μM (0.59 mg/mL). The molar TH/lipid ratio is 6.6×10^{-4}. The buffer used for the reconstitution is buffer A. The mixture is incubated for 45 min. TH is a temperature-sensitive protein so the mixture is kept in a cold room and rolled on a small rolling table during incubation (17) (*see* **Notes 7** and **9**).
2. After incubation the detergent needs to be removed. When using Triton X-100 as the detergent it can be removed using Bio-Beads. Bio-Beads are macroporous polystyrene beads used for hydrophobic interaction. Prior to the use of Bio-Beads they need to be washed in methanol and water according to the manufacturer's protocol. Bio-Beads are added to the proteoliposome solution in three sequential additions of 0.05 g Bio-Beads/mL proteoliposome solution with an incubation time between the Bio-Bead additions of 90 min for the first two and 60 min for the last addition (*see* **Note 9** and **10**).

3.4. Sensor Chip Surface Cleaning

The sensor chips can be used several times if the cleaning is done correctly (*see* **Notes 13** and **14**).

1. The sensor chips are incubated in a glass container in a water solution containing 10 mM SDS for at least 30 min but they can be incubated for a few days in the SDS solution if that is more suitable since the SDS is not damaging to the sensor surface (*see* **Note 15**).
2. After the SDS treatment the sensor chips are immersed for 10 min into a heated (70°C) solution containing $NH_3/H_2O_2/H_2O$, one part NH_3, one part H_2O_2 and six parts H_2O.
3. The sensor chips are then thoroughly rinsed with H_2O, dried using a stream of N_2 and stored in a dust-free environment until use.
4. Just prior to use the sensor chips are treated with UV-ozone for 2×10 min with a thorough rinse of water followed by drying in between. After the second round of UV-ozone treatment the sensor chips are ready to be used in the SPR experiments (*see* **Note 16**).

3.5. SPR Experiment

The SPR sensing machine used in this study is a Biacore 2000 and the instructions are based on using this or a similar machine. The SPR measurements are performed using a constant flow of 5 μL/min.

1. Assemble the sensor chips according to the manufacturer's instructions. Insert the sensor chip into the SPR machine.

2. Add buffer A to the sensor chip and make sure that a stable baseline is established.
3. Add biotinylated BSA to the gold surface in a concentration of 10 μg/mL in buffer A. The addition should last for 20 min or until the binding has reached saturation (*see* **Note 11**).
4. Add Neutravidin in a concentration of 10 μg/mL in buffer A. The addition should last for 15 min or until the binding has reached saturation (*see* **Notes 11** and **12**).
5. Add biotinylated DNA1 in a concentration of 0.2 μM. The addition should last for 20 min or until the binding is saturated.
6. The first layer of proteoliposomes (DNA2-loaded) is added at this stage. The concentration of proteoliposomes is 0.5 mg/mL (lipid concentration). The addition should last for 30 min. Make sure that the binding has reached saturation.
7. Before the second layer of proteoliposomes (DNA1-loaded) an addition of the same cholesterol-DNA as the first layer (DNA2-loaded) of proteoliposomes must be made in order to attach the second layer of proteoliposomes. Add 50 nM of cholesterol-DNA2 for 10 min or until saturation has been reached.
8. Continue by repeating the additions of proteoliposomes functionalized with altering DNA strands (DNA1 and DNA2). After saturated binding of each layer of liposomes there should be an additional addition of extra cholesterol-DNA (same DNA strand as the latest layer of proteoliposomes). To efficiently enhance the detection signal four to five proteoliposome layers are enough for the multilayer structure (*see* **Fig. 16.2**).
9. To confirm that the method allows the transmembrane protein TH to reside within the liposome structure a trypsin addition was made. Trypsin cleaves off 43 kDa of the 105 kDa of the total mass of the protein. Trypsin is added to the multilayer structure in a concentration of 10 μg/mL in buffer A. The addition of trypsin should last for 25 min or until saturation has been reached (*see* **Fig. 16.3**).

3.6. Analysis Using SPR

An SPR apparatus measures the mass load on the surface by measuring the change in refractive index near the surface as a change in SPR-angle as the biomolecules are binding to the surface. The results are given as resonance units (ΔRU). As seen in **Figs. 16.2** and **16.3** the response in RU from each layer decreases with layer number. This is a phenomenon which is due to the exponential decay of the evanescent field as illustrated in **Fig. 16.2**

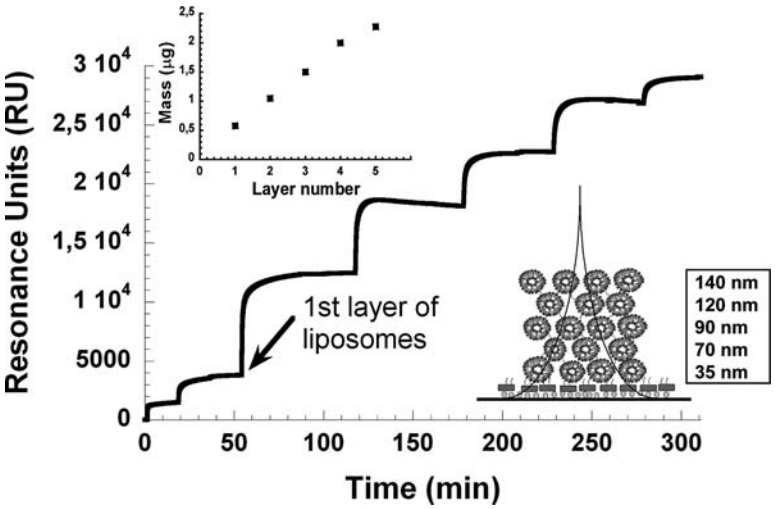

Fig. 16.2. An SPR measurement of the building up of the multilayer structure using PC-liposomes (100 nm without transmembrane proteins) is shown. The figure shows in the *right lower corner* a schematic of the bound layers and the layer thickness that has been calculated using a quartz crystal microbalance with dissipation monitoring (further described later in the text). The figure also shows the evanescent field of the SPR. The *top left corner* shows the actual mass that is added with each liposome layer.

(*see* **Section 3.5**). The evanescent field has a sensing depth of ~300 nm and this means that the further away from the surface the less mass is sensed even though each layer consists of the same amount of biomolecules. Therefore there is a need to compensate for the exponentially decaying sensing depth when calculating the mass that is adsorbed in each layer of the multilayer structure. The actual mass that is adsorbed in an SPR measurement, when the adsorbed structure approaches the same magnitude as the sensing depth of the evanescent wave, is described by the following equation (13):

$$\Delta m = C_{\mathrm{SPR}}.\Delta \mathrm{RU}.\frac{2d}{d_z}\left(1 - e^{\left(-\frac{2d}{d_z}\right)}\right)^{-1} \qquad [1]$$

In **Eq. [1]** C_{SPR} is 0.059 ng/cm^2 for lipids (most of the mass consists of lipids since the protein concentration is very low compared to the lipid concentration), d_z is the sensing depth (300 nm) and d the layer thickness (13). The layer thickness cannot be obtained from SPR measurements; one suitable technique is instead quartz crystal microbalance with dissipation monitoring (QCM-D) (18). **Figure 16.2** shows results from such calculation for pure PC-liposomes. It is shown that the different layers of pure PC-liposomes are packed in the multilayer structure in such a way that each layer only builds up the multilayer structure by

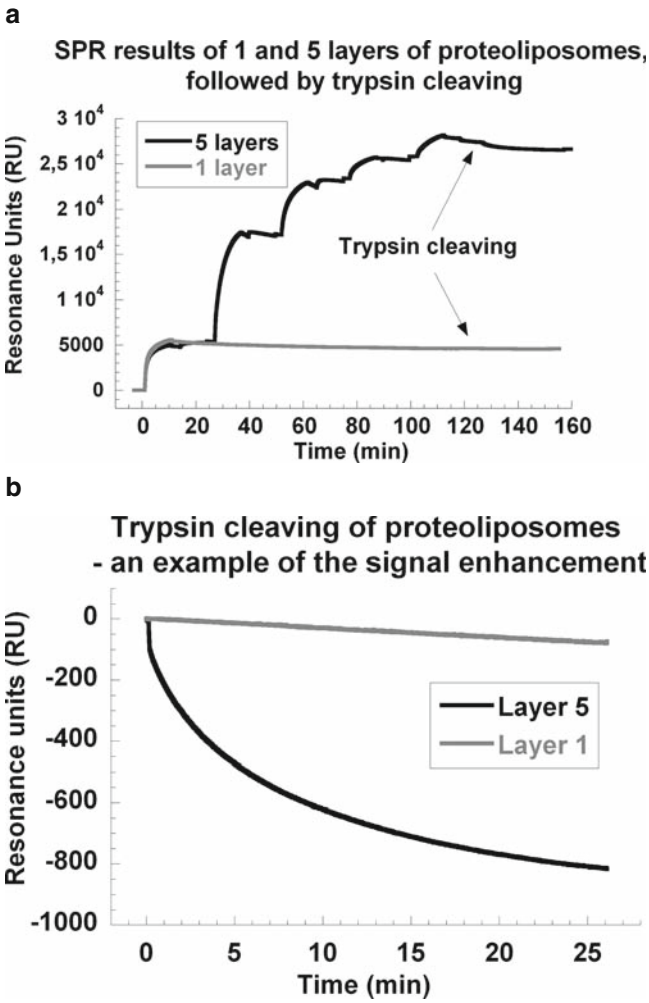

Fig. 16.3. (**a**) SPR measurement of the build-up of the proteoliposome multilayer structure and subsequent cleaving of TH using trypsin within the multilayer structure for one layer (*grey* trace) and five layers (*black* trace). (**b**) Close-up of the effect of trypsin cleavage on the SPR signal for one liposome layer (*grey* trace) and for five layers (*black* trace), demonstrating that the multilayer structure enhances the detection signal.

20–30 nm even though the liposomes are 100 nm in diameter. When using the lipid mixture that is suitable for the transmembrane protein TH (50% PC, 45% PE and 5% PS) the layer thickness becomes different as shown in **Fig. 16.3**, which only illustrates that it is very important to confirm the layer thickness when using different lipid mixtures. The details about the QCM-D measurements have been described elsewhere (14). Since the intensity of the evanescent field decreases with distance from the surface it is enough to use four to five proteoliposome layers for increasing the detection.

4. Notes

4.1. Lipids/Liposomes

1. The method can also be used with liposomes without protein if the interaction of interest is with a lipid membrane or the interior of the liposomes.
2. A small change in pH (between pH 7 and 8) when preparing the liposomes can be made depending on the desired pH for the specific transmembrane protein.
3. The lipid concentration in the extruding process can easily be varied from 5 to 20 mg/mL depending on the desired concentration.
4. Liposomes that have been prepared by extrusion should be used within 4 days according to the extruder manufacturer otherwise they start to decompose. The prepared liposomes can often be stored for more than 4 days if they are properly stored in a tightly sealed container in an oxygen-free environment. The liposomes should not be stored for more than 2 weeks.
5. It is important that the lipids are stored in an oxygen-free environment since the lipids can otherwise be oxidized. The lipids should therefore be stored in chloroform or a water-based buffer under nitrogen in a tightly sealed container.

4.2. Proteoliposomes/ Reconstitution

6. This method has only been tried out using the transmembrane protein TH. Even so, the method could still work for other transmembrane proteins. When trying another protein there are several important factors to consider.
7. There should be a well-functioning reconstitution procedure to use to make sure that the transmembrane protein can reside within the lipid bilayer of the liposomes in a natural and functioning way.
8. The lipid mixture can vary as long as the lipids are suitable for liposome preparation. Be careful, though, when using too much charged lipids since the liposomes then can affect each other in the different layers.
9. The detergent used for the reconstitution can be changed but make sure to use a detergent that can be removed from the solution after reconstitution and use the proper way of removing the detergent.
10. After the protein reconstitution the proteoliposomes should be used within 4 days.

4.3. Surface Preparation

11. It is important that the whole surface area be covered by the biotin-BSA and Neutravidin otherwise the liposomes/proteoliposmes will adsorb to the surface and the liposomes/proteoliposomes will break.
12. It is also possible to use Streptavidin or Avidin instead of Neutravidin but note that the DNA has a tendency to be attracted by the Streptavidin that is positively charged in neutral pH.

4.4. Surface Cleaning

13. The most important thing to notice when working with surface-sensitive techniques is to keep all parts involved extremely clean. All glassware that is used to prepare the samples and to store buffers should be cleaned with a powerful detergent such as Hellmanex®II (Hellma, Germany), which is a detergent especially designed to clean glass and quartz. Make sure that the glassware is well rinsed after cleaning with detergent, otherwise the detergent can cause problems in the SPR measurements.
14. The sensor chips can be used several times but it is important to clean them properly between the experiments. The sensor chips should be cleaned in the same way as prior to the first use as previously described in Section 3.
15. To make sure that all the buffers are without contamination they can be filtered through a sterile filter. To make sure that the experiments are not disturbed by air bubbles in the buffers, they can be degassed prior to use. Also make sure that the buffers have room temperature before degassing so that no air bubbles are created while the buffers are heated.
16. A UV-ozone chamber is a device where the surfaces are cleaned. Depending on the device used the efficiency can vary so the optimal time used for cleaning of the sensor surface must be tried out. If the cleaning is done inefficiently the adsorption of the proteins closest to the surface will be lowered.

Acknowledgments

A patent that is based on the protocol described in this method has been filed by Layerlab AB, Göteborg, Sweden. The patent has the patent number WO2004090165.

References

1. Berggard, T., Linse, S., and James, P. (2007) Methods for the detection and analysis of protein–protein interactions. *Proteomics* **7(16)**, 2833–42.
2. Lopez, P. H., and Schnaar, R. L. (2006) Determination of glycolipid-protein interaction specificity. *Methods Enzymol.* **417**, 205–20.
3. Majka, J., and Speck, C. (2007) Analysis of protein-DNA interactions using surface plasmon resonance. *Adv. Biochem. Eng. Biotechnol.* **104**, 13–36.
4. Nguyen, B., Tanious, F. A., and Wilson, W. D. (2007) Biosensor-surface plasmon resonance: quantitative analysis of small molecule-nucleic acid interactions. *Methods* **42(2)**, 150–61.
5. Anamelechi, C. C., et al. (2007) Streptavidin binding and endothelial cell adhesion to biotinylated fibronectin. *Langmuir* **23(25)**, 12583–88.
6. Satomi, T., et al. (2007) Physicochemical characterization of densely packed poly(ethylene glycol) layer for minimizing nonspecific protein adsorption. *J. Nanosci. Nanotechnol.* **7 (7)**, 2394–99.
7. Wang, Z., et al. (2008) Development of air-stable, supported membrane arrays with photolithography for study of phosphoinositide-protein interactions using surface plasmon resonance imaging. *Anal. Chem.* **80(16)**, 6397–404.
8. Naumann, R., et al. (2002) Proton transport through a peptide-tethered bilayer lipid membrane by the H(+)-ATP synthase from chloroplasts measured by impedance spectroscopy. *Biosens. Bioelectron.* **17(1–2)**, 25–34.
9. Wagner, M. L., and Tamm, L. K. (2000) Tethered polymer-supported planar lipid bilayers for reconstitution of integral membrane proteins: silane-polyethyleneglycol-lipid as a cushion and covalent linker. *Biophys. J.* **79(3)**, 1400–14.
10. Fix, M., et al. (2004) Imaging single membrane fusion events mediated by SNARE proteins. *Proc. Natl. Acad. Sci. USA* **101(19)**, 7311–16.
11. McConnell, H. M., et al. (1986) Supported planar membranes in studies of cell-cell recognition in the immune system. *Biochim. Biophys. Acta* **864(1)**, 95–106.
12. Salafsky, J., Groves, J. T., and Boxer, S. G. (1996) Architecture and function of membrane proteins in planar supported bilayers: a study with photosynthetic reaction centers. *Biochemistry* **35(47)**, 14773–81.
13. Graneli, A., Benkoski, J. J., and Hook, F. (2007) Characterization of a proton pumping transmembrane protein incorporated into a supported three-dimensional matrix of proteoliposomes. *Anal. Biochem.* **367(1)**, 87–94.
14. Graneli, A., Edvardsson, M., and Hook, F. (2004) DNA-based formation of a supported, three-dimensional lipid vesicle matrix probed by QCM-D and SPR. *ChemPhysChem.* **5(5)**, 729–33.
15. Meuller, J., et al. (1997) Properties of a cysteine-free proton-pumping nicotinamide nucleotide transhydrogenase. *Biochem. J.* **324(Pt 2)**, 681–87.
16. Tong, R. C., Glavas, N. A., and Bragg, P. D. (1991) Topological analysis of the pyridine nucleotide transhydrogenase of Escherichia coli using proteolytic enzymes. *Biochim. Biophys. Acta* **1080(1)**, 19–28.
17. Richard, P., Rigaud, J. L., and Graber, P. (1990) Reconstitution of CF0F1 into liposomes using a new reconstitution procedure. *Eur. J. Biochem.* **193(3)**, 921–25.
18. Hook, F., et al. (2001) Variations in coupled water, viscoelastic properties, and film thickness of a Mefp-1 protein film during adsorption and cross-linking: a quartz crystal microbalance with dissipation monitoring, ellipsometry, and surface plasmon resonance study. *Anal. Chem.* **73(24)**, 5796–804.

Chapter 17

Application of Surface Plasmon Resonance Spectroscopy to Study G-Protein Coupled Receptor Signalling

Konstantin E. Komolov and Karl-Wilhelm Koch

Abstract

The G-protein coupled receptor rhodopsin is a classical example of a seven transmembrane helix receptor; it is photoexcited and transmits this light signal to a G-protein mediated cascade. Many components of this receptor-triggered cascade can be purified in their native forms from natural sources making this system most suitable for biophysical studies. A central aspect of cellular signal transduction routes is to understand protein–protein interactions in a quantitative way. Surface plasmon resonance (SPR) spectroscopy is a biosensor-based technique that allows investigating molecular interactions by determining kinetic parameters. We here show how dark-adapted rhodopsin can be immobilized on the sensor chip surface. A laser device implemented in the SPR system allowed us to trigger light-induced conformational changes in rhodopsin and to monitor light-dependent binding of the photoreceptor cell G-protein transducin to rhodopsin. The sensor chip surface can be regenerated and used for several rounds of interaction analysis. Furthermore, illuminated rhodopsin can be regenerated by applying 9-*cis*-retinal on the sensor chip surface.

Key words: Surface plasmon resonance, rhodopsin, G-protein coupled receptor, G-protein.

1. Introduction

The superfamily of G-protein coupled receptors (GPCR) is involved in the transmission of hormones, neurotransmitters or sensory signals. These diverse signals are further processed by specific receptor coupling to heterotrimeric G-proteins that can interact and regulate effector molecules like adenylate cyclases, phosphodiesterases and ion channels (1–3). A well-understood example of a GPCR pathway is the light-triggered enzyme cascade of vertebrate photoreceptor cells (4, 5). Absorption of single

N.J. de Mol, M.J.E. Fischer (eds.), *Surface Plasmon Resonance*, Methods in Molecular Biology 627,
DOI 10.1007/978-1-60761-670-2_17,

photons by the visual pigment rhodopsin is sufficient to produce a photoresponse from a rod cell. This remarkable performance is achieved by a precise arrangement of interacting proteins that leads to a highly amplified hydrolysis of the second messenger guanosine-3′,5′-cyclic monophosphate (cGMP). The heterotrimeric G-protein transducin (G_t) is activated by the light-activated form of rhodopsin, Meta II, which catalyses a GDP/GTP-exchange at the G_t α-subunit. The effector molecule of G_t is the cGMP-specific phosphodiesterase PDE6 that hydrolyses its substrate cGMP with a high turnover number. The downstream target of cGMP is a cyclic nucleotide-gated channel located in the plasma membrane of the photoreceptor cell, which is opened by cGMP and is closed upon hydrolysis of cGMP causing a halt of cation influx and a hyperpolarization of the cell (6).

Investigation of protein–protein interactions that involve membrane-bound proteins like receptor molecules is a challenging task, because for many experimental approaches the receptor needs to be extracted from the membrane while maintaining its structural and functional integrity. The application of SPR spectroscopy for the study of membrane proteins has recently attained increasing interest (7–12). SPR is an optical phenomenon that depends on an ultra-thin metal layer, which is located at the interface of two media of different refractive indices (13). In commercial systems like Biacore© these two media are a prism and a compartment containing an aqueous buffer. When light hits the prism under the angle of total internal reflection, the electric field of the photons extends beyond the reflecting interface into the medium of lower refractive index (e.g. compartment with an aqueous buffer) thereby creating a so-called evanescent electric field. Depending on the conditions of the measuring system a resonance phenomenon is observed that reduces the intensity of the reflected light beam. This phenomenon is highly sensitive to the geometry of the optical system, the wavelength of the incident light, the thickness of the metal layer and the refractive index of the medium. It therefore allows detecting any changes in refractive index close to the sensor chip surface, when all other parameters are kept constant during an analysis.

Protein–protein interaction studies using SPR require the immobilization of one binding partner, while the other partner is supplied in a buffer stream flowing over the sensor surface. Membrane receptor molecules could be immobilized via binding to an immobilized lectin, when they harbour a carbohydrate moiety. We made use of the mannose-rich oligosaccharide chains in rhodopsin to specifically bind the receptor via its amino-terminal part to immobilized concanavalin A (ConA) on the sensor surface (10, 11). This arrangement exposes the loops and the carboxy terminus of rhodopsin to the buffer flow allowing the supply of

interacting partners that bind to the cytoplasmic regions of rhodopsin. In order to trigger rhodopsin activation by light directly on the sensor chip surface, we integrated a laser system into the commercial SPR device. Flashes of light or constant illumination are channelled onto the sensor surface from the light source (laser) by an optic fibre (11).

2. Materials

2.1. Preparation of Bovine Rod Outer Segment Membranes and Proteins

1. Hypotonic buffer: 5 mM Tris–HCl, pH 7.5, 0.5 mM $MgCl_2$, 0.4 mM EDTA, 1 mM DTT. Store at 4°C.
2. GTP (Sigma-Aldrich) solution: 20 μM GTP in hypotonic buffer (see above).
3. Resuspension buffer: 20 mM Tris–HCl, pH 7.5.
4. CHAPS stock solution: 250 mM 3-[(3-Cholamidopropyl) dimethylammonio]-1-propanesulfonate (Serva) in H_2O. Store at room temperature.
5. Potter homogenizer.
6. PD-10 column (GE Healthcare).
7. Liquid nitrogen.

2.2. Immobilization of ConA and Rhodopsin

1. CM5 sensor chips were from Biacore AB (GE Healthcare).
2. NHS solution: 50 mM *N*-hydroxysuccinimide dissolved in H_2O. Prepare a stock and store aliquots at –20°C.
3. EDC solution: 200 mM *N*-ethyl-*N′*-[(dimethylamino)propyl]carbodiimide dissolved in H_2O. Prepare a stock and store aliquots at –20°C.
4. Ethanolamine solution: 1 M ethanolamine hydrochloride, pH 8.5.
5. Concanavalin A stock solution: 5 mg/mL ConA (from *Canavalia ensiformis*, type IV, Sigma-Aldrich) in 100 mM sodium acetate, pH 5.0. Store at –80°C.
6. MES-buffer: 50 mM 2-(*N*-morpholino)ethanesulfonic acid (MES), pH 6.0, 1 mM $CaCl_2$ and 1 mM $MnCl_2$. Store at 4°C.

2.3. SPR Measurements

1. Recordings were performed with a Biacore 2000.
2. Running buffer: 50 mM 3-morpholinopropane-1-sulfonic acid (MOPS), pH 7.5, 150 mM NaCl, 3 mM $MgSO_4$, 10 μM $CaCl_2$, 10 μM $MnCl_2$. Filtrate the running buffer before use (0.22 μm filter, Millipore). Check running buffer daily for particles. Repeat filtration, if necessary.

3. 200 μM GTP solution: prepared from a 50 mM stock solution by dilution with running buffer.
4. Diode-pumped Nd:YAG solid state laser (monochromatic light of $\lambda = 532$ nm, model LL-11 qps) was from Laser-Compact Co. Ltd. The optic fibre had a diameter of 0.5 mm.
5. BIAevaluation 4.1 software.

2.4. Regeneration of Rhodopsin and of Rhodopsin-Coated Surfaces

1. Solution of 9-*cis*-retinal (Sigma-Aldrich): 100 mM stock in dimethyl sulfoxide (DMSO). Store aliquots in light-protected vials at –80°C.
2. Running buffer for regeneration procedure is the same as for SPR measurements.
3. Regeneration solution I: 100 mM methyl α-D-mannopyranoside (Sigma-Aldrich) supplemented with 30 mM *n*-octyl-β-glucoside (Sigma-Aldrich).
4. Regeneration solution II: 6 M urea.
5. Filter all solutions except the 9-*cis*-retinal stock before use in the Biacore device.

3. Methods

The starting material for the preparation of rod outer segment (ROS) membranes, rhodopsin and transducin, is a highly purified sample of rod outer segments. In particular the preparation of bovine rod outer segments from isolated retinae is a well-established procedure and outlined in detail in several publications (e.g. 14, 15). It is not described here. ROS can be stored at –80°C under protection from light for many years without loss of biological activity of most key proteins. All handling of ROS must occur under very dim red light. It is also important to operate the Biacore system in a dark room. While routine steps like washing of the system, activation of the sensor chip surface and immobilization of ConA can be performed under daylight conditions, it is necessary to exclude any light from the rhodopsin sample. A summarizing scheme of all steps is displayed in **Fig. 17.1**.

3.1. Preparation of Rhodopsin and G_t for SPR Interaction Studies

1. For preparation of washed dark ROS membranes, take a sample of bovine ROS (1 mL containing rhodopsin at a concentration of 5–10 mg/mL) and add 5 mL of hypotonic buffer. Homogenize by vortexing and centrifuge (300,000*g*, 15 min). Discard the supernatant and repeat this washing step three times. Keep samples cool at 4°C all the time.

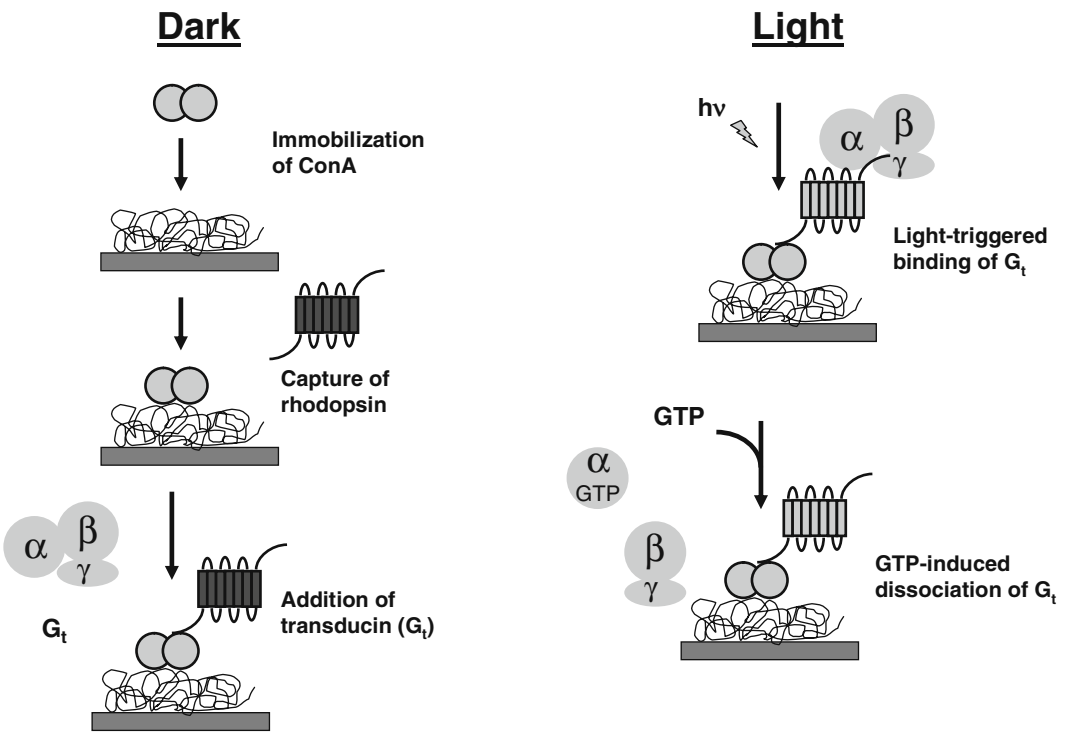

Fig. 17.1. Summary of all steps performed on the SPR sensor chip involving rhodopsin. *Dark*: ConA is immobilized via its free amino groups on a surface with activated carboxy groups. Rhodopsin is captured from the flowing buffer solution by interaction of its carbohydrate moiety with ConA. This allows a site-directed immobilization of rhodopsin on the amino terminus leaving the carboxy-terminal region (i.e. cytoplasmic parts) free for protein–protein interaction analysis. Injection of G_t into the buffer flow leads to a negligible binding to the surface. *Light* : illumination of the sensor chip surface by a laser light triggers interaction of G_t with rhodopsin. Addition of GTP induces the rapid dissociation of G_t from rhodopsin.

Suspend the final pellet of washed membranes in resuspension buffer and store it in aliquots at –80°C.

2. For the isolation of G_t (16, 17) take 1 mL of bovine ROS (rhodopsin concentration 5–10 mg/mL) and illuminate it with normal white light for 20 min on ice. Then add 5 mL of hypotonic buffer and homogenize the suspension of ROS by using a Potter homogenizer. Avoid foaming of the sample. Centrifuge at 300,000*g* for 15 min. Discard supernatant and repeat this washing step five times. Elute G_t from the membranes by incubation of ROS membranes for 5 min with 2.5 mL of 20 μM GTP in hypotonic buffer. Centrifuge once more (300,000*g*, 15 min) and then use a PD-10 column to remove GTP. Removal of GTP is important to observe light-dependent G_t–rhodopsin interaction. In order to minimize bulk refractive index changes during the injection of G_t samples into the microfluidic system of the Biacore device equilibrate the PD-10 column with running buffer. Use liquid N_2

to freeze the final sample of G_t and store aliquots at –80°C until use (*see* **Note 1**).

3. Measure protein concentration of G_t by a Coomassie blue assay (18) and of the rhodopsin preparation by the absorbance at 498 nm ($\varepsilon_{498} = 42{,}000\ M^{-1}\ cm^{-1}$). Analyse samples by sodium dodecyl sulfate polyacrylamide gel electrophoresis (19).
4. Rhodopsin is solubilized from a suspension of washed ROS membranes (50–100 μg of rhodopsin) by addition of CHAPS to reach a final concentration of 25 mM in resuspension buffer. After 30 min of gentle shaking at 4°C, nonsolubilized material was sedimented by centrifugation at 18,000*g* for 15 min. Take the supernatant, protect from light and store on ice until use. The resulting preparation is highly enriched in rhodopsin (11) and can be used without further purification for immobilization on the sensor chip surface (*see* **Note 2**).

3.2. Immobilization of Proteins on the SPR Chip Surface

1. CM5 sensor chips (Biacore) contain a carboxy-methylated matrix that can be activated by a fresh mixture of *N*-hydroxysuccinimide (NHS) and *N*-ethyl-*N*′-[(dimethylamino)propyl]carbodiimide (EDC) to allow the covalent coupling of proteins via its free amino groups. Set the flow rate to 5 μL/min. In order to couple ConA activate the matrix first by 35 μL of 50 mM NHS and 200 mM EDC.
2. Inject 35 μL of 0.1 mg/mL ConA in 100 mM sodium acetate buffer, pH 5.0.
3. Activated carboxy groups that have not been reacted with ConA need to be deactivated before start of any interaction analysis. Therefore, deactivate the surface by injection of 35 μL of ethanolamine solution.
4. Take a freshly prepared stock solution of rhodopsin in CHAPS (*see* step 4 of **Section 3.1**). Just before immobilization, dilute the solution with MES-buffer fivefold (this buffer contains Ca^{2+} and Mn^{2+} cations which are essential for carbohydrate binding by ConA) and set the flow rate to 2 μL/min. Inject 50 μL of solubilized rhodopsin (4–400 μg/mL) (*see* **Note 3**).
5. When the injection and immobilization are finished, set the flow rate to 30 μL/min. Wash the system with running buffer until a stable baseline is recorded. This will take at least 30 min. A sensorgram displaying all steps of activation, coupling, deactivation and binding is shown in **Fig. 17.2**.
6. Calculate the amount of immobilized ConA and immobilized rhodopsin by measuring the difference in resonance

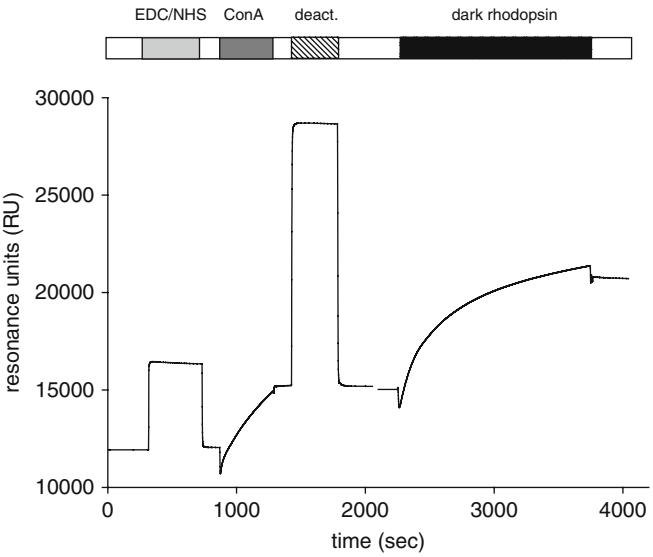

Fig. 17.2. Sensorgram displaying the immobilization of ConA and rhodopsin. A mixture of EDC and NHS activates the carboxy-methylated matrix of a CM5 sensor chip for subsequent coupling of free amino groups (*light grey bar*). Injection of ConA (*dark grey bar*) leads to a reaction of free amino groups in ConA with activated carboxy groups on the surface. Deactivation of nonreacted carboxy groups is performed by flushing the system with ethanolamine (*hatched bar*). Injected rhodopsin is captured by ConA (*dark bar*).

units (RU) before and after injection of ConA and rhodopsin. A change of 1 RU corresponds to an amount of 1 pg protein per mm^2.

3.3. Interaction of G_t with Immobilized Rhodopsin

The analysis of a G-protein/receptor interacting pair has to look for the G-protein binding step that is triggered by ligand activation of the receptor and the GTP-induced dissociation of the G-protein from its receptor. In the case of native rhodopsin 11-*cis*-retinal is a covalently bound ligand located in a receptor-binding pocket. Light triggers the conversion of the inactive ligand to an active form leading finally to the catalytically active Meta II state of rhodopsin. Commercial SPR systems are not equipped with an external light source to illuminate the sensor chip surface. The system used in this study was modified by integration of an optical fibre (diameter = 0.5 mm) that was placed directly on the interfluid cartridge (IFC) device from Biacore by fixing it with scotch tape. The fibre was connected to a diode-pumped Nd:YAG solid state laser (model LL-11 qps; Laser-Compact Co. Ltd.), which allows to illuminate the sensor chip surface with light of λ = 532 nm (*see* **Note 4**).

1. Check how the illumination of the sensor chip surface by the laser will disturb the performance of the system, in particular whether artefact signals are produced. For this

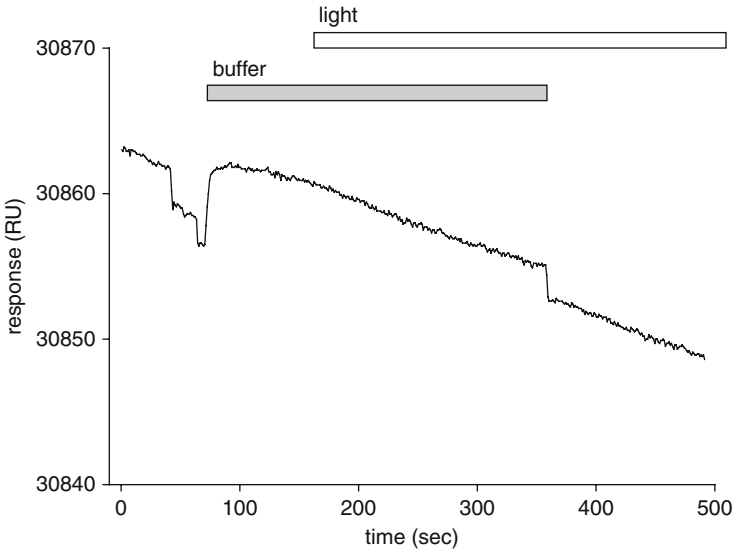

Fig. 17.3. Control recording showing the influence of the laser illumination on the resonance signal. Running buffer is injected into running buffer that is flowing over a ConA-coated surface. Injection is indicated by the *grey bar*. The laser light is switched on as indicated by the *white bar*. Disturbance of the system is very low in the order of maximal 1–2 RU, which is similar to the noise of the system.

purpose run the system without immobilized rhodopsin or after rhodopsin has been bleached by laser light. The Biacore signal should not be affected by light from the laser light source. *See* for example **Fig. 17.3**.

2. Set the flow rate to 5 μL/min and keep the system in the dark. Inject 35 μL of purified G_t (*see* step 2 of **Section 3.1**) at different concentrations (0.0175–0.7 μM).
3. Observe possible dark (or nonspecific) binding of G_t to the surface (*see* **Note 5**). Let the signal reach a plateau (usually within 1 min) and start illumination by switching on the laser. Use either flash illumination or constant illumination depending on the aim of the experiment.
4. When the injection of G_t is finished, wash the flow cell for 5 min with running buffer. Initiate dissociation of G_t from bleached rhodopsin by application of 200 μM GTP (inject 25 μL). The sequence of binding and dissociation events can be seen in **Fig. 17.4**.

3.4. Regeneration of Rhodopsin and of a Rhodopsin-Coated Sensor Chip Surface

Due to a limited supply of 11-*cis*-retinal one can also use the commercially available 9-*cis*-retinal to regenerate rhodopsin. Regeneration can be performed directly on the chip surface by injecting 9-*cis*-retinal into the flow cell. Alternatively, the surface can be regenerated by removing rhodopsin from ConA. This can be achieved by injection of the competing carbohydrate

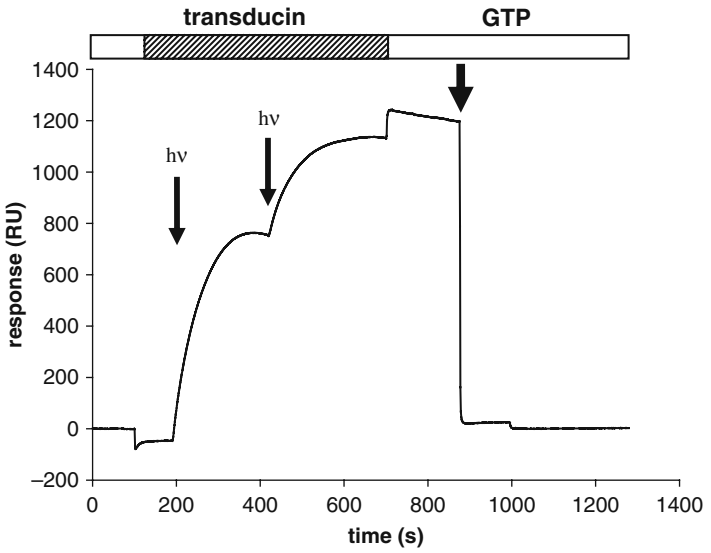

Fig. 17.4. Light-triggered binding of G_t to rhodopsin. G_t is injected into the flow cell (*hatched bar*) under dark conditions, which causes first a small decrease of the resonance signal due to bulk refractive index changes and then a small increase indicating binding of G_t to the surface. Illumination of the system is indicated by two *thin arrows*. Bleaching of rhodopsin triggers binding of G_t as is seen by the positive changes in RU. Running buffer without G_t causes only slow dissociation of G_t (see small change in RU from the end of G_t injection to the third arrow). GTP leads to complete dissociation of G_t from rhodopsin (*thick arrow*).

methyl-α-D-mannopyranoside in a detergent mix and by injection of urea (*see* **Note 6**).

1. Set the flow rate to 5 μL/min. Inject consequently 35 μL of regeneration solution I and 5 μL of regeneration solution II. Wait until the baseline is stable and measure the RU. Compare the value with the starting RU before addition of rhodopsin to the system (*see* **Note 7**).
2. Alternatively, regenerate rhodopsin online by applying 9-*cis*-retinal in the dark. Inject 120 μL of 10 μM solution of 9-*cis*-retinal (diluted from 100 mM stock solution by running buffer just before injection) at low flow rate (1 μL/min) (*see* **Note 7**).

4. Notes

1. G_t is a very labile protein. Therefore, freeze it only once in liquid nitrogen (shock freezing) directly after purification, when the prepared sample is not used immediately. Do not freeze an aliquot of G_t again, when it has been thawed and

used for experiments. It is also important to remove completely GTP before starting the binding experiments with rhodopsin. That is necessary, because in the presence of an even negligible amount of remaining GTP (as well as GDP) in the sample we observed low or no G_t binding to rhodopsin. Instead of a purified sample of G_t it is also possible to use an extract enriched in G_t that could be obtained according to 17 and as described above (*see* step 2 of **Section 3.1**). Such a preparation also contains a small amount of photoreceptor-specific PDE6 and some other retinal proteins in low quantities. However, the presence of these proteins does not interfere with the G_t–rhodopsin interaction monitored by SPR on a Biacore sensor chip.

2. Best results were obtained with a freshly solubilized and prepared sample of rhodopsin on the day of the experiment. The lifetime of immobilized dark-adapted rhodopsin on a sensor chip is surprisingly long (several days), but there are some factors that may decrease its functional properties. For instance, long exposure of rhodopsin deposited on sensor chip surfaces to detergents may cause loss of receptor function. Therefore we usually do not include detergent to Biacore running buffer, but we assume that a mixture of lipid and detergent molecules is interacting tightly with the hydrophobic parts of rhodopsin forming probably a protecting shelf.
3. We found that CHAPS is the best choice among other detergents that are frequently used for rhodopsin solubilization. It probably helps in maintaining the structural integrity during subsequent experiments on the sensor chip surface. When other detergents were used during solubilization (for example, dodecyl-β-D-maltoside, *n*-octyl-β-D-glycoside or Triton X-100), rhodopsin was less stable and interaction with G_t was less efficient.
4. As a light source for this purpose we used a laser of $\lambda = 532$ nm connected to a thin and flexible optic fibre. The fibre can be connected with the Biacore system without disturbing the SPR signal. It was fixed on the interfluid cartridge (IFC) in a distance of 1 cm away from the capillary system on the sensor chip surface (**Fig. 17.5**). It is important to check that the surface is homogeneously illuminated. Filters can be used to attenuate the light intensity. Alternatively, one can use a strong source of white light instead of a laser.
5. Injection of G_t over dark-adapted rhodopsin can give small positive changes in RU, which originates from either nonspecific interaction of G_t with the sensor chip dextran matrix or binding of G_t to pre-bleached rhodopsin. We could not exclude the presence of small amounts of illuminated

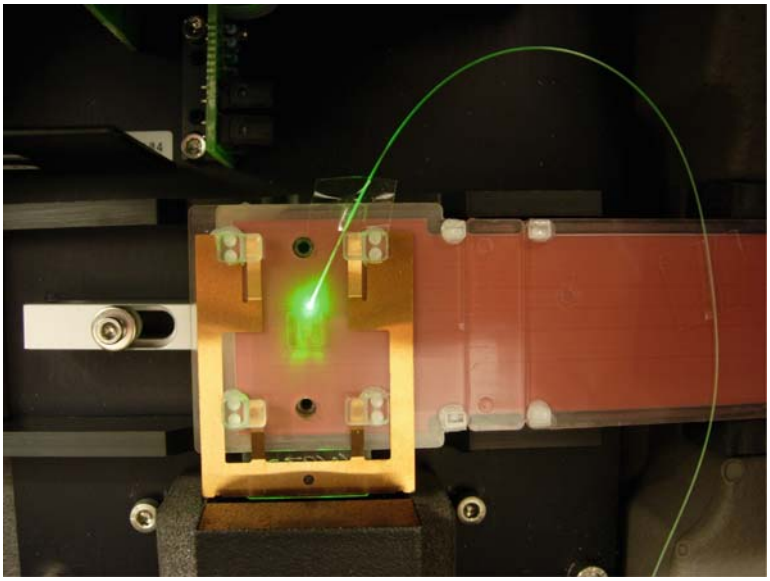

Fig. 17.5. Connection of an optic fibre with the IFC of the Biacore system. The *green light* of the laser is focussed via the optic fibre on the capillary system. The sensor chip has been removed for better visualization.

rhodopsin in a sample of dark-adapted rhodopsin due to the extreme light sensitivity of the receptor. Depending on the purpose of the experiment dark binding of G_t could be subtracted using a corresponding control injection.

6. We observed that the ConA-coated surface has a limited lifetime and we used the surface for approximately 20–30 cycles of immobilization–regeneration. Afterwards, it is advisable to prepare a new surface of ConA. The maximal binding capacity for rhodopsin was only achieved with a fresh surface of ConA. During subsequent cycles of regeneration and immobilization the amount of immobilized rhodopsin decreased steadily indicating a loss of effective ConA-binding sites.
7. Regeneration of rhodopsin by 9-*cis*-retinal was never complete and in the best cases gave 90% recovery of original rhodopsin activity towards G_t binding.

Acknowledgments

This work was supported by grants from the Deutsche Forschungsgemeinschaft and the EWE-Stiftung.

References

1. Helmreich, E. J. M., and Hofmann, K. P. (1996) Structure and function of proteins in G-protein-coupled signal transfer. *Biochim. Biophys. Acta* **1286**, 285–322.
2. Pierce, K. L., Premont, R. T., and Lefkowitz, R. J. (2002) Seven-transmembrane receptors. *Mol. Cell Biol.* **3**, 639–50.
3. Oldham, W. M., and Hamm, H. E. (2008) Heterotrimeric G Protein activation by G-protein-coupled receptors. *Nature Rev. Mol. Cell. Biol.* **9**, 60–71.
4. Arshavsky, V. Y., Lamb, T. D., and Pugh, E. N. Jr. (2002) G proteins and phototransduction. *Annu. Rev. Physiol.* **64**, 153–87.
5. Filipek, S., Stenkamp, R. E., Teller, D. C., and Palczewski, K. (2003) G protein–coupled receptor rhodopsin: a prospectus. *Annu. Rev. Physiol.* **65**, 851–79.
6. Kaupp, U. B., and Seifert, R. (2002) Cyclic nucleotide-gated ion channels. *Physiol. Rev.* **82**, 769–824.
7. Salamon, Z., Cowell, S., Varga, E., Yamamura, H. I., Hruby, V. J., and Tollin, G. (2000) Plasmon resonance studies of agonist/antagonist binding to the human δ–opioid receptor: new structural insights into receptor ligand interactions. *Biophys. J.* **79**, 2463–74.
8. Neumann, L., Wohland, T., Whelan, R. J., Zare, R. N., and Kobilka, B. K. (2002) Functional immobilization of a ligand-activated G-protein-coupled receptor. *ChemBioChem.* **3**, 993–98.
9. Bieri, C., Ernst, O. P., Heyse, S., Hofmann, K. P., and Vogel, H. (1999) Micropatterned immobilization of a G-protein-coupled receptor and direct detection of G protein activation. *Nat. Biotechnol.* **17**, 1105–08.
10. Clark, W. A., Jian, X., Chen, L., and Northup, J. K. (2001) Independent and synergistic interaction of retinal G-protein subunits with bovine rhodopsin measured by surface plasmon resonance. *Biochem. J.* **358**, 389–97.
11. Komolov, K. E., Senin, I. I., Philippov, P. P., and Koch, K.-W. (2006) Surface Plasmon Resonance study of G protein/receptor coupling in a lipid bilayer-free system. *Anal. Chem.* **78**, 1228–34.
12. Vidic, J., Pla-Roca, M., Grosclaude, J., Persuy, M.-A., Monnerie, R., Caballero, D., Errachid, A., Hou, Y., Jaffrezic-Reanult, N., Salesse, R., Pajot-Augy, E. „ and Samitier, J. (2007) Gold surface functionalization and patterning for specific immobilization of olfactory receptors carried by nanosomes. *Anal. Chem.* **79**, 3280–90.
13. Schuck, P. (1997) Use of surface plasmon resonance to probe the equilibrium and dynamic aspects of interactions between biological macromolecules. *Annu. Rev. Biophys. Struct.* **26**, 541–66.
14. Schnetkamp, P. P. M., and Daemen, F. J. M. (1982) Isolation and characterization of osmotically sealed bovine rod outer segments. *Methods Enzymol.* **81**, 110–16.
15. Koch, K.-W., Lambrecht, H.-G., Haberecht, M., Redburn, D., and Schmidt, H. H. (1994) Functional coupling of a Ca^{2+}/calmodulin-dependent nitric oxide synthase and a soluble guanylyl cyclase in vertebrate photoreceptor cells. *EMBO J.* **13**, 3312–20.
16. Kühn, H. (1981) Interactions of rod cell protein with the disk membrane: influence of light, ionic strength, and nucleotides. *Curr. Top. Membr. Transp.* **15**, 171–201.
17. Bornancin, F., Pfister, C., and Chabre, M. (1989) The transitory complex between photoexcited rhodopsin and transducin. Reciprocal interaction between the retinal site in rhodopsin and the nucleotide site in transducin. *Eur. J. Biochem.* **184**, 687–98.
18. Bradford, M. M. (1976) A rapid and sensitive method for the quantitation of microgram quantities of protein utilizing the principle of protein-dye binding. *Anal. Biochem.* **72**, 248–54.
19. Laemmli, U. K. (1970) Cleavage of structural proteins during the assembly of the head of bacteriophage T4. *Nature* **227**, 680–85.

Chapter 18

Integration of SPR Biosensors with Mass Spectrometry (SPR-MS)

Dobrin Nedelkov

Abstract

The combination of surface plasmon resonance (SPR) and mass spectrometry (MS) creates a comprehensive protein investigation approach wherein SPR is employed for protein quantification and MS is utilized to structurally characterize the proteins. In such, MS utterly complements the SPR detection and reveals intrinsic protein structural modifications that go unregistered via the SPR detection. Protein complexes and non-specific binding can also be delineated via the SPR-MS approach. Described here are the protocols and know-how for successful and reproducible integration of SPR and MS. The individual steps of the entire SPR-MS process are illustrated via an example showing analysis of myoglobin from human plasma.

Key words: SPR, mass spectrometry, MALDI-TOF, SPR-MS, protein interactions.

1. Introduction

The major technological advances that ushered the field of proteomics have mainly been driven by developments in the mass spectrometric methods of detection. Mass spectrometry, in the form of matrix-assisted laser desorption ionization time-of-flight (MALDI-TOF) and electrospray ionization (ESI), has taken center stage in the investigation of the human proteome. Coupled with powerful single (2D-gels) or multidimensional (liquid chromatography, LC/LC) separation approaches, mass spectrometry offers a unique way of detecting proteins and their smaller peptide fragments. MS interrogation can also be performed on proteins analyzed by surface plasmon resonance (SPR) biosensors, another

N.J. de Mol, M.J.E. Fischer (eds.), *Surface Plasmon Resonance*, Methods in Molecular Biology 627,
DOI 10.1007/978-1-60761-670-2_18,

relatively new technology that has come to dominate the field of protein interactions since its commercialization in the early 1990s. The combination of SPR biosensors with mass spectrometry has become known as SPR-MS or BIA/MS (biomolecular interaction analysis MS) and offers a unique way of analyzing proteins: SPR is employed for protein quantification, and MS is utilized to delineate the structural features of the analyzed proteins. Proteins are initially affinity-captured from solution via ligands covalently attached on the SPR sensor surface. These ligands are most commonly antibodies, although other types of interacting molecules can also be utilized. Because the SPR detection is non-destructive, proteins retrieved on the SPR sensing surface can be further analyzed via mass spectrometry, either directly from the sensor/chip surface or separately, following an elution and microrecovery. The MS analysis offers a unique opportunity to delineate non-specific binding (NSB) of other biomolecules to the surface-immobilized biomolecules (or to the underivatized sensor surface itself), binding of protein fragments, protein variants (existing due to post-translational modifications and point mutations), and complexed (with other molecules) proteins. The SPR sensing alone cannot detect any of the above events due to its non-discriminatory character (i.e., uniform detection of all binding events via mass change on the sensor surface).

The SPR-MS approach was first demonstrated in 1996 (1) and was subsequently described in several proof-of-principle articles (2–3). Almost all of the early work and technology development was performed in our laboratory (4–11). Other investigators have also utilized the approach and advanced it into new applications (12–22). Described here are the protocols, know-how, nuances, and the "little tricks" we do in our laboratory for successful and reproducible integration of SPR and MS, using the "from-the-chip" MS analysis approach.

2. Materials

Any SPR biosensor that utilizes a planar SPR chip can be utilized for the SPR analysis and protein retrieval (the dominant player in the SPR instruments field is Biacore, Biacore Life Sciences, Piscataway, NJ; another manufacturer of SPR biosensors is GWC Technologies, Inc., Madison, WI). In the case of the Biacore instruments, ligands (e.g., antibodies) are most commonly immobilized on the carboxymethyldextran surface of a CM5 Research Grade Sensor Chip (Biacore, Cat. No. BR. 1000-14) using amine coupling kit chemicals (Biacore, Cat. No. BR-1000-50).

The interface between the SPR biosensor and the mass spectrometer, as practiced in our laboratory, consists of a chip cutter and matrix applicator. The chip cutter is used for excising the chip from its plastic support so that it can be placed in an appropriately milled MALDI target. The chip cutter contains a circular heated cutter-head that, when pressed against the plastic mount, excises a chip/plastic mount of a defined circular shape that fits into our MALDI mass spectrometer target (23). The MALDI matrix applicator is an aerosol-spraying device also developed in our laboratory (23). The device consists of an aspirating/sheath gas needle (~30 μm orifice) backed by ~30 psi of compressed air. The air/matrix solution ratio can be adjusted to produce a fine mist of matrix solution that is aimed at the entire surface of the cutout chip. The matrix of choice is α-cyano-4-hydroxycinnamic acid (ACCA, Aldrich, Milwaukee, WI, USA, Cat. No. 47,687-0), which is further processed by powder-flash re-crystallization from a low-heat saturated acetone solution of the original stock.

MALDI-TOF mass spectrometry analysis from the chip surface can be performed on any commercially available mass spectrometer. In our laboratory, a custom-made MALDI-TOF mass spectrometer (Intrinsic Bioprobes, Inc.) is used for the SPR-MS analysis. The instrument consists of a linear translation stage/ion source capable of precise targeting of each of the flow cells under a focused laser spot. Ions generated during a 4 ns laser pulse (357 nm, nitrogen) are accelerated to a potential of 30 kV over a single-stage ion extraction source distance of ~2 cm, before entering a 1.5 m field-free drift region. The ion signals are detected using a two-stage hybrid (channel plate/discrete dynode) electron multiplier. Time-of-flight spectra are produced by signal averaging of individual spectra from 50 to 100 laser pulses (using a 500 MHz; 500 Ms/s digital transient recorder). Custom software is used in acquisition and analysis of the mass spectra. All protein spectra are obtained in the positive ion mode.

3. Methods

The individual steps of the entire SPR-MS process will be illustrated via an example showing analysis of myoglobin from human plasma. Two antibodies to myoglobin were utilized: goat anti-human (Fitzgerald, Concord, MA, Cat. No. 70-MG60, 5.2 mg/mL) was immobilized in flow cell 1 (FC1) on a surface of a CM5 Research Grade Sensor Chip (*see* **Note 1**), using standard EDC/NHS coupling protocol and reagents supplied by Biacore. Rabbit anti-human myoglobin antibody (Fitzgerald,

Cat. No. 70-MR13, 3.9 mg/mL) was immobilized in a similar manner in flow cell 2 (FC2) on the same chip. Both antibodies were diluted 100-fold into 10 mM acetate buffer, pH 5.0. The SPR signals observed at the end of the immobilization process indicated successful immobilization of ~100 fmoles antibody in each flow cell (*see* **Note 2**). HBS-EP (0.01 M HEPES, pH 7.4, 0.15 M NaCl, 0.005% (v/v) polysorbate 20, and 3 mM EDTA) at a flow rate of 5 μL/min (*see* **Note 3**) was used as a running buffer in the SPR experiments. Following buffer equilibration in both flow cells, a single 50-μL aliquot of twofold diluted human plasma (ProMedDX, Norton, MA) was injected over both flow cells simultaneously. The resulting sensorgram (**Fig. 18.1**)indicates binding responses of 324 RUs (response units) in FC1 and 1,031 RUs in FC2. Immediately following the end of the injection, the buffer flow was stopped (*see* **Note 4**), the chip removed from the biosensor, washed with three 200-μL aliquots of ultra pure sterile water, cut from its plastic housing (*see* **Note 5**), and prepared for MALDI-TOF mass spectrometry by application of MALDI matrix (*see* **Note 6**) with the help of the matrix applicator device (*see* **Note 7**). **Figure 18.2** shows the mass spectra obtained from the surfaces of the two flow cells. Both mass spectra contain multiply charged myoglobin signals, at expected m/z values ($MW_{myoglobin}$=17,052.6 Da). The signals and the overall quality of the mass spectrum obtained from the surface of flow cell 2 are little better than those obtained from FC1. This is somewhat expected, as there was more material bound in FC2, judging from the SPR response in **Fig. 18.1**. Hence, from the SPR-MS experiment it was concluded that the rabbit anti-human myoglobin antibody exhibited better affinity for human myoglobin and was chosen for further experiments.

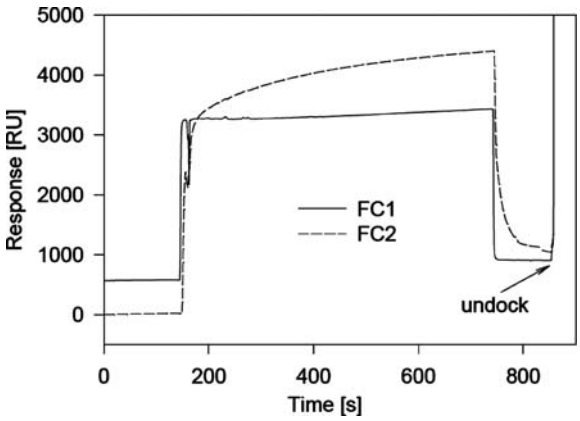

Fig. 18.1. SPR sensorgrams showing the injection of a 50-μL aliquot of twofold diluted human plasma over FC1 and FC2, derivatized with goat and rabbit anti-human myoglobin antibodies, respectively.

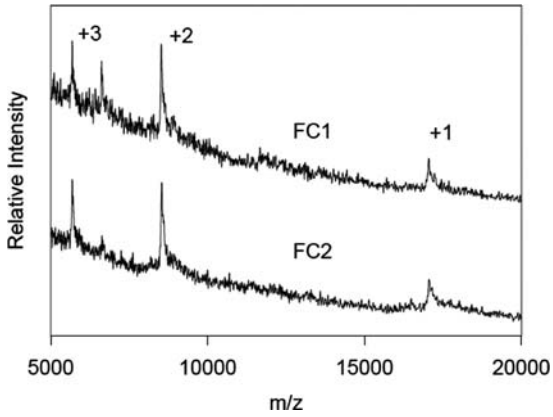

Fig. 18.2. Mass spectra taken from the surfaces of FC1 and FC2, showing the presence of multiply charged myoglobin ions ($MW_{myoglobin}$=17,052.6 Da).

4. Notes

1. Prior to insertion into the instrument, the sensor chip should be removed from the plastic housing cassette and washed with several aliquots of ultra pure water, to remove any residual stabilizers that might interfere with the post-SPR mass spectrometry analysis.
2. It is highly recommended that the ligand is immobilized in a high density on the flow cell surface. High ligand densities can be somewhat detrimental to the generation of good kinetics data (i.e., re-binding of the analyte might complicate the kinetics analysis), but are very beneficial for the subsequent MS analysis because the amount of protein analyte captured from solution is increased.
3. Another way of increasing the amount of captured analyte is to decrease the flow rate of the sample over the ligand-derivatized flow cell surface. Decreased rates promote mass transport effects, which in turn increase the amount of protein analyte captured on the chip. On the other hand, at high flow rates typically used for SPR kinetics experiments (60–100 μL/min), low-concentration analytes will not be captured in amounts permissible to downstream MS analysis.
4. To minimize the loss of protein during the post-capture steps, it is of great importance to minimize the time between the end of the SPR analysis and the subsequent preparation steps for MS. Following the end of the sample injection step,

the SPR response should be promptly recorded, the flow of the running buffer stopped, and the chip removed from the biosensor (the fastest way to undocking is via the root control software of the biosensor). The chip itself should be removed from the cassette and washed with several aliquots of ultra pure water to remove the residual buffer which contains detergent molecules that cause interferences in the mass spectra.

5. We have used, in the past, and with great success, a chip cutter with circular heated cutter-head (Intrinsic Bioprobes Inc., Tempe, AZ) for excising a chip/plastic mount of a defined circular shape that fits into an appropriately configured MALDI mass spectrometer target (12). However, most commercially available mass spectrometers can accommodate the large footprint of the entire chip-housing, as long as the MALDI target is appropriately machined/milled to accommodate the entire chip.
6. In most MS experiments, higher quality mass spectra are obtained with α-cyano-4-hydroxycinnamic acid (ACCA) for proteins smaller than ~25 kDa, whereas sinapic acid (SA) yields better results for higher molecular mass (>25 kDa) proteins. For the MS analysis from the chips, however, ACCA is superior in that it is a better energy-absorbing matrix and, consequently, requires less laser power. Lower laser power means that more spectra can be obtained from a single spot and the fast burning through the matrix/sample layer is avoided. (It should be noted that the analyte is captured in a very thin layer on the surface of the chip, and aggressive interrogation with the laser (at high frequency) can rapidly deplete the sample spot.) Hence, for big proteins, the appearance and intensity of multi-charged ion analyte signals obtained with ACCA are better indicators of the presence and the mass of the on-chip retained proteins. Re-application of more matrix (following initial application and MS analysis) does not yield better signals and generally results in decreased S/N ratio.
7. The application of MALDI matrix is the most critical step in the entire SPR-MS process. The matrix mist generated by the matrix applicator should moisten, but not completely wet the chip surface (i.e., the tiny matrix droplets should stay as individual drops on the surface and not be connected into one large liquid drop). The matrix droplets will desorb the proteins from their respective capturing affinity ligand and, upon rapid drying, the matrix/protein mixture will be re-deposited on the same area from where the proteins were originally captured in the SPR analysis.

Acknowledgments

This publication was supported in part by grant number 5 R44 CA82079-04 from the National Institutes of Health. Its contents are solely the responsibility of the author and do not necessarily represent the official views of the National Institutes of Health.

References

1. Krone, J. R., Nelson, R. W., Dogruel, D., Williams, P., and Granzow, R. (1996) Interfacing mass spectrometric immunoassays with BIA. *BIAJournal* **3**, 16–17.
2. Krone, J. R., Nelson, R. W., Dogruel, D., Williams, P., and Granzow, R. (1997) BIA/MS: interfacing biomolecular interaction analysis with mass spectrometry. *Anal. Biochem.* **244**, 124–32.
3. Nelson, R. W., Krone, J. R., and Jansson, O. (1997) Surface plasmon resonance biomolecular interaction analysis mass spectrometry. 1. Chip-based analysis. *Anal. Chem.* **69**, 4363–68.
4. Nelson, R. W., Jarvik, J. W., Taillon, B. E., and Tubbs, K. A. (1999) BIA/MS of epitope-tagged peptides directly from E. coli lysate: multiplex detection and protein identification at low-femtomole to subfemtomole levels. *Anal. Chem.* **71**, 2858–65.
5. Nelson, R. W., Nedelkov, D., and Tubbs, K. A. (2000) Biosensor chip mass spectrometry: a chip-based proteomics approach. *Electrophoresis* **21**, 1155–63.
6. Nedelkov, D., and Nelson, R. W. (2001) Analysis of human urine protein biomarkers via biomolecular interaction analysis mass spectrometry. *Am. J. Kidney Dis.* **38**, 481–87.
7. Nedelkov, D., and Nelson, R. W. (2001) Delineation of in vivo assembled multiprotein complexes via biomolecular interaction analysis mass spectrometry. *Proteomics* **1**, 1441–46.
8. Nedelkov, D., and Nelson, R. W. (2003) Design and use of multi-affinity surfaces in biomolecular interaction analysis-mass spectrometry (BIA/MS): a step toward the design of SPR/MS arrays. *J. Mol. Recognit.* **16**, 15–19.
9. Nedelkov, D., and Nelson, R. W. (2003) Delineating protein-protein interactions via biomolecular interaction analysis-mass spectrometry. *J. Mol. Recognit.* **16**, 9–14.
10. Nedelkov, D., and Nelson, R. W. (2003) Surface plasmon resonance mass spectrometry: recent progress and outlooks. *Trends Biotechnol.* **21**, 301–05.
11. Nedelkov, D., Nelson, R. W., Kiernan, U. A., Niederkofler, E. E., and Tubbs, K. A. (2003) Detection of bound and free IGF-1 and IGF-2 in human plasma via biomolecular interaction analysis mass spectrometry. *FEBS Lett.* **536**, 130–34.
12. Borch, J., and Roepstorff, P. (2004) Screening for enzyme inhibitors by surface plasmon resonance combined with mass spectrometry. *Anal. Chem.* **76**, 5243–48.
13. Bouffartigues, E., Leh, H., Anger-Leroy, M., Rimsky, S., and Buckle, M. (2007) Rapid coupling of Surface Plasmon Resonance (SPR and SPRi) and ProteinChip based mass spectrometry for the identification of proteins in nucleoprotein interactions. *Nucleic Acids Res.* **35**, e39.
14. Gilligan, J. J., Schuck, P., and Yergey, A. L. (2002) Mass spectrometry after capture and small-volume elution of analyte from a surface plasmon resonance biosensor. *Anal. Chem.* **74**, 2041–47.
15. Grote, J., Dankbar, N., Gedig, E., and Koenig, S. (2005) Surface plasmon resonance/mass spectrometry interface. *Anal. Chem.* **77**, 1157–62.
16. Kikuchi, J., Furukawa, Y., and Hayashi, N. (2003) Identification of novel p53-binding proteins by biomolecular interaction analysis combined with tandem mass Spectrometry. *Mol. Biotechnol.* **23**, 203–12.
17. Larsericsdotter, H., Jansson, O., Zhukov, A., Areskoug, D., Oscarsson, S., and Buijs, J. (2006) Optimizing the surface plasmon resonance/mass spectrometry interface for functional proteomics applications: how to avoid and utilize nonspecific adsorption. *Proteomics* **6**, 2355–64.
18. Lopez, F., Pichereaux, C., Burlet-Schiltz, O., Pradayrol, L., Monsarrat, B., and Esteve, J. P. (2003) Improved sensitivity of biomolecular interaction analysis mass spectrometry for the identification of interacting molecules. *Proteomics* **3**, 402–12.

19. Mattei, B., Borch, J., and Roepstorff, P. (2004) Biomolecular interaction analysis and MS. *Anal. Chem.* **76**, 18A–25A.
20. Natsume, T., Taoka, M., Manki, H., Kume, S., Isobe, T., and Mikoshiba, K. (2002) Rapid analysis of protein interactions: on-chip micropurification of recombinant protein expressed in Escherichia coli. *Proteomics* **2**, 1247–53.
21. Zhukov, A., Schurenberg, M., Jansson, O., Areskoug, D., and Buijs, J. (2004) Integration of surface plasmon resonance with mass spectrometry: automated ligand fishing and sample preparation for MALDI MS using a Biacore 3000 biosensor. *J. Biomol. Tech.* **15**, 112–19.
22. Zhukov, A., Suckau, D., and Buijs, J. (2002, March/April) From isolation to identification: using surface plasmon resonance-mass spectrometry in proteomics. *Pharmagenomics* **1**, 18–28.
23. Nedelkov, D., and Nelson, R. W. (2000) Practical considerations in BIA/MS: optimizing the biosensor-mass spectrometry interface. *J. Mol. Recognit.* **13**, 140–45.

Chapter 19

SPR/MS: Recovery from Sensorchips for Protein Identification by MALDI-TOF Mass Spectrometry

Jonas Borch and Peter Roepstorff

Abstract

Surface plasmon resonance is widely used to study binding interactions with proteins, potentially yielding information on kinetics, thermodynamics and active concentrations. However, the technology cannot identify the involved interaction partners. Mass spectrometry, on the other hand, can be used for specific identification of proteins in amounts comparable to the levels that can be captured on a Biacore SPR sensorchip. Here we present protocols for capturing, washing and eluting proteins from Biacore instruments as well as for robust sample preparation for sensitive mass spectrometric identification.

Key words: Surface plasmon resonance, mass spectrometry, 14-3-3 proteins, H^+-ATPase, phosphorylation-dependent interaction.

1. Introduction

Epitope-tagged proteins are routinely used for capture of proteins by Biacore sensorchips and for affinity purification of the tagged protein from cell lysates by capturing the epitope-tagged protein with an immobilized reagent that specifically recognizes the tag. Furthermore, they can be used for co-precipitation or affinity purification of proteins that interact with the tagged protein (1). The capture step as well as subsequent binding events can be followed by surface plasmon resonance (SPR), a technique that specifically detects how much and how fast analytes in solution bind to an immobilized ligand. Because Biacore's SPR technology employs an immobilized ligand, its microfluidic system is

N.J. de Mol, M.J.E. Fischer (eds.), *Surface Plasmon Resonance*, Methods in Molecular Biology 627,
DOI 10.1007/978-1-60761-670-2_19, © Springer Science+Business Media, LLC 2010

automatically controlled and can monitor binding events even in complex mixtures; it can be used for automated affinity purification of the tagged protein directly from a lysate (2, 3). However, to assure that the captured protein is the tagged one and to investigate if and what it co-purified with, it is important to confirm the identity of the proteins captured by the sensorchip. Once the identity of the captured protein has been verified it can be used for characterization of interactions of proteins that interact with the captured protein. Furthermore, it can be used for identification of interaction partners of the captured protein by injection of cell lysates or chromatographic fractions over the protein that has been captured on the sensorchip by subsequent elution and mass spectrometric analysis (4).

6xHis-tagged proteins are widely used for affinity purification of recombinant proteins because of the relatively tight binding of the six consecutive histidines in the tag to Ni^{2+} ions in immobilized metal ion affinity chromatography and because of the small size of the tag. In the following, we provide protocols for capture of 6xHis-tagged proteins directly from cell lysates by commercially available SPR Ni^{2+}-capturing nitrilotriacetic acid (NTA) derivatized sensorchips, followed by elution from the sensorchip and mass spectrometric identification of eluted protein.

Surface plasmon resonance: For a general introduction to SPR techniques for biomolecular interaction analysis, please refer to **Chapter 1** by de Mol and Fischer, this volume.

1.1. Mass Spectrometric Analysis of Proteins

Intact proteins and peptides resulting from digests of proteins can be transferred to the gas phase by soft ionization techniques in the ion source of mass spectrometers. The two major ionization methods used for protein mass spectrometry (MS) are matrix-assisted laser desorption (MALDI) and electrospray ionization (ESI) (5, 6). In the present chapter we only introduce the background of MALDI. The ion source in a MALDI instrument consists of a metal plate on which the analyte has been co-crystallized with UV-light absorbing low molecular weight compounds, the matrix. A laser shoots on the matrix/analyte mixture and causes desorption of the matrix with the embedded analyte. In addition to assisting desorption, the matrix also protects the analytes from destruction by the UV-light energy and ionizes the analyte by transfer of protons. The analyte ions are accelerated in the ion source and enter the field free time-of-flight (TOF) mass analyser in which they are separated in time and space according to their mass to charge ratios (m/z) before they arrive at the detector. The flight time through the tube correlates to the m/z by $m/z = 2eV(t/L)2$, where e is the electron charge, V is the acceleration voltage, L is the length of the field free flight tube and t is the flight time. Thus the m/z ratios can be calculated from the time it takes the ions to travel through the flight tube to a detector of ion

intensities. By plotting the ion intensity against the recorded flight time a mass spectrum is produced. Most peptide ions observed in MALDI MS are singly charged, even though many large peptides and proteins are also observed at higher charge states. Resolution, sensitivity and mass accuracy have been improved considerably in modern MALDI instruments by modification of the ion source using delayed extraction and of the flight tube by adding a reflector (7). These correct for the kinetic and spatial energy distributions of the desorbed ions with the result that isotopic resolution can be obtained for peptides up to 5–10 kDa. Sensitivities are in the low femtomole to high attomole range and mass accuracy better than 15 ppm can be achieved.

MALDI MS mainly generates molecular weight information of the components. Additional information can be obtained by so-called tandem mass spectrometry (or MS/MS). In MS/MS experiments an ion of interest is selected and submitted to increased internal energy, for example by collision with neutral gas molecules. This results in fragmentation of the ion upon which the formed fragment ions are analysed in a second mass analyser in the tandem mass spectrometer. In the case of peptide analysis this generates sequence information in addition to the molecular weight information generated in the MS experiment (8).

1.2. Protein Identification by MALDI MS and MS/MS

Intact proteins can usually not be identified relative to genome sequences based on their mass alone, because the mass accuracy of MALDI-TOF MS is not good enough at high masses and because the actual proteins may be the result of alternative splicing, be truncated or be co- or post-translationally modified. But upon digestion of a protein with a specific protease, for example trypsin, the protein is cleaved into well-defined peptides. The masses of these peptides can be compared to the calculated masses for the peptides generated by a theoretical digestion with the same enzyme for the proteins in databases. This is termed protein identification by peptide mass fingerprinting (PMF) (9–12). Additional identification can be obtained by combining the PMF data with sequencing of selected peptides in the generated peptide mixture by MS/MS (13).

1.3. SPR/MS

Two major concepts of MS after binding to SPR sensorchip exist: (1) MALDI-TOF directly on the sensorchip and (2) elution of captured analyte from the sensorchip followed by mass spectrometric characterization. The former concept was developed in 1997 by Krone et al. (14). The concept of MALDI-TOF MS directly on the sensorchip is described elsewhere in **Chapter 18**.

Elution of analyte captured by the sensorchip was developed in 1998 by Sönksen et al. (15). After binding the analyte to the immobilized ligand and washing out loosely bound and non-binding material from the sensorchip and the flow system,

the analyte is eluted with a small volume of buffer that disrupts the interaction. After elution from the sensorchip the eluent may be collected from the flow system by microfluidic liquid handling. The autosampler dispenses the eluted protein into a vial or directly onto a MALDI target positioned in the autosampler (16, 17). The elution method from the Biacore system has the advantage that post-processing of the eluted analyte is possible: for example desalting, proteolytic digestion for peptide mass fingerprinting or chemical modification. Additionally, eluted analytes from several experiments can be pooled with the purpose of increasing the amount for more robust mass spectrometric analysis.

The ability of SPR to identify specific binding activity to immobilized ligands in biological fluids, extracts or purification fractions can be combined with mass spectrometric strategies for identification of binding partners. The identity of the novel interaction partner may then provide clues to the function of the immobilized ligand. However, most of the examples provided in the literature are confirmatory: Ligands with known interaction partners have been immobilized and the known interaction partners have been eluted and identified. For example, small protein interaction partners have been identified by their molecular weight alone from urine (18). Borch et al. also identified small proteins by intact masses after screening for carboxypeptidase B enzyme inhibitors (4).

Identification of proteins based on their molecular weight is generally only possible for very small unmodified proteins as mentioned in the introduction. Consequently, peptide mass fingerprinting after proteolytic digestion of the protein often combined with mass spectrometric sequencing of the proteolytic peptides is required for identification. An example of identification by peptide mass fingerprinting is the identification of 14-3-3 proteins bound to a 14-3-3 binding phosphopeptide. Based on the sequence of the 14-3-3 protein binding C-terminus from a plant plasma membrane proton pump the phosphopeptide was synthesized and immobilized on the sensorchip. A 14-3-3 protein could be identified after passing a cauliflower extract over the sensorchip followed by elution, tryptic digestion, MALDI-TOF MS and database searching (19). Other studies have identified proteins eluted from the Biacore sensorchip by reversed phase high-performance liquid chromatography coupled to electrospray ionization tandem mass spectrometers (LC-ESI MS/MS) (20–22).

The protocol presented in this article outlines a general experiment of binding a 6xHis-tagged protein expressed in *Escherichia coli* to a sensorchip coated with Ni^{2+} ions, washing of the fluidic system and elution from the sensorchip to an autosampler vial. Additionally, we provide protocols for tryptic digestion,

upconcentration and desalting of the protein and for mass spectrometric analysis including database searching of the peptide masses (*see* **Note 1**).

2. Materials

All chemicals are analytical grade of highest purity, unless otherwise stated.

2.1. Binding and Recovery from the Biacore Sensorchip

1. Dispensor buffer: 10 mM 4-(2-hydroxyethyl)piperazine-1-ethanesulfonic acid (HEPES), 150 mM NaCl, 1 mM DL-dithiothreitol (DTT), 0.5 mM ethylenediaminetetraacetic acid (EDTA); pH 7.4.
2. Running buffer: 10 mM 4-(2-hydroxyethyl)piperazine-1-ethanesulfonic acid (HEPES), 150 mM NaCl, 1 mM DL-dithiothreitol (DTT); pH 7.4.
3. Nickel chloride solution: 0.5 mM $NiCl_2$ in running buffer. From a 50 mM (100X) stock solution.
4. EDTA stock solution: 300 mM (600X) EDTA, adjusted to pH 8.6 with NaOH.
5. Sensorchip wash solution: running buffer.
6. Integrated fluidic cartridge IFC wash solution 1: 70% formic acid.
7. IFC wash solution 2: 10 mM ammonium acetate.
8. Recovery buffer: 30% formic acid.
9. Sensorchip NTA.

2.2. In-Solution Digestion

1. Digestion buffer: 100 mM ammonium bicarbonate, 2 M guanidinium hydrochloride.
2. *Optional:* reducing solution: 2 mM DTT in digestion buffer.
3. *Optional:* alkylation buffer: 100 mM iodoacetamide. Make the iodoacetamide solution fresh; it is unstable and light sensitive. Iodoacetamide is toxic; wear suitable protection.
4. *Optional:* alkylation quench buffer: 100 mM DTT.
5. Trypsin: Promega, sequencing grade. 100 μg/mL stock in 0.01% HCl.
6. Digestion quenching solution: 10% trifluoroacetic acid (TFA) in water.

2.3. Sample Preparation for MALDI-TOF MS

All solutions that contain organic solvents should be stored in glass vials or used within a few days to prevent contamination with polymer residues from the plastic vials.

1. Matrix solution: sinapinic acid solution 1: 20 mg/mL in 99% acetone, 0.9% water, 0.1% TFA.
2. Matrix solution: sinapinic acid solution 2: 20 mg/mL in isopropanol, formic acid and water (2:1:3).
3. Matrix solution: α-hydroxy-4-cyano cinnamic acid (HCCA) solution: 20 mg/mL in 70% acetonitrile, 30% water with 0.1% TFA.
4. Reversed phase beads: Poros R1-50, Poros R2-20 (Applied Biosystems, Foster City, CA); resuspended in 100% acetonitrile. Store in tightly capped glass vials.
5. Washing solution: isopropanol, formic acid, water (2:3:1).
6. Equilibration/washing solution: 0.1% TFA in water.
7. Washing solution for proteins: 98% water, 2% isopropanol, 0.1% TFA.
8. Eppendorf GELoader tips.
9. Polished stainless steel MALDI-TOF target.
10. MALDI-TOF instrument.

3. Methods

3.1. Binding and Recovery from the Biacore Sensorchip

1. Prepare 500 mL running buffer by degassing and filtering through 0.22 μm nitrocellulose filter. Split the buffer in two bottles, each with 250 mL buffer; add EDTA to a final concentration of 0.5 mM to one of the bottles. Mix by swirling gently and place the inlet-tubing for the dispenser pump in the bottle that contains EDTA. Place the inlet-tubing for the eluent pump in the bottle without EDTA (*see* **Note 2**).
2. Dock a Ni-NTA sensorchip. Equilibrate the Biacore fluidic system with the buffers by running the working tool procedure PRIME (*see* **Notes 3** and **4**).
3. Load the "Analyte recover wizard" for binding, wash and recovery. The wizard contains parameters for which flow cells to use, the flow rate during binding positions of the vials in the autosampler, analyte injection time, time for incubation of the elution buffer on the flow cells, names of solutions and number of cycles to run. Adjust the parameters as desired.
4. Place vials containing 0.5 mM $NiCl_2$, sensorchip washing solution, IFC washing solutions 1 and 2, water, an empty vial, lysate from *E. coli* and elution solution (*see* **Note 5**). The vials are to be placed as specified in the recovery wizard with

the specified minimal volumes. Run the control method. At the end of the method, take out the vial that contains the material eluted from the sensorchip, cap it and store frozen or proceed to **Section 3.2** (*see* **Notes 6,** 7 and **8**).

5. Evaluate the sensorgram according to the level of analyte binding the sensorchip and how efficient elution from the sensorchip was. *See* **Fig. 19.1** for an outline of the observations in an analyte recovery experiment. A result wizard automatically reports the amount of recovered analyte and baseline stability to aid the evaluation of the efficiency when multiple cycles are run.

3.2. In-Solution Digestion

1. Lyophilize the eluted protein to remove the formic acid/water solution.
2. Add 10 μL digestion buffer to the vial that contains the eluted protein, heat to 56°C for 30 min to unfold the protein.
3. Add 1 μL trypsin from a 100 μL/ml stock to the protein solution and incubate at 37°C overnight.
   Optional: For disulfide cross-linked proteins it is an advantage to reduce and alkylate the disulfide bridges to cysteine residues before addition of trypsin solution: include 2 mM DTT in the digestion buffer (without trypsin) and heat the protein to 56°C for 30 min. Alkylation with iodoacetamide is carried out by addition of 0.8 μL of a 100 mM

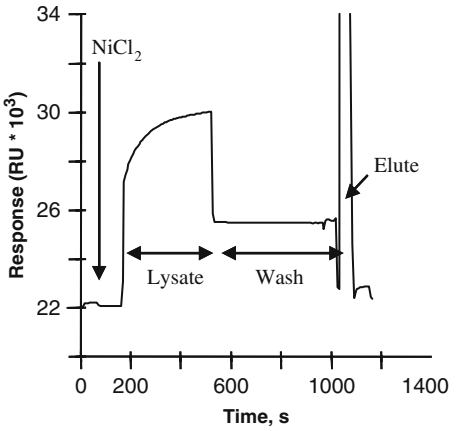

Fig. 19.1. First a flow of running buffer is passed over the sensorchip, next an injection of $NiCl_2$. After washing with running buffer the lysate is injected. Then sensorchip wash solution 1 is injected over the sensorchip and left there while the rest of the flow system that will come in contact with the sample is washed with flow system wash solution 1 and flow system wash solution 2. Finally the recovery solution is injected over the sensorchip. The wash solutions and recovery solutions are separated from each other with air bubbles to avoid mixing. Adapted from (19).

iodoacetamide to the solution after it has cooled down to room temperature and incubation 60 min in the dark.

4. Add 0.5 μL 100 mM DTT to quench unreacted iodoacetamide that might otherwise react with primary amine groups and trypsin to a final concentration of 10 ng/μL. Incubate at 37°C overnight.
5. Stop the digestion by addition of 1/10th volume of 10% TFA in water.

3.3. Sample Preparation of Proteins for MALDI-TOF MS

Intact proteins are prepared by concentration and desalting on microcolumns of Poros R1-50 perfusion chromatography beads (C4 reversed phase material) packed in Eppendorf GELoader tips. Subsequently they are eluted directly onto a drop of water on a thin layer of sinapinic acid (23).

1. Prepare thin sinapinic acid layers by deposition of 0.5 μL 20 mg/mL sinapinic acid in 99% acetone, 0.9% water, 0.1% TFA on the target. The drop spreads out and evaporates quickly.
2. Prepare the microcolumns by making a partial restriction near the end of the gel-loader tip, for example by squeezing with a cap from a microcentrifuge tube vial, and then pipetting a suitable amount of the Poros beads suspended in 100% acetonitrile into the top of the gel-loader tip. Squeeze the suspension through the tip with air pressure from a syringe (all additions to the microcolumn are performed by pipetting into the top and squeezing through with air pressure). The beads should be retained in the end of the eppendorf tip. A suitable length of columns for proteins is 3–4 mm.
3. Wash the column with 20 μL of a mixture of isopropanol, formic acid and water (2:1:3) and subsequently with 20 μL 0.1% TFA.
4. Add the protein solution that was eluted from the sensorchip by slowly pushing it through the column and wash off salts with 2 × 20 μL with 98% water, 2% isopropanol, 0.1% TFA.
5. Apply a 0.5 μL drop of water on the thin sinapinic acid layer that was deposited on the MALDI target.
6. Elute the protein solution directly onto the drop with 0.5 μL 20 mg/mL sinapinic acid in 0.1% TFA in a mixture of isopropanol, formic acid and water (2:1:3). Let the solution dry.

3.4. Sample Preparation of Peptide Digest for MALDI-TOF MS

1. Prepare the microcolumns as described in **Section 3.3** with the following changes: the perfusion chromatography resin should be Poros R2-20 (C18 reversed phase material). The microcolumn bed should be 1–2 mm after packing.

2. Wash first with 70% acetonitrile, 30% water, 0.1% TFA and then with 0.1% TFA in water.
3. Apply the peptide digest and wash with 0.1% TFA in water.
4. Finally, the peptides are eluted directly onto the MALDI target (i.e. no thin layer) with approximately 0.2 μL 20 mg/mL α-cyano-4-hydroxy cinnamic acid dissolved in 70% acetonitrile, 30% water, 0.1% TFA. Let the solution dry.

3.5. MALDI-TOF MS

1. Load the MALDI target into the instrument.
2. Select a parameter file for the positive ion mode with delayed extraction, in the linear mode for intact proteins and reflector mode for peptide digests. The parameter file defines voltage settings and delay times optimized on your instrument for the expected mass ranges.
3. Adjust the laser energy to produce spectra of sufficient intensity while maintaining acceptable resolution. Examples of mass spectra of intact protein and of tryptic digest are shown in **Fig. 19.2**. Sum up spectra and move the laser to a new spot when the intensity of the protein or peptide peaks decrease. Continue to record and sum up spectra until the intensity and resolution of the spectra is acceptable.

3.6. Peptide Mass Searches

1. Open the spectra with suitable software for displaying and processing the mass spectra. Process the mass spectra according to the recommendations of software vendors. Calibrate the spectrum with at least two peaks resulting from trypsin autodigestion products. Extract peak lists of the mass spectra from the software using suitable cut-offs for signal to noise ratios. Peak lists that contain monoisotopic masses are suitable for peptide mass searches (*see* **Note 9**).
2. Paste the peak list into the peptide mass fingerprint search form of the MASCOT search engine (http://www.matrixscience.com/cgi/search_form.pl?FORMVER=2&SEARCH=PMF). Set the requested parameters, e.g. the estimated mass deviation, expected modifications, enzyme used for proteolytic digestion (trypsin in this work), sequence database and taxonomy (*see* **Note 10**).
3. Submit the search.
4. Evaluate the results. The identified protein should have a MASCOT score above the significance threshold reported by MASCOT. A more comprehensive discussion of evaluation of peptide mass searches is beyond the scope of this chapter, but more information can be found in reference (24).

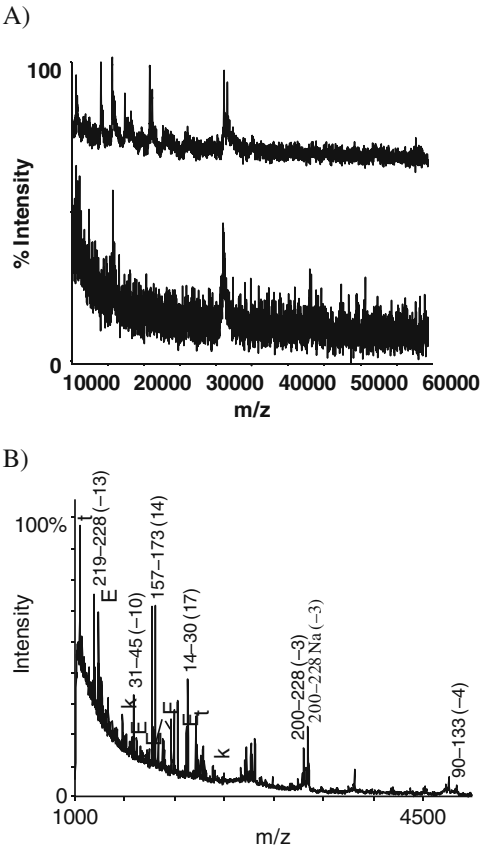

Fig. 19.2. Protein mass spectra of 14-3-3 protein eluted from a Biacore sensorchip. (**a**) Intact protein mass spectra. The *upper trace* displays a mass spectrum of the lysate deposited directly on target, while the *lower trace* displays a mass spectrum of the 14-3-3 protein captured from the cell lysate. (**b**) Annotated spectrum of a tryptic digest of the eluted protein. Peptides annotated to 14-3-3 omega are denoted with the first and last amino acid residues of the corresponding peptide match and the deviation in parts per million (ppm). Peaks that match commonly observed trypsin peptides are labelled with *t* and peaks that match commonly observed keratin peptides are labelled *k*. Peptide labelled with *E* are peaks that match elongation factor Tu, an abundant protein from *E. coli* in which the 14-3-3 protein was expressed. Adapted from (19).

4. Notes

1. The washing solutions and binding times should be optimized for your specific protein. The reference (25) provides an example of systematic optimization of the washing and elution solutions.
2. EDTA protects the stainless steel autosampler needle, but is omitted from the flow over the sensorchip to avoid stripping the Ni^{2+} off.

3. It is important to work with a clean instrument; otherwise excessive amounts of unspecifically binding materials can be eluted from the liquid handling system. We run desorb (flushing with 0.5% SDS, 50 mM glycine, pH 9.5) followed by three PRIME routines with water and overnight standby run with water the day before an SPR/MS recovery experiment to wash out potential contaminants and detergents that interfere with mass spectrometric analysis. It is also advisable to sonicate the injection port and autosampler needle in 70% methanol, 30% water and subsequent rinsing with water before connecting the injection port again.
4. It is advisable to cool the autosampler compartment when running multiple cycles of binding, wash and recovery because proteins in cell lysates are prone to proteolytic and chemical degradation, when they are placed at room temperature for extended time.
5. It is important that all solutions are particle free to avoid blocking the system, thus it is important to filter all solutions through a 0.22 μm filter. Alternatively, to prevent losses caused by filtration, the lysate can be centrifuged at 20,000*g* for 30 min at 4°C.
6. Occasionally the droplet is not deposited in the bottom of the vial, but sits at the edge of the autosampler needle, presumably due to surface tension. To help deposit the droplet in the vial, place 10 μL digestion water or digestion buffer in the bottom of the vial and close the vial with a penetrable silicone cap.
7. Often one cycle is not enough for robust mass spectrometric analysis; in our hands at least a total of 3,000 RU (~3 ng protein) of protein eluted from the sensorchip is required. This corresponds to 100 fmol of a 30 kDa protein. In the case that the amounts are low increase the number of binding, wash and recovery cycles. Alternatively, a larger area of the sensorchip can be employed for capture by a special device, called a surface prep unit, or by manual handling (pipetting). However, neither the surface prep unit nor manual handling allows real-time SPR measurements.
8. Even when the recovered amounts are expected to be sufficiently high as judged from the sensorgram, losses of recovered analyte to the surfaces of the liquid handling system may prevent robust analysis. In that case, try to include a MALDI-TOF compatible detergent in the binding, wash and elution buffers, e.g. *n*-octyl glycopyranoside at 10 mg/mL. Reference (25) devises a different strategy to transport out the eluted protein with minimized losses, based on capture of the eluted protein on nanobeads

during incubation with the elution buffer in the flow cells. The surface prep unit, mentioned in **Note 6**, has minimized contact surfaces for the elution solvent, leading to decreased non-specific binding.

9. The peak lists can also be calibrated after extraction, for example by the software Peak-erazor that also allows common keratin peptides to be used for calibration and can remove the peaks used for calibration and other contaminating masses commonly observed in your project (26).
10. For a detailed description of the contents and parameters choice of the search page, use the Help function of the MASCOT homepage (http://www.matrixscience.com/help_index.html).

References

1. Collins, M. O., and Choudhary, J. S. (2008) Mapping multiprotein complexes by affinity purification and mass spectrometry. *Curr. Opin. Biotechnol.* **19**, 324–30.
2. Visser, N. F. C., and Heck, A. J. R. (2008) Surface plasmon resonance mass spectrometry in proteomics. *Expert Rev. Proteomics* **5**, 425–33.
3. Mattei, B., Borch, J., and Roepstorff, P. (2004) Biomolecular interaction analysis and MS. *Anal. Chem.* **76**, 18A–25A.
4. Borch, J., and Roepstorff, P. (2004) Screening for enzyme inhibitors by surface plasmon resonance combined with mass spectrometry. *Anal. Chem.* **76**, 5243–48.
5. Domon, B., and Aebersold, R. (2006) Review – Mass spectrometry and protein analysis. *Science* **312**, 212–17.
6. Han, X. M., Aslanian, A., and Yates, J. R. (2008) Mass spectrometry for proteomics. *Curr. Opin. Chem. Biol.* **12**, 483–90.
7. Vestal, M. L., Juhasz, P., and Martin, S. A. (1995) Delayed extraction matrix-assisted laser-desorption time-of-flight mass-spectrometry. *Rapid Commun. Mass Spectrom.* **9**, 1044–50.
8. Medzihradszky, K. F., Campbell, J. M., Baldwin, M. A., Falick, A. M., Juhasz, P., Vestal, M. L., and Burlingame, A. L. (2000) The characteristics of peptide collision-induced dissociation using a high-performance MALDI-TOF/TOF tandem mass spectrometer. *Anal. Chem.* **72**, 552–58.
9. James, P., Quadroni, M., Carafoli, E., and Gonnet, G. (1993) Protein identification by mass profile fingerprinting. *Biochem. Biophys. Res. Commun.* **195**, 58–64.
10. Pappin, D. J. C., Hojrup, P., and Bleasby, A. J. (1993) Rapid identification of proteins by peptide-mass fingerprinting. *Curr. Biol.* **3**, 327–32.
11. Henzel, W. J., Billeci, T. M., Stults, J. T., Wong, S. C., Grimley, C., and Watanabe, C. (1993) Identifying proteins from 2-dimensional gels by molecular mass searching of peptide-fragments in protein-sequence databases. *Proc. Natl. Acad. Sci. USA* **90**, 5011–15.
12. Mann, M., Hojrup, P., and Roepstorff, P. (1993) Use of mass-spectrometric molecular-weight information to identify proteins in sequence databases. *Biol. Mass Spectrom.* **22**, 338–45.
13. Medzihradszky, K. F. (2005) *Methods Enzymol.* **402**, 209–44.
14. Krone, J., Nelson, R., Dogruel, D., Williams, P., and Granzow, R. (1997) BIA/MS: interfacing biomolecular interaction analysis with mass spectrometry. *Anal. Biochem.* **244**, 124–32.
15. Sonksen, C. P., Nordhoff, E., Jansson, O., Malmqvist, M., and Roepstorff, P. (1998) Combining MALDI mass spectrometry and biomolecular interaction analysis using a biomolecular interaction analysis instrument. *Anal. Chem.* **70**, 2731–36.
16. Zhi, Z. L., Laurent, N., Powel, A. K., Karamanska, R., Fais, M., Voglmeir, J., Wright, A., Blackburn, J. M., Crocker, P. R., Russell, D. A., Flitsch, S., Field, R. A., and Turnbull, J. E. (2008) A versatile gold surface approach for fabrication and interrogation of glycoarrays. *ChemBioChem* **9**, 1568–75.

17. Sonksen, C. P., Roepstorff, P., Markgren, P. O., Danielson, U. H., Hamalainen, M. D., and Jansson, O. (2001) Capture and analysis of low molecular weight ligands by surface plasmon resonance combined with mass spectrometry. *Eur. J. Mass Spectrom.* **7**, 385–91.
18. Nedelkov, D., and Nelson, R. W. (2003) Delineating protein-protein interactions via biomolecular interaction analysis-mass spectrometry. *J. Mol. Recognit.* **16**, 9–14.
19. Borch, J., and Roepstorff, P. (2006) Combinations of SPR arid MS for characterization of native and recombinant proteins in cell lysates. *Mol. Biotechnol.* **33**, 179–90.
20. Visser, N. F. C., Scholten, A., van den Heuvel, R. H. H., and Heck, A. J. R. (2007) Surface-plasmon-resonance-based chemical proteomics: efficient specific extraction and semiquantitative identification of cyclic nucleotide-binding proteins from cellular lysates by using a combination of surface plasmon resonance, sequential elution and liquid chromatography-tandem mass spectrometry. *ChemBioChem* **8**, 298–305.
21. Natsume, T., Nakayama, H., Jansson, O., Isobe, T., Takio, K., and Mikoshiba, K. (2000) Combination of biomolecular interaction analysis and mass spectrometric amino acid sequencing. *Anal. Chem.* **72**, 4193–98.
22. Ohman, E., Nilsson, A., Madeira, A., Sjogren, B., Andren, P. E., and Svenningsson, P. (2008) Use of Surface Plasmon Resonance Coupled with Mass Spectrometry Reveals an Interaction between the Voltage-Gated Sodium Channel Type X alpha-Subunit and Caveolin-1. *J. Proteome Res.* **7**, 5333–38.
23. Kussmann, M., Nordhoff, E., RahbekNielsen, H., Haebel, S., Rossel Larsen, M., Jakobsen, L., Gobom, J., Mirgorodskaya, E., KrollKristensen, A., Palm, L., and Roepstorff, P. (1996) *"44th ASMS Conference on Mass Spectrometry and Allied Topics"*. pp. 593–601, John Wiley & Sons Ltd, Portland, OR.
24. Hjerno, K. (2007) Protein identification by peptide mass fingerprinting. In Matthiesen, R. (Ed.) *Mass Spectrometry Data Analysis in Proteomics*. pp. 61–75, Humana, Totowa NJ.
25. Larsericsdotter, H., Jansson, O., Zhukov, A., Areskoug, D., Oscarsson, S., and Buijs, J. (2006) Optimizing the surface plasmon resonance/mass spectrometry interface for functional proteomics applications: how to avoid and utilize nonspecific adsorption. *Proteomics* **6**, 2355–64.
26. Hjerno, K., and Hojrup, P. (2002) In Kamp, R. M., Calvete, J. J., and Choli-Papadopoulou, T., (Ed.)*"14th Meeting on Methods in Protein Structural Analysis"*. pp. 359–70.

Subject Index

N.J. de Mol, M.J.E. Fischer (eds.), *Surface Plasmon Resonance*, Methods in Molecular Biology 627,
DOI 10.1007/978-1-60761-670-2,

E

F

G

H

I

K

L

M

N

O

P

Q

R

S

T

U

V

W